# Bubbles – catalysts – oil interactions at elevated temperature and pressure in Fischer Tropsch synthesis

by

**EMILIA NOWAK**

A thesis submitted to

The University of Birmingham

for the degree of

**DOCTOR OF PHILOSOPHY**

School of Chemical Engineering

The University of Birmingham

February 2013

TO MY FAMILY

# ACKNOWLEDGEMENTS

I owe genuine and earnest thankfulness to my academic supervisor and major contributor of this work, Prof. Andrzej W. Pacek, without whom this thesis would not have been possible. I'm truly grateful to my industrial supervisor, Dr Gary Combes, for his constructive guidance, constant support and infinite patience in this endless process of learning. I also would like to thank Prof. E. Hugh Stitt for his valuable recommendations.

I am very thankful to Johnson Matthey PLC, EPSRC and the University of Birmingham for the financial support and for giving me the opportunity to carry out this work.

It is a great pleasure to thank everyone who helped me during the typical struggle of carrying out the PhD, in specific Lynn Draper with all the administration related things, Tom Eddelston with all the laboratory struggles and Bob Sharpe with the technical solutions.

I want to thank my Colleagues for making Uni such a cool place to be. Especially, my thanks goes to Ola, Ourania, Christine, Marie, Flora, Isaac, Roman and my other friends - I will never forget all the fun and experiences we shared and I hope that in the future our friendship will survive.

Dziękuję również Mamie, Siostrom i Braciom za wsparcie, wiarę we mnie, bezwzględną akceptację moich dziwności i w ogóle bycie takimi wyjątkowo-super ludźmi. Dziękuję również Sławkowi, za bycie przy mnie, gdy tego potrzebowałam.

# ABSTRACT

Driving force for this research is dictated by the fact that resources of crude oil, key source of energy in our everyday life, are limited. Therefore the extensive work is currently carried out to find alternatives such as fully synthetic fuels - Fisher Tropsch synthesis (FTS). Though FTS was developed in 1923 until recently it was nearly forgotten. Recent prices of crude oil make this technology attractive again and new research aimed at optimisation is necessary. Crucial step in development/application of this process are new catalyst for complex, three phase, slurry reactors. To certain approximation the most efficient catalyst can be identified by analysis of the bubble size (interfacial area), as it often determines overall reaction rate. Investigations of mass transfer rates at similar to reaction conditions, i.e. high temperature and pressure in oily liquid, are usually carried out using dry nitrogen/air as a model of gas phase, forming non-polar gas/non-polar liquid interface. However in a real system, presence of water as a steam (at high T, P) can change dramatically chemistry of interface that in turn might affect the particles behaviour at polar gas/non polar liquid interface.

The aim of this work was to investigate the behaviour of different catalyst in gas/oil dispersion and the effect on overall mass transfer rate. Efficiency of the entire synthesis, specifically, what is the effect of steam at those conditions was investigated, since there is practically no information in open literature.

Results showed that the effect of particles on the bubble size strongly depends on the interface nature, i.e. non-polar gas/non-polar liquids behaviour is entirely different than polar gas/non-polar liquid. Apparently, reduction of mass transfer rates might occur when steam is present in the system caused by decrease of interfacial area due to larger cohesive forces, hence less efficient breakage. Presence of catalyst particles, such as $Al_2O_3$ might reduce the mass transfer rates of dry gas since the nitrogen/oil interfacial area was decreased, but the same catalyst might increase the rate of mass transfer because of the boost of the steam/oil

interfacial area as compared to the steam/oil (two phase) system. It can be therefore concluded that the simulation of FT synthesis or similar kind of catalysed, slurry reactions using dry gas might lead to incorrect conclusions. This work shows summary of the similarities and differences of properties of all the investigated catalyst and evaluation of their performance. It was shown that the interactions and ultimately the effect that particles have on the bubble size made of either polar or non-polar gas depends on the particles lyophobicity. Subsequently two mechanisms are required to explain such behaviour: particles form bridge and enhance coalescence of bubbles made of nitrogen (non-polar) whereas bubbles made of steam (polar gas) are reduced due to stabilising abilities of particles firmly attached to the interface.

Commonly used contact angle as a parameter enabling quantification of the interactions between catalyst/oil/gas was a) measured and b) evaluated using fundamental (single drop) and practical (emulsion) approach. Several, common methods were tested and the most accurate for the particles contact angle determination was identified for both types of liquids (polar, non-polar). The measurements revealed several issues, such as invalidity of Washburn equation when applied to the liquid rising in highly porous particles bed. Additional set of experiments aiming at the visualisation of the particles in respect to the air/oil interface proved that the contact angle not only does not describe three phase interactions of such system but also leads to wrong conclusions. Therefore novel method, based on thermodynamical approach, was developed and applied for the quantification of the gas/liquid/oil interactions. It was shown that most and least favourable attachment, calculated based on the interfacial energies only, correspond to the experimental observations of the particle to bubble attachment in oil.

# TABLE OF CONTENTS

# LIST OF FIGURES

# LIST OF TABLES

# NOMENCLATURE

$a$ – gas-liquid interfacial area, $m^2$

$a_p$ – the cross-sectional area of the probe on the surface-reported quantity, $m^2$

$D$ – impeller diameter, m

$d_{32}$ – Sauter mean diameter, m

$e$ – effectiveness factor for the first order reaction of CO with rate constant $(k'_{CO}\overline{Cs_{H2}})$.

$f_s$ – is the solid loading,

$F$ – flow rate, $m^3/s$

$G$ – Gibbs free energy per unit area, $J/m^2$

$G_{ads}$ – adsorption energy, J

$j$ – James-Martin factor for the correction of gas compressibility

$k_g$ – gas film coefficient,

$k_l$ – liquid film coefficient,

$k_s$ – film liquid-solid mass transfer coefficient,

$P_{H2O}$ – water vapour pressure in the bubble flowmeter, Pa

$P_{in}$ – pressure at the column inlet, Pa

$P_{out}$ – pressure at the column outlet, Pa

$S$ – constant (Zwieterning) depending from the impeller geometry and clearance; 5 for Rushton 6-blade disc turbine with D=T/2 (Nienow 1968)

$S_{BET}$ – surface area of the column filled with solid particles, $m^2$

$t_o$ – retention time of non-adsorbing probe, s

$T_{col}$ – column temperature, K

$T_{meter}$ – temperature of atmosphere, K

$W_{adh,\,coh}$ – work of adhesion and cohesion, $J/m^2$

$X$ – solid particles loading, $100\frac{\rho_s vol\%}{\rho_l(100-vol\%)}$

Φ – gas hold-up, -

ε – specific energy dissipation rate, W/kg

γ – surface/interfacial tension, N/m

μ – viscosity, Pa·s

$\eta_K$ – Kolmogoroff length scale, m

$\varepsilon_s$ – geometrical factor of the particles packing within the adhering layer for the spheres 0.5236 (Omota et al. 2006)

$\pi_0$ – pressure of the adsorbed state, 338 μN/m

$\rho_p$ – density of porous particle with pores filled with liquid (θ<0° the pores are filled with liquid), so the actual density of porous particles (Vinke et al. 1991): $\rho_p = \frac{\left(1+V_p\rho_l\right)\rho_s}{1+V_p\rho_s}$

Dimensionless numbers and equations:

Henry's constant: $He = p_{CO}/C_{CO,l}$

Mean specific energy dissipation rate: $\varepsilon = \frac{P}{\rho V}$

Weber number: $We = \frac{\rho N^2 D^3}{\gamma}$

Power number: $P_0 = \frac{P}{\rho N^3 D^5}$

Reynolds number: $\mathrm{Re} = \frac{\rho N D^2}{\mu}$

# Chapter 1

# 1 Introduction

## 1.1 Background

Three phase gas/solid/liquid systems are widely used in a range of processes in the chemical, biological (fermentation), petrochemical industry and separation processes such as flotation. The most common application of such systems are the heterogeneous catalytic processes such as oxidation and hydrogenation (of fatty acids), hydroformylation and carbonylation or high pressure reactions catalysed by heavy metal acetylides, called Reppe chemistry. Large scale industrial examples of these include methanol and dimethyl ether synthesis, although the largest by far is Fisher Tropsch (FT) synthesis. Such a gas-liquid-solid system is very complex and one of the underlying problems is the interaction between the gas bubbles and particles in a slurry reactors. In the case of the FT processes, the additional complexity aside from the high temperature and pressure is the presence of steam in the gas phase. All of them have an effect on the catalyzed reaction efficiency however the understanding of their impact is rather poor. The FT synthesis presents only one example of the complex three phase process but because of its current industrial relevance, it is briefly discussed below.

Brief description of Fischer Tropsch synthesis

Energy industries are constantly searching for economically efficient ways to manufacture high quality and environmentally clean petrochemicals (Maretto *et al.* 1999). Historically, interest in FT synthesis development varied according to the changes of the price of crude oil, however ongoing research (from 1985) is no longer driven only by the petroleum price but *"by the desire to monetize stranded natural gas and/or terminate flaring the gas associated with petroleum production and other environmental concerns"* (Davis 2002).

Synthetic fuels production was discovered by two German scientists: Franz Fischer and Hans Tropsch at the Kaiser Wilhelm Institute for Coal Research in Müllheim in 1923 (Davis 2002). In FT synthesis, the carbon monoxide and hydrogen are converted into liquid hydrocarbons and water. The feedstock, syngas ($CO+H_2$), can be obtained from any carbon based sources. The cheapest is natural gas but there are also other sources of feedstock, such as biomass, coal, hydrocarbons and hydroleum coke (Wilhelm *et al.* 2001).

In the FT synthesis two gases, carbon monoxide and hydrogen, react on the surface of catalyst (Figure 1.1) giving the following products with water as a major by-product:

- alkanes: $(2n+1)H_2 + nCO = C_nH_{(2n+2)} + nH_2O$
- olefins: $2nH_2 + nCO = C_nH_{2n} + nH_2O$
- minor quantities of oxygenates, aromatics, naphthenes and carboxylates (Klerk 2007).

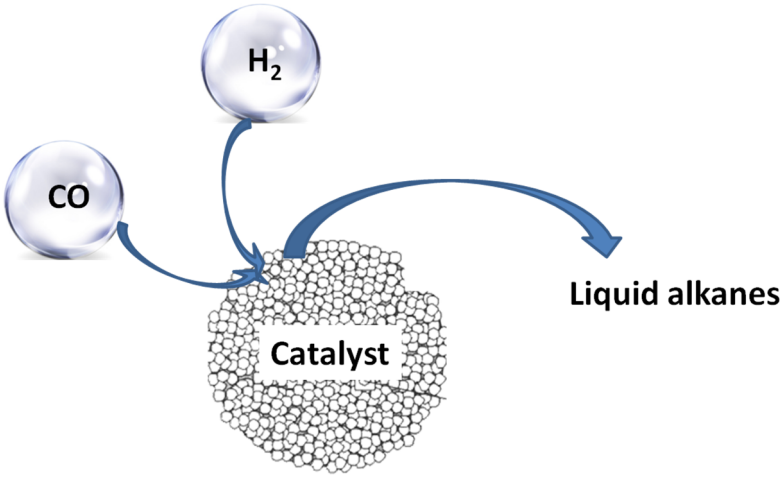


Figure 1.1 Illustration of Fischer Tropsch synthesis

The FT process is based on building hydrocarbon chains by the addition of methyl monomers $-CH_2-$ to the growing molecule so to some extent it can be seen as polymerization reaction (Dry 1996; Guettel *et al.* 2008). The literature extensively describes the possible mechanisms of the reaction, and the following steps are commonly proposed (Kollar *et al.* 2010; Cao *et al.* 2011; Voillequin *et al.* 2011):

a) Carbene mechanism – carbon monoxide molecule undergo chemisorption on the catalyst surface which is followed by the completed dissociation of CO to carbon and oxygen atoms (initiation). Subsequently, the carbon atom is hydrogenated producing $CH_x$ entities, which subsequently form the chains of hydrocarbons due to the propagation of the reaction and finally a termination process (Figure 1.2).

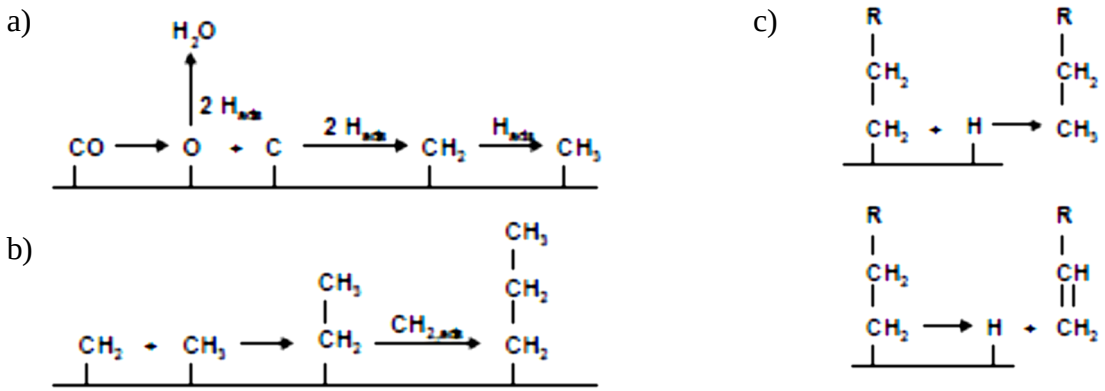


Figure 1.2 Carbene mechanism of hydrocarbons production, a) chemisorptions and dissociation, b) propagation and c) termination

b) Hydroxycarbene mechanism - CO molecules undergo chemisorption and hydroxycarbene is produced by the hydrogenation of CO molecules (initiation). The chain growth of hydrocarbon occurs when oxygen containing species are linked and water molecules are removed (propagation). Figure 1.3 shows the main steps of the hydroxycarbene mechanism.

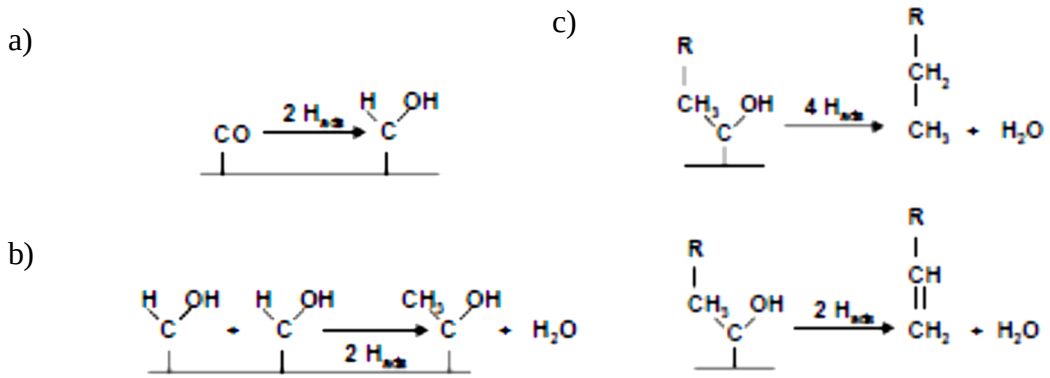

Figure 1.3 Hydroxycarbene mechanism of hydrocarbons production, a) chemisorption and hydrogenation, b) propagation and c) termination

c) CO-insertion mechanism - chemisorption of CO molecule without its dissociation. Adsorbed CO is inserted into catalyst surface-C or metal-H bonds which is schematically presented on Figure 1.4.

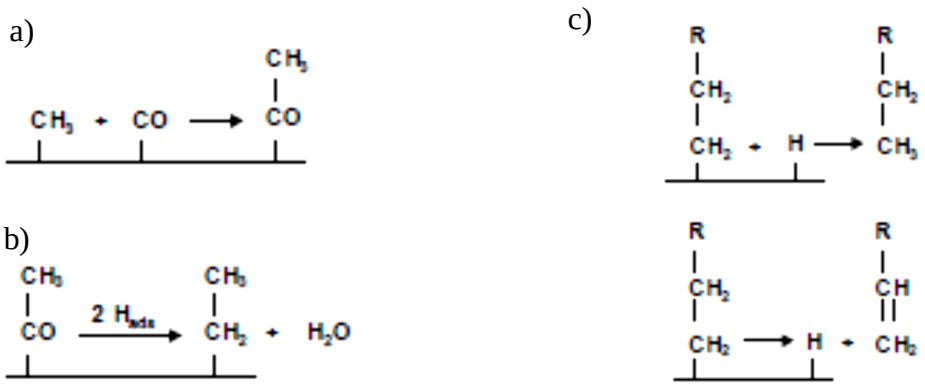


Figure 1.4 CO insertion mechanism of hydrocarbons production, a) chemisorption and insertion, b) propagation and c) termination

The mechanisms of the Fischer-Tropsch synthesis described above provide an insight in the molecular scale of the process of the chain growth. Details of Fischer Tropsch reaction at the molecular level might be useful when interactions between catalyst particles and gas bubbles are analysed. Undeniably, the polymerization like nature of the synthetic fuel production requires prolonged proximity of gas and catalyst to assure the chain growth and such knowledge is important in the design process. Therefore, for the low solubility gases [ in FT liquids: 4bar, 523K: $C^*_{H2}$ and $C^*_{CO}$ larger than 0.3 kmol/m$^3$ (Deimling *et al.* 1984)] it appears that the ideal situation is the catalyst sticking to the $H_2$/CO gas bubble surface, reducing the diffusion through the liquid environment. In such case, the gas concentration near the catalyst active sites is high and the polymerization process is more efficient.

FT synthesis can be carried out in different types of reactor and there are 3 basic designs for the hydrocarbons production on a large scale: fixed bed, fluidized bed and slurry reactors. The overview and the development of Fischer Tropsch reactors to the current solutions can be found in (Davis 2002; Dry 2002; Samiran 2007; Guettel *et al.* 2008).

The selectivity towards desired product can be altered by selecting the type of catalyst and operating conditions, like pressure and temperature, as well as the feed gas $H_2$:CO ratio which subsequently determine the type of reactor that can be used (Cheng *et al.* 2008; Guettel *et al.* 2008). The main challenge in reactor design is the highly exothermic nature of this reaction, i.e. enthalpy ranging -150kJ per mole converted carbon monoxide (Guettel *et al.* 2008). Liquid environment of the slurry reactors ensures a more uniform temperature profile up the reactor, avoiding hot spots and almost isothermal conditions during the synthesis (Geerlings *et al.* 1999). Slurry reactors are economical, the catalyst loading is relatively low and continuous feed with fresh catalyst is possible (Dry 1990). Moreover, the small size of catalyst particles assure enhanced intraparticle gases diffusion although the separation of the fine particles might be difficult (Geerlings *et al.* 1999).

Slurry reactors where the gas bubbles are sparged through the liquid phase in which catalyst particles are suspended have rather simple design and are relatively inexpensive both in terms of investment and running costs. Therefore these types of reactors are commonly used as heterogeneous reactors despite the fact that scaling up of these reactors is rather difficult and the reaction kinetics and heat/mass transfer are predicted experimentally. Empirical correlations based on laboratory studies are very useful and essential for the correct design of industrial processes; however the limited fundamental understanding of the behaviour and interactions in gas-liquid-solid systems can lead to enormous errors and costly mistakes. Whilst the kinetics of the reaction is the system specific are predominantly

determined by the catalyst activity, the mass transfer rate depends on many processing parameters and is generic, therefore applicable for analogous gas-liquid-solid systems.

Understanding of the hydrodynamics, reaction kinetics and mass/heat transfer rates as well as the parameters affecting them are essential for the accurate design, modelling and scale up of slurry reactors. Reactants present in the gas phase are transferred into the liquid phase (which can contain a second reactant) and the reaction takes place on the surface of solid catalyst (Figure 1.5).

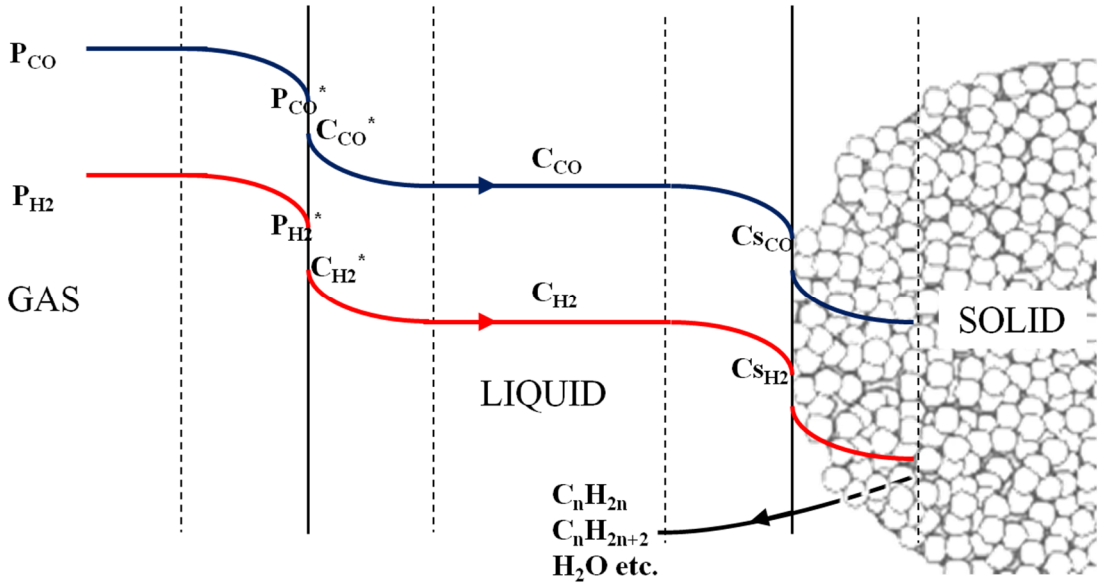


Figure 1.5 Mass transfer of reagents in Fischer Tropsch synthesis

The efficiency (overall yield) of slurry reactors depends of the kinetics of the chemical catalytic reactions and mass transfer of reactants from gas phase through the bulk of liquid phase to the surface of catalyst (external followed by internal diffusion) and assuming first order reaction the overall FT synthesis rate with respect to CO (Levenspiel 1999):

$$r_{CO} = \frac{1}{\frac{1}{Hek_{CO,g}a_g} + \frac{1}{k_{CO,l}a} + \frac{1}{k_{CO,s}a_s} + \frac{1}{\left(k_{CO}^{'}\overline{C_{s,H_2}}\right)e_{CO}f_s}} \frac{p_{CO}}{He} \qquad (1.1)$$

where $k_l a$ is the volumetric mass transfer rate in given phase, Henry's constant (*He)* and *p* partial pressure of gas and effectiveness factor (*e*). Since diffusion, convection and reaction on catalyst occur simultaneously, the slowest step determines the overall reaction rate. It was shown that at given gas phase composition the kinetic of Fisher Tropsch reaction is determined by the catalyst activity and concentration and that the overall reaction is mass transfer limited for the high concentration and activity of catalyst (Inga *et al.* 1996). Therefore, the efficiency of the process is currently limited by the mass transfer rates rather than the catalyst itself.

Therefore, despite use 'excellent' catalysts, the overall reaction rate is expected to be limited by the rate of mass transfer which can be controlled (increased) by appropriate process conditions.

One of the key steps of mass transfer which might control the overall reaction rate is mass transfer from gas bubbles to the liquid phase (Figure 1.5). The resistance in the gas phase from the bulk of the gas bubble to the gas/liquid interface is usually negligible. If the gas is highly soluble, the gas-phase resistance has to be taken into account, otherwise only liquid-side resistance dominates mass transfer. For example, ammonia in water or hydrocarbon in mineral oil is highly soluble, therefore the resistance lies in gas-phase side, whereas oxygen in aqueous solutions are liquid-side resistance controlled. For pure gas there is no gas-side resistance. The mass transfer to and from catalyst is largely controlled by gas in liquid solubility and processing conditions especially by energy dissipation rate in turbulent flow and shear rate in laminar flow. Presence of chemical reactions in slurry reactors increases the liquid-solid mass transfer and the gas-liquid mass transfer becomes determining step of the transfer processes since the driving force (concentration) increases (Jin *et al.* 2006).

The above considerations lead to the conclusion that the gas–liquid mass transfer is the parameter that plays a key role in the overall mass transfer. Gas to liquid mass transfer with the resistance lying on the liquid side is driven by the difference between the equilibrium concentration at the interface and in the bulk of liquid with the volumetric mass transfer coefficient, $k_l a$.

For a multiphase reaction, the correlations for the mass transfer coefficients ($k_l a$) that can be found in literature are often inconsistent because the gas liquid mass transfers experiments were carried out at elevated temperature but at atmospheric pressure (Behkish *et al.* 2002) or at the range of pressures but at ambient temperature (Albal *et al.* 1984; Chilekar *et al.* 2010) or with the particles but at ambient conditions (Vinke *et al.* 1993; Ozkan *et al.* 2000). Elevated temperature and pressure noticeably affect the physicochemical properties of fluids and consequently alter the mass/energy transport and hydrodynamic. Typically, the effect of temperature and pressure has been investigated without particles (Fillion *et al.* 2000). Furthermore, correlations of tested liquids, gases and solids are usually different than those in FT synthesis, i.e. the Fisher Tropsch liquids are simulated by organic and even aqueous liquids, the non-porous particles are used and most importantly, the gas phase contains no water/steam. The presence of water in a gas phase was shown to strongly affect the reaction rates (Storsæter *et al.* 2005; Das *et al.* 2007), hence ignoring this in mass transfer tests and using 'dry' gas can be misleading for the design and scale up purposes. It was shown that in a case of water saturated gas bubbles ($H_2$ and CO) in FT liquids $k_l a$ changes drastically for instance, at 3.3MPa and 423K the $k_l a$ of CO increased from $0.0625 s^{-1}$ to $0.1 s^{-1}$ when the gas was saturated but the $k_l a$ of $H_2$ decreased from $0.3 s^{-1}$ to $0.15 s^{-1}$ (Karandikar *et al.* 1986). It has to be stressed here that the presence of steam in the gas phase was often neglected in the gas-liquid mass transfer experiments (Das *et al.* 2007) (Israelachvili 2011).

Addition of solid particles to gas/liquid system increases the complexity of the mass transfer mechanism. Numerous studies showed that the particles enhance the mass transfer rates in non reactive systems (Alper *et al.* 1980; Vinke *et al.* 1991; Tinge *et al.* 1995; Kluytmans *et al.* 2003; Ruthiya *et al.* 2003; Junmei *et al.* 2006; Junmei *et al.* 2008) but also the completely opposite effect, the reduction of mass transfer rates was reported (Boon *et al.* 1992; Chang *et al.* 1992). Table 1.1 summarizes the studies on the effect of particles on the mass transfer rates in different types of reactors with the indication whether the particles effect was found to enhanced, reduced or unaltered the mass transfer.

Reported contradictory effects of particles on the mass transfer proves that this process is still poorly understood in three phase system (Kluytmans *et al.* 2003). In literature there are several mechanisms and explanations for the mass transfer enhancement or reduction. For example, though the mass transfer resistances in series has physical meaning, frequently showed inaccuracy in modelling (Dumont *et al.* 2003) leads the researchers to seek for alternative modelling, such as the shorter route of gas to solid transfer, where the mass transfer through liquid phase can be significantly reduced (Ruthiya *et al.* 2003) (Figure 1.6).

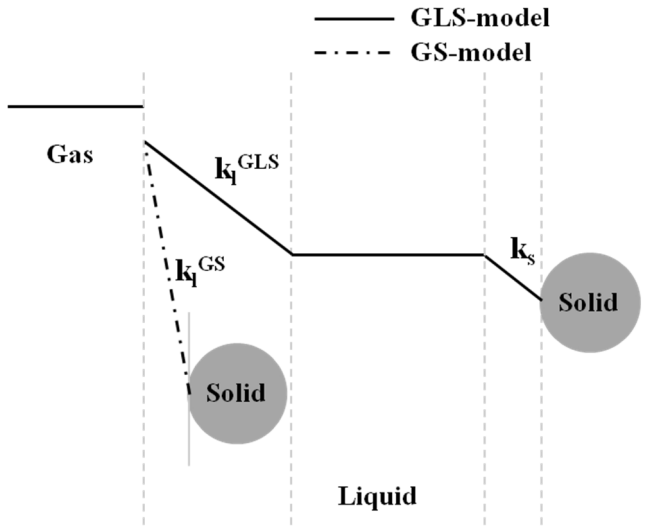


Figure 1.6 Transport of the gaseous reactant to the particle surface through gas-liquid phases ($k_l^{GLS}$) and through gas phase ($k_l^{GS}$)

Clearly, the gas transfer route is the shortest for the particle 'sticking' to the gas bubble which might result in significant reduction of mass transfer rate. Such close proximity of particle and gas bubble brings not only the shorter time for the mass transfer but several other phenomena can occur, such as: reaction in the boundary layer, mixing of the boundary liquid layer, shuttling or grazing effect (absorption of gas from bubble and desorption in the bulk of liquid), bubble coalescence inhibition/enactment (van der Zon *et al.* 1999; Kluytmans *et al.* 2003; Junmei *et al.* 2006; Omota *et al.* 2006; Junmei *et al.* 2008).

Table 1.1 Effect of the solid particles on the mass transfer rates in slurry reactors

| Author | Reactor | Gas/liquid | Solid | Effect of particles on $k_la$ |
|---|---|---|---|---|
| Kluytmans *et al.* (2003) | SAR | $O_2$/Water with sodium gluconate | Carbon particles | Increase |
| Ruhiya *et al.* (2003) | SAR | $O_2$, $H_2$/glucose solituion, methyl styrene | $SiO_2$, C particles | Increase at low concentrations |
| Behkish *et al.* (2002) | SBC | $H_2$, CO, $N_2$ $CH_4$/mixtures of organic liquids (M-isopar, hexane) | iron oxides, glass beads | No effect at low concentration, Decrease at higher concentration |
| Fillion *et al.* (2002) | SAR | $H_2$, $N_2$/ soybean oil | $Ni/Al_2O_{3=}$ | No effect at low concentration (<0.16%) |
| Ozkan *et al.* (2000) | SAR | $O_2$/water, butanol | AcC,Kieselguhr, $CaCO_3$, $TiO_2$, $BaSO_4$, $Fe_2O_3$ | Increase and decrease in both liquids for different particles at low concentrations |
| Inga *et al.* (1997) | SAR | $H_2$, $N_2$, CO, $CH_4$, $C_2H_2$/Hexane mixture | Iron oxide catalyst | Increase at low concentration and decrease at higher conc (12.5%wt) |
| Joly *et al.* (1996) | SAR | $H_2$/mixture of diamine, alcohol and water | Raney Ni catalyst; inert particles | Increase with catalyst Decrease with inert particles |

| | | | | |
|---|---|---|---|---|
| Tinge *et al.* (1995) | SAR | propane, methane, $H_2$/aqueous | Carbon | Increase |
| Vinke *et al.* (1993) | SAR | $H_2$/water | Pd(Rh)/C and Pd(Rh)/$Al_2O_3$ | Increase with C supported and decrease with $Al_2O_3$ |
| Boon *et al.* (1992) | SAR | $O_2$/coal slurries | Coal | Increase |
| Dietrich *et al.* (1992) | SAR | $N_2$,$H_2$/Ethanol, water | Ni Raney particles | Increase at low concentrations and decrease at higher concentration (>3%wt) |
| Hichri *et al.* (1992) | SAR | $H_2$/propanol, o-cresol | Pyrex beads | No effect and low increase at increasing concentration |
| Lindner *et al.* (1988) | SAR, SBC | $H_2$,$O_2$,air/$NH_4NO_3$,$H_3PO_4$ buffer | Pd/C | Increase |
| Alper *et al.* (1986) | SAR | $O_2$/$Na_2S$ | C,$SiO_2$,avicell celluloze | Increase with C<br>Increase with avice cellulose<br>Decrease with $SiO_2$, |
| Deimling *et al.* (1984) | SAR | $H_2$,CO/FT liquids | Glass beads | Decrease with increasing solid concentration |
| Albal *et al.* (1983) | SAR | He, $O_2$/glycerine, water with CMC | Glass beads, oil shale particles | Increase at low concentrations and decrease at higher concentrations (>5%v/v) |
| Joosten *et al.* (1977) | SAR | He, $N_2$/kerosene | Propylene, sugar, pyrex beads | Increase at low concentration and decrease at higher concentrations |

[1]Reactors: SAR – agitated slurry reactor, SBC – slurry bubble column

Almost every explanation of the mass transfer enhancement/reduction is related to the presence of the particles in proximity of the gas bubble. Obviously several mechanisms can occur at the same time, which complicates the understanding how the particles and operating conditions affect the mass transfer. Typically, the product of mass transfer coefficient $k_l$ and interfacial area $a$, $k_la$ is investigated instead of the separated values, and such generalization leads to the limited understanding of the effect of particles on mass transfer (Bouaifi *et al.*

2001; Alves *et al*. 2002). For a better view and understanding, the investigations could be improved by the separation of the component in $k_l a$.

Gas/liquid interfacial area can be determined independently from the $k_l a$, by the measurements of flow rate and mean bubble size. The $k_l a$ was found to follow the interfacial area (Behkish *et al.* 2002). The understanding of the effect of particles and processing conditions on the interfacial area enhance the understanding of the mass transfer in complex multiphase system.

It is clear that the type of particle has an impact on the mass transfer rates and the ability of particles to attach to the gas/liquid interface is responsible for the effect, i.e. as long as the particle attachment occurs there are expected mass transfer variations (Vinke *et al.* 1993). Subsequently, it was shown that the carbon particles are able to remain attached to the gas bubbles whereas silica particles have no such ability in aqueous solution (Ruthiya *et al.* 2003). Also similar tendency, i.e. particles to bubble attachment, was reported for the carbon supported palladium and no attachment was shown for alumina supported palladium (Vinke *et al.* 1993). In both cases the particles wettability by water was claimed to be different, i.e. carbon particles were badly wetted by water as compared to the well wetted alumina/silica particles. The effect of particles was also observed in organic liquids, where the presence of silica, alumina and graphite reduced the bubbles size in high-viscosity organic liquids but the effect was not observed with the low viscosity propanol (Hu *et al.* 2005).

In bubble columns or stirred reactors where the gas phase is dispersed, the resistance to mass transfer across the interface is inversely proportional to the interfacial area or to the bubble size, e.g. the smaller the bubble the larger the ratio of interfacial area to volume and the smaller the resistance to mass transfer. The interfacial area of 1% gas hold-up, the

decrease of bubble size from 1 to 0.1mm gives the increase of interfacial area from 60 to $600m^3$.

In principle, dispersing gas into very small bubbles appears to be the best way of reducing resistance to mass transfer (in the limit it becomes zero). This approach is not very practical because of: a) large amount of energy necessary to produce very small bubbles and b) serious difficulties with removing very small bubbles from the liquid. Therefore the better approach is to control the bubble size by varying energy input and flow rate of both phases and their composition which requires good understanding of the effect of processing conditions on bubble size and/or bubble size distributions.

There is a large body of literature dealing with the bubble size problem in diluted two phase gas/liquid systems where simple mechanistic models are used to relate maximum stable bubble size to average energy dissipation rate (Parthasarathy *et al.* 1991; Machon *et al.* 1997; Alves *et al.* 2002; Hu *et al.* 2006). Obviously such simple models require experimental data to calculate unknown constants resulting in semi-empirical correlations relating bubble size to energy dissipation rate, surface tension and physical properties of liquid phase.

It was frequently reported that the presence of particles significantly affects the bubble size (Nagaraj *et al.* 1987; van der Zon *et al.* 1999; Hu *et al.* 2005; Behkish *et al.* 2007) but the detailed mechanism is unclear. Though there is obvious effect of particles on the slurry properties such as viscosity and density, the studies showed that similar shape and size particles affected the mass transfer rates differently (Vinke *et al.* 1993; Ruthiya *et al.* 2003). It appears that the most important factor is the particles location in the slurry reactor, where in principle (catalyst) particles can be suspended homogenously in liquid, they can agglomerate or they can adhere to gas bubbles (Figure 1.7).

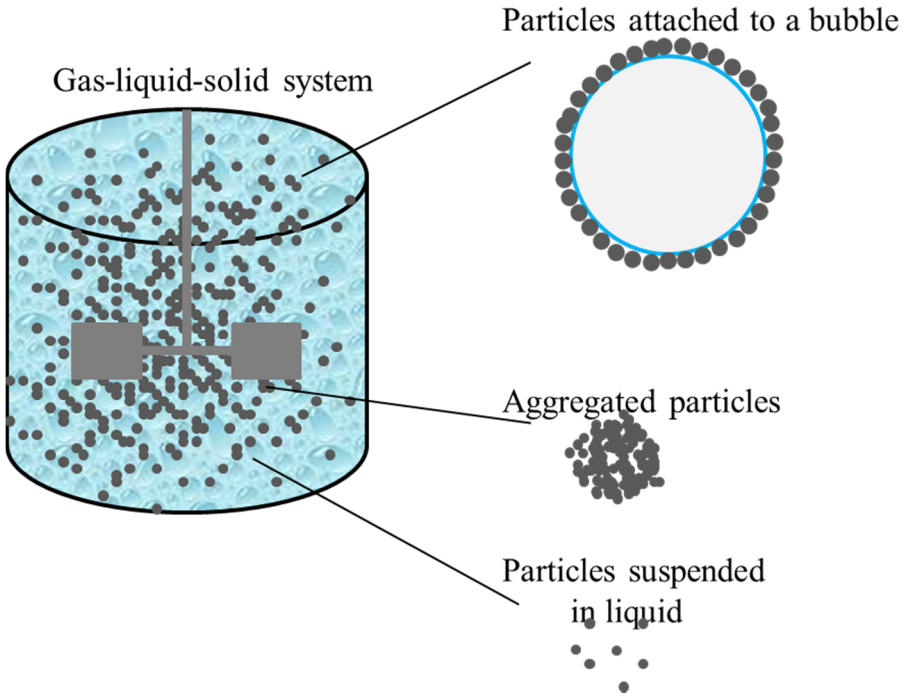


Figure 1.7 The position of particles in the slurry reactor

The effect of fine particles on the bubble size is expected to be pronounced when they are present at the gas liquid interface, commonly expressed as the particle to bubble attachment (Vinke *et al.* 1991). If strong, repulsive forces exist between the liquid and the non wettable particles it is very likely that particles will tend to agglomerate in the bulk of liquid or they will tend to attach to the gas-liquid interface area (Ruthiya *et al.* 2005).

Since in gas-liquid system it is expected that the fine hydrophobic (lyophobic) particles attach to the gas bubble (at given hydrodynamic conditions), the particles wettability seems to be the most important parameter that is considered when the effect of particles on the bubble size is investigated. For a given hydrodynamical conditions, the position of fine particles at the interface is mostly determined by the gas-liquid-solid interaction, described by the three phase contact angle. In aqueous solutions is called hydrophobicity and in non-aqueous liquids lyophobicity, and the three phase contact angle is a measure of the solid

wettability. The solid is hydrophobic, i.e. badly wetted by liquid, when the contact angle formed with the liquid exceeds $90^o$ and hydrophilic, i.e. well wetted by liquid, when the contact angle is below $90^o$.

Clearly the knowledge of the three phase contact angle enables prediction of the particles to bubble attachment (Vinke *et al.* 1991; Dai *et al.* 1999). It is straightforward to measure the contact angle on the flat solid surface (angle that the droplet creates with the surface) but the measurements complicates significantly for the particles. In the literature there are several methods for the measurements of particles contact angle (Lazghab *et al.* 2005; Chau 2009). Determination of the contact angle of particles significantly complicates when the particles are porous and/or of irregular shape.

Presence of particles in the interfacial area can act as a coalescence inhibitor, similarly to the Pickering effect in oil/water emulsions, where the particles sitting at the oil-water interface create the physical barrier for the droplets to coalesce (Pickering 1907; Stiller *et al.* 2004; Binks *et al.* 2005; Saukowski *et al.* 2005). On the other hand, the presence of particles can increase liquid film thinning and enhance the bubbles coalescence which is commonly exploited in antifoaming studies (Frye *et al.* 1989; Garrett 1993; Karakashev *et al.* 2012).

Coalescence inhibition was proposed in numerous studies, where the mass transfer enhancement with the particles was observed (Ruthiya *et al.* 2003; Ruthiya *et al.* 2003; Chilekar *et al.* 2010). Frequently, the coalescence suppression was attributed to the fine particles hydrophobicity, i.e. the hydrophobic particles could remain on the interface and act as a physical barrier for proximal bubbles whereas hydrophilic remained suspended in the liquid, away from the interface.

Controversially, the negative effect of particles on the mass transfer rates was claimed to be an effect of the improved bubbles coalescence caused, again, by the hydrophobic

particles (van der Zon *et al.* 2002). Though completely opposite particles effects, the suggested mechanisms lead to the conclusion that the particle to bubble attachment plays a key role and the main parameter. That the hydrophobic particles are able to stick to the interface is well known and commonly used in the flotation fields, where the particles separation and recovery is based on the difference in particles wettability (Schulze 1977; Yotsumoto 2006; Miettinen *et al.* 2010; Muganda *et al.* 2011).

Undoubtedly, the effect of particles on the mass transfer rates in slurry reactors is strongly dependent on the ability of particles to remain attached to the gas bubble. Particles to bubble attachment might change the interfacial area by the effect on the bubbles coalescence. Apparently, the crucial factor is the fine particles wettability, described by the three phase contact angle which is very difficult to measure for the porous particles. In complex systems, such as Fischer Tropsch reactions, elevated temperature and pressure and the presence of water in the gas phase additionally complicates the analysis of the effect of particles on the bubble size which is mainly manifested by the particle to bubble attachment. Information on the catalyst wettability by the high molecular liquid together with the consistent study of the effect of the energy input, operational temperature and pressure gives the understanding of the major parameters influencing the mass transfer rates in organic liquids, essential for the correct design/scale up of the process.

## 1.2 Aims and Objectives

Crucial step in the development/application of catalysed processes such as Fisher Tropsch synthesis is the production of suitable catalyst. The aim of this work was to investigate the behaviour of different catalyst, supplied by Johnson Matthey, in gas/oil dispersion in order to establish which might produce the largest overall mass transfer rate therefore efficiency of the process.

Specifically, this work aims to establish how the presence of steam affects the mass transfer rates via bubble size in gas/liquid but also how it affects catalysts performance at reaction conditions since there is practically no information in open literature.

Though several recent papers demonstrate the impact of the particles on the bubble size (and bubble size distribution) in aqueous solutions, there is lack of information on the particles effect on the bubbles made of steam in organic liquids (non-polar) and this work attempts to fill this gap.

This work attempts to find the best and most accurate way of quantifying the interactions between catalyst/oil/gas. One of the research goal is to establish which are the key properties of catalyst that affect the bubble size, e.g. particles wettability, size, shape etc.

The work subsequently focuses on the prediction whether the particles are prone to remain at the gas/oil interface. In this context, the most accurate method for the porous catalyst particles wettability measurements was identified. The results were further compared with the images that aimed to visualise the particles at the gas/liquid interface.

## 1.3 Thesis outline

The outline of this thesis consists of six chapters, first introducing the background for the research, the aims and objectives, and last chapter ($6^{th}$) summarizes conclusions that can and further recommendations and work. Three experimental chapters are constructed of short literature review, experimental part, followed by results and discussion and finally conclusions. The layout of this thesis consists of the following chapters:

*Chapter 1* provides background on the Fischer Tropsch synthesis, the main challenges related to such catalysed multiphase reactions, followed by the aims and objectives for this research.

*Chapter 2* describes the effect of four commonly used catalyst supports on the bubble size made of varying steam concentration in a model of FT synthesis. Semi-empirical correlations relating bubble size to hydrodynamic conditions at elevated temperature and pressure were developed for gas/liquid and gas/liquid solid systems with varying gas volume fraction.

*Chapter 3* summarizes measurements of contact angle for porous and non-porous particles.

*Chapter 4* describes novel method for gas/liquid/solid interaction quantification based on the energy changes of the system. The ability of particles to spontaneous attachment to the gas bubble in paraffin oil was determined using equilibrium thermodynamics, based on the experimentally obtained surface energy of particles using inverse gas chromatography.

*Chapter 5* presents set of experiments aimed at imagining/visualisation of the catalyst particles at the interface. The particles attachment to air bubble suspended in water and in oil was investigated for porous and non-porous particles. Interactions of the particles with the polar and non-polar liquid were investigated using fundamental approach (single droplet/bubble in liquid) and more practical approach (emulsions).

*Chapter 6* summarizes key findings and conclusions followed by the recommendations.

*Appendixes* contain peer review published work.

## 1.4 Publications and presentations

Findings from this study have been published in the following journals:

1. E. Nowak, P. Robbins, G.B. Combes, E.H. Stitt, A.W. Pacek, Measurements of contact angle between fine, non-porous particles with varying hydrophobicity and water and non-polar liquids of different viscosities, Powder Technology, accepted, 2013 (see Appendixes)

2. E. Nowak, G.B. Combes, E.H. Stitt, A.W. Pacek, A comparison of contact angle measurement techniques applied to highly porous catalyst supports, Powder Technology, 233 (2013) 52–64 (see Appendixes)

Parts of this work have been presented at:

1. E. Nowak, M. J. H. Simmons, A. W. Pacek, Analysis Of Common Methods For Measurement Of Contact Angle Between Different Particles and Liquids, OKiChiP21, Kołobrzeg, Poland, 2013

2. E. Nowak, G.B. Combes, E.H. Stitt, A.W. Pacek, Critical analysis of different methods for measurement of contact angle of catalyst support, Poster, CAMURE 8 & ISMR-7, Naantali, Finland, 2011

3. E. Nowak, G.B. Combes, E.H. Stitt, A.W. Pacek, Effect of contact angle between catalyst particles and liquids on bubble size in a heterogeneous reactor at elevated pressure and temperature, Presentation, JMAC, Loughborough, UK, 2011

4. E. Nowak, G.B. Combes, E.H. Stitt, A.W. Pacek, Effect of catalyst particles on bubble size and mass transfer rate in mixed solvents in a heterogeneous reactor at elevated pressure and temperature, Poster, JMAC, Loughborough, UK, 2010

5. E. Nowak, G.B. Combes, E.H. Stitt, A.W. Pacek, Effect of catalyst particles on bubble size and mass transfer rate in mixed solvents at elevated pressure and temperature, Poster, JMAC, Loughborough, UK, 2009

# Chapter 2

# 2 Effect of the particles on the bubble size of the particles on the bubble size

## 2.1 Introduction

Fisher Tropsch synthesis is an example of a three phase reaction frequently carried out in a slurry reactor. It is a rather complex system not only because of the presence of three phases but because the mixture of CO and $H_2$ reacts on the catalyst (porous particles) suspended in the high molecular hydrocarbon liquid at elevated temperature and pressure, which consequently leads to the presence of steam in the gas phase.

The overall reaction rate in slurry reactors depends on the reaction and mass transfer kinetics of which a detailed description is essential for the accurate design of multiphase process. The limiting step that controls the overall rate of the reaction in bubble columns or stirred reactors where the gas phase is dispersed in the liquid is often the mass gas-liquid transfer, as previously described in Chapter 1. As the mass transfer from the gas bubble to the bulk of liquid is directly proportional to the volumetric mass transfer coefficient, $k_l a$, is proportional to the gas hold-up ($\Phi$) and inversely proportional to the gas bubble size ($d_{32}$):

$$a = \frac{6\Phi}{d_{32}} \tag{2.1}$$

Though several studies showed that the bubble size depends on the gas composition (Wilkinson *et al.* 1990), there is no data in the open literature on the effect of steam in the gas phase on the bubble size in hydrocarbon liquids. For instance it was reported that the presence of steam in the gas phase changes $k_l a$ for gases in Fisher Tropsch liquids where the $k_l a$ for $H_2$ was decreased and for CO increased with the presence of steam (Karandikar *et al.* 1986; Karandikar *et al.* 1987) but the mechanism was not given. Studies also showed that in Fischer Tropsch liquids the overall reaction rates depends on steam concentration in the gas phase (Storsæter *et al.* 2005). For different catalyst supports ($Co/Al_2O_3$, $Co/SiO_2$, $Co/TiO_2$) that

have same number of cobalt active centres and similar dispersion it has been shown that the presence of steam had a significant effect on the reaction rate (Storsæter *et al.* 2005). Investigation of the effect of the type of surface (hydrophobic, hydrophilic) of the catalyst support on the reaction rate showed that hydrophobicity of particles had an important effect on the $k_l a$ (Ruthiya *et al.* 2003). Gas phase that contain steam at elevated temperature and pressure might become polar and hence the bubble behaviour in the polar gas – non-polar liquid can change drastically as compared to the non-polar gas/non-polar liquid system. Therefore, in this work the effect of different catalyst supports on the gas/liquid interfacial areas with the presence of steam in gas phase has been investigated in order to establish the effect on the mass transfer rates and ultimately on the overall reaction rates.

With a given gas hold-up, dispersing gas into very small bubbles appears to be the best way of reducing resistance to mass transfer since the smaller the bubble the larger the interfacial area and the smaller the resistance to mass transfer. Traditionally, the bubble size in dilute gas-liquid systems is frequently described in terms of energy dissipation rate which results in semi-empirical correlations with experimental data necessary to determine unknown constants (Parthasarathy *et al.* 1991; Machon *et al.* 1997; Alves *et al.* 2002; Hu *et al.* 2006). Such an approach leads to the correlating of data with the dimensionless *We* number which describes the ratio of disrupting and restoring forces acting on the bubble. Alternatively, a completely experimental approach has been reported where based on a large number of experiments, the average bubble size is expressed in terms of the dimensionless numbers (Calderbank 1958; Akita *et al.* 1974; Bouaifi *et al.* 2001; Alves *et al.* 2002), and for a bubble column (Akita *et al.* 1974):

$$\frac{d_b}{D} = 26\left(\frac{gD^2\rho_l}{\gamma}\right)^{-0.50}\left(\frac{gD^3}{\upsilon_l^2}\right)^{-0.12}\left(\frac{U_g}{\sqrt{gD}}\right)^{-0.12} \tag{2.2}$$

where the bubble size ($d_b$) depends on the liquid properties, kinematic viscosity ($\upsilon_l$), density ($\rho_l$) and surface tension ($\gamma$). Also diameter (D), gravity (g) and gas velocity ($U_g$) affect the bubble size.

Another approach was to relate the bubble size directly to physical properties and processing conditions (Wilkinson *et al.* 1994):

$$d_b = 3g^{-0.44}\gamma^{0.34}\mu^{0.22}\rho_l^{-0.45}\rho_g^{-0.11}U_g^{-0.02} \tag{2.3}$$

### 2.1.1 The concept of Weber number

Theoretical prediction of the bubble size is currently unavailable due to the complexity of turbulence, especially in three phase systems. The correlations for bubble size in liquid dispersion (Calderbank 1958) have its origin in the field of liquid/liquid dispersion with the pioneering work of Kolmogoroff (1941) isotropic turbulence theory that was subsequently used by Hinze (1955). According to Kolmogoroff's theory, the complex turbulent motions can be seen as a cascade of eddies. The largest energy containing eddies are of the order of magnitude of the turbulence generator, e.g. the impeller diameter in agitated reactors, from which the eddy takes its kinetic energy. Large eddies are unstable and break into smaller and smaller ones with no loss of energy and the resulting smallest eddies dissipate the energy into the heat (Parthasarathy *et al.* 1991). Smaller eddies are isotropic and independent from the main flow. Between the largest and smallest eddies there exist the range of eddies with the energy transfer entirely due to the inertia, independent of the viscous effects and geometry. The Kolmogoroff's scale separates the inertial sub-range and viscous sub-range accordingly to the following ratio of kinematic viscosity ($\upsilon$) and energy dissipation rates ($\varepsilon$) (Hinze 1955):

$$\eta_K = \left( \frac{\upsilon^3}{\varepsilon} \right)^{1/4} \tag{2.4}$$

To a first approximation there are two major forces acting on the gas bubble dispersed in liquid, i.e. the deforming bubble inertial forces and the restoring surface tension forces (Parthasarathy *et al.* 1991; Pacek *et al.* 1998; Hu *et al.* 2006). Inertial forces result from the turbulent velocity fluctuations (pressure variations) at the bubble surface that act disruptively on the bubble whereas the surface tension attempts to preserve the bubble size. Inertial range eddies are believed to be responsible for the bubble breakage since they carry enough kinetic energy; largest eddies just convey the bubbles whereas the smallest are too weak and therefore unable to break the bubble (Parthasarathy *et al.* 1994).

In equilibrium, there is a dynamic balance between break up and coalescence that depends on physical properties of the system and hydrodynamics. The coalescence rate depends on the collision frequency, the efficiency (i.e. the kinetics of liquid film thinning) and the frequency becomes negligible for the diluted dispersions, therefore in such systems it can be assumed that the bubble size is determined by breakage only. The bubble will break when the kinetic energy of oscillations on the bubble surface, expressed as $\rho\overline{u^2(d)}d^3$, exceeds the surface energy of bubble, i.e. $\gamma d^2$ (Tavlarides *et al.* 1981). In an agitated reactor, the mean velocity fluctuations in the inertial sub-range is expressed in terms of the energy dissipation rate as $\bar{u}d \propto (\varepsilon d)^{1/3}$ where $\varepsilon = P_0 N^3 D^5 / V$. Hence the ratio of the kinetic to surface energy of the bubble describes the maximum size above which the stable bubble is broken. Hinze (1955) proposed that there exists a critical ratio of inertial to surface forces in stirred tank reactors above which the bubble will break, called the critical Weber number:

$$We_c = \frac{\rho \varepsilon^{2/3} d^{5/3}}{\gamma} = const \tag{2.5}$$

and $d_{max} \propto \varepsilon^{-2/5}$ in a stirred tank reactor and the mean energy dissipation rate per unit volume is $\varepsilon \propto N^3D^2$ so the $d_{max} \propto We^{-3/5}$ relation applies and:

$$We = \frac{\rho N^2 D^3}{\gamma} \tag{2.6}$$

$$d_{\max} = C_1 \left( \gamma / \rho \right)^{3/5} \varepsilon^{-2/5} \tag{2.7}$$

where $d_{32} \propto d_{max}$ i.e. the volume to surface of bubble ratio, $d_{32}$. The expression is used as a semi-empirical correlation for low fractions of a dispersed phase (Pacek *et al.* 1998):

$$d_{32} = C_1 \varepsilon^{-2/5} \tag{2.8}$$

$$\frac{d_{32}}{D} = C_2 We^{-3/5} \tag{2.9}$$

where the constants $C_{1,2}$ are system specific, obtained experimentally and mostly depend on the impeller type (power number), reactor geometry and also on the maximum energy dissipation rate (Pacek *et al.* 1998; Hu *et al.* 2003).

It was frequently reported that the exponents in the bubble size correlated with energy dissipation rate and *We* were larger than the theoretical ones, i.e. larger than -0.4 and -0.6 respectively, in liquid/liquid dispersion (Pacek *et al.* 1998; Desnoyer *et al.* 2003) as well as gas/liquid dispersion (Takahashi *et al.* 1992; Hu *et al.* 2006). The correlation of the bubble size with the energy dissipation and/or surface tension is therefore ambiguous and it seems that the bubbles coalescence cannot be neglected, even in highly diluted systems. Moreover, it was shown that the bubble size cannot be correlated with the interfacial tension of water-alcohol/electrolytes mixtures (Machon *et al.* 1997; Hu *et al.* 2005). It is therefore clear that

the bubble size is not only controlled by breakage but also by coalescence, especially when the volume fraction of the gas phase is high (>>1% v/v).

A large and growing body of literature has investigated the bubble size in aqueous solutions, usually with the application to the fermentation processes in biochemical studies. Far less published literature deals with the bubble size in organic liquids and available studies are limited to air, helium, $CO_2$ bubbles, i.e. dry gases (Wilkinson *et al.* 1990; Schäfer *et al.* 2002; Chilekar *et al.* 2010). The presence of steam and its effect on bubble size was notoriously neglected though a range of reaction involves water at elevated temperature. For instance, Karandikar et al. (1986) showed that the mass transfer of CO and $H_2$ was affected by the presence of water/steam in the Fischer Tropsch synthesis though the understanding of the underlying mechanisms behind such changes was not explained.

Except for the scattered experimental results on the bubbles in organic liquids there is a lack of fundamental understanding. It therefore appears that the investigation of the effect of the presence of water in the gas phase on the bubble sizes in organic liquids can be critical in the understanding of the underlying mass transfer mechanisms. Also a lack of information on the relationship between bubbles in viscous organic liquids and process parameters such as the temperature and pressure might lead to enormous errors during reactor design.

### 2.1.2 Effect of operating conditions on the bubble size

The effect of temperature and pressure on the slurry hydrodynamics are essential for the optimum design and subsequently correct operation of multiphase reactors. Empirical correlations based on laboratory studies are useful in the design of industrial processes. However, the limited fundamental understanding of the behaviour and interactions in the gas-liquid and gas-liquid-solid systems can lead to critical errors in scaling up and costly

mistakes. Inaccuracy increases additionally when the results at ambient conditions are transferred into different operating conditions, such as elevated temperature and pressure, or the composition of the phases are altered (Lin *et al.* 1998; Behkish *et al.* 2007). Elevated temperature and pressure noticeably affect the physicochemical properties of fluids and consequently alter the mass and energy transport as well as overall hydrodynamics. Therefore it is obvious that studies on the multiphase systems that were carried out under ambient conditions convey insufficient information (Alves *et al.* 2002; Schäfer *et al.* 2002) to extrapolate to high temperature and to a lesser extent pressure.

#### 2.1.2.1 Effect of elevated pressure on the bubble size

The studies of the effect of elevated pressure on the bubble size in organic liquids in agitated reactors and/or bubbles column appear to be inconsistent. It was found that the increase in pressure leads to smaller bubbles in agitated reactors (Hu *et al.* 2003) and in bubble columns (Lin *et al.* 1998). Also Jiang et al. (1995) showed that the bubble size decreases as the pressure increases up to 1.5 MPa but no further effect was observed. However, it has been also shown that pressure has no effect on the bubble size in an agitated reactor (Albal *et al.* 1983) as well as in a bubble column (Pohorecki *et al.* 2001).

Generally, pressure can affect bubble size because of:

- changes in interfacial tension (Chun *et al.* 1995; Jiang *et al.* 1995)
- changes of gas density (Wilkinson *et al.* 1990; Wilkinson *et al.* 1994; Lin *et al.* 1998; Schäfer *et al.* 2002)

since it does not affect the liquid properties (density and viscosity).

The reduction of interfacial tension with pressure can be attributed to the reduction of surface tension due to the gas absorption on the liquid surface (Lin *et al.* 1998) and it has been

suggested that such decrease is almost linear (Massoudi *et al.* 1974; Massoudi *et al.* 1974). Also Chun et el. (1995) showed a linear decrease of the interfacial tension with rising pressure of carbon dioxide in water-alcohols mixtures. Deimling et al. (1984) suggested that the $k_l a$ increase in Fischer-Tropsch liquids with the pressure was caused by the changes of the interfacial tension and reported at 4MPa FT liquids interfacial tension is reduced by 35-40% as compared to atmospheric pressure due to the increased solubility of gases in the liquid.

The bubble size in the bubble columns, where the initial bubble size is initially established by the size of the gas sparger, depends on the gas density such that smaller bubbles are produced for denser gases due to the higher gas momentum (Wilkinson *et al.* 1990). Also, higher kinetic energy cause bubble distortion leading to enhanced breakage (Behkish *et al.* 2007). Takahashi et al. (1992) however showed no difference in bubble size for different densities gases (molecular weights from 4 to 131) in an agitated reactor which means that another reason must be responsible for the reduction of bubble size with pressure (Clark 1990).

#### 2.1.2.2 Effect of elevated temperature on the bubble size

The Arrhenius equation describes the viscosity dependence on the temperature, i.e. shows that as the temperature increases the viscosity of liquid decreases. Reduction of viscosity with temperature leads to enhanced turbulence and bubble breakage intensifies (Schäfer *et al.* 2002) and surface tension also decreases with temperature. Since the magnitude of disruptive forces increases whereas the magnitude of cohesive forces decreases with temperature, the bubble size also decreases. Indeed, it was frequently reported that the bubbles in organic liquids decrease as the temperature increases (Sridhar *et al.* 1980; Deimling *et al.* 1984; Lin *et al.* 1998; Schäfer *et al.* 2002; Behkish *et al.* 2007) though in the

study by *Deckwer et al.* (1980) of paraffin liquid, the bubble size was similar at 250 and 270°C.

Table 2.1 Effect of physical properties on bubble size

| | | | |
|---|---|---|---|
| Density of gas, $\rho_g$ ↑ | Inertia forces ↑ | ⇒ | $d_{32}$ ↓ |
| Viscosity of liquid, $\mu_l$ ↓ | Turbulence ↑ | ⇒ | $d_{32}$ ↓ |
| Surface tension, $\gamma$ ↓ | Cohesive forces ↓ | ⇒ | $d_{32}$ ↓ |

↓ - decreases, ↑ increases

Table 2.2 Effect of operating conditions on bubble size

| | | | | | |
|---|---|---|---|---|---|
| T ↑ | $\rho_g$ ↓ | $\mu_l$ ↓ | $\gamma$ ↓ | ⇒ | $d_{32}$ ↓ |
| P ↑ | $\rho_g$ ↑ | $\mu_l$ - | $\gamma$ ↘ | ⇒ | $d_{32}$ ↓ |

↓ - decreases, ↑ increases, ↘ slightly decreases, - remains the same

The results of the investigation of the effect of temperature and pressure on the bubble size in non-aqueous solutions in bubble columns and agitated reactors are summarized in Table 2.3. Clearly not much data can be found on the bubble size in organic liquids, moreover, only few studies investigated simultaneous effect of presence of particles and temperature/pressure. To the author's knowledge, there is no published work on the effect of steam on bubble size in organic liquids.

Table 2.3 Effect of particles and operating conditions on the bubble size in non/aqueous sol.

| Reactor type | Conditions | G/L/S | Effect of P, T on bubble size | Effect of particles on bubble size | Literature |
|---|---|---|---|---|---|
| BC | 0.1-1.3 Mpa; Cs <3% | $N_2$, air/ water, isopar-m oil/C 30μm, $SiO_2$ 44μm | ↑ P => $d_{32}$↓ (irrespective on particles type) | No effect of particles (wettability) | (Chilekar *et al.* 2010) |
| BC | 300-473°C; 0.67-3MPa; 0.07-0.39m/s; Cs 0-20% | $N_2$,He/isopar-M/ $Al_2O_3$ (32-42μm) | P↑ => $d_{32}$↓ T↑=>$d_{32}$↓ | Cs↑=>$d_{32}$↓ | (Behkish *et al.* 2007) |
| STR | Ambient | air/alcohol /alumina, silica (~20-~200um), graphite ~20um | - | Particles reduce $d_{32}$ | (Hu *et al.* 2005) |
| BC | 30-160°C; 0.2-1.1 MPa; $u_g$=0.002-0.055 m/s | $N_2$/cyclohexane | No effect of T and P on $d_{32}$ | | (Pohorecki *et al.* 2001) |
| BC | 25-175°C; 1-50 bar | $N_2$/cyclohexane, cyclohexanol, water, ethanol | P↑ => $d_{32}$↓ T↑=>$d_{32}$↓ | | (Schäfer *et al.* 2002) |
| BC | Ambient | air/water/carbon | | Cs↑=>$d_{32}$↑ | (van der Zon *et al.* 2002) |
| BC | 27, 78°C; 0.1-15.2MPa; 0.02-0.08m/s | $N_2$/paratherm NF heat transfer fluid | P↑=$d_{32}$↓ T↑=>$d_{32}$↓ | | (Lin *et al.* 1998) |
| STR | 373-523K, 10-40 bar, TV 2.0L, 800-1100 RPM, Solid up to 30 wt.% | $H_2$, CO/FT light($C_6$-$C_{11}$)/ FT medium ($C_{12}$-$C_{21}$)/FT heavy(≥$C_{22}$)/solid: glass bed (125-177μm) | P↑ => $d_{32}$↓ T↑=>$d_{32}$↓ | | (Deimling *et al.* 1984) |
| STR | 295K,13.8-96.5 bar, 400-1000 RPM, TD 10.2 cm, Solid up to 30 vol% | He, $O_2$/ Glycerin,water+CMC/ glass beads (75-150μm), oil shale particles | No influence of P; | | (Albal *et al.* 1983) |
| STR | 297-423K, 480-1800 RPM, 1-10 bar, | $N_2$/cyclohexane | T↑=>$d_{32}$↓ | | (Sridhar *et al.* 1980) |

BC – slurry bubble column, STR – stirred tank reactor, Cs – solid particles concentration

### 2.1.3 Effect of gas volume fraction on the bubble size

In the bubble column, bubbles are formed at the gas distributor which determines the initial size together with the liquid properties. In the surface aerated agitated reactors however, bubbles are formed by the action of impeller and baffles, where initially the gas is sucked into the bulk of liquid and then disrupted into smaller bubbles. In this case the equilibrium size depends on the energy input and liquid and gas properties which affect the bubble breakage. On the other hand there is coalescence of bubbles involved. The coalescence rate depends on the collision frequency and efficiency (Laari *et al.* 2003), therefore the higher gas hold-up, the higher probability of collision. Therefore for the larger gas phase where the collisions are inevitable, the bubble is controlled not only by the breakage but considerable coalescence occurs and the larger the gas phase volume fraction, the higher the coalescence (Hu *et al.* 2003).

Increasing the gas holdup results in dampening of the energy dissipation rates (turbulence) and a larger coalescence probability and both lead to larger bubble sizes (Razzaghi *et al.* 2010). There were attempts to include the bubble coalescence effect due to highly concentrated systems and the following expression was proposed:

$$\frac{d_{32}}{D} = C_3\left(1 + C_4\Phi\right)We^{-3/5} \tag{2.10}$$

where the constant $C_4$ is related to the coalescence behaviour of a system with the experimental values ranging from 3 to 20 and $\Phi$ represents the fraction of gas phase (Zhou *et al.* 1998; Hu *et al.* 2003). $C_4\phi$ also indicates dampening of turbulence for highly diluted systems (Pacek *et al.* 1998).

### 2.1.4 Effect of particles on the bubble size

It is commonly reported that the presence of particles affect the bubble size. A number of parameters and solid properties are suggested to be important, such as solids concentration, size, wettability, ionic strength, etc. though the relative significance of these is still not clear (Nagaraj *et al.* 1987; Vinke *et al.* 1991; Vinke *et al.* 1993; van der Zon *et al.* 1999; Hu *et al.* 2005; Behkish *et al.* 2007). Moreover, the effect of particles on the slurry properties such as viscosity and density was often attributed to the observed effect on the bubble size (Deimling *et al.* 1984; Karandikar *et al.* 1986). However, antifoaming studies (Frye *et al.* 1989; Garrett 1993; Karakashev *et al.* 2012) and emulsion related studies (Pickering 1907; Binks *et al.* 2005; Saukowski *et al.* 2005) reveal the importance of the particles behaviour at the fluid-fluid interface rather than the effect on properties of the bulk of liquid. Such particles activity on the interface were used to explain differences in the bubble size when similar concentrations of particles with similar size that produce similar slurry properties ($\mu$, $\rho$) were suspended in the gas-liquid dispersion (Vinke *et al.* 1993; Ruthiya *et al.* 2003).

One of the most difficult problems of gas-liquid-solid systems is the interaction between the gas bubble and particle in the liquid environment. Addition of solid particles to gas/liquid systems drastically increases the complexity of the interaction between phases and there is rather limited information on such systems in open literature. It appears however, that the particles location in the slurry reactor, i.e. homogenously suspended in the liquid or concentrated on the bubble surfaces, is the crucial factor affecting the bubble size. In catalysed reactions the particles have even larger significance since reactants (gas/liquid) has to first absorb on the catalyst surface for the reaction to occur. It therefore is possible to speculate that the most active catalyst should a) form the smallest bubbles to increase the

mass transfer rates and b) remain in the close proximity to the gas-liquid interface for efficient reactants absorption.

If strong, repulsive forces exist between the liquid and the particles it is very likely that particles will tend to attach to the gas/liquid interface (Ruthiya *et al.* 2005). Inherently, such tendency depends on the particles wettability. For given hydrodynamic conditions, the position of fine particles in relation to the interface is often determined by the gas-liquid-solid interaction, described by the three phase contact angle.

Particle wettability (hydrophobicity in aqueous and lyophobicity in organic solutions), quantified by the three phase contact angle has a straightforward interpretation when a flat solid surface is considered (Figure 2.1). The three phase contact angle, formed when the solid-liquid, solid-vapour surface energies and liquid-vapour interfacial tension are balanced:

$$\gamma_{sl} = \gamma_{sv} - \gamma_{lv} \cos\theta \tag{2.11}$$

In other words, surface and interfacial forces at a certain contact angle are in equilibrium. The solid with $\theta > 90^o$ is called hydrophobic (lyophobic) and $\theta < 90^o$ hydrophilic (lyophilic).

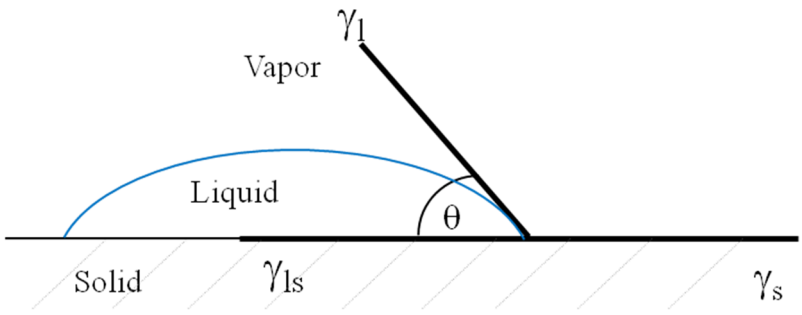


Figure 2.1 Physical meaning of contact angle

Similarly, when the same concept is applied to the system, where the particles are suspended in the gas-liquid dispersion, the higher the three phase contact angle the higher the affinity of particles to bubbles (Figure 2.2).

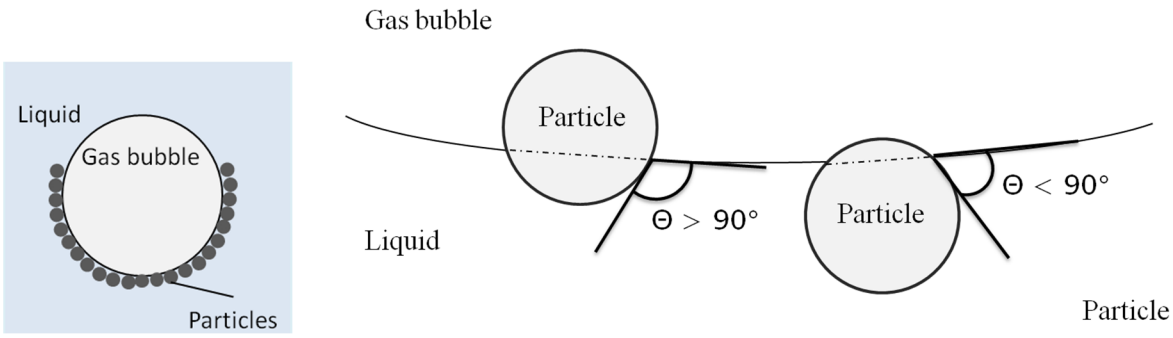


Figure 2.2 Particles to bubble attachment (left) as a function of the contact angle (right)

A fine particle to bubble attachment is caused by the capillary force arising from the hydrophobicity (large θ). Thermodynamically, the change in the energy (Gibbs, $\Delta G$) per unit interfacial area at the particle to bubble attachment is a function of energies of all three interfaces:

$$\Delta G = \gamma_s - \left(\gamma_{sl} + \gamma_l\right) \tag{2.12}$$

which combined with Young's equation gives:

$$\Delta G = \gamma_l \left(\cos\theta - 1\right) \tag{2.13}$$

These changes of free energy correspond to the work of particle-bubble adhesion and express the work done on the liquid removal from the solid and bubble surface followed by formation of the solid-gas interface. Clearly, the attachment is favourable for the θ > 0° and attachment probability increases with increasing θ (Norde 2003). It can be concluded that the higher the

three phase contact angle the higher the particles to bubble attachment and particles are expected to remain on the gas-liquid interface. The strength of particles attachment on the interface is related to the magnitude of energy of desorption:

$$E \approx 4\pi r^2 \gamma_{lv} \left(1 - \left|\cos\theta\right|\right)^2 \tag{2.14}$$

Therefore at the contact angle ~ 90°, and high surface/interfacial tension large particles are strongly attached to bubble.

According to previous studies (van der Zon *et al.* 2002; Ruthiya *et al.* 2003; Ruthiya 2005; Chilekar *et al.* 2010; Karakashev *et al.* 2011), the presence of particles on the interface lead to the changes of bubble coalescence rate and for high gas hold-up, bubbles coalescence could become as important as breakage. Unlike the breakage, the coalescence involves not only interaction of a bubble with the liquid but also involves another bubble which significantly complicates the description. Coalescence can be seen as the action of the external flow (continuous phase) and internal flow between bubbles flow (Figure 2.3) (Chesters 1991). The former determines the frequency and force of the collision, but also duration of the contact. The latter determines the drainage of the thin liquid film separating bubbles and the deformation of the bubble surface. Coalescence frequency results from the collision frequency and efficiency (Paul *et al.* 2004). In principle however, the coalescence is a fast process that normally takes less than 1s, the controlling step is believed to be the draining of the liquid film to a critical thickness under the action of the turbulent (external) flow (Chaudhari *et al.* 1994).

The presence of particles can decrease the turbulence intensity and subsequently the bubbles collision frequency and contact force by not only increasing the apparent liquid

viscosity and density but also the particles can influence the thickness of liquid film and the rate of its thinning/draining.

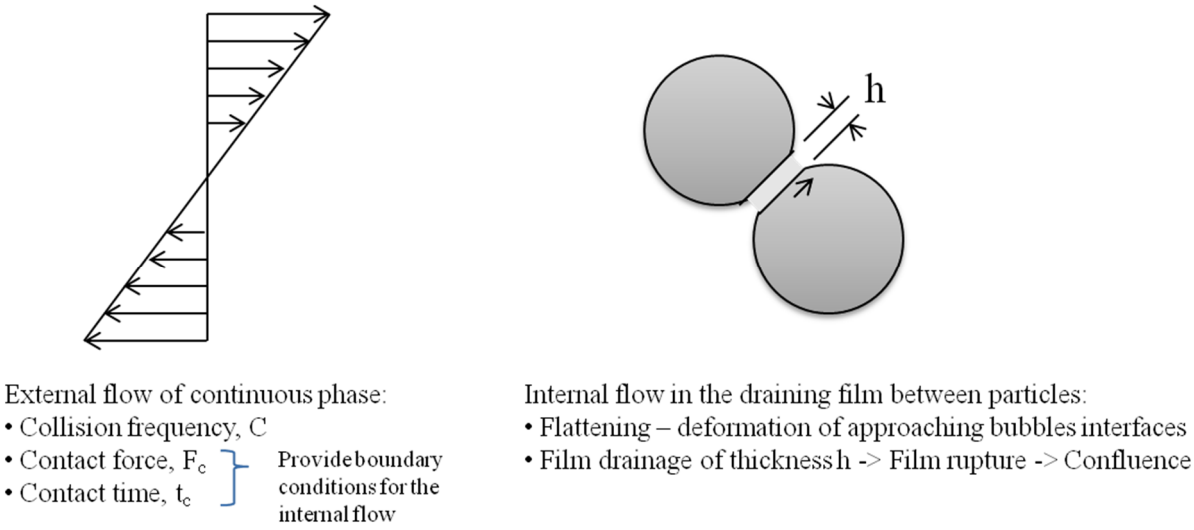


Figure 2.3 Sub-processes of the bubbles coalescence (Chesters 1991)

In a three phase system the presence of particles at the interface suppress bubble coalescence (Ruthiya *et al.* 2003; Ruthiya *et al.* 2003; Chilekar *et al.* 2010), however others argue that the particles enhance the bubble coalescence rate and increase the bubble size (Nagaraj *et al.* 1987; van der Zon *et al.* 2002).

Particles can suppress bubble coalescence in a similar manner as they suppress coalescence of liquid drops (Pickering 1907; Stiller *et al.* 2004; Binks *et al.* 2005; Saukowski *et al.* 2005) but also in the formation of stable foams (Karakashev *et al.* 2011; Karakashev *et al.* 2012). The particles present on the fluid-liquid interface create the dense coverage mesh; a physical barrier preventing the droplets/bubbles from coalescing. The strength of particles attachment to the fluid-liquid interface is related to the magnitude of energy of desorption expressed by equation (2.14) When the contact angle that the particle forms with the liquid and fluid (gas or other liquid) phase reaches 90°, the energy of desorption reaches maximum

and the removal of particles from the interface becomes difficult. Therefore the hydrophobic particles can form a stable barrier for the coalescing bubbles (Figure 2.4).

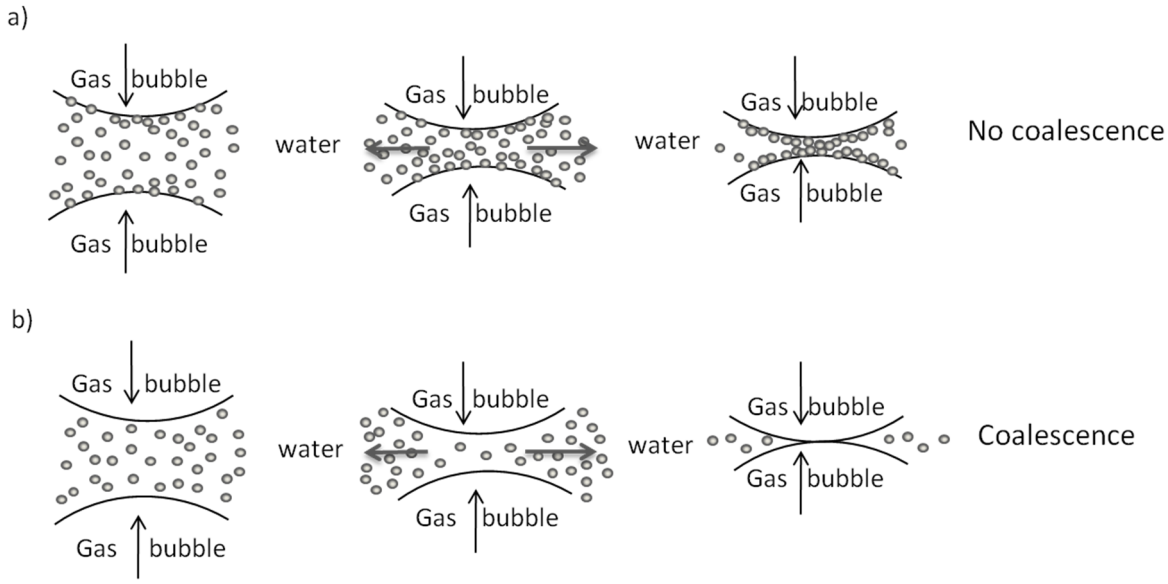


Figure 2.4 The effect of a) hydrophobic and b) hydrophilic particles on the gas bubble coalescence (Chilekar *et al.* 2010)

On the other hand, the presence of particles on the interface can enhance the bubbles coalescence when the bubble coverage with particles is poor which is commonly exploited in antifoaming studies (Frye *et al.* 1989; Garrett 1993; Karakashev *et al.* 2012). Thinly dispersed particles at the interface are unable to form the physical barrier. Moreover, particles attached to the bubble surface can form a 'bridge' when another bubble approaches. Bridging effects becomes more pronounced for the highly hydrophobic particles (large θ), where the liquid is removed by the gas as shown on Figure 2.5 (Murray *et al.* 2004). Subsequently the thin liquid film between two bubbles drains faster and the rupture occurs leading to coalescence. For instance, the coalescence of bubbles in the foam, due to the liquid film rupture, can be hindered by increase of interfacial elasticity due to the presence of particles (Karakashev *et al.* 2011). In a similar way the particles produce viscoeleastic properties at the water-oil interface

(Tambe *et al.* 1994). For instance it was observed in the froth that bubbles were stable with the intermediate hydrophobicity of 26-44μm quartz (~65°) and higher hydrophobic particles tend to destabilise the froth (Johansson *et al.* 1992). The reason is that the particles with high hydrophobicity penetrate the gas-liquid interface to much higher degree and destabilise the liquid film by bridging effect.

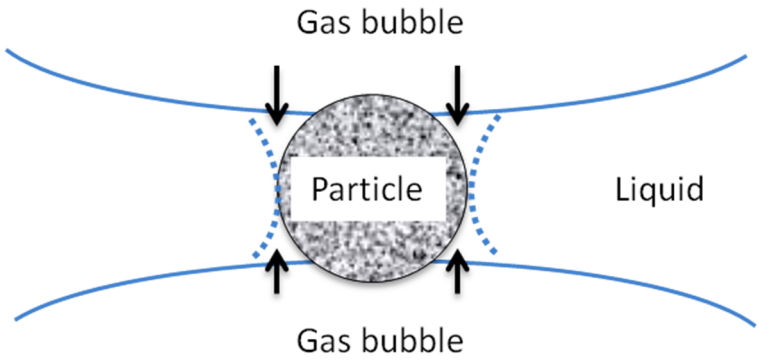


Figure 2.5 Particle bridging two bubbles – liquid around hydrophobic (lyophobic) particle is removed by the gas

Clearly, the particle's effect on the bubble coalescence rate is a very interesting subject where several aspects appear to be significant. However, the importance of particles wettability, quantified by the three phase contact angle, on the bubbles coalescence is unquestionable. Nonetheless, the energy of adsorption/desorption, particle size and the coverage of bubbles by particles are also important contributors.

Unfortunately, there is a lack of information on the particle's effect on the bubbles in organic liquids. Foaming/antifoaming studies often involve the aqueous solutions and emulsions involve two liquids, usually oil and water, therefore the mechanisms suggested for those systems is not necessarily relevant to the bubbles dispersed in paraffin oils. The presence of water in the gas phase (steam) can drastically change the particles behaviour on

the interface and to the author's knowledge the effect of particles on the steam bubbles size/coalescence in paraffin oils has yet to be investigated.

The aim of this chapter is to investigate the effect of bubble composition, type of particles (catalyst support), energy input on bubble size distribution in system similar to the Fisher Tropsch or methanol slurry synthesis. In those processes carried out at elevated temperature/pressure, water/steam is frequently present in the gas phase.

The bubbles were investigated using a video-camera system (Hu *et al.* 2007) in a turbulent, dead end stirred vessel. A paraffin oil similar to a Fischer Tropsch product liquid was used as a liquid phase in which a mixture of nitrogen and different concentrations of steam were dispersed. The effect of the gas composition in the gas-liquid and the effect of presence of different catalyst supports were tested at elevated temperature, pressure and at a range of energy dissipation rates.

Analysis of the effect of properties of gas, particles and slurry are discussed in terms of establishing all the possible factors/properties that might influence the bubble size. The detailed analysis is divided into two categories: a) how the properties of multiphase system affect the bubble size at elevated temperature and pressure and b) how different particles behaviour on the gas-liquid interface affects the bubble sizes.

## 2.2 Experimental methodology

In this chapter the experimental rigs and methodology employed for the bubble size measurements and the physical properties and interfacial tension between oil and selected fluids are described. Details of the steam addition to the reactor are also given as well as the analysis of the accuracy and repeatability of the bubble size measurements.

### 2.2.1 Experimental rig and materials

The effect of type of particles, gas type and holdup and energy dissipation rates on the bubble size in oil at elevated temperature and pressure was investigated in an agitated reactor (Figure 2.6). The experiments were carried out in a batch mode in a jacketed 3L vessel (diameter T=15cm, height H=T) fitted with 4 baffles (width T/10) and Rushton turbine (diameter T/2) placed at clearance of C=T/3. The images of the three-phase system were recorded through a glass window which slightly protruded into the vessel (Pacek *et al.* 1994). Video technique was used not only to measure the bubble size but also to determine the position of solid particles in the dispersion.

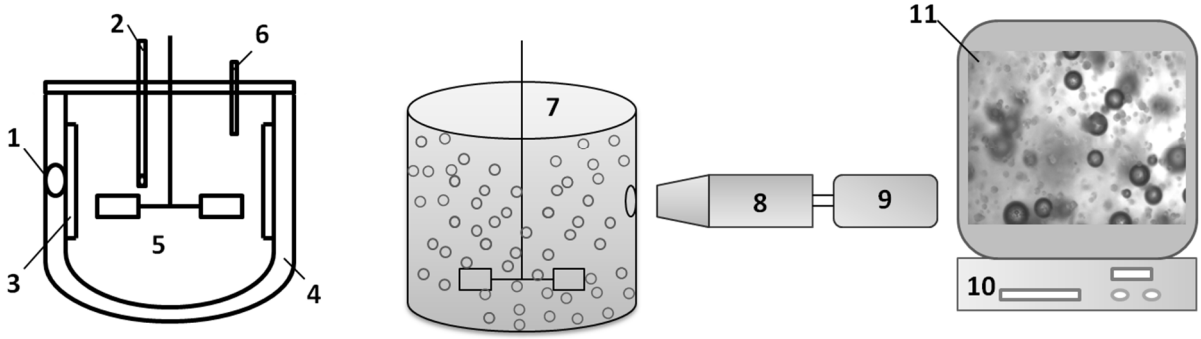


Figure 2.6 Experimental rig for the bubble size measurements

1 side window, 2 strobe lamp, 3 baffle, 4 oil jacket, 5 Rushton impeller, 6 thermocouple, 7 agitated vessel, 8 microscope, 9 camera, 10 computer, 11 photos from the inside of reactor

As the experiments aimed to mimic Fischer Tropsch synthesis, a long chain paraffin oil (provided by Johnson Matthey) was used as a liquid phase and nitrogen, air, $H_2O$ and mixtures of these as a gas phase. Alumina, silica, titania and zirconia catalyst supports ($d_{32}$ between 2-26μm) were added to the reactor. The temperature in the vessel (up to 210°C) was controlled by the oil bath connected to the reactor jacket. The pressure (up to 20bar) was controlled by the control valve installed between the $N_2$ cylinder and inlet to the reactor. The volume fraction of gas phase was controlled by addition of precise volume of oil into the vessel corrected by thermal expansion. The oil and particles were added to the reactor at room temperature and the reactor was sealed prior to the heating. Whilst addition of nitrogen/air to the vessel was straightforward, the methodology developed for the steam addition is discussed below.

#### 2.2.1.1 Steam addition

Initially, it was attempted to generate steam in the reactor by evaporating water drops. However it was very difficult to completely evaporate water and it was observed that large number of water droplets as well as steam bubbles was present even at 170°C at 1bar. The difference between the refractive index of steam and water enabled the resolution of water drops and bubbles (Figure 2.7). Also, when the stirrer was switched off, the droplets (water) tend to sink and bubbles (steam) to rise upwards.

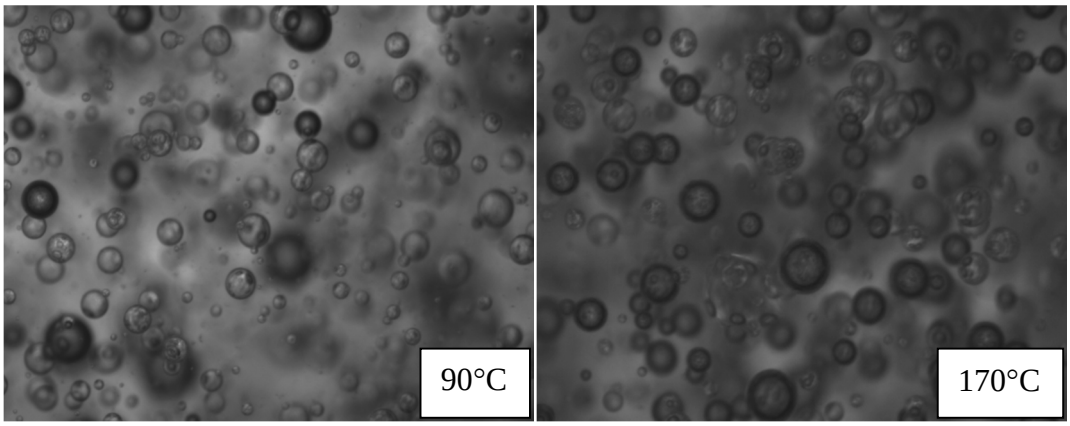


Figure 2.7 Bubbles (dark) and droplets (bright) of water in the paraffin oil at 1bar

Difficulties with the water drop evaporation in the hot oil were also observed in a glass beaker. The pendant drop submersed in oil was stable even at 130°C (Figure 2.8). Droplets of water detached from the needle tend to sink to the bottom of the beaker rather than evaporate.

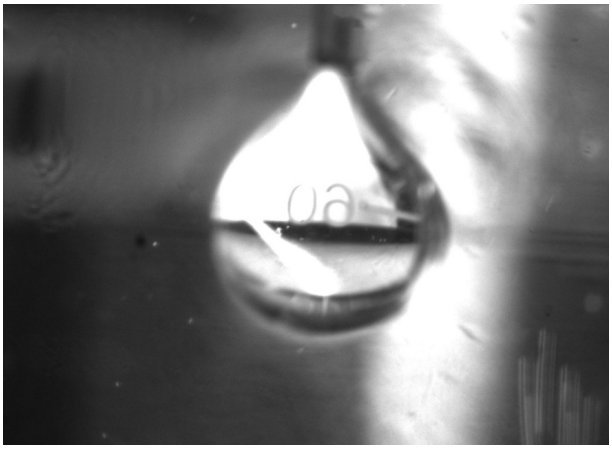

Figure 2.8 Stable water droplet in paraffin oil at 130°C

Therefore, to avoid problems with water evaporation it was decided to add steam produced outside the reactor. For this purpose, the external steam generator was specially designed and built. It consisted of a 5L stainless steel vessel equipped with three ports: inlet (distilled water) and an outlet (steam) at the top cover of the vessel and the outlet (water) at the bottom. The connections between the steam generating vessel and the reactor were made

from metal tubing and were air tight. To avoid condensation, the metal pipes were heavily insulated. The steam generator vessel was also heavily insulated as well as the pipes directing the steam to the reactor. Furthermore all metal lines were heated prior to steam introduction to the reactor by passing the steam through the metal pipes for a minimum of half an hour. The volume of water in the steam generator was controlled by measuring its mass. The experimental set up for the steam addition is shown in Figure 2.9.

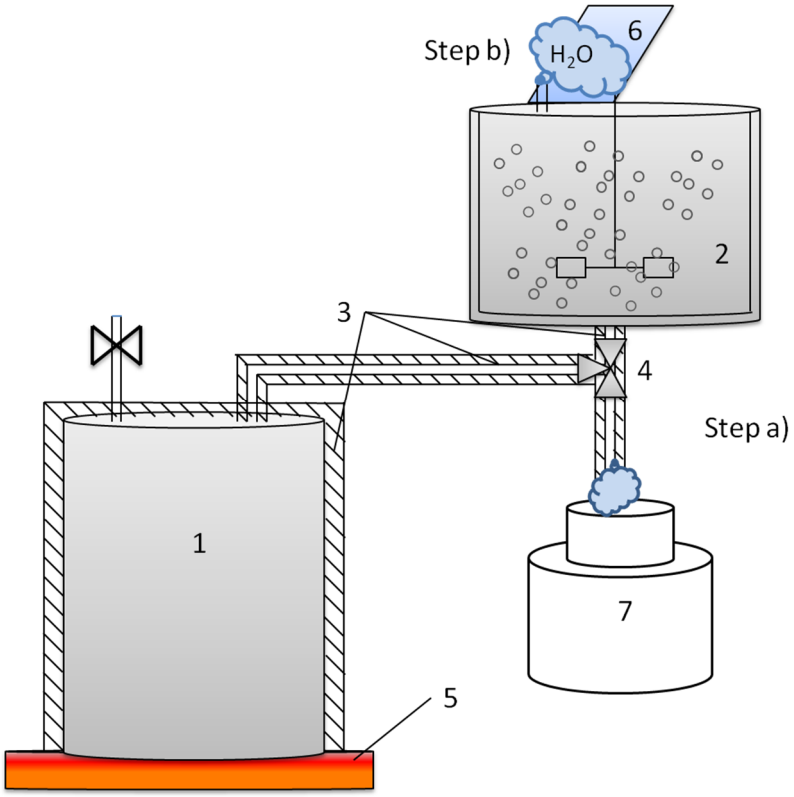


Figure 2.9 Steam addition to the particle-oil suspension in a stirred vessel
1 steam generator, 2 agitated vessel, 3 insulation, 4 three way valve, 5 hot plate, 6 mirror, 7 water container

The steam generator (1) was placed on the hot plate (5) below the reactor (2). The steam generator was completely filled with water in order to produce steam at a slightly higher pressure than atmospheric. Higher pressure ensured that during the steam addition to the reactor through the inlet placed at its bottom, oil did not flow into the steam generator.

The pipe at the outlet from the steam generator was equipped with a three way valve (4), enabling the steam to be directed into the reactor or to the vent. Prior to the steam addition, the reactor containing required amount of paraffin oil was heated to 150°C. Initially (step a in Figure 2.9), steam was passed through the cold metal pipes for approximately 0.5h into the container with cold water (7) using the three way valve. After such time, all metal connections were hot enough to avoid steam condensation. Subsequently, the steam was directed into the reactor with hot (150°C) oil through the inlet at the bottom. After a few minutes of steam addition, the reactor was completely sealed. It was noticed that if the volume of oil in the reactor was too large, the mixture of steam and oil tend to overflow and the maximum volume of oil enabling controlled addition was determined as 1.85L.

The presence of steam in the reactor was qualitatively assessed by:

- the steam condensation on the mirror placed near the outlet from the reactor
- the images taken before and during the steam addition (Figure 2.10).

The images clearly showed that no gas was present before steam addition (Figure 2.10a) and when the steam was directed into the vessel, the images clearly show steam bubbles (Figure 2.10b).

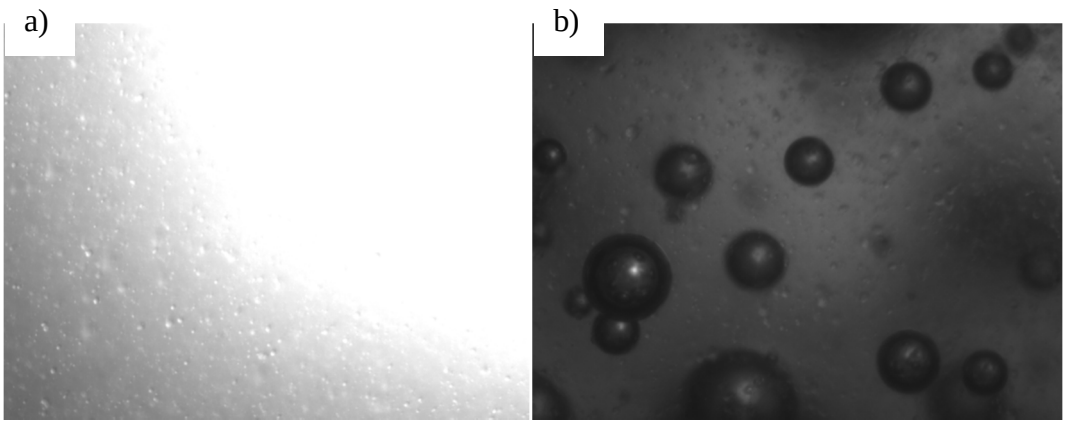


Figure 2.10 Images of oil in the reactor before steam addition (a) and after steam was introduced (b)

When the steam was introduced to the system, the gas phase contained 100% of steam at atmospheric pressure. The gas composition was controlled using the pressurized cylinder with nitrogen connected to the reactor. The gas composition was changed and steam concentration reduced when the nitrogen was introduced to the reactor. Pressurizing the reactor to 10 and 20bar with nitrogen caused further reduction of the steam concentration in the gas phase. At the pressure of 10bar the gas phase contained 10% of steam and 90% of nitrogen and at 20bar 95% of nitrogen and 5% of steam was present in the reactor. Use of such high pressure, i.e. 20bar at 210°C might lead to the steam condensation (saturation pressure $19.08 \cdot 10^5$Pa, (Hobler 1979)). Condensation of ~1L of steam would produce ~0.5g of water, therefore such amount is negligible when ~1L of gas volume fraction is present in the system at 20bar and 210°C. Also, the images recorded at 20bar and 210°C when the rotor was stopped, showed that the bubbles were present in the system (Figure 2.11).

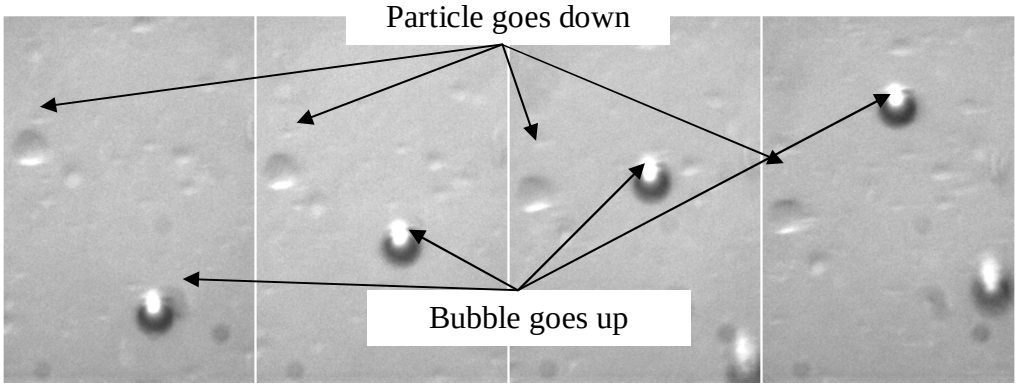


Figure 2.11 Alumina particles and steam bubbles at 20bar and 210°C with (no agitation)

#### 2.2.1.2 Gas/particles dispersion in oil

As surface aeration was employed, the additional experiments aimed at the determination of the impeller speed necessary for complete dispersion were carried out. The minimum impeller speed for the complete gas dispersion by surface aeration with the highest

gas concentration (35% v/v) was determined in a glass vessel of the same geometry as the reactor. Since it was not possible to heat oil to 210°C in this vessel decane, having similar properties at 20°C as paraffin oil at 210°C, was used as a liquid phase and air as a gas phase. It was determined that the minimum power input necessary for the reasonable number of bubbles production for the comparative study between different particles using 35% volume fraction of gas was 1 W/kg which corresponded to an impeller speed of 380rpm (Figure 2.12).

Figure 2.12 The gas dispersion at the lowest, 1W/kg energy dissipation rate

In a similar qualitative way, the required power input for the alumina suspension was assessed by placing the light source outside the bottom of the vessel. As more particles were suspended in the bulk liquid the intensity of transmitted light increased. It was observed that at a power input even lower than 1W/kg, the particles were uniformly suspended. This was compared with the calculated minimum impeller speed for the uniform solids suspension using Zwietering correlation (Nienow 1968; Kresta *et al.* 2004):

$$N_{sus} = S\upsilon^{0.1}\left(\frac{g(\rho_s - \rho_l)}{\rho_l}\right)^{0.45} X^{0.13} d_p^{0.2} D^{-0.85} \qquad (2.15)$$

The minimum impeller speed for the 1% v/v of the alumina particles was calculated to be 310rpm which corresponds to 0.53 W/kg. Therefore, the 1W/kg, as the lowest power input for the experiments with high gas concentration was employed to get both uniform gas dispersion and particles suspension. Though the power number decreases with the increasing gas filling cavities around the Rushton turbine and behind the blades, the power number taken was 5 for the similar geometry of the vessel and impeller (Bujalski *et al.* 1987). For surface aeration, the prediction of the power decrease in the gassed system is not yet possible since the amount of gas drawn back into the cavities is not known (Harnby *et al.* 1997).

#### 2.2.1.3 Investigated systems

The effect of $Al_2O_3$, $SiO_2$, $TiO_2$ and $ZrO_2$ (catalyst supports), operating conditions, gas type and holdup on the bubble sizes dispersed in paraffin oil was investigated. The experimental matrixes for the varying volume of gas phase are given in Table 2.4-5.

Table 2.4 Experimental matrix for low volume of gas phase (in total 33 experiments)

| Gas fraction, %v/v | Type of particles | Type of gas | T, °C | P, bar | ε, W/kg | Re, - |
|---|---|---|---|---|---|---|
| ~1<br>5 | No particles | Air<br>$N_2$ | 90<br>120<br>170<br>210 | 1<br>10 | 4<br>9.4<br>18.3 | 4,000-80,000 |
| 5 | 1% v/v $Al_2O_3$ | $N_2$ | 210 | 10 | 4<br>9.4<br>18.3 | 48,000-80,000 |
| 5 | 1% v/v $SiO_2$ | $N_2$ | 210 | 10 | 4<br>9.4<br>18.3 | 48,000-80,000 |
| 5 | 1% v/v $TiO_2$ | $N_2$ | 210 | 10 | 4<br>9.4<br>18.3 | 48,000-80,000 |
| 5 | 1% v/v $ZrO_2$ | $N_2$ | 210 | 10 | 4<br>9.4<br>18.3 | 48,000-80,000 |

Table 2.5 Experimental matrix for the 35% v/v of gas phase (in total 160 experiments)

| Type of particles | Type of gas | P, bar | T, °C | ε, W/kg | Re |
|---|---|---|---|---|---|
| No particles<br>1% v/v $Al_2O_3$<br>1% v/v $SiO_2$<br>1% v/v $TiO_2$<br>1% v/v $ZrO_2$ | Nitrogen | 1<br>10<br>20 | 170<br>210 | 1<br>4<br>9.4<br>18.3 | 16,000-80,000 |
| No particles<br>1% v/v $Al_2O_3$<br>1% v/v $SiO_2$<br>1% v/v $TiO_2$<br>1% v/v $ZrO_2$ | Steam | 1 | 170<br>210 | 1<br>4<br>9.4<br>18.3 | 16,000-80,000 |
| No particles<br>1% v/v $Al_2O_3$<br>1% v/v $SiO_2$<br>1% v/v $TiO_2$<br>1% v/v $ZrO_2$ | 10% steam - 90% $N_2$ | 10 | 210 | 1<br>4<br>9.4<br>18.3 | 16,000-80,000 |
| No particles<br>1% v/v $Al_2O_3$<br>1% v/v $SiO_2$<br>1% v/v $TiO_2$<br>1% v/v $ZrO_2$ | 5% steam - 90% $N_2$ | 20 | 210 | 1<br>4<br>9.4<br>18.3 | 16,000-80,000 |

### 2.2.2 Physical properties of materials used

The Fisher Tropsch synthesis liquid was simulated using mixture of highly refined hydrocarbons, heavy liquid paraffin (VARA Oil 600/240 PB, CAS No: 8042-47-5) supplied by Meade-King, Robinson & Co. Ltd. The physical properties of paraffin oil were measured at different temperatures and subsequently extrapolated to the temperatures used in experiments. Metal oxides, used as catalyst support, were supplied by Johnson Matthey® and their properties such as: size, size distribution, density, contact angle and surface energy are discussed in Chapter 3 (Contact angle) and Chapter 4 (Particles adsorption on interface).

Increasing the temperature of the paraffin oil leads to drastic increase of pressure in the closed reactor due to thermal expansion of oil. For instance, heating of the reactor completely filled with oil from 23°C to 37°C caused pressure increase to 30bar. In order to keep the required gas volume, the degree of oil expansion was experimentally determined and compared with the calculations based on the thermal expansion coefficient that relates the increase of the liquid volume as temperature increases. The thermal expansion coefficient of oil used in this work was taken for the mineral oil of similar composition (www.pantherlubes.com) as $0.00064°C^{-1}$. Experimentally, the degree of oil expansion was measured by collecting the liquid flowing from initially full reactor (3L) during heating. Measured volume of oil that left the reactor when heated from the room temperature to 80°C was 105ml and to 120°C was 178ml. The calculated thermal expansion of oil, based on initial 3L, gives 111ml of excessive oil when heated to 80°C oil and 192ml when heated to 120°C. The calculated volumes are slightly larger than the measured ones because of the flowing oil cooling when transported from the hot reactor to the measuring beaker. Nevertheless, the volume of expanding oil could be accurately predicted at elevated temperature from $V_{exp}$=2.0384*T[°C]-50.659 and it was possible to calculate the amount of paraffin oil that needed to be added to the reactor prior to heating.

The rheology of the paraffin oil and the suspensions of catalyst supports were measured with a Rheometer AR1000. The liquid was Newtonian (Figure 2.13) with a viscosity 100 times of water at room temperature.

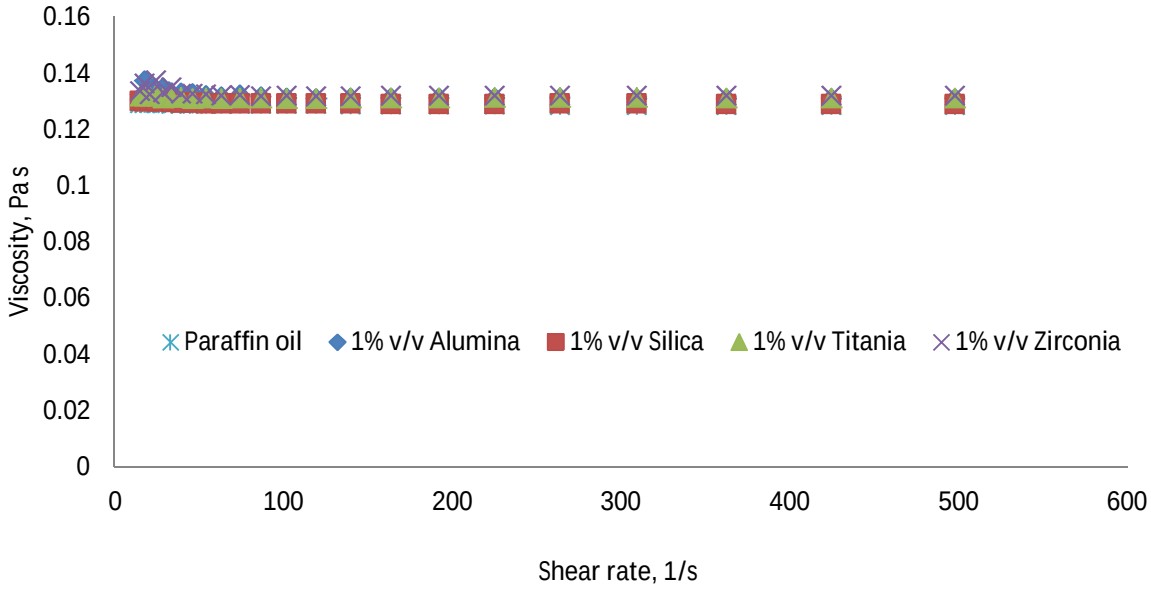


Figure 2.13 Viscosity of paraffin oil at 20°C

Measurements were also carried out at 25, 40, 60 and 80°C and the viscosity of the paraffin oil at those temperatures (Figure 2.14) was correlated with the Arrhenius equation:

$$\mu = 0.000414 \cdot e^{\frac{30827}{R \cdot T[K]}} \text{ cP}$$

There is good agreement between correlation and the experimental data, indicating that the extrapolation is accurate.

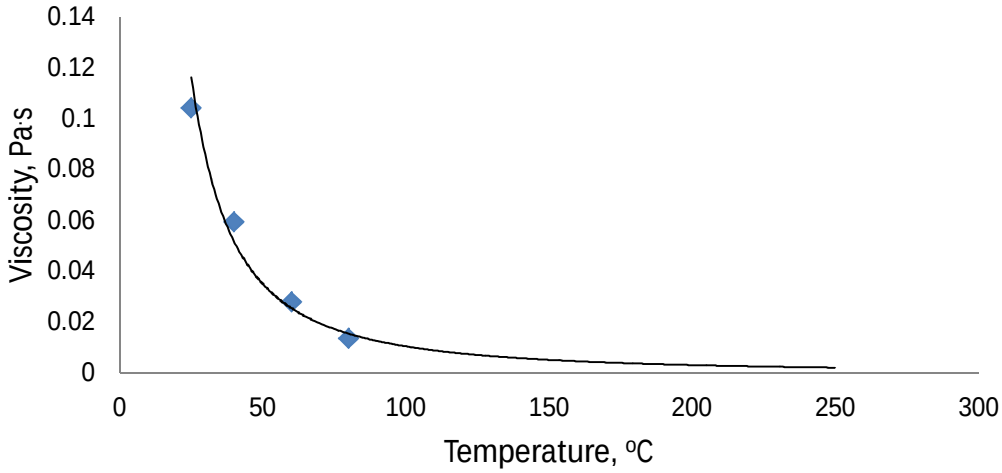


Figure 2.14 Viscosity of paraffin oil at elevated temperature

Density of paraffin oil was also measured as a function of temperature and the following correlation was obtained (Figure 2.15):

$$\rho = 0.6494 \cdot T[°C] + 885.91 \text{ kg/m}^3$$

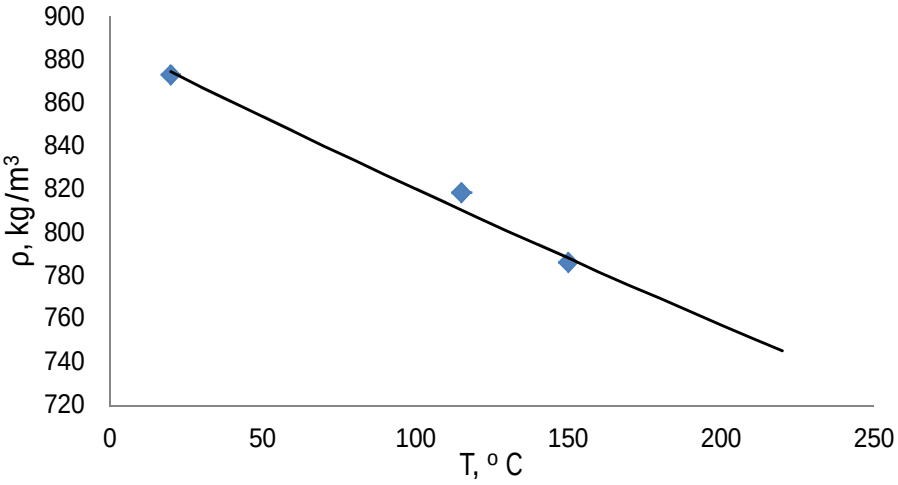


Figure 2.15 Density of paraffin oil at elevated temperature

Surface tension of the paraffin oil was measured using a Kruss Tensiometer. This equipment employs the Wilhelmy plate method (Miller 1985) and surface tension, σ, is calculated from the following equation:

$$\sigma = \frac{F}{L \cdot cos\theta}$$

where $F$ is the force applied to the plate, $L$ wetted length and θ contact angle between liquid and a plate. In this method, a force is recorded at the moment when rising liquid forms zero angle with the platinum plate. The Tensiometer was fitted with the water bath enabling temperature control of tested liquid. However the heating of oil that was opened to the atmosphere was very slow. Therefore the measurements at higher temperatures were carried out with the oil preheated to the required temperature. The linear extrapolation of the obtained surface tensions at 25, 60 and 86°C was found to follow the Macleod-Sugden linear correlation for randomly chosen molecular weight hydrocarbon (Balasubrahmanyam 2008).

The surface tension of paraffin oil was linearly dependent on the temperature (Figure 2.16):

$$\gamma = 0.04879 - 0.6 \cdot 10^{-4} \cdot T[K] \text{ N/m}$$

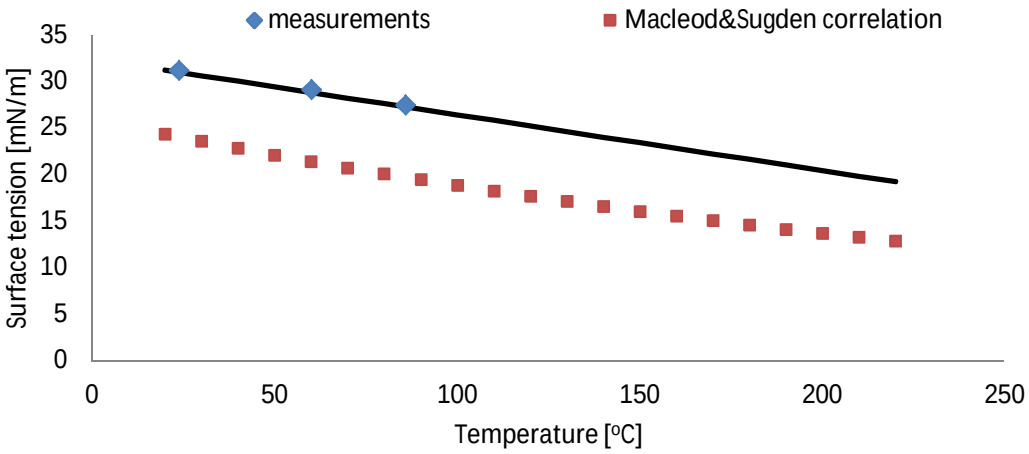


Figure 2.16 Surface tension of paraffin oil at elevated temperatures

It was also attempted to use the pendant drop method to measure the interfacial tension between paraffin oil and steam (Figure 2.16). In this case surface tension was calculated from (Miller 1985):

$$\gamma_i = \frac{V_{drop}\,\Delta\rho g}{2\pi r_{needle}}$$

In order to avoid steam condensation, the metal needle tip was wrapped with strongly hydrophobic PTFE tape. Measured interfacial tension (39.5±3mN/m) was almost 25% larger than the surface tension of oil with air (see Figure 2.16).

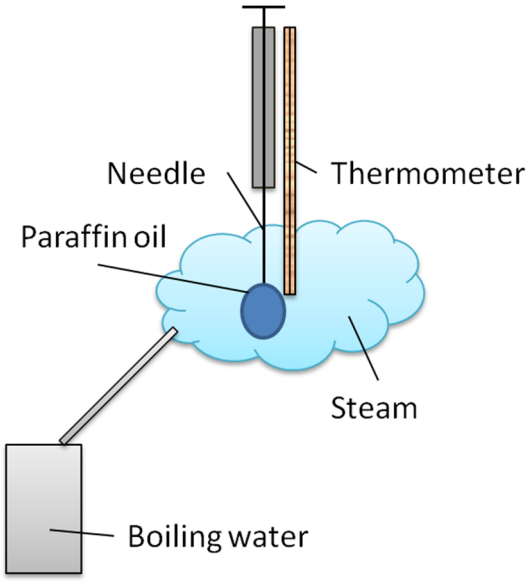


Figure 2.17 Interfacial tension measurements between paraffin oil and steam

The higher surface tension between paraffin oil and steam was also obtained by the measurements of oil-water interfacial tension (Figure 2.18) using the Wilhelmy plate method (KRUSS Tensiometer). The measurements were also performed at elevated temperature and similarly as for surface tension measurements, the liquids were heated up to the required temperatures prior to the measurements.

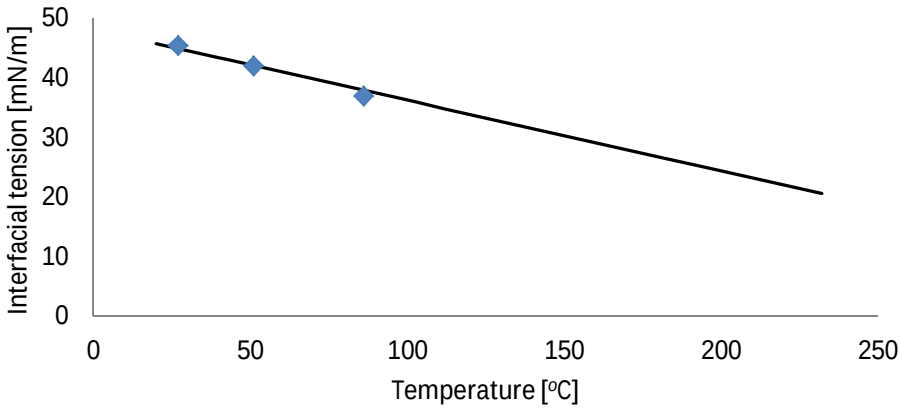


Figure 2.18 Interfacial tension of oil-water at elevated temperature

Properties of paraffin oil are summarized in Table 2.6 and the properties of investigated catalyst supports can be found in Chapter 2. Table 2.7 shows that increasing pressure from 1 bar up to 10 and 20 bar causes an increase of gas density of 10 and 20 times.

Table 2.6 Paraffin oil properties at experimental temperatures

| Paraffin oil | Density, $kg/m^3$ | Viscosity, cP | Surface tension, mN/m |
|---|---|---|---|
| 20°C | 873 | 128.43 | 31.21 |
| 90°C | 827 | 11.19 | 27.01 |
| 120°C | 807 | 5.13 | 25.21 |
| 170°C | 775 | 1.77 | 22.21 |
| 210°C | 749 | 0.88 | 19.81 |

Table 2.7 Density (kg/m3) of nitrogen and steam at elevated T and P

| | | 170°C | 210°C |
|---|---|---|---|
| 1bar | $N_2$ | 0.76 | 0.697 |
| | Steam | 0.49 | 0.45 |
| 10 bar | $N_2$ | | 6.97 |
| | 10% steam + 90% $N_2$ | | 6.72 |
| 20 bar | $N_2$ | | 13.9 |
| | 5% steam + 95% $N_2$ | | 13.7 |

### 2.2.3 Accuracy of the bubble size measurements

Images taken by the microscope-video system were analyzed using the software "BubblePro" (Figure 2.19) developed at University of Birmingham since the automatic bubble size/shape detection could not be used because of the bubbles overlapping and often poor quality of images. The images were uploaded to the software and the bubbles were manually marked by placing the cursor on the three points of the bubble perimeter.

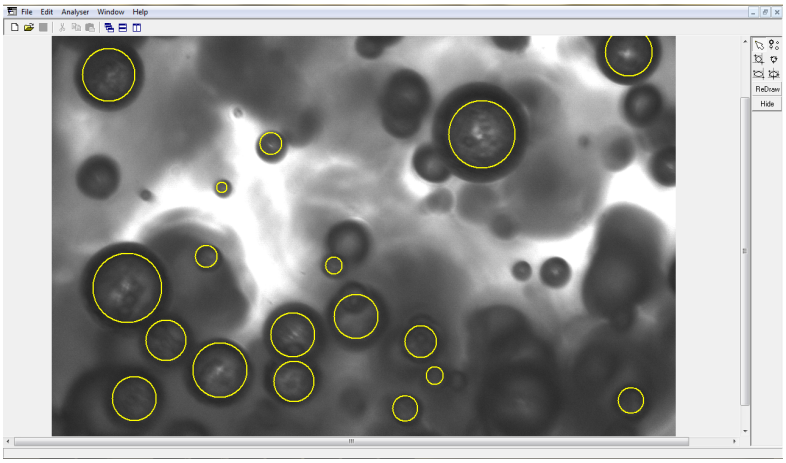

Figure 2.19 Bubble size measurements with BubblePro

Though the imaging method for the bubble size and bubble size distribution measurement is a very accurate method, several errors are inherently incorporated. The representative number of analysed bubbles might be one of the sources of errors which might also arise from counting bubbles out of focus (blurred) and inaccuracy of placing the cursor on bubble perimeter. Each of these sources of errors is further considered in details and the total error for the bubble size measurement is calculated.

In order to establish the representative sample population, the system with the highest gas concentration (35% v/v) was analysed since the widest bubble size distribution was expected and the images at different energy dissipation rates (1; 4; 9.4 and 18.3 W/kg) were analysed. Up to 500 bubbles were measured for chosen system (35% v/v $N_2$ in oil at 170°C and 1bar) and $d_{32}$ and bubble size distribution was compared for approximately 100, 150, 200, 250, 300, 350, 400, 450, 500 bubbles (Figure 2.20 and Table 2.8).

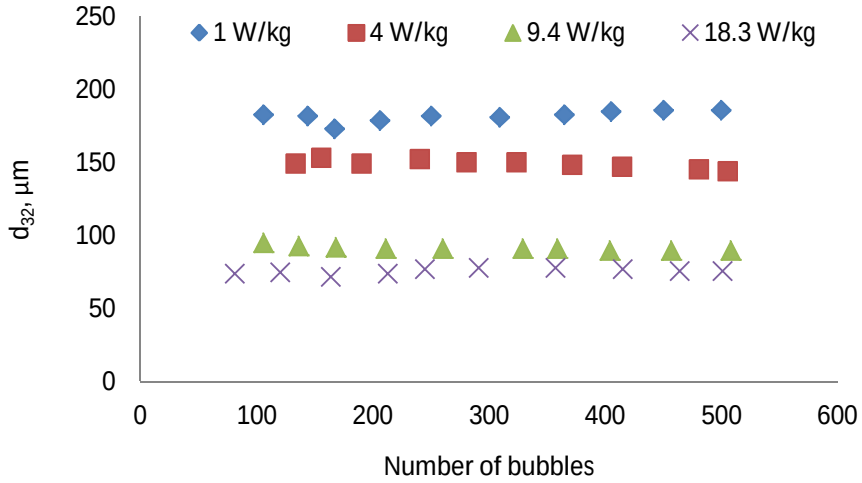


Figure 2.20 Sauter mean diameter calculated from different number of bubbles ($N_2$/oil at 170°C, 1bar)

Table 2.8 Average bubble size and standard deviations from 500 bubbles

| ε, W/kg | Average $d_{32}$, µm | StDev, µm |
|---|---|---|
| 1 | 182 | 3.8 |
| 4 | 149 | 2.8 |
| 9.4 | 92 | 1.5 |
| 18.3 | 76 | 1.9 |

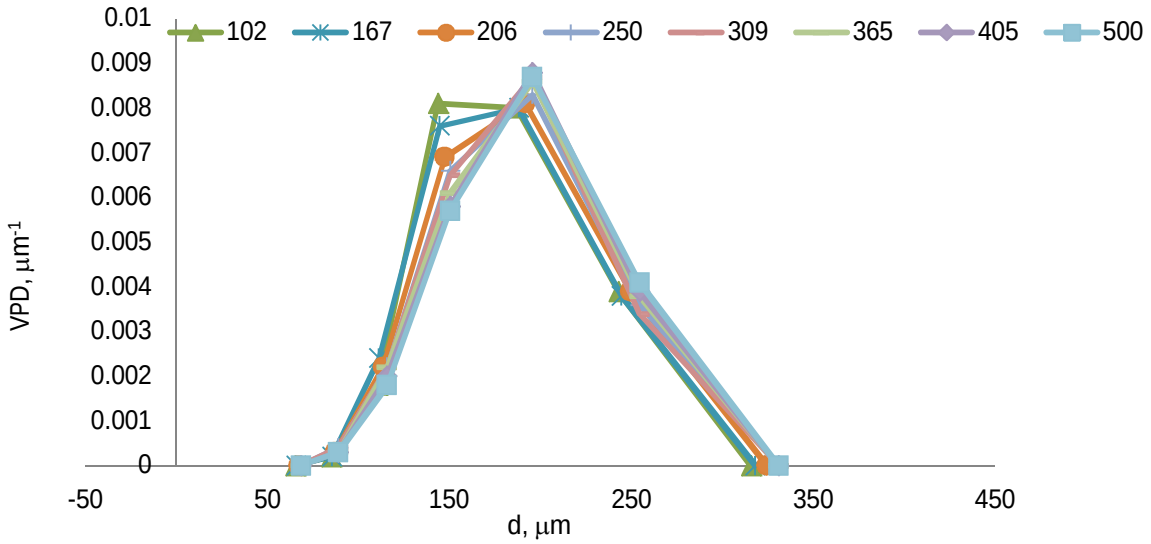


Figure 2.21 Bubble size distribution as a function of a number of bubbles (N in oil at 170°C, 1bar, 1 W/kg)

It appears that the representative sample in investigated system was obtained with 200 bubbles (Figure 2.20) indicating a narrow size range of nitrogen bubbles in paraffin oil (Figure 2.21). Therefore, for the analysis it was decided to account for 200-300 bubbles depending on the bubble size distribution, i.e. for the wider distribution, more bubbles were accounted.

At higher energy dissipation rates, the lighting sometime becomes insufficient with the result that bubbles tended to be blurred and it became difficult to distinguish the ones out of focus. Therefore it was attempted to assess the error due to the counted bubbles out of focus. For this purpose, a pencil and ruler as a small and large object were measured by putting them out of focus with the same microscope magnification as in experiments. The object was moved back and forth from the position where sharp edges were visible and images were recorded. It was noticed that the object was completely out of focus for the shift of approx. 2-3mm from the sharp position, and was not visible after that range. This suggests that the bubbles that are far away (or too close) from the focus position are not visible on the pictures.

The error associated with the blurred picture of the bubble where the sharp edges are difficult to distinguish decreases with the decreasing bubble size (Table 2.9). The bubble size found in the experiments were below 200um therefore the percentage error (standard deviation divided by the average size) is assumed to be 2% maximum so to unify the absolute value.

Table 2.9 Error associated with the bubbles out of focus and human eye and/or software resolution

| | Out of focus (Sharp/blurred) | | Eye resolution | | |
|---|---|---|---|---|---|
| | Pencil, D(μm) | Ruler, D(μm) | Big bubble | Medium bubble | Small bubble |
| | 773 | 212 | 236 | 157 | 82 |
| | 726 | 207 | 233 | 150 | 81 |
| | 662 | 198 | 235 | 153 | 79 |
| | 650 | 203 | 236 | 153 | 80 |
| | 674 | 199 | 234 | 155 | 78 |
| | 670 | 205 | 232 | 156 | 76 |
| Avg, μm | 693 | 204 | 234 | 154 | 79 |
| StDev | 47.5 | 5.3 | 1.6 | 2.7 | 2.1 |
| StDev/Avg, % | 6.8% | 2.6% | 0.7% | 1.7% | 2.7% |

The resolution of the operator eye that marks the bubbles was assessed based on the marking of the same bubble 7 times (Table 2.9). Three different sized, sharp bubbles were chosen in order to derive the associated error of different sizes bubbles created by different degree of energy dissipation rate. The limited resolution of the human eye and software pixels create the increasing error with decreasing bubble size (Table 2.9).

The overall experimental error associated with different sources can be therefore summarized for different ranges of the bubble size as shown in Table 2.10. The total error in different bubble size ranges does not exceed 10% indicating very good accuracy of the measurements. The highest power input that produces the smallest bubbles carries also the highest error though it remains within 10%. It can be concluded, that in systems containing different particles the differences in measured bubble sizes are significant when they exceed 10% of the average size.

Table 2.10 Total experimental error at different power input: StDev/Avg, %

| Source of error | 1 W/kg | 4 W/kg | 9.4 W/kg | 18.3 W/kg |
|---|---|---|---|---|
| Representative sample | 2.0% | 2.1% | 2.8% | 4.2% |
| Bubble out of focus | 2.6% | 2.0% | 1.5% | 1.0% |
| Cursor resolution | 0.7% | 1.7% | 2.7% | 2.7% |
| Total | 5.30% | 5.80% | 7.00% | 7.90% |

## 2.3 Bubbles in model Fisher Tropsch synthesis

Initially, the effect of particles on the bubble size was investigated for low gas phase volume fraction (5% v/v) as the experiments aimed to relate the bubble size to the hydrodynamic and physical properties using semi-theoretical correlations. However, it was impossible to add steam to such a large oil volume, therefore the experiments were conducted with significantly larger gas phase volume fractions (35% v/v). Additionally, elevated temperature caused oil thermal expansion which subsequently led to increased gas pressure. Such highly concentrated dispersion however mimics the industrial multiphase reactions, such as Fisher Tropsch synthesis (Krishna *et al.* 1997; Maretto *et al.* 1999). Also, as the bubbles coalescence is significantly higher in a concentrated dispersion, the effect of the particles on the coalescence rate is expected to be more pronounced with 35% v/v of gas phase.

### 2.3.1 Bubbles in diluted (1-5% v/v) dispersions

#### 2.3.1.1 Effect of type of gas on the bubble size at elevated temperature

The effect of the type of gas on the bubble size and bubble size distributions in paraffin oil was investigated in diluted system at elevated temperatures of 90°C, 120°C and

170°C at 1bar in closed reactor. The gas phase consisted of either air or nitrogen and the gas volume fraction in the reactor was decreased from approximately 5% v/v at 90°C to ~1% v/v/ at 170°C due to the thermal expansion of oil.

Typical images of air and $N_2$ bubbles at 90°C and 170°C at low energy dissipation rate (4W/kg) are shown on Figure 2.22. As expected, the mean bubble sizes and bubble size distributions are very similar for air and nitrogen. In both cases the bubble size is significantly reduced at elevated temperature due to the decrease in viscosity (e.g. *Re*: 4,100 $\Rightarrow$ 25,000) and surface tension. The bubbles were found to be spherical at lower mixing intensity whereas the bubbles produced at the highest energy dissipation rates suggest coalescence occurrence since larger and non-spherical bubbles are found (compare Figure 2.22 and Figure 2.23). Though the numbers of such large bubbles were found to be rather scarce, nonetheless their presence at high mixing intensity could be attributed to the higher collision rate and higher efficiency of colliding bubbles since. On the other hand, large eddies formed around baffles and vortices (Figure 2.24) facilitate gas suspension and higher mixing intensity that might cause engulfment of larger volumes of gas. Entrapment of such large gas bubble when the highest energy dissipation rate is applied results in subsequent disruption in the impeller region, where the velocity fluctuations are the highest.

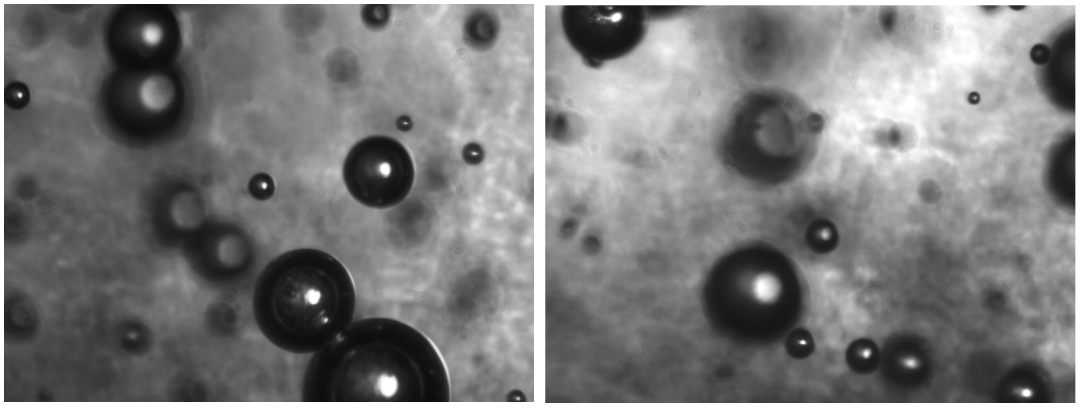

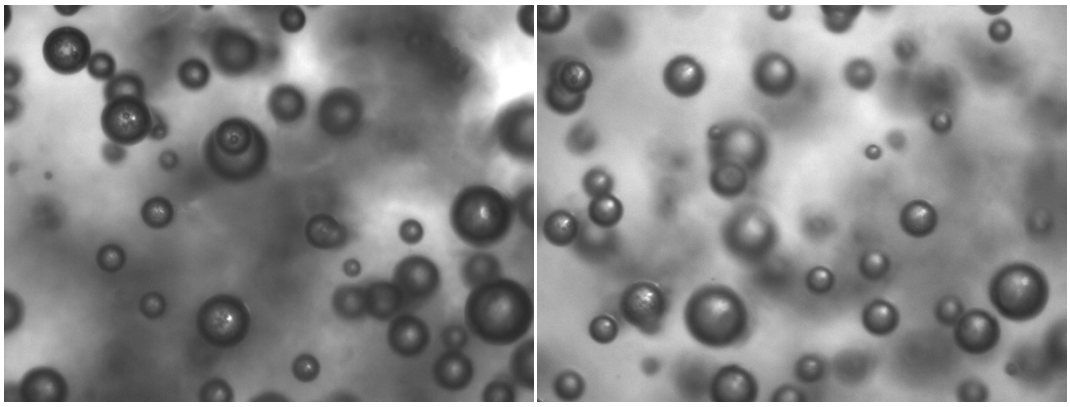

Figure 2.22 Nitrogen (left column) and air (right column) bubbles in oil at 90°C and 170°C respectively at 4W/kg (1.85 x 1.4 mm)

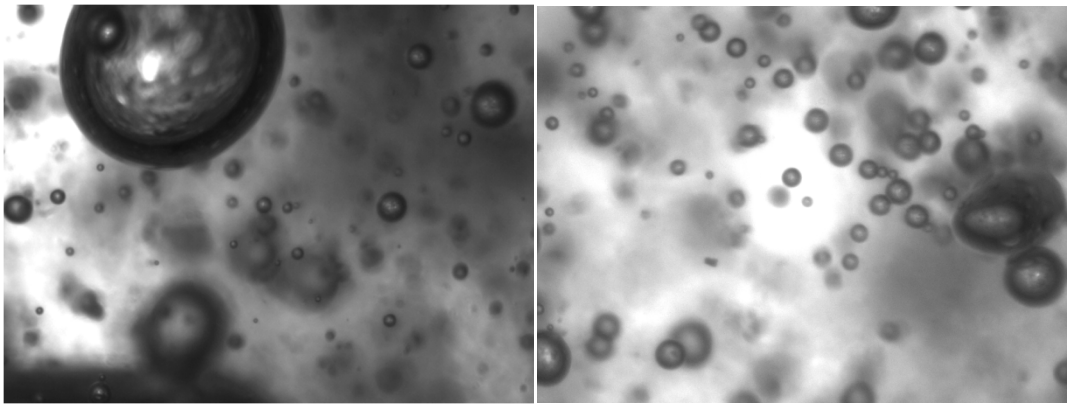

Figure 2.23 $N_2$ bubbles at 90°C (left) and 170°C (right) at the highest energy dissipation rates (18.3W/kg)

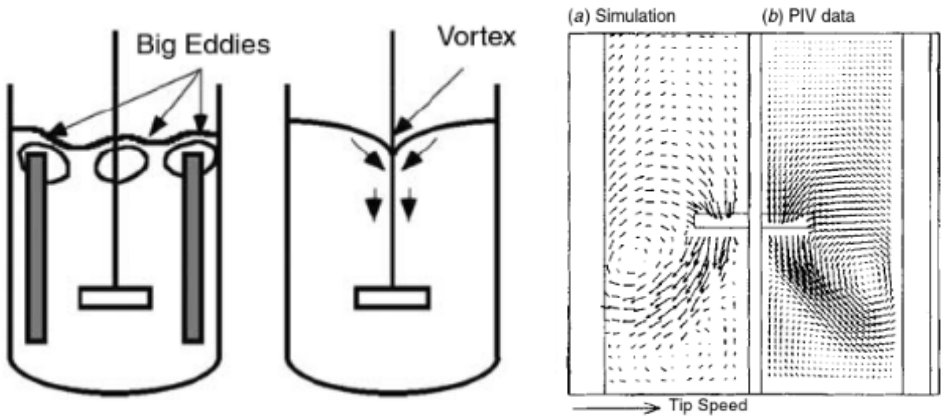

Figure 2.24 Surface aeration and velocity profiles in Rushton agitated reactor (Paul *et al.* 2004)

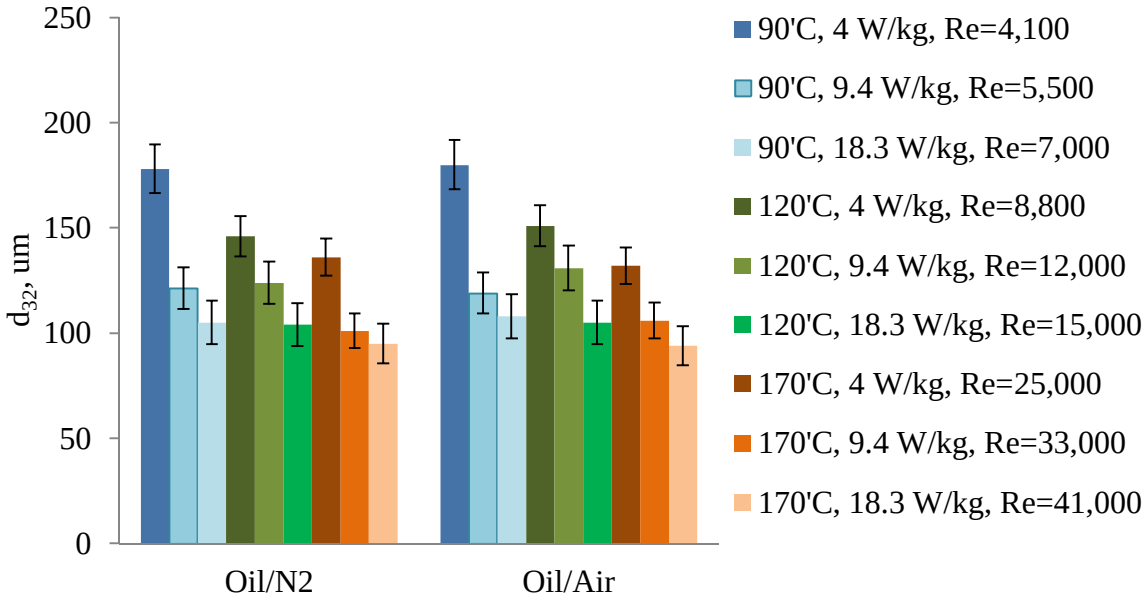


Figure 2.25 Effect of the gas type on the mean bubble size at elevated temperatures and turbulence intensity in diluted system (1%) at 1bar

The air and $N_2$ mean bubble sizes at different energy dissipation rates are shown in Figure 2.25. Clearly, there is an insignificant difference between air and nitrogen bubble sizes. It is not surprising since the air is composed of 78% of nitrogen and clearly the presence of oxygen (21%) doesn't affect the bubble size. Moreover, these results additionally validate the reproducibility of the video method in multiphase systems.

There is a clear effect of temperature on the bubble size (Figure 2.25) regardless of the type of gas used. The increase of temperature affects the bubble size stronger at the lowest energy dissipation rate with a reduction of bubble size of 31% compared to the highest energy dissipation rates (11% reduction). At 90°C and 120°C the flow is transitional (4,000 < *Re* < 15,000), whereas at 170°C the flow is turbulent (*Re* > 25,000). However, the comparable bubble size at all temperatures at the highest rotor speed indicates that even though the *Re*

numbers are significantly lower at $Re_{90°C} << Re_{120°C} << Re_{170°C}$ the disruptive forces are similar indicating turbulent flow even at low *Re* (7,000). The difference in the bubble size at different temperatures is directly related to the changes of the physicochemical properties of the liquid. The disruptive forces are enlarged with a decrease of liquid density and viscosity with temperature whereas the restoring forces (surface tension) also decreases.

Number probability density functions show that at lower temperatures (in the transitional flow regime) the bubble size distribution changes insignificantly with energy dissipation (compare distributions in a) and b) in Figure 2.27). As the temperature increases, the flow becomes turbulent and the larger fraction of small bubbles is produced due to breakage as can be clearly seen on Figure 2.26. Evidently, the probability density functions clearly show that increasing the agitation speed resulted in a reduction of bubble diameter with a narrower size distribution. It is evident in graphs in Figure 2.27 that in all cases, the distribution moves toward the smaller bubble sizes with increasing energy dissipation rate. The reason obviously goes back to the breakage of bigger bubbles due to the high ε. Another factor important in industrial applications is the width of the bubble size distributions or in other words the range of bubbles sizes. Observation proves that the majority of bubbles are in a range between 50-250μm, however, some bubbles were as small as 15μm and the maximum bubble size was close to 480μm.

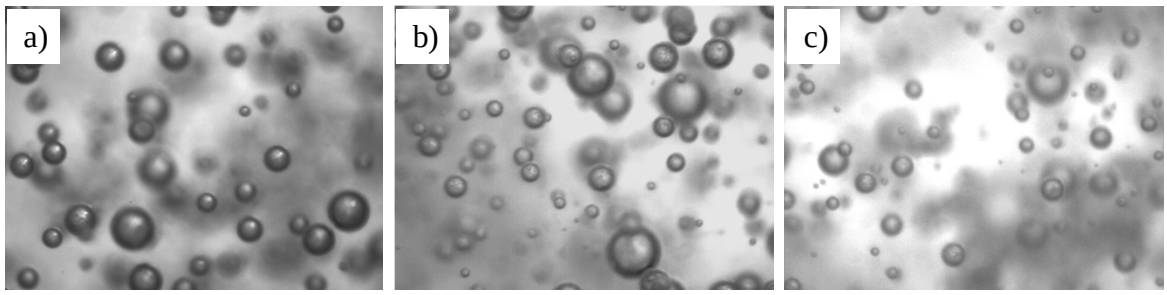


Figure 2.26 1% v/v air dispersed in oil at 170°C with varying mean energy dissipation rates: a) 4 W/kg, b) 9.4 W/kg and c) 18.3 W/kg (1.85 x 1.4 mm)

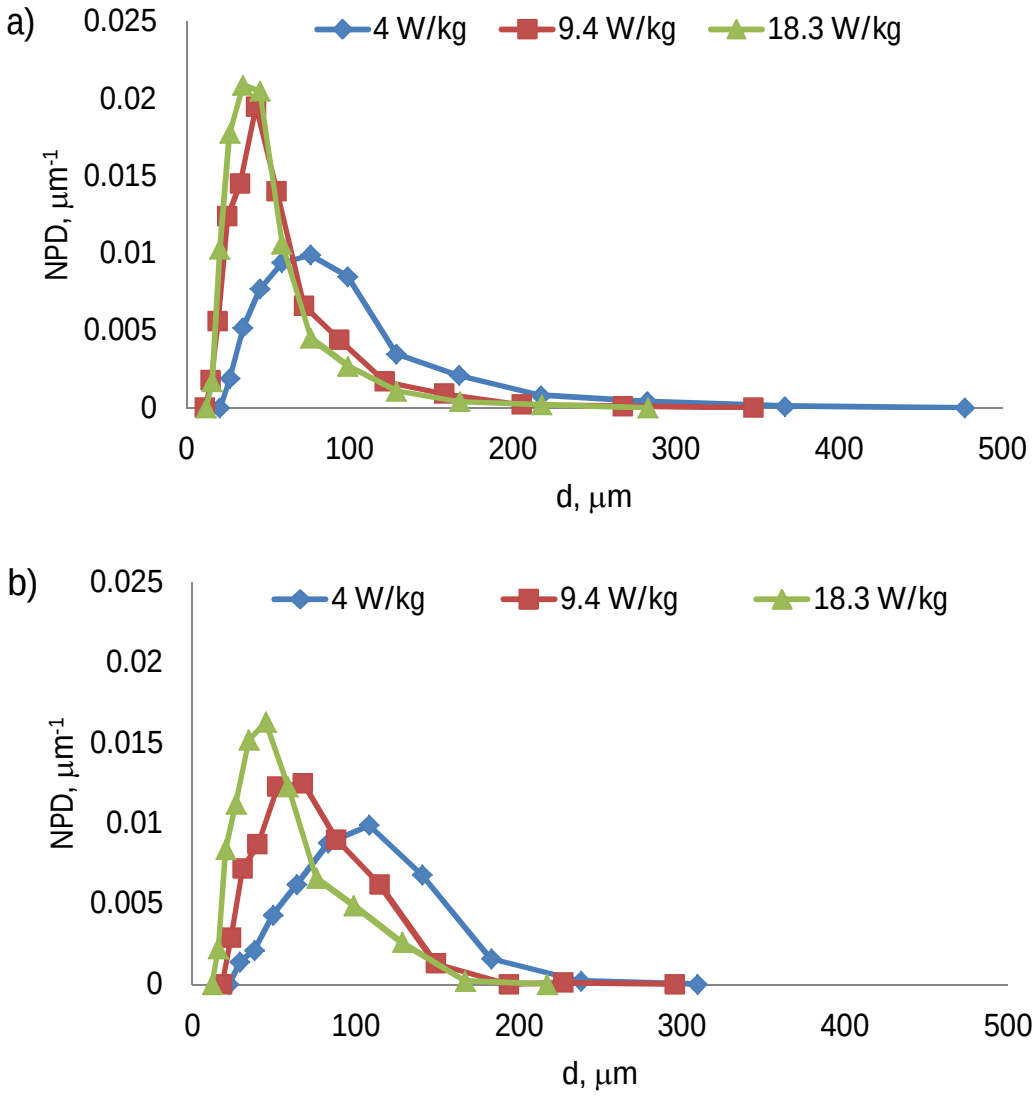


Figure 2.27 Number probability density functions 1% v/v nitrogen bubbles with varying mixing intensity at a) 90°C and b) 170°C

#### 2.3.1.1.1 Correlating the data

The effect of the hydrodynamics conditions and surface tension on the bubble size is traditionally correlated using the dimensionless *We* number, i.e. the ratio of breaking to stabilising forces, developed for liquid/liquid dispersions (Kolmogorov 1949; Hinze 1955; Nienow 1997). Air and nitrogen bubble size (Sauter mean diameters) correlations with the *We*

number *($d_{32}$/D vs We)* at elevated temperature are shown in Figure 2.28 where the following correlations were found:

1% of air at 90°C: $\frac{d_{32}}{D} = 0.0896 \cdot We^{-0.51}$ $R^2 = 0.9283$,

1% of air at 120°C: $\frac{d_{32}}{D} = 0.0256 \cdot We^{-0.35}$ $R^2 = 0.9613$,

1% of air at 170°C: $\frac{d_{32}}{D} = 0.0201 \cdot We^{-0.335}$ $R^2 = 0.9911$,

1% of $N_2$ at 90°C: $\frac{d_{32}}{D} = 0.0986 \cdot We^{-0.524}$, $R^2 = 0.9674$,

1% of $N_2$ at 120°C: $\frac{d_{32}}{D} = 0.0211 \cdot We^{-0.329}$, $R^2 = 0.9853$,

1% of $N_2$ at 170°C: $\frac{d_{32}}{D} = 0.0242 \cdot We^{-0.359}$, $R^2 = 0.9179$,

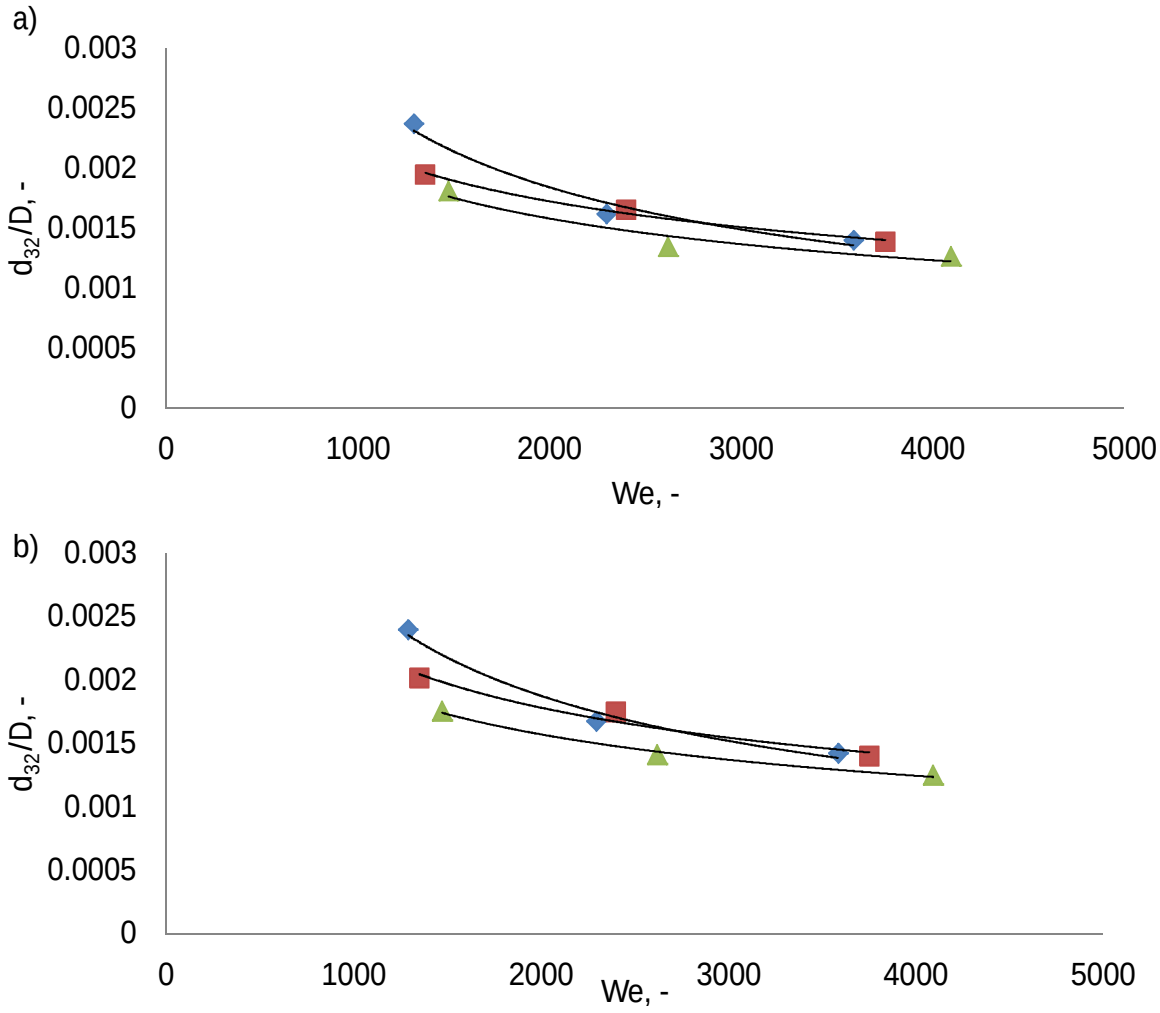


Figure 2.28 Correlation of a) nitrogen and b) air mean bubble sizes with We number (90°C-blue, 120°C-red and 170°C-green)

Clearly, the exponent of *We* number are different from the theoretical values (*-0.6)* expected for breakage dominated dispersion in turbulent flow. The exponents were found to be substantially higher, -0.335 with air and -0.359 with nitrogen. These values indicate that breakage is not the only mechanism responsible for the equilibrium bubble size. This might indicate that even at such low gas phase volume fraction, that coalescence occurs. Similar results were reported for the bubble size correlations with the *We* number (*Re>32,000*) where the 1% v/v air/alcohol systems gave the -0.38 exponents (Hu *et al.* 2005). With the slightly higher gas phase fraction (5% v/v), where the coalescence was suppressed using low

concentration proteins in aqueous system, the bubble size correlation with the We number gave the exponent *-0.4*, which is again larger than the theoretical one (Hu *et al.* 2003). The rate of bubble coalescence is higher than for liquid droplets (Chan *et al.* 2011) therefore the semi-empirical correlations developed for liquid/liquid dispersions that assume no coalescence in diluted dispersions must be invalid for the bubbles, given the weight of data across a range of systems. The driving force for thin liquid film drainage between bubbles is much stronger than between droplets since the density difference in gas-liquid dispersion is much higher than in liquid/liquid dispersion. It might also be expected that high internal circulation within the non-viscous bubble increases the rate of thin film drainage.

The transitional flow (at 90°C) produced the bubble size that when correlated with the *We* number gave exponents that are more similar to the theoretically predicted, i.e. -0.51 for air and -0.524 for nitrogen bubbles. Though there is not much information on the bubble/droplet size in transitional flows (Zhou *et al.* 1998), Hu *et al.* (2005) found even higher exponents than the theoretically predicted, i.e. -0.70 for the 1% of air in non-aqueous solutions in the transitional flow. It appears that the extent of disruptive forces are comparable to those in turbulent flow even for the 4,100 < Re < 7,000.

Table 2.11 Flow regimes of the 1% gas in oil in different operating conditions

| ε, W/kg | T, °C | Re, - | $\eta_K$, um | Flow |
|---|---|---|---|---|
| 4 | 90 | 4160 | 158 | Transitional |
| 9.4 | 90 | 5540 | 128 | |
| 18.3 | 90 | 6930 | 108 | |
| 4 | 120 | 8850 | 90 | |
| 9.4 | 120 | 11800 | 72 | |
| 18.3 | 120 | 14750 | 61 | |
| 4 | 170 | 24660 | 42 | Turbulent |
| 9.4 | 170 | 32880 | 34 | |
| 18.3 | 170 | 41100 | 28 | |

Mean energy dissipation rate used for Kolmogoroff length scale calculation $\varepsilon = PN^3D^5/V$

The correlations based on *We* assume that the breakage results from the turbulence fluctuations of inertial range eddies, comparable to the bubble size where the viscous effects are negligible, i.e. $\eta_K << d_{max} << D_{impeller}$. However, in the transitional flow, at 90°C, the mean bubble size is of the order of the Kolmogoroff scale (compare Table 2.11 and Figure 2.25). Also, at 120°C the mean bubble sizes are only 68-72% larger than the Kolmogoroff length scale. Therefore, to correlate the bubbles that are as small as $\eta_K$, where the stress on the bubble arises from the inertial sub-range eddies, the following equation was proposed (Shinnar 1961; Calabrese *et al.* 2000; Hu *et al.* 2006):

$$\frac{d_{32}}{D} = C_3 \left( \mathrm{Re} \cdot We \right)^{-1/3} \tag{2.16}$$

The correlation for the 1% v/v air bubble size in transitional flow at 90°C where the mean bubble size is similar to the Kolmogoroff length scale is:

$$\frac{d_{32}}{D} = 0.4509 (Re \cdot We)^{-0.34}$$

and for nitrogen:

$$\frac{d_{32}}{D} = 0.5176 (Re \cdot We)^{-0.349}$$

Clearly, the exponents are comparable to those predicted by the theoretical consideration of the bubble of the order of $\eta_K$. Correlated bubble sizes that were produced at 120°C and 170°C gave the exponents -0.234 and -0.223 respectively.

The mean bubble size of air and nitrogen were also correlated with the mean energy dissipation rate in turbulent flow for power input from 4-18 W/kg.

For air:

90C: $d_{32} = 0.0003 \cdot \varepsilon^{-0.34}$ $R^2 = 0.9283$,

120C: $d_{32} = 0.0002 \cdot \varepsilon^{-0.234}$ $R^2 = 0.9613$,

170C: $d_{32} = 0.0002 \cdot \varepsilon^{-0.223}$ $R^2 = 0.9911$,

For nitrogen:

90C:, $d_{32} = 0.0003 \cdot \varepsilon^{-0.349}$ $R^2 = 0.9674$,

120C:, $d_{32} = 0.0002 \cdot \varepsilon^{-0.219}$ $R^2 = 0.9853$,

170C:, $d_{32} = 0.0002 \cdot \varepsilon^{-0.239}$ $R^2 = 0.9179$,

Here again, as in the We correlations, the exponents are larger (closer to theoretical -*0.4*) in transitional flow at 90°C, whereas they increase in turbulent region. A similar discrepancy was observed by Hu *et al.* (2006), where the bubbles in water/alcohol solutions correlated with energy to *-0.25*.

#### 2.3.1.2 Effect of the particles on the 5% $N_2$ bubble size at high temperature and pressure

##### 2.3.1.2.1 Repeatability of the bubble size (distribution) measurements in identical system

Initially, the repeatability of the measurements of $d_{32}$ in identical three-phase systems was analysed. Since the great majority of experiments were carried out at elevated temperature and pressure, the 1% v/v of titania in (5% v/v) nitrogen - paraffin oil dispersion at 210°C and 10bar was tested. Such conditions produced turbulent flow (Re = 48,000). In order to assess the degree of error for the different range of bubble sizes, different energy

dissipation rates were applied, i.e. low and high energy dissipation rates produced large and small bubbles respectively.

The mean bubble sizes measured in three identical experiments are showed in Table 2.12. The bubble sizes are almost identical for the same energy dissipation rates. The accuracy of the measurements of Sauter mean diameters ($d_{32}$) proves to be very high therefore it was not repeated for other systems. The bubble volume probability density functions (Figure 2.29) of three identical experiments at different energy dissipation rates are fairly similar which additionally confirms the accuracy of the technique used.

Table 2.12 $d_{32}$ and standard deviations of the 5% $N_2$, 1% Titania, 210°C, 10bar system measured in 3 different experiments

| | 4 W/kg | 9.4 W/kg | 18.3 W/kg |
|---|---|---|---|
| Exp. I | 120μm | 99μm | 90μm |
| Exp. II | 119μm | 98μm | 92μm |
| Exp. III | 119μm | 100μm | 94μm |
| Average $d_{32}$ | 119μm | 99μm | 92μm |
| StDev | 0.8μm | 1.2μm | 1.79μm |

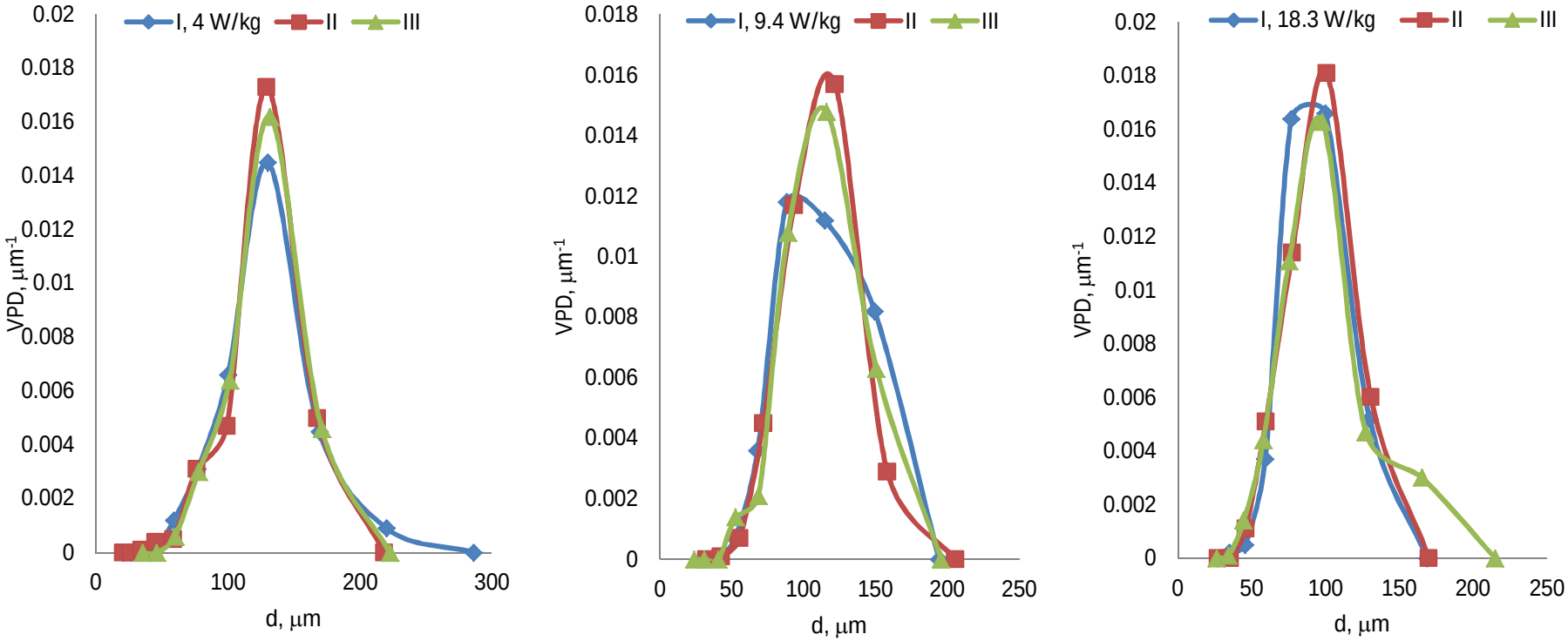


Figure 2.29 Bubble size distribution of the 5% $N_2$, 1% Titania, 210°C, 10bar system reproduced and repeated 3 times for different energy dissipation rates

#### 2.3.1.2.2 Effect of the type of particles on the bubble size in 5% nitrogen dispersion

The effect of different particles on the bubble size was investigated at the 5% v/v gas phase fraction. As discussed in the introduction, the particles can increase or reduce the bubble size through mostly affecting the bubbles coalescence. Studying more concentrated dispersions is rarely investigated and may reveal the coalescence more clearly. Also, higher solids loadings and larger gas holdups are employed in practical applications, e.g. Fischer Tropsch synthesis employ gas holdups in SBCR in the range of 0.3 – 0.4.

The effect of the particles on the bubble sizes at high temperature (210°C) and pressure (10bar) was investigated with 5% v/v of nitrogen in oil and typical images with and without particle are shown in Figure 2.30. At the steady state, the bubbles produced with 4 W/kg energy dissipation rate were spherical but at the highest energy dissipation rates (18W/kg) the non-spherical bubbles were also observed (Figure 2.31). This observation might indicate fast coalescence at 1% v/v gas volume fractions.

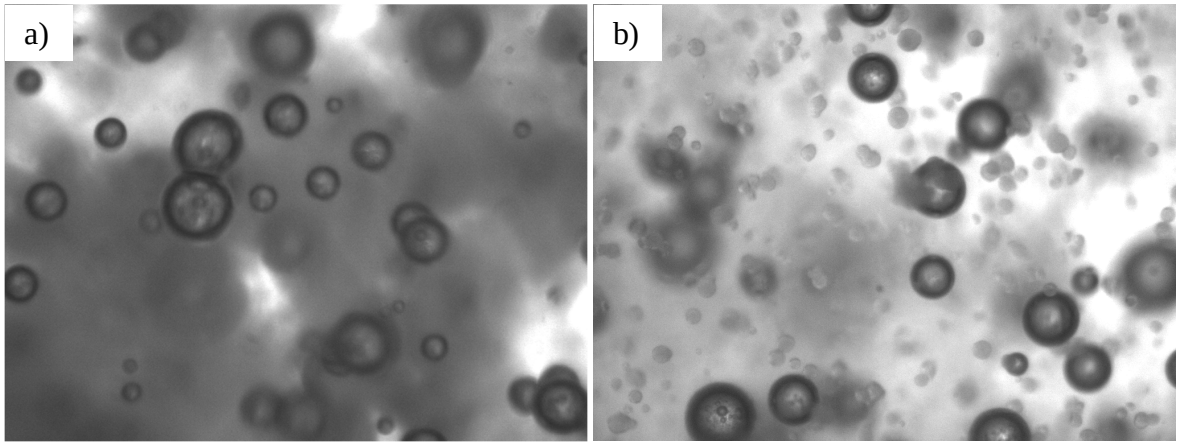


Figure 2.30 Typical images of nitrogen dispersed in a) oil and b) 1% v/v Al2l3-oil at 210°C and 10 bar at low mean specific dissipation rate (4 W/kg) (1.85 x 1.4 mm)

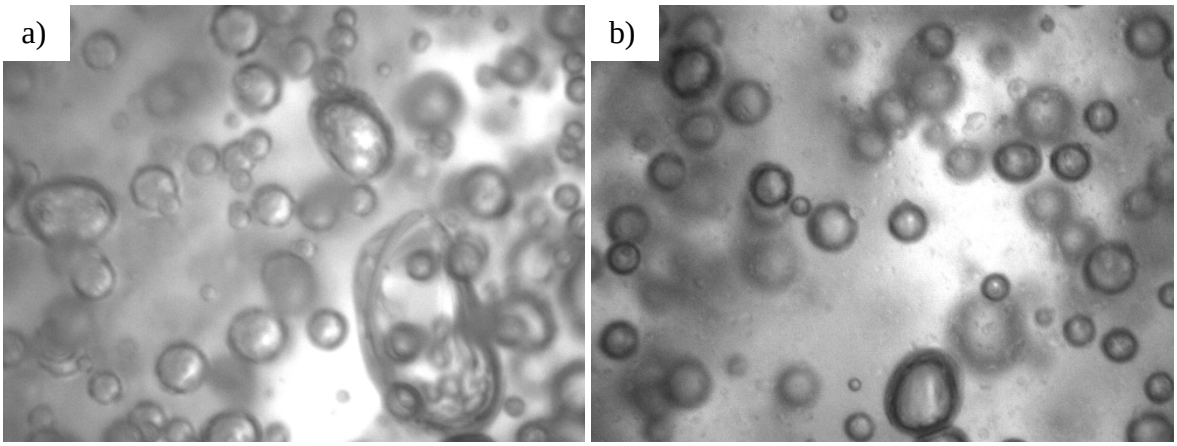


Figure 2.31 Typical images of nitrogen dispersed in a) oil and b) 1% v/v Al2l3-oil at 210°C and 10 bar at high mean specific dissipation rate (18 W/kg) (1.85 x 1.4 mm)

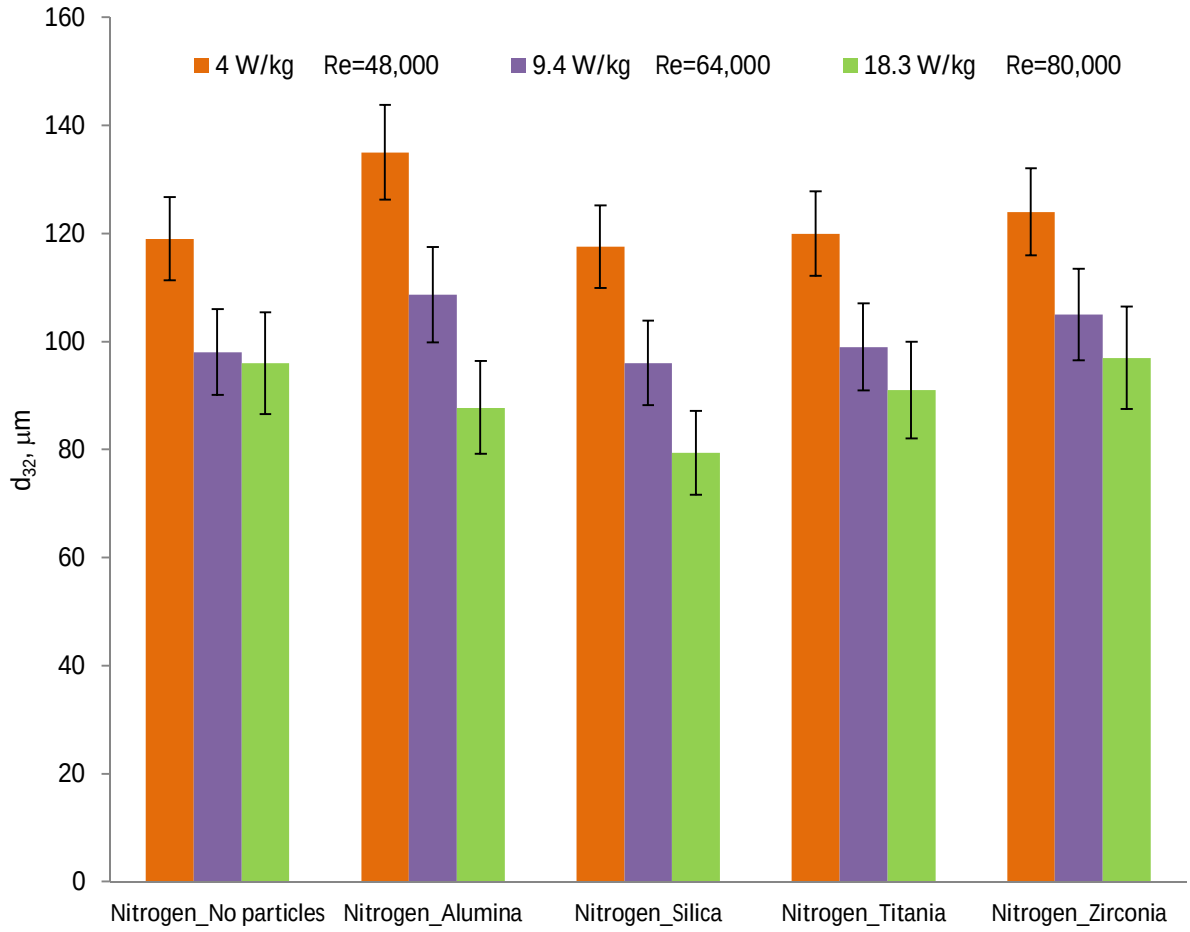


Figure 2.32 Sauter mean diameters of nitrogen bubbles of investigated systems at 210°C, 10bar

Figure 2.32 shows the bubble size (5% v/v $N_2$) dispersed in oil containing 1% v/v particles/oil at 210°C and 10bar with mean energy dissipation rates from 4 to 18 W/kg. Though the effect of different particles on the bubble size was below 12%, there can be distinguished certain differences between bubbles with and without particles. At the lowest energy dissipation rates the larger bubbles were produced when 1% v/v of $N_2$ was dispersed in alumina/oil suspension (Figure 2.32) whereas the suspensions of silica, titania and zirconia gave similar mean bubble sizes. With the increase of mean energy dissipation rate to 9.4 W/kg, the trend remains the same, i.e. the bubbles in alumina suspension were larger by approx. 10%. Surprisingly, a further increase of energy dissipation rate to 18.3W/kg led to a reduction of bubble size in all the particles suspensions. Bubble size in oil without particles remained similar at 9.4 and 18.3W/kg which can be ascribed to the formation of large, non-spherical bubbles at the highest energy dissipation rate as shown in Figure 2.31a. The bubble size distributions for the nitrogen bubbles in oil without particles shown in Figure 2.33 (volume probability density functions) indicate that at the highest energy dissipation rate (18.3W/kg) there are larger bubbles (>200μm) than at 9.4W/kg (<200μm). Relatively larger size and non-spherical shape of bubbles indicates that coalescence occurs.

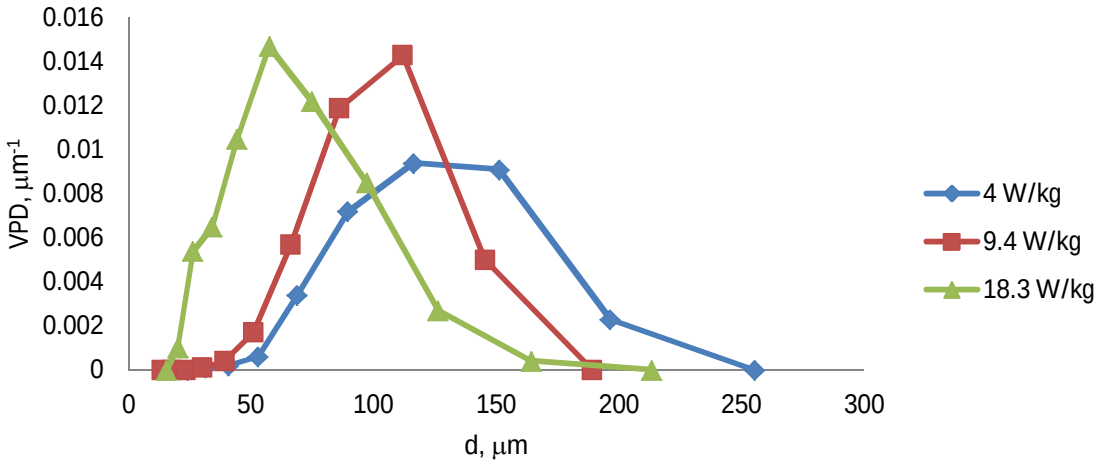


Figure 2.33 Volume probability density function of 5% v/v N2 in oil at 210°C and 10 bar

#### 2.3.1.2.3 Correlating the data

It is evident that the bubble size follows the mean energy dissipation rates regardless whether it is a two or three phase system. Smaller drop formation at higher energy dissipation rates have been reported in numerous liquid/liquid studies (Shinnar 1961; Pacek *et al.* 1994; Pacek *et al.* 1998; Zhou *et al.* 1998; Zhou *et al.* 1998) and gas/liquid dispersion studies (Parthasarathy *et al.* 1991; Parthasarathy *et al.* 1994; Machon *et al.* 1997; Hu *et al.* 2003; Hu *et al.* 2005; Hu *et al.* 2006; Hu *et al.* 2007).

All the investigated systems were well within the turbulent region (Re > 48,000) and the bubble sizes were higher than Komogoroffs length scale, $\eta_K$ (<25μm). The bubble size as a function of *We* and ε are shown in Figure 2.34 and the following correlations were obtained:

No particles: $\frac{d_{32}}{D} = 0.0077 \cdot We^{-0.216}$ $R^2 = 0.8735$,

$Al_2O_3$/oil: $\frac{d_{32}}{D} = 0.04 \cdot We^{-0.419}$ $R^2 = 0.9953$,

$SiO_2$/oil: $\frac{d_{32}}{D} = 0.0265 \cdot We^{-0.383}$ $R^2 = 0.9969$,

$TiO_2$/oil: $\frac{d_{32}}{D} = 0.0119 \cdot We^{-0.274}$ $R^2 = 0.9779$,

$ZrO_2$/oil: $\frac{d_{32}}{D} = 0.0098 \cdot We^{-0.243}$, $R^2 = 0.9834$,

No particles: $d_{32} = 0.0001 \cdot \varepsilon^{-0.144}$ $R^2 = 0.8735$,

$Al_2O_3$/oil: $d_{32} = 0.0002 \cdot \varepsilon^{-0.28}$ $R^2 = 0.9953$,

$SiO_2$/oil: $d_{32} = 0.0002 \cdot \varepsilon^{-0.255}$ $R^2 = 0.9969$,

$TiO_2$/oil: $d_{32} = 0.0003 \cdot \varepsilon^{-0.183}$ $R^2 = 0.9779$,

$ZrO_2$/oil: $d_{32} = 0.0002 \cdot \varepsilon^{-0.162}$ $R^2 = 0.9834$,

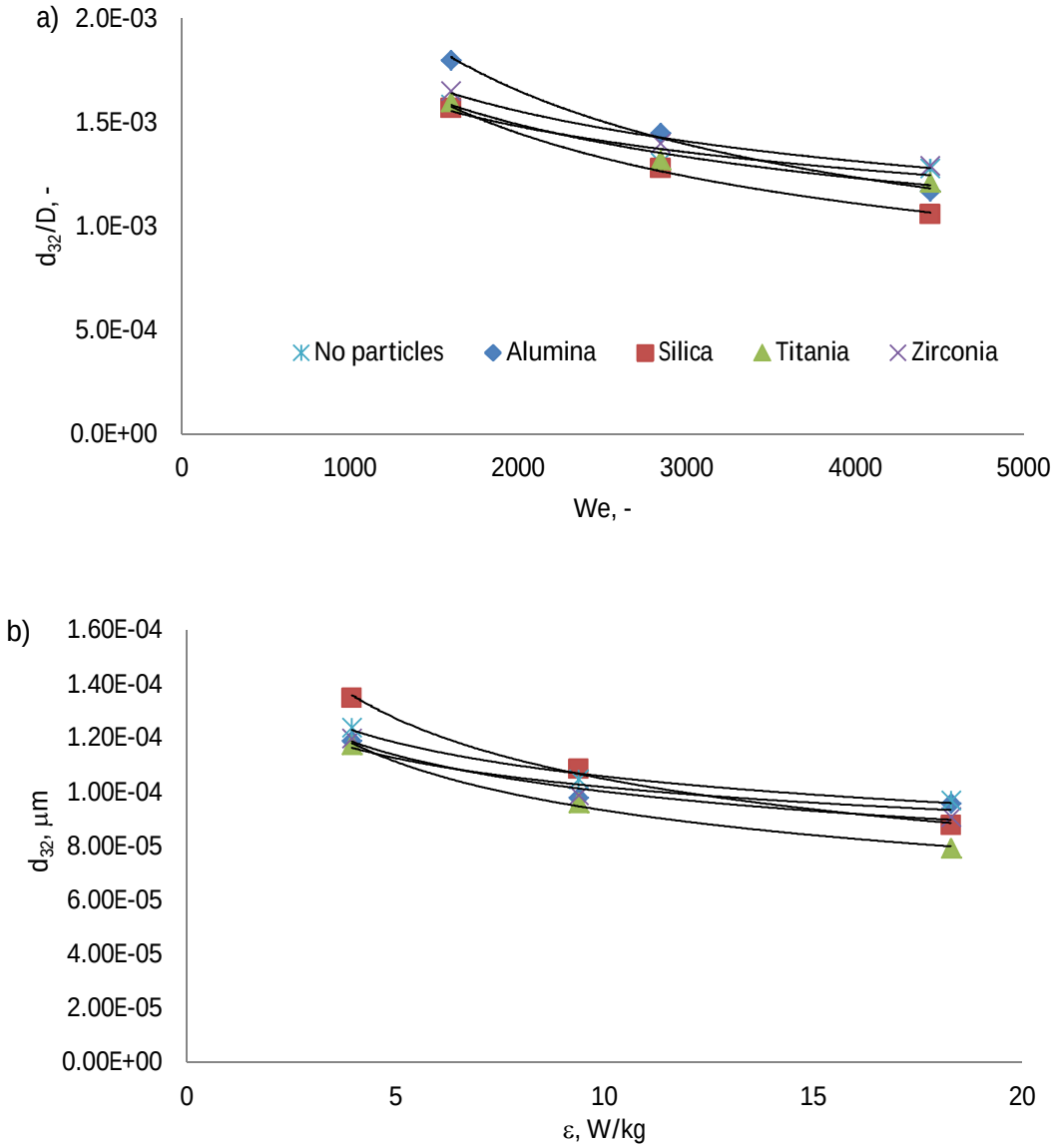


Figure 2.34 Bubble size as a function of a) We and b) ε in 5% N2 dispersed in oil with and without particles

In two and three phase systems the exponents are larger in correlations than theoretical ones indicating the presence of bubble coalescence, hence the assumption on the breakage as the only factor determining the bubble size can not be correct. Though the bubble size is well correlated as an exponential function of the energy dissipation rates, the exponent determined experimentally is different from theoretical one (-2/5).

The bubble size correlated with ε and *We* that gives theoretical exponents of -2/5 and -3/5 were developed with the assumption that the coalescence is negligible, i.e. for the dilute dispersions (~1%) where the collision probability is very low. Therefore, the larger than theoretical exponents obtained indicate that at higher gas hold up (5%) the assumption of negligible coalescence is not valid. Clearly, the correlation between energy dissipation rates necessary to break the bubble must be corrected by the coalescence effect, which, as we have seen previously, is significant even for diluted dispersion (1% of gas). If the gas-liquid systems with 1% and 5% gas dispersion are compared, the exponents of *We* of more diluted system (1% v/v gas) is smaller (-0.335, -0.359) than that of higher gas phase fraction (5% v/v gas) without particles (-0.216) which indicates pronounced coalescence of the latter. This agrees with the concept of the presence of coalescence at larger gas phase fractions.

The coalescence can be accounted for by including the volume fraction of dispersed gas phase into correlation relating bubble size to *We* (Pacek *et al.* 1998) in the same way as it is done for liquid/liquid systems:

$$\frac{d_{32}}{D} = a(1+b\cdot\phi)We^{c} \tag{2.17}$$

Table 2.13 Coefficients of the bubble size correlated with eq. : $\frac{d_{32}}{D} = a(1+b\cdot\phi)We^{c}$

| System | a | B | c | $R^2$ |
|---|---|---|---|---|
| $N_2$-No particles | 0.0060 | 7.6024 | -0.2261 | 0.8888 |
| $N_2$-Alumina | 0.0189 | 20.1563 | -0.4128 | 0.9958 |
| $N_2$-Silica | 0.0147 | 14.8598 | -0.3782 | 0.9972 |
| $N_2$-Titania | 0.0077 | 12.4498 | -0.2800 | 0.9804 |
| $N_2$-Zirconia | 0.0070 | 9.2163 | -0.2469 | 0.9850 |

For the $\phi = 0.05$ (5% gas dispersed) the parameters *a*, *b* and *c* and $R^2$ that were fit to the (equation (2.17)) are shown in Table 2.13. Clearly, the exponents of the *We* number are again significantly different from the theoretical one (-3/5) but it can be seen that they shifted slightly towards this value as compared to the correlation (equation (2.9)). Hu *et al.* (2003) studied bubble sizes in aqueous/proteins solution with different air concentration (5-20%) and found that the coefficients were *a = 0.027, b = 3.85* and *c = -0.4* which is similar to the above results. The coefficient *b* that is related to the degree of coalescence in the system normally ranges from 2.5-22 for liquid/liquid dispersions (Zhou *et al.* 1998; Hu *et al.* 2003) and the higher value, the stronger coalescence. The lowest value of coefficient *b* of the system with no particles might indicate that the coalescence is stronger when the particles are present in the system. A value of *b* as high as 23 was reported in the chlorobenzene/water dispersions, whereas the exponent was c=-0.43 (Pacek *et al.* 1999).

### 2.3.2 Effect of steam and type of particles on the bubble size in concentrated dispersions

The steam addition with the 5% gas holdup was impossible (see Experimental and methodology) therefore the higher gas hold up used was (35%). In practical applications the higher gas volume fraction is commonly used, especially in bubble columns, e.g. gas hold-ups in the Fisher Tropsch synthesis in slurry bubble columns was in the range of 0.025-0.3 (Deckwer *et al.* 1980) or higher (Krishna *et al.* 1997; Maretto *et al.* 1999). Additionally, the effect of the particles on the bubble sizes proved to be rather insignificant at 5% v/v of gas phase which did not bring noticeable difference in the bubbles. As discussed in the Introduction the particles can act in a similar way as a surfactant, e.g. they inhibit or prevent coalescence of droplets or bubbles. On the other hand however, particles are used as

antifoaming agents, and can enhance the coalescence of bubbles. Therefore, in order to observe the effect of particles on the bubbles coalescence, higher volumes of the gas phase should be employed, because in such conditions, i.e. high gas volume fraction, the coalescence of bubbles becomes significant.

The combined effect of the presence of steam at different concentrations and the type of particles on the bubble size was also investigated. Since the effect of particles on the bubble size is expected to remain similar in mechanically agitated reactors and in bubble columns, (trend rather than absolute values), the range of energy input in mechanically agitated reactors was adjusted to resemble those existing in bubble columns. The mean energy dissipation rates in bubble column is determined by the gas velocity: $\varepsilon = g \cdot u_g$ (Deckwer *et al.* 1980). The gas velocities are essentially different for different applications and the energy dissipation rate ranges from 0.1 to 0.64 W/kg for the three phase bubble columns (Zhang *et al.* 2008) but in Fisher Tropsch synthesis, the energy dissipation rate is within 0.26-0.6 W/kg (Schlesinger *et al.* 1951) and it does not exceed 0.3 W/kg (Deckwer *et al.* 1980). Therefore in the current study the investigated range of energy input was extended and the minimum energy dissipation rate, that still enabled the dispersing of the particles and the gas phase was employed, resulting in the range of 1-18.3 W/kg being investigated.

#### 2.3.2.1 Bubble size models

Measurements of the bubble size were carried out in the conditions that mimic the Fischer Tropsch synthesis, without and with 1% v/v particles ($Al_2O_3$, $SiO_2$, $TiO_2$ and $ZrO_2$) at elevated temperature (170-210°C) and pressure (1-20bar). Since the presence of water in the system is highly relevant, e.g. in Fischer Tropsch synthesis, different concentrations of steam were used in the reactor: 100%, 10% and 5%vol.

Typical images of bubbles taken at steady state are shown in Figure 2.36. The bubbles were sufficiently detectable for the measurements. The mean bubble size are shown in Figure 2.37 and the typical bubble size distributions are shown in Figure 2.35.

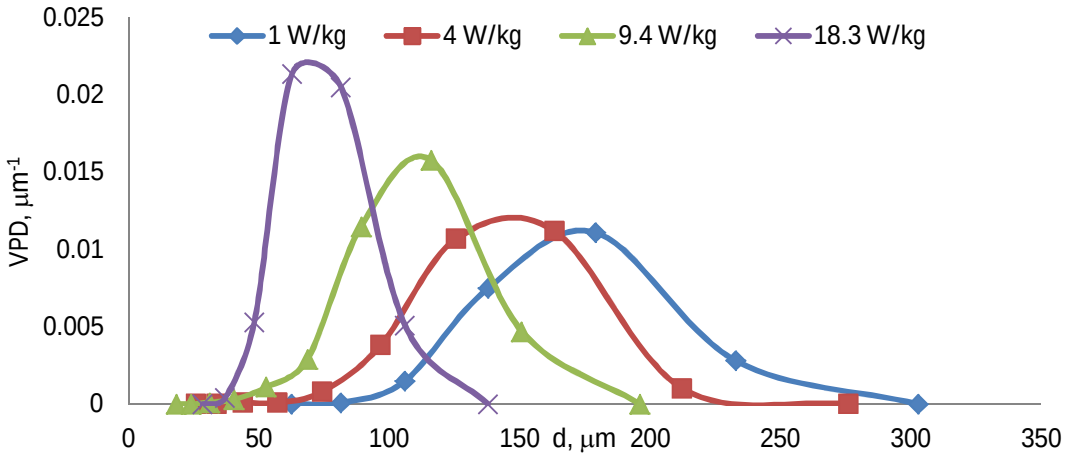


Figure 2.35 Bubble size distribution of nitrogen dispersed in paraffin oil at 210C and 1bar

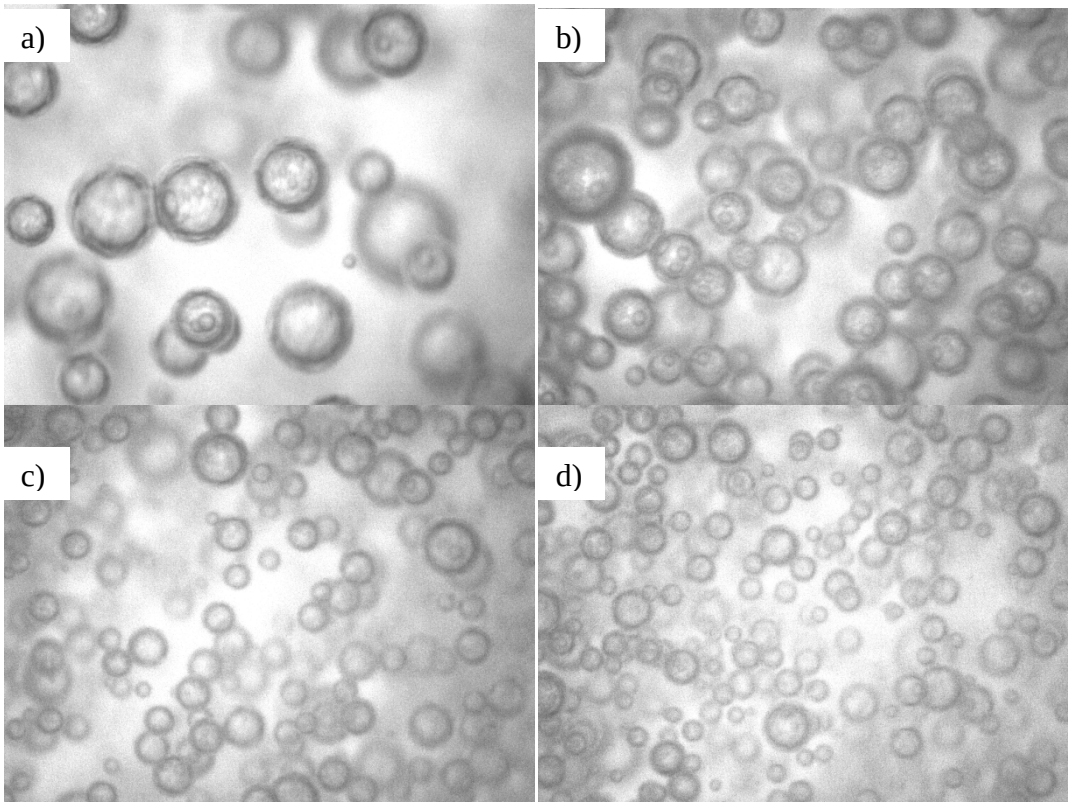


Figure 2.36 Typical images of 35% nitrogen dispersed in paraffin oil at 170°C, at 1bar at different energy dissipation rate: a) 1W/kg, b) 4 W/kg, c) 9.4W/kg and d) 18.3W/kg (1.85 x 1.4 mm)

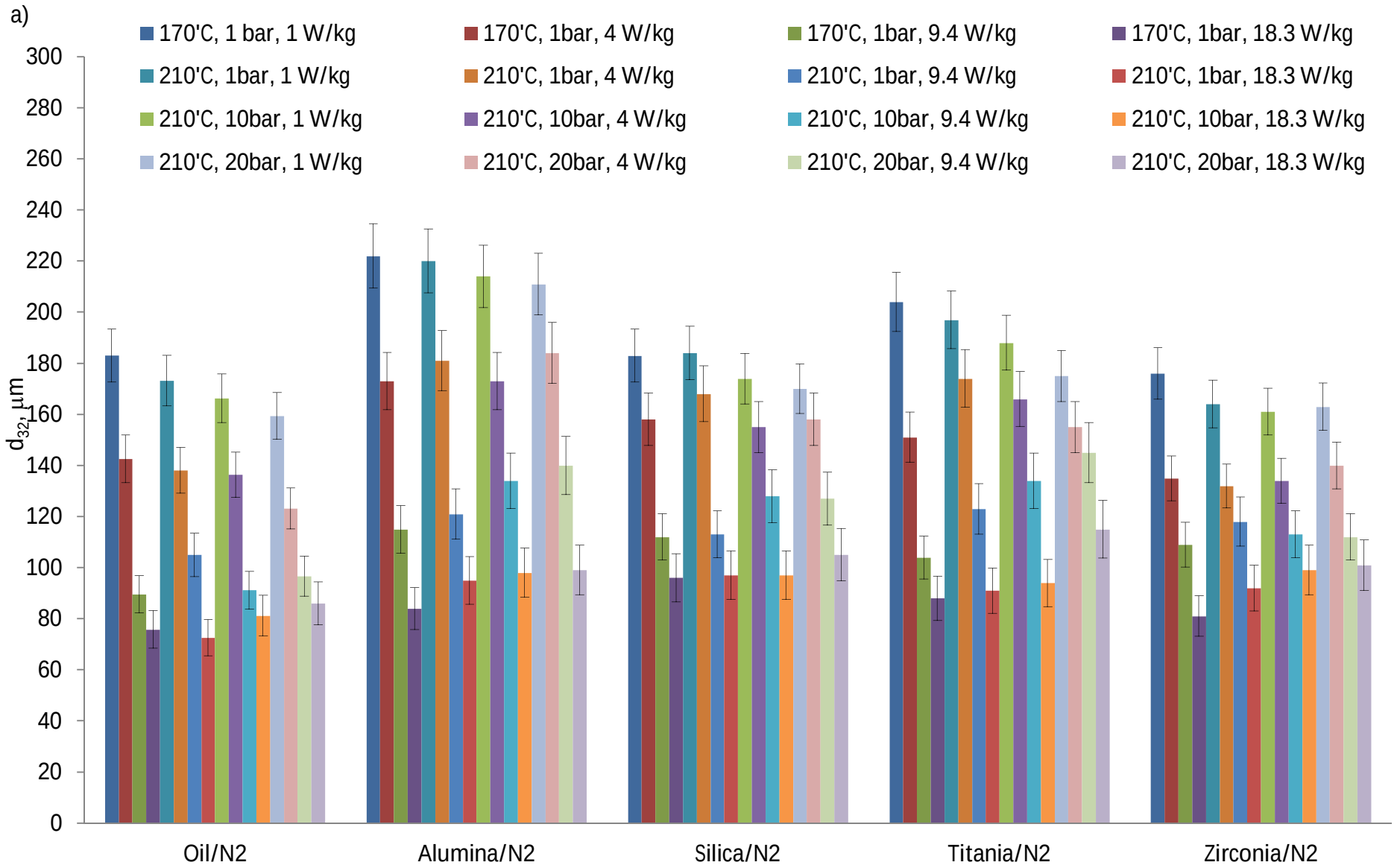
a)
170'C, 1 bar, 1 W/kg
170'C, 1bar, 4 W/kg
170'C, 1bar, 9.4 W/kg
170'C, 1bar, 18.3 W/kg
210'C, 1bar, 1 W/kg
210'C, 1bar, 4 W/kg
210'C, 1bar, 9.4 W/kg
210'C, 1bar, 18.3 W/kg
210'C, 10bar, 1 W/kg
210'C, 10bar, 4 W/kg
210'C, 10bar, 9.4 W/kg
210'C, 10bar, 18.3 W/kg
210'C, 20bar, 1 W/kg
210'C, 20bar, 4 W/kg
210'C, 20bar, 9.4 W/kg
210'C, 20bar, 18.3 W/kg
300
280
260
240
220
200
180
160
140
120
100
80
60
40
20
0
$d_{32}$, µm
Oil/N2
Alumina/N2
Silica/N2
Titania/N2
Zirconia/N2

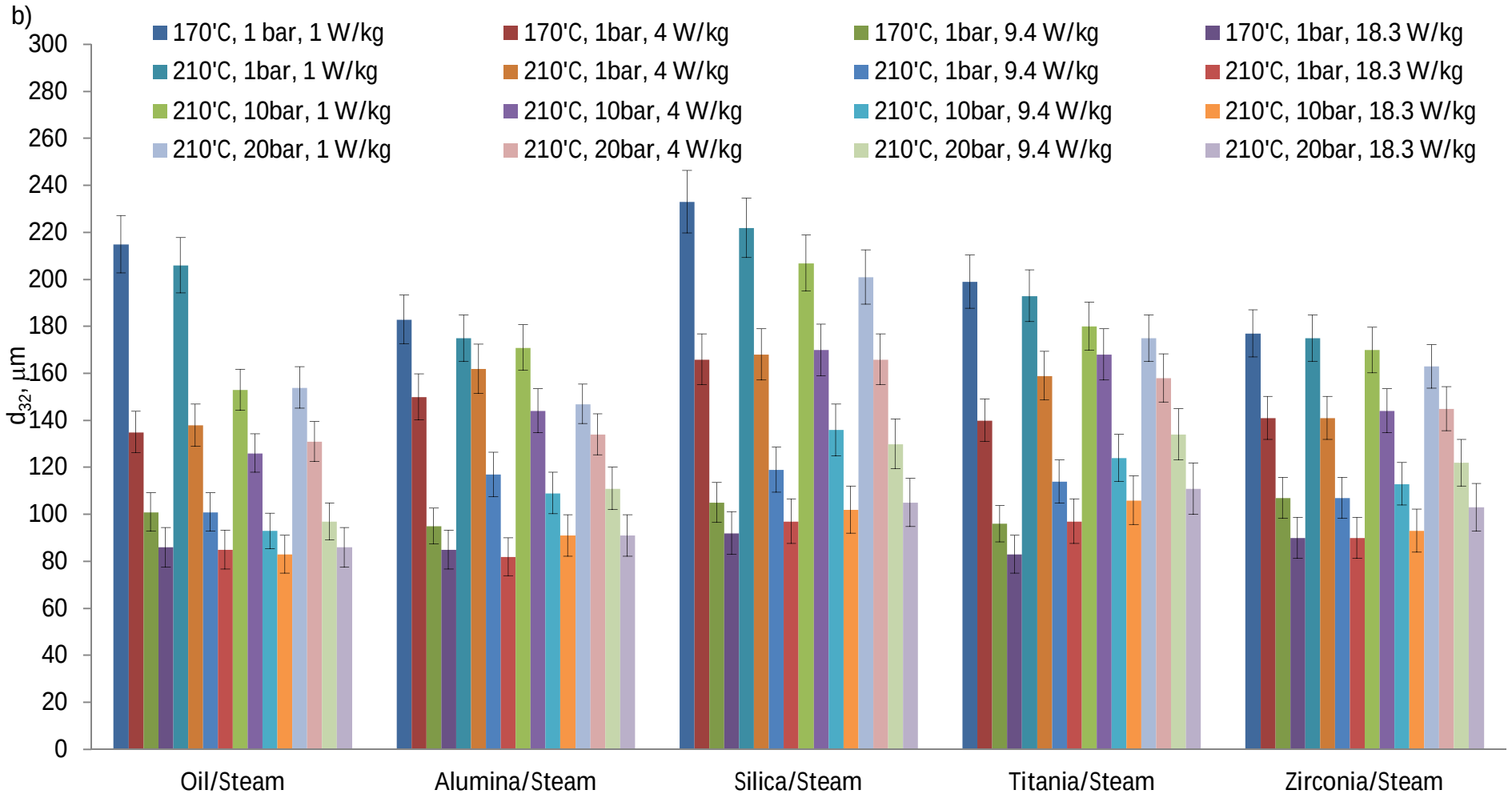


Figure 2.37 Experimental data on the Sauter diameter of bubbles in 35% v/v of a) nitrogen and b) steam (+nitrogen)

#### 2.3.2.1.1 Effect of hydrodynamic conditions and surface/interfacial tension

Clearly, the bubble size decreases with increasing power input (Figure 2.37). The results were lumped together in different *T* and *P* conditions and correlated with *We,* e.g. in Figure 2.38 the bubbles size are correlated for nitrogen dispersed in paraffin oil without particles. Since the systems are concentrated and the coalescence cannot be neglected, the data were correlated using the equation (2.17) as shown on Figure 2.39.

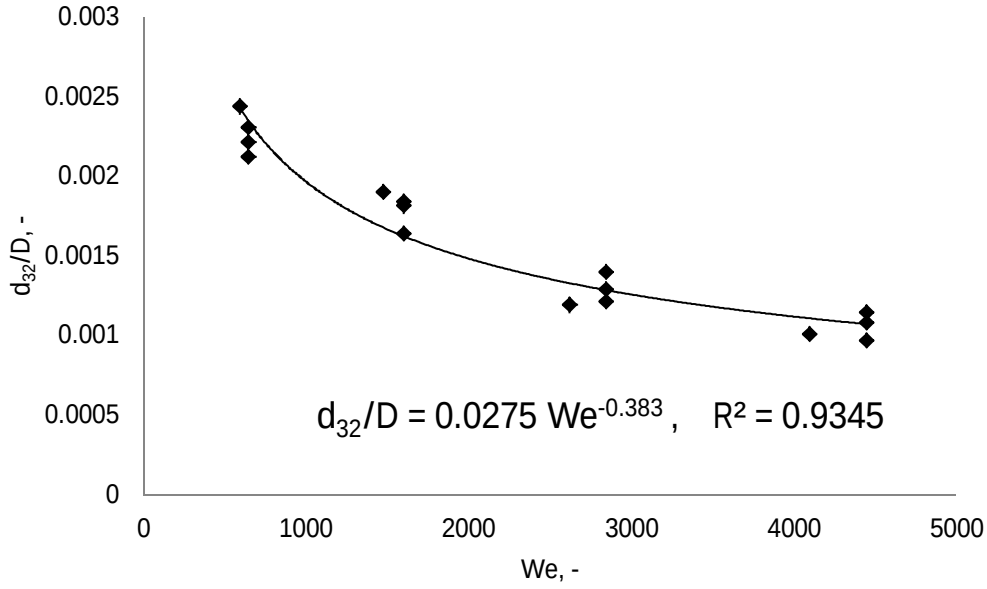


Figure 2.38 Bubble size correlated with We number for 35% of nitrogen in oil at elevated temperature and pressure (170°C - 210°C; 1-20bar)

Table 2.14 Correlations of the bubble sizes of all systems according to $d_{32}/D = aWe^{b}$

| | System | a | b | $R^2$ |
|---|---|---|---|---|
| $N_2$ | No particles | 0.0324 | -0.406 | 0.9301 |
| | Alumina | 0.0476 | -0.424 | 0.8966 |
| | Silica | 0.0179 | -0.305 | 0.874 |
| | Titania | 0.0241 | -0.341 | 0.8157 |
| | Zirconia | 0.0148 | -0.291 | 0.9175 |

| | | | | |
|---|---|---|---|---|
| 100-10% steam | No particles | 0.0317 | -0.398 | 0.9236 |
| | Alumina | 0.0216 | -0.342 | 0.8559 |
| | Silica | 0.0402 | -0.404 | 0.9240 |
| | Titania | 0.0218 | -0.331 | 0.8183 |
| | Zirconia | 0.0174 | -0.31 | 0.9289 |

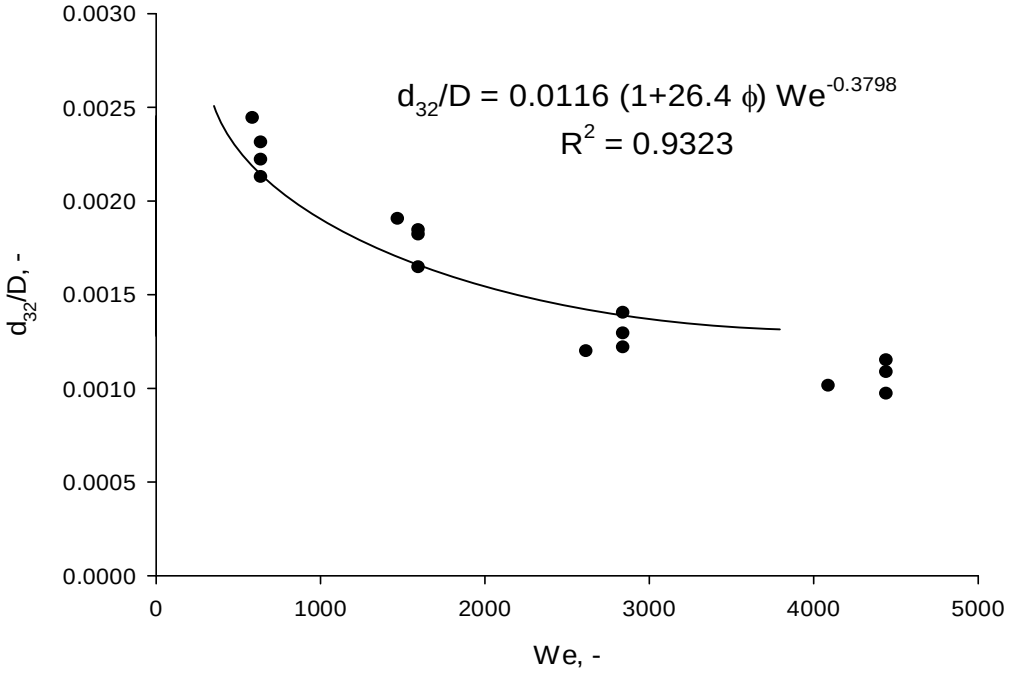


Figure 2.39 Bubble size correlated with We number and gas volume fraction

Table 2.15 s Coefficients in $d_{32}/D = a(1+b\cdot\phi)We^{c}$ for different systems

| | System | a | b | c | $R^2$ |
|---|---|---|---|---|---|
| $N_2$ | No particles | 0.0116 | 26.4 | -0.3798 | 0.9219 |
| | Alumina | 0.0206 | 13.1 | -0.3779 | 0.8562 |
| | Silica | 0.0086 | 14.3 | -0.2773 | 0.839 |
| | Titania | 0.0098 | 19.2 | -0.309 | 0.8087 |
| | Zirconia | 0.0082 | 12.97 | -0.2791 | 0.9417 |
| 100-5% steam | No particles | 0.0127 | 30.9 | -0.4003 | 0.8774 |
| | Alumina | 0.0093 | 17.4 | -0.3121 | 0.8393 |
| | Silica | 0.0207 | 12.88 | -0.3807 | 0.8319 |
| | Titania | 0.0097 | 18.8 | -0.3103 | 0.8476 |
| | Zirconia | 0.0087 | 15.1 | -0.2926 | 0.9357 |

The exponents in correlation with *We* are all in the range 0.29-0.398 (Table 2.14) whereas in the correlations that include the gas hold up they are within 0.2773-0.4003 (Table 2.15). The flow in all cases is turbulent (25,000-80,000) apart from the lowest energy dissipation rate (1W/kg) at 170°C (16,000). Obviously, the exponents are very different form the theoretical value (-0.6) but rather consistent with those obtained previously for the turbulent flow with 1% v/v dispersed gas and 5% v/v dispersed in two- and three-phase systems. Obviously, in such a concentrated dispersion, coalescence is inevitable and the coalescence rate is considerably increased. The coalescence rate depends on the collision frequency which substantially increases with the larger gas volume fraction (Prince *et al.* 1990). The bubble collision frequency is much higher and so the equilibrium bubble size is controlled not only by breakage which ultimately leads to the higher exponents when correlated with *We*. The collision efficiency, which depends on the time that the bubbles remain in proximity during which the thin liquid film drainage occurs (Laari *et al.* 2005), is to a certain approximation, independent from the gas volume fraction.

#### 2.3.2.1.2 Effect of mean specific energy dissipation rate on equilibrium bubble size

The mean bubble sizes were correlated utilizing the mean specific energy dissipation rate, where data for each system were combined together at different temperatures (170, 210°C) and pressures (1, 10, 20bar). The proportionality coefficients and exponents of such combined bubbles size correlated with the energy dissipation rates are listed in Table 2.16. The constant *a* directly follows the sizes of bubbles, in that the larger parameter is related to larger observed bubbles, e.g. bubbles in alumina/nitrogen suspension are larger than bubbles in nitrogen (compare Figure 2.37a and Table 2.16). The exponents from the correlations are in a range of -0.196 to -0.285. Again, these numbers are much higher than the theoretical one (-

0.4) but consistent with the results obtained for diluted gas nitrogen dispersion in paraffin oil/particles suspension (-0.144 to -0.28).

Table 2.16 Correlations of the bubble sizes of all systems with ε according to $d_{32} = a\varepsilon^b$

| | System | a | b | R2 |
|---|---|---|---|---|
| $N_2$ | No particles | 181 | -0.278 | 0.92 |
| | Alumina | 233 | -0.285 | 0.9077 |
| | Silica | 189 | -0.204 | 0.8804 |
| | Titania | 202 | -0.229 | 0.8309 |
| | Zirconia | 170 | -0.196 | 0.9269 |
| 100-5% steam | No particles | 183 | -0.265 | 0.9149 |
| | Alumina | 179 | -0.229 | 0.8604 |
| | Silica | 225 | -0.271 | 0.9331 |
| | Titania | 195 | -0.224 | 0.8401 |
| | Zirconia | 178 | -0.208 | 0.9351 |

Table 2.17 Bubbles sizes correlated with mean energy dissipation rate $d_{32} = a\varepsilon^b$

| The exponents (b) of the bubbles correlated with energy dissipation rates (1-18.3 W/kg) | | | | |
|---|---|---|---|---|
| | 170°C, 1bar | 210°C, 1bar | 210°C, 10bar | 210°C, 20bar |
| $N_2$ | -0.317 | -0.288 | -0.261 | -0.218 |
| Steam | -0.32 | -0.31 | -0.219 | -0.209 |
| $Al_2O_3$ / $N_2$ | -0.335 | -0.294 | -0.26 | -0.251 |
| $Al_2O_3$ /steam | -0.282 | -0.253 | -0.22 | -0.161 |
| $SiO_2$ / $N_2$ | -0.23 | -0.231 | -0.192 | -0.164 |
| $SiO_2$ /steam | -0.336 | -0.29 | -0.235 | -0.222 |
| $TiO_2$ / $N_2$ | -0.298 | -0.263 | -0.225 | -0.131 |
| $TiO_2$ /steam | -0.312 | -0.244 | -0.188 | -0.152 |
| $ZrO_2$ / $N_2$ | -0.258 | -0.187 | -0.167 | -0.17 |
| $ZrO_2$ /steam | -0.236 | -0.232 | -0.207 | -0.155 |

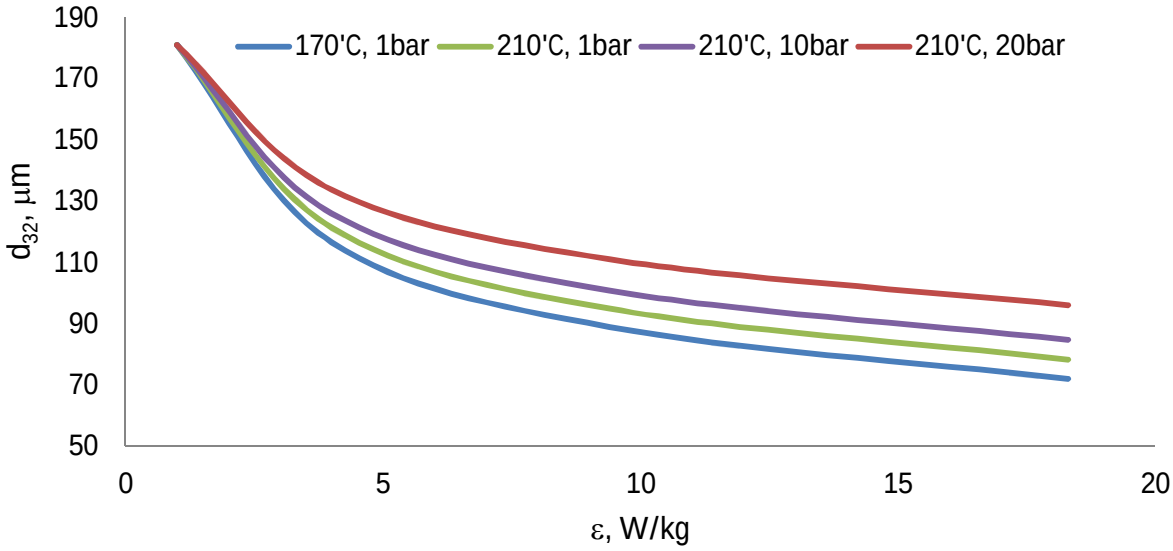


Figure 2.40 Sauter mean diameter of nitrogen bubbles correlated with energy dissipation rates in different T and P (constant proportionality coefficient, a, exponent according to Table 2.17)

The data were also correlated with energy dissipation for all investigated conditions as shown in Table 2.17. The exponent (*b*) in the bubbles correlations for the energy dissipation rate (Table 2.17) clearly increase when the temperature increases (170->210°C) and subsequently when the pressure increases (1->10->20bar). Therefore the energy dissipation rates had larger effect on the bubble sizes at lower temperature and lower pressure, than at higher temperature and pressure, i.e. the bubbles size reduction was more pronounced in less severe conditions (Figure 2.40). The character of flow at 170°C and 1bar changes from the transitional to turbulent (*Re* 16,000 -> 41,000) which is the reason for the larger exponents at those conditions, i.e. bubble size reduction with energy dissipation rate. Such a flow regime is similar to all investigated systems which explain the larger exponents in the correlations at lower temperature and pressure. Whereas at higher temperature and pressure the *Re* number is larger than 30,000, therefore the flow is turbulent.

#### 2.3.2.2 Bubble size – qualitative approach

In order to determine the effect of different particles on the bubble size, qualitative rather than a quantitative approach was employed. The results show that the bubble size depends not only on the energy dissipation rate but also of the type of the particles used and the gas composition. It is worth to note that the bubbles produced with 4W/kg power input are of the same size as those produced with only 1W/kg power input. For instance, nitrogen bubbles in $Al_2O_3$/oil at ε=4W/kg are of similar size as bubbles at ε=1W/kg in oil and in $SiO_2$/oil and $ZrO_2$/oil (Figure 2.37). Steam bubbles were also found to be of similar size even though energy dissipation rates were four times higher. For instance, steam bubbles in $SiO_2$/oil at ε=4W/kg are of similar size as steam bubbles in $Al_2O_3$/oil and $ZrO_2$/oil at only ε=1W/kg. Clearly, the energy dissipation rates can be significantly reduced (e.g. from 4 to 1W/kg, energy saving) and the same bubble size can be obtained by simple addition of a particular particle type. As the continuous phase properties remain the same at given *T* and *P* with the same particles concentration, the bubble size must result from the effect of the type of particles and/or the gas composition on the bubble size.

The effect of different particles on the bubble size in this section is analysed qualitatively, via their effect on the bubbles coalescence rate. At the highest energy dissipation rates, there is an insignificant effect of operating conditions and the type of particles and gas type (Figure 2.41 and Figure 2.42). However, at the most severe conditions, i.e. 210°C and 20bar, the bubbles have a noticeably larger size than in all other investigated systems. A similar trend was observed for most of the systems at 9.4W/kg and for some systems at 4W/kg, i.e. the bubbles tend to be larger at 20 bar and 210°C than at lower pressure/temperature. The reason could be due to the condensation of steam and presence of water as either droplets or as a layer in the gas-liquid interface. In the Experimental and

methodology section it was shown however that the steam bubbles were present rather than water droplets since the bubbles were going up. But if the condensation occurs and the water remains at the interface, the increase of interfacial tension which occurs should lead to an increase of bubble size. Such effect however was not observed with the lowest energy dissipation rates. Therefore, it can reasonably be concluded that this is not the most likely of reasons.

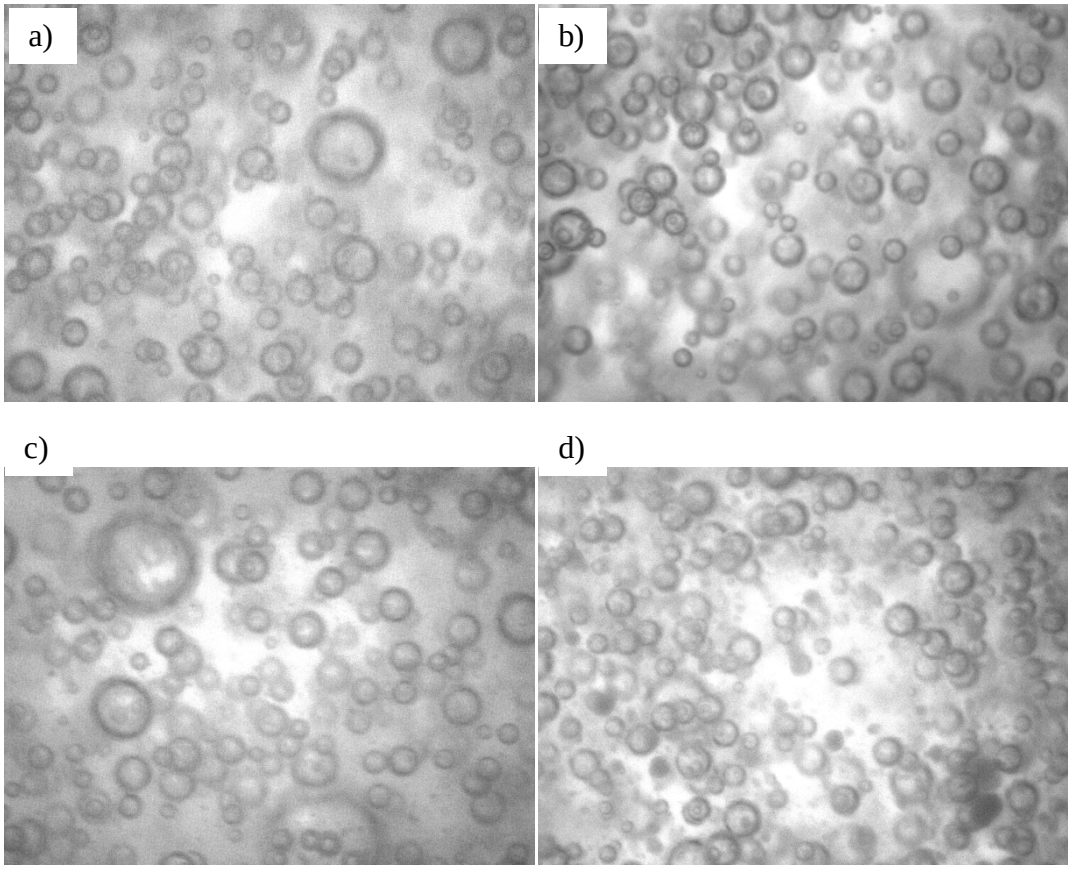


Figure 2.41 Nitrogen bubbles in a) oil, b) SiO2/oil, c) TiO2/oil and d) ZrO2/oil with the 18.3W/kg power input at 170°C and 1bar (1.85 x 1.4 mm)

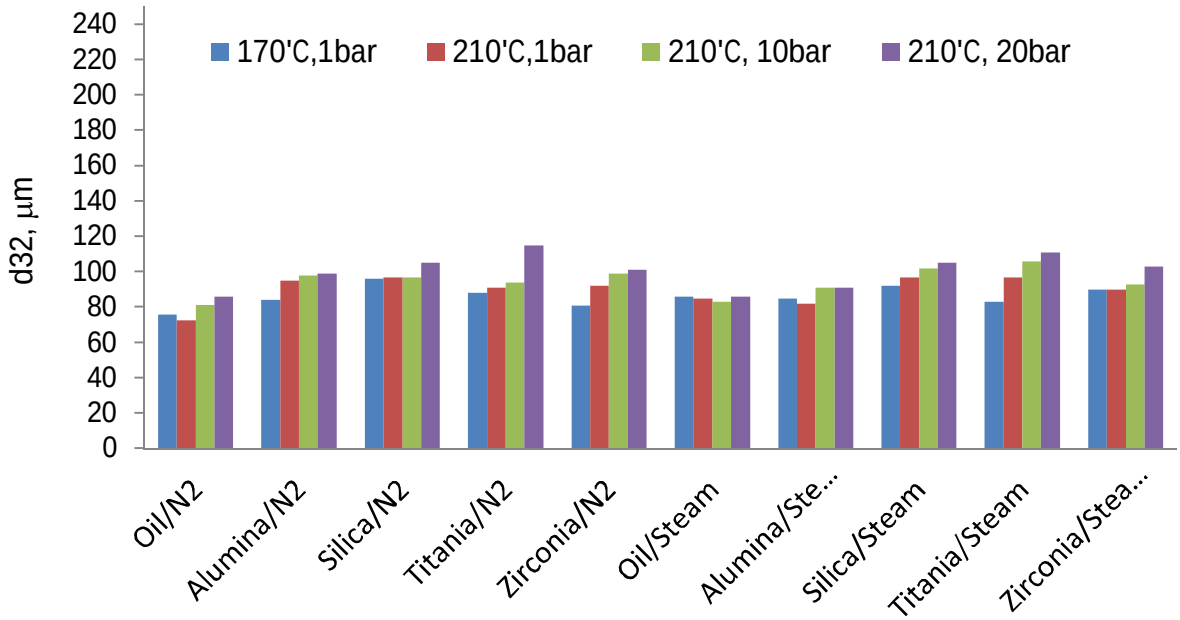


Figure 2.42 Sauter mean diameter of investigated systems at the highest energy dissipation rates (18.3W/kg)

The largest differences in the bubble size of investigated systems at different conditions can be observed when the lowest mixing intensity is applied (Figure 2.43 and Figure 2.44) and these data seem to be the most interesting from the industrial point of view, where usually lower power inputs are used in the slurry bubble columns.

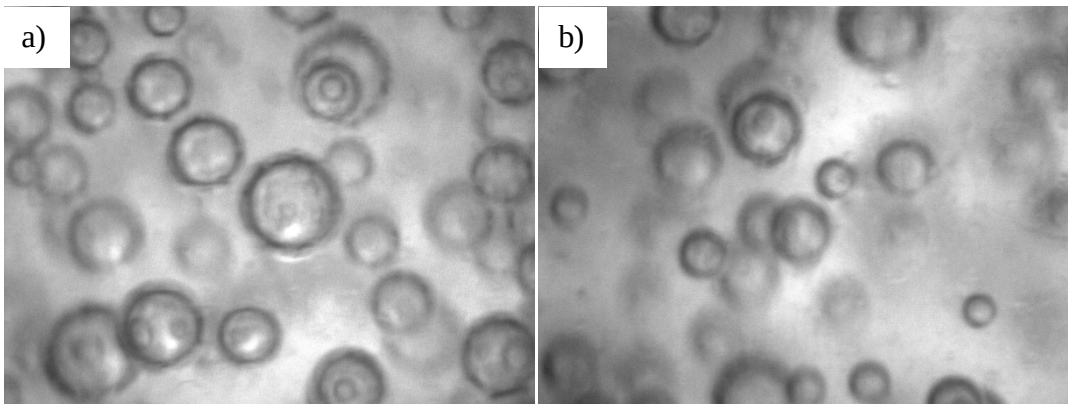

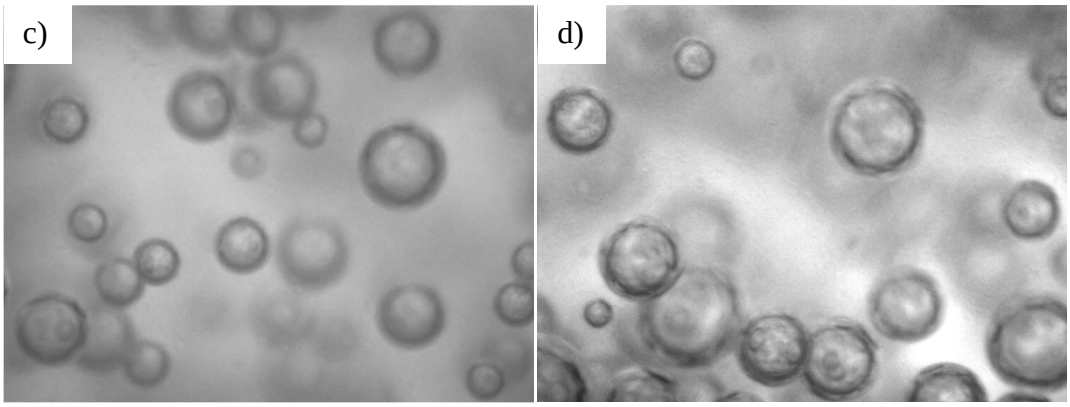


Figure 2.43 Bubbles at 1 W/kg energy input, 210°C and 1bar in a) N2/ Al2O3/oil, b) Steam/ Al2O3/oil SiO2, c) N2/ SiO2/oil and d) Steam/ SiO2/oil (1.85 x 1.4 mm)

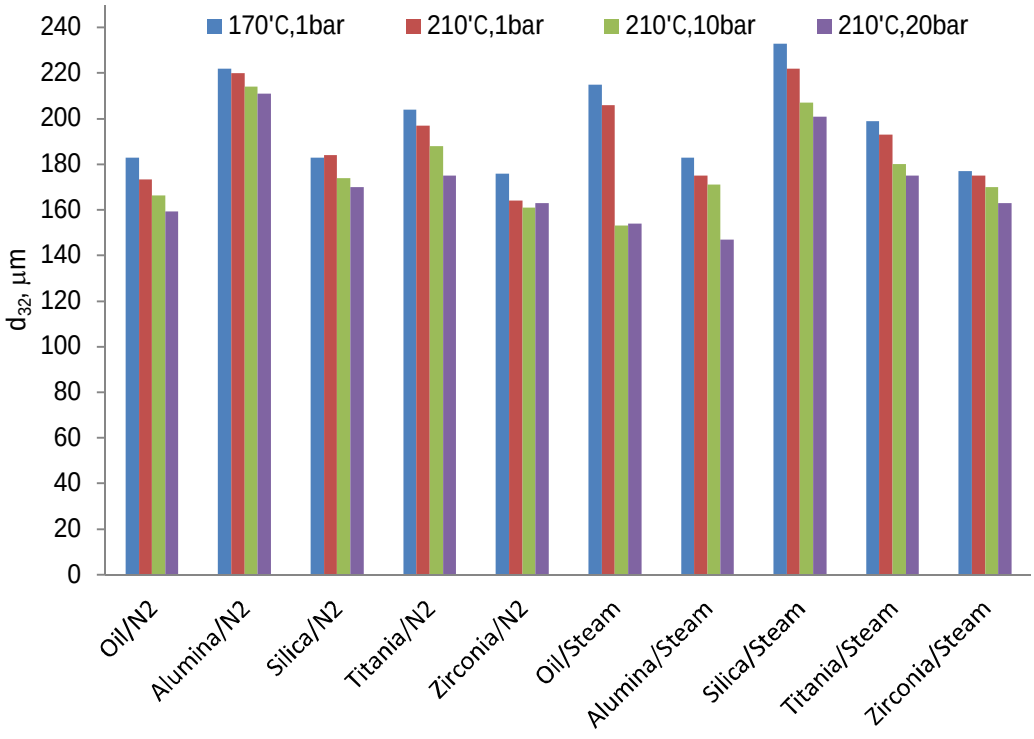


Figure 2.44 Bubble sizes of investigated systems at 1 W/kg energy dissipation rate

It appears that in gas-liquid system, without particles, the presence of steam strongly affects the bubble size at low pressure (1 bar). Clearly, in pure nitrogen and pure steam results, the steam bubbles are larger. However, in presence of the nitrogen in the steam (10 and 20bar), the bubble size becomes similar as those made of nitrogen only.

Bubble sizes are different for different particles regardless of the type of gas, for instance, bubbles in suspension of zirconia are always the smallest. Also, there is a combined effect of the type of particles and the composition of gas on the bubble sizes. Alumina particles increase the nitrogen bubbles but reduce the size of steam bubbles as compared to the bubbles observed in the system without particles. Silica particles do not affect nitrogen bubbles but only slightly increase the size of steam bubbles as compared to $N_2$/oil and steam/oil bubbles. Also titania particles increase the size of nitrogen bubbles and only slightly affect the steam bubbles. The particles seem to be strongly affecting bubble size, since at the same *T*, *P* and gas composition, the bubble size is measurably different. Elimination of the possible factors allows establishing what actually influence the bubble size, bringing understanding but it also offers the possibility of bubble size control by adjusting the particles properties like size, wettability etc.

Using such approach for the qualitative analysis, first, the effect of liquid/slurry properties on the bubble size will be considered in terms of the effect of operating conditions. Subsequently, the presence of particles on the liquid properties will be considered.

#### 2.3.2.2.1 Effect of operating conditions on the liquid properties

The bubble sizes slightly decrease with increasing temperature and pressure. It is well known that as temperature increases density and surface tension decrease linearly and viscosity decreases according to Arrhenius equation. Elevated pressure however does not affect liquid density and viscosity and although there are some studies on the effect of pressure on the surface tension, in general it can be assumed that the surface tension does not change significantly (Poling *et al.* 2001).

The values of viscosity, density and surface tension at elevated temperature can be found in Chapter 2. The viscosity of oil at 170°C to 210°C is 0.177 Pa·s and 0.0885 Pa·s respectively, so decreases by 100% with the temperature increase of 40°C (Table 2.6). With such a temperature increase, the paraffin oil density decreases by only 3.5% ($\rho_{l(170°C)}$ = 775.5 kg/m$^3$, $\rho_{l(210°C)}$ = 749.5 kg/m$^3$). Similarly, with the temperature increase from 170°C to 210°C, the surface tension of paraffin oil decreases by 12% ($\gamma_{(170°C)}$ = 22.21 mN/m, $\gamma_{(210°C)}$ = 19.81 mN/m).

As showed in the Introduction, the bubble size change with the temperature (Table 2.1) which is a combined effect of viscosity, density and surface tension. Decrease of viscosity increases the turbulence in the reactor, therefore the energy of eddies and bubble breakage intensifies which leads to the smaller bubble size (Schäfer *et al.* 2002). The disruptive forces in the turbulent flow depend on the density, according to $\tau \approx \rho \cdot (\langle \varepsilon \rangle \cdot d_{max})^{2/3}$, therefore the larger density, the larger the disruptive forces and improved bubble breakage. Also, the cohesive forces are reduced when the surface tension of liquid is reduced.

Pressure increase leads to an increase in gas density which causes larger inertia of the bubbles. It has been postulated that larger inertia of the gas in the fluctuating bubble causes increased bubble breakage (Sagert *et al.* 1977; Wilkinson *et al.* 1994; Behkish *et al.* 2007). Increasing pressure from 1 bar up to 10 and 20 bar causes an increase of gas density 10 and 20 times (Table 2.7) so this might explain the smaller bubbles at higher pressure but does not explain the differences in the bubbles made of nitrogen and steam in paraffin oil (Figure 2.44).

#### 2.3.2.2.2 The effect of particles on the properties of the liquid phase

The presence of nitrogen in alumina and titania in oil results in larger bubbles. The presence of particles in the liquid leads to the increase of viscosity and density and consequently reduces breakage of the bubbles due to reduction of disruptive forces. Viscosities of 1% v/v particles suspended in oil (Experimental and methodology) changes insignificantly. The measured alumina/oil viscosity increased by 3%, silica by 1.7%, titania by 2.2% and zirconia by 3.1% as compared to the pure paraffin oil. Such an insignificant viscosity increase for 1% v/v particles also agrees with the literature correlations, and for all investigated systems, there is only 1.5% viscosity increase according to $\mu_{sl} = \mu_l \left[1 + 2.5\phi + 10\phi^2 + 0.00273(16.6\phi)\right]$ or $\mu_{sl} = \mu_l \exp\left[(5/3)\phi/(1-\phi)\right]$ (Thomas 1965, Barnea at al. 1973).

The density of particles/oil suspension, calculated from

$$\rho = \Phi_l \cdot \rho_l + \Phi_s \cdot \rho_s$$

also show insignificant changes (<1%) with 1% v/v particles.

Therefore the combined effect of the density and viscosity increase does not explain different bubble size in presence of different particles. For example, zirconia and silica particles do not affect the nitrogen bubble. Additionally, the viscosity and density of the 'slurry' where 1% v/v particles were suspended in oil with any chosen particles remains the same.

Surface tension measurements of micron-sized particles in oil did not reveal differences. Suspended particles sedimented in the beaker before the measurement with the Wilhelm plate could be performed. However, the particles can affect the properties of the gas-liquid interface, and the results on the bubble size measurements show a clear effect of the varying gas composition, i.e. nitrogen bubbles are significantly larger in alumina/oil than

steam ones and silica has the reversed effect, i.e. steam bubbles are larger than nitrogen ones (Figure 2.44). It also appears, that at intense turbulence (Re > 40,000), the bubbles remain similar for each type of particles (Figure 2.37). Apparently, particles tend to affect the interface at lower energy dissipation rates, as they might remain in the gas-liquid interface. Nevertheless, the bulk properties of the continuous phase are unaffected by the presence of solids which is in according with the published conclusions.

#### 2.3.2.2.3 Combined effect of gas composition and type of particles on the bubble size

##### 2.3.2.2.3.1 Gas phase

It appears that steam in the gas phase is a main reason for the significant difference in the bubble size in paraffin oil without particles (Figure 2.45). The insignificant change of the gas density does not explain the larger steam bubbles (Table 2.7). Therefore the effect of paraffin oil-air and oil-steam surface tension was considered in details on the bubble size in system without solids.

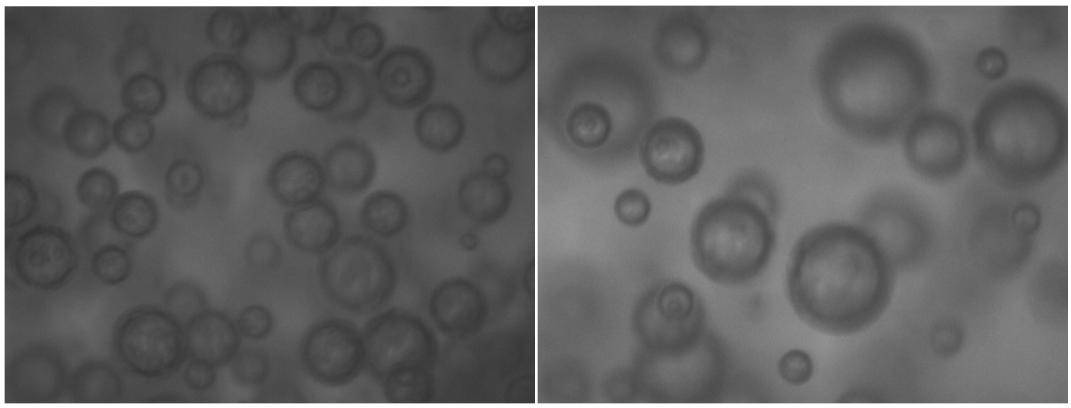

Figure 2.45 Nitrogen (a) and steam (b) dispersed in oil at 210C and 1bar (1.85 x 1.4 mm)

Measured oil-steam surface tension was much higher than the surface tension of oil-air (see Experimental and methodology), which were 31mN/m and 40 mN/m respectively. When

water replaces the air contacting the oil, the oil surface energy increases. This was confirmed by measurements of the oil-water interfacial tension (46mN/m,

Figure 2.18). This is caused by the nature of these liquids, i.e. water is polar (high dielectric constant) and oil non-polar (low dielectric constant). Polar liquid interacts through dispersive and polar forces; water surface tension divides into the dispersive part (20±2mN/m) and polar part (53mN/m) (Israelachvili 2011). Non-polar oil molecules interact with each other or with other molecules only through dispersive forces and $\gamma_o=\gamma_o^d$ (31mN/m) and hence with water interact only through dispersive forces. The water-paraffin oil interfacial tension can be calculated from the Dupré equation where the work of adhesion describes oil-water interactions through dispersive forces:

$$\gamma_{ow} = \gamma_o + \gamma_w - W_{ow} = \gamma_o + \gamma_w - 2\sqrt{\gamma_o^d \gamma_w^d}$$

Though calculated interfacial tension is larger (~53mN/m) than the measured one, the values clearly show that the surface/interfacial tension of oil increases when the air is replaced by water, i.e. with steam, the interfacial tension increases.

The above considerations agree with the results obtained for gas-liquid system, where nitrogen bubbles are smaller than those made of steam. The cohesive forces increase and the breakage is lower. Also, once the pressure of oil-steam is increased (up to 10, 20 bar) and the concentration of steam is significantly reduced (up to 10, 5%) the bubble sizes are comparable with the bubbles made of nitrogen only.

#### 2.3.2.2.3.2 Particles at the nitrogen-oil and steam-oil interface

The effect of particles on the gas bubbles changes considerably when the nitrogen is replaced by steam and the most pronounced differences are observed with alumina and silica particles. Though different studies argue whether bubble behaviour is altered by particles due to bubble coalescence suppression (as in emulsions) or enhancement (e.g. antifoaming behaviour), the attachment of the particles to the interface is inevitable for both mechanisms (Pickering 1907; Frye *et al.* 1989; Garrett 1993; Binks 2002; Binks *et al.* 2005). The results (Figure 2.37) suggest that nitrogen bubbles dispersed in the oil are affected by the particles that enhance coalescence, which is the case when alumina and titania particles are used. However, with the steam dispersed in oil, alumina and zirconia suppress bubbles coalescence but silica slightly increases the coalescence rate. If the particles presence in the gas-liquid interface is the key parameter, it can be concluded that alumina and titania are present in the nitrogen/liquid interface and silica and zirconia are not. It appears however that all particles are present in steam-oil interface but influence the bubbles coalescence differently, i.e. alumina and zirconia significantly reduce coalescence rate and to lower extent titania but silica enhances steam bubbles coalescence.

The coalescence inhibition, as a result of steric repulsion of the bubbles caused by the particles sitting at the interface (Pickering stabilisation) requires high coverage of bubbles by particles. In general, the higher the surface coverage, the better the Pickering stabilisation of the emulsions since the physical barrier is formed (Boode *et al.* 1993).

The extent of coverage of bubble by particles is important and can be accounted for by the concentration of particles used and the bubble sizes for each system. The maximum coverage that can be obtained is 78.54%, assuming that particles on the bubble surface are touching each other tightly, creating gaps in between the uncovered bubble surface area. The

coverage of bubbles in oil can be calculated from the number of particles of given surface area that occupy the total gas-liquid interfacial area (Boode *et al.* 1993):

$$Coverage = \frac{A_p \cdot n_p}{A_i}$$

where the surface area of cross section of single particle $A_p = \pi \cdot d_p^2/4$, number of particles $n_p = V_{p\,tot}/V_p$ and total surface area of dispersed gas $A_i = 6\,V_{gas}/d_b$. The volume of single particles $V_p = \pi \cdot d_p^3/6$ and the diameters of particles and bubbles are assumed to be equal Sauter mean diameters.

The coverage was calculated for the smallest and the highest energy dissipation rates with nitrogen and steam as dispersed gas. The coverage model enables an estimate of the maximum coverage that can be obtained with the amount of particles used and at the highest mixing intensity, the total gas is entrapped in the liquid therefore the coverage's are reliable. Assuming that the maximum coverage obtainable by tightly sticking particles to each other (78.54% as above) is equal to 100%, the coverage at 170°C and 1 bar is summarized in Table 2.18, where the example of calculated coverage is displayed for alumina particles (up to scale).

Table 2.18 The coverage of bubble with varying energy dissipation rate at 170°C, 1bar and the coverage by alumina up to scale

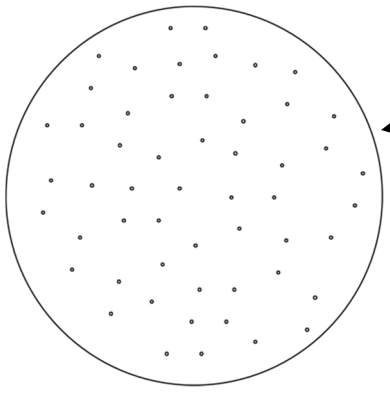

| | 36% Nitrogen 1 W/kg | 36% Nitrogen 18.3 W/kg | 36% Steam 1W/kg |
|---|---|---|---|
| Al2O3 | 12.2% | 4.6% | 10.1% |
| SiO2 | 12.4% | 6.5% | 15.8% |
| TiO2 | 89.9% | 38.8% | 87.7% |
| ZrO2 | 5.9% | 2.7% | 6.0% |

The coverage increases for increasing bubble size since the interfacial area decreases and the same number of particles are used. At the highest power input (18.3 W/kg) the coverage is the highest for the titania particles since is the smallest particle (compare $d_{32}$ and SEM). The coverage by the silica, alumina and zirconia are rather similar at the highest power input and this corresponds to the reversed proportionality of the particles diameter, i.e. largest zirconia forms the lowest coverage. The coverage obviously increases for the lower power input (1 W/kg) but the trend remains the same, i.e. the highest coverage found for titania and the lowest for zirconia. The example of coverage of the nitrogen bubble by alumina particles up to scale (Table 2.18) clearly shows that the alumina, silica and zirconia dispersion on the bubble surface is scarce assuming the total gas is entrapped in the liquid. As zirconia can form always the lowest coverage, caused by the large size, the effect on the bubble size is expected to be the lowest. In case of titania particles however the coverage is the highest due to the small particles size.

Such a simplistic model of bubble coverage can resolve the differences in the use of different particles on the bubble size. The coverage with the highest mixing intensity can explain why there is a small difference in bubble size when different particles are used, i.e. the maximum coverage by all the particles is the lowest, therefore their effect is less pronounced. Also, at such high energy dissipation rates, the time of bubbles remaining in close proximity might not be long enough to allow drainage of the liquid film between the bubbles and coalescence might not occur.

Nitrogen bubbles are unaffected by the zirconia particles (Figure 2.37). Zirconia particles creates the lowest coverage and are not able to form a dense cap around the nitrogen bubble, therefore stabilisation of bubble against the coalescence is inefficient. The lack of

influence of the zirconia on the nitrogen bubbles suggests that the particles have high affinity to the oil phase, i.e. are suspended in the liquid and remain absent at the bubble surface. Though the coverage of steam bubbles is similar, the steam bubble (Figure 2.37) are affected, i.e. the size decreases as compared to the steam-oil system without particles. This indicates interactions between zirconia particles and the steam-oil interface in a way that they suppress bubbles coalescence, although the steric repulsion of steam bubbles by the particles adsorbed at the interface is rather unlikely due to the low coverage (Table 2.18).

The results show that titania particles affect the bubbles differently: nitrogen bubble size is increased whereas steam bubble size is slightly decreased as compared to the system without particles (Figure 2.37). Titania particles are able to form dense coverage on nitrogen and steam bubbles (Table 2.18). It appears that in the case of nitrogen, the bridging mechanism occurs whereas with steam, bubbles coalescence seems to be suppressed by Pickering stabilisation. In the case of bubbles made of nitrogen, particles might have higher affinity to the air, i.e. are better wetted by an air than paraffin oil and particles remaining at the interface tend to be pushed into the bubble, drying out the oil film between bubbles. On the other hand, when bubbles are made of steam and with such high coverage (more than 100%) titania particles might remain strongly adsorbed at the interface without preference as for the steam or paraffin oil, effectively suppressing the coalescence rate through Pickering stabilisation.

Silica particles revealed no effect on nitrogen bubble size and only slightly increased steam bubble size. The coverage that particles are able to form on the steam bubbles is almost as twice as much as for steam bubbles, so the effect of particles on the bubbles is expected to be more pronounced with steam bubbles. However, comparable bubble sizes with the systems

without particles suggest lack of silica activity at the interface, i.e. particles tend to remain in the bulk of one phase.

Alumina particles tend to increase the nitrogen bubble size in the reactor whereas significantly decrease steam bubble size (at 170°C). Apparently, the bridging effect is responsible for the larger nitrogen bubbles where the thin liquid film between two approaching bubbles is drained more efficiently. Steam bubbles coalescence inhibition is present only at lower temperatures and the bubbles are enlarged at higher temperatures.

## 2.4 Conclusions

Differences in the bubble sizes were significantly different between different systems at low energy dissipation rates, i.e. in a range of crucial energies in the industrial slurry bubble columns. At high energy dissipation rates the differences between bubble sizes in different systems were insignificant what implies that at high energy dissipation rates the type of gas and /or particles does not affect interfacial area. Bubble sizes correlated with *We* gave higher exponents than theoretical ones for all investigated systems. The obtained exponents in systems with and without particles with different gas phase volume fractions were as follows:

1% v/v ~ -0.35; 25,000 < Re < 41,000 and ~ -0.52; 4,000 < Re < 7,000

5% v/v -0.22 to -42; 48,000 < Re < 80,000

35% v/v -0.29 to -0.425; 16,000 < Re < 80,000

Similarly, diluted as well as highly concentrated gas dispersions in oil with and without particles gave exponents of $\varepsilon$ within the range of -0.145 to -0.28 regardless of the gas volume fraction. This indicates that bubble breakage is not the only process determining the bubble size but also strong coalescence occurs.

There can be two reasons for such differences of the empirical and theoretical powers discrepancies. Firstly, at high energy dissipation rate, the amount of gas dispersed in liquid from the head space increases which lead to a) decrease of power input, therefore less efficient breakage and b) increased coalescence rate caused by larger volume fraction of dispersed gas. Secondly, there might be an error in the measurements of the bubble size with the Mastersizer, i.e. small bubbles (< 20μm) might remain undetected, therefore the equilibrium size shifted towards larger bubbles.

Correlations/theory with *We* and ε does not explain (Figure 2.46):

- Larger bubbles when steam is present in the system
- Different effect of catalyst supports on the bubble size

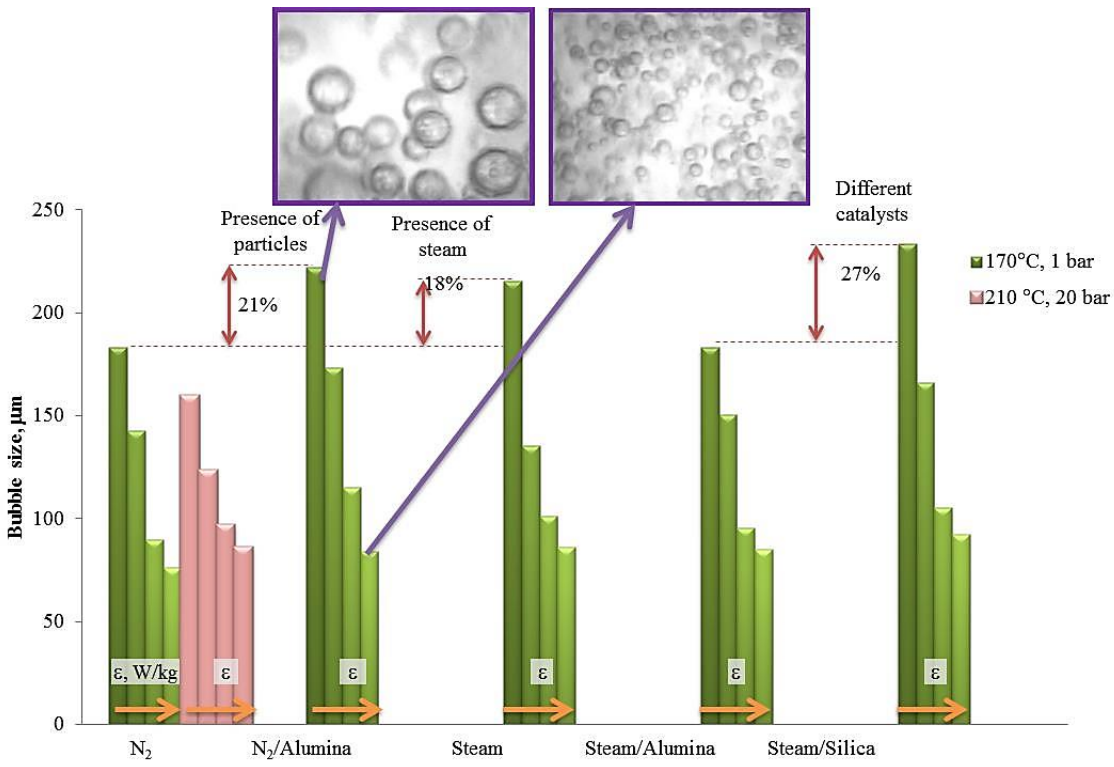


Figure 2.46 Nitrogen and steam bubble size (35%v/v) in oil at elevated temperature and pressure with and without catalyst

The effect of temperature on the bubbles sizes was significant in diluted dispersions where the temperature changed from 90->170°C at low energy dissipation rates. In the same systems however, the effect of temperature was insignificant at higher energy dissipation rates. With the high volume fraction the temperature change from 170 to 210°C show no difference in the bubble size. In highly concentrated systems, the effect of elevated pressure was significant when the gas phase consisted of steam. In such cases, the increase of pressure, i.e. decrease of steam concentration, led to decrease of bubble size.

Presence of steam might lead to significant mass transfer reduction and simulation of the FTS with dry gas is likely to bring wrong conclusions. Bubbles made of steam were significantly larger than those made of nitrogen (Figure 2.46) which is a direct result of increased interfacial tension between steam and oil as compared to air-oil surface tension, i.e. cohesive forces in steam bubbles are larger, i.e. less effective bubble breakage. Diluted systems showed no difference in the bubble size when air and nitrogen were compared.

Bubble sizes are different with different particles which in turn strongly depend on the type of gas used (Figure 2.47). At low gas volume fraction (1-5%) the effect of particles on the bubble size is unimportant whereas more significant differences are observed at a) high gas volume fractions (35%) and b) low energy dissipation rates that imitate the bubble columns conditions (Figure 2.46). The density and viscosity of paraffin oil were unaffected by the presence of particles, therefore the observed effect on bubbles is due to the particles activity at the gas-liquid interface.

Clearly, the particles affect the bubble behaviour, i.e. in the non-polar gas/ non-polar liquid the increase of bubbles occurs whereas in the polar gas/ non-polar liquid the reduction of bubbles was observed (Table 2.19). Presence of alumina and titania tend to increase

nitrogen bubbles whereas alumina and zirconia decreased the bubbles made of steam. Also, steam bubbles were slightly increased by silica particles and marginally decreased by titania. Though silica and alumina have similar size, there is clear difference between the bubbles made of either nitrogen of steam. It can be concluded that the surface properties of these particles are responsible for the observed bubbles size differences.

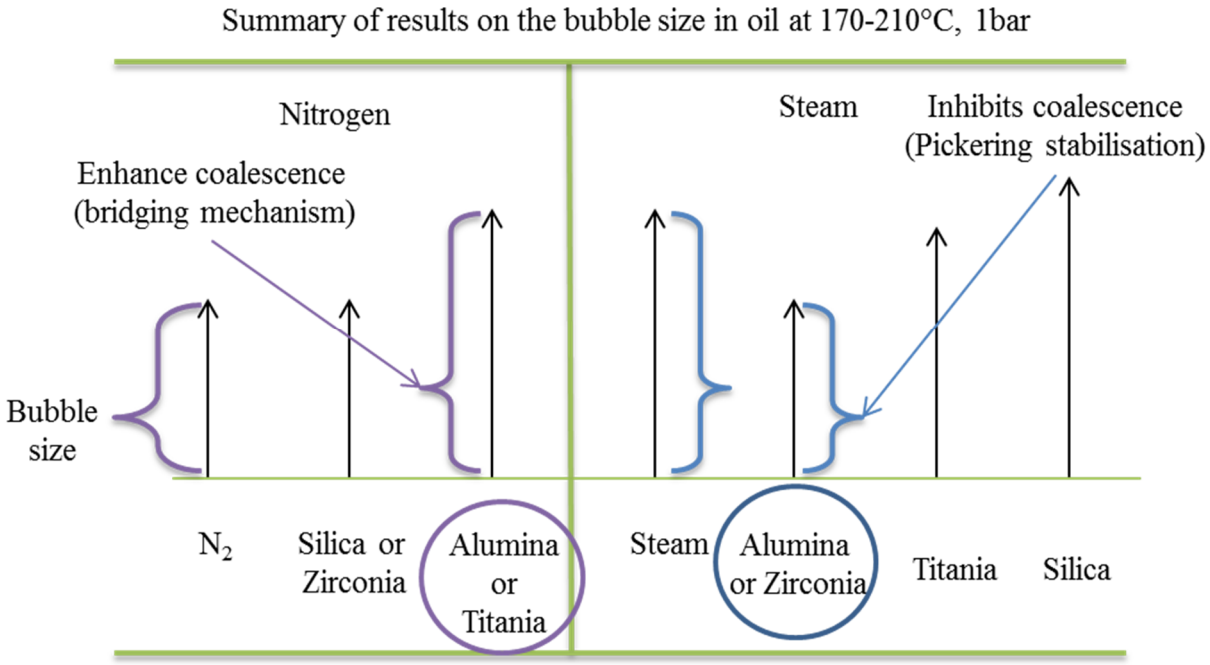


Figure 2.47 Effect of the catalyst particles on the bubble size (35% v/v dispersion)

Table 2.19 Effect of particles on the bubble size in 35% dispersion

| Gas type | Alumina | Silica | Titania | Zirconia |
|---|---|---|---|---|
| Non-polar (nitrogen) | ↑ | = | ↑ | = |
| Polar (steam) | ↓ | ↗ | ↘ | ↓ |

= does not affect, ↑ increases, ↓ decreases, ↗ slightly increases, ↘ slightly decreases

# Chapter 3

# 3 Contact angle measurements

Three phase interactions were investigated measuring the contact angle between particles and paraffin oil and water. Series of experiments were undertaken and initially carried out with the investigated porous particles. Experiments revealed several issues and the results were published in *Powder Technology* (see Appendix). It was found that different techniques produced variables contact angles and the porous particles. Therefore to identify the best technique for the measurements of contact angle between particles and water and paraffin oil, the non-porous particles with varying degree of hydrophobicity were tested and the findings were submitted for publication in *Powder Technology* (see Appendix).

Three phase contact angles do not fully describe the interactions between paraffin oil – catalyst particles – gas bubble. The complete spreading of oil over silica, zirconia and alumina particles (contact angle close to 0) makes differentiation between particles very difficult, and indicate that none are lyophobic therefore none of these particles tend to remain at the gas-liquid interface. Contact angle measured at room temperature however can be misleading when elevated temperature is considered, e.g. in the reaction conditions, since it is known that the surface tension/energy is a function of temperature. The wettability of particles is also affected.

The aim of the next chapters, Chapter 4 and 5, was to investigate and assess the particles attachment to fluid/liquid interface. In the first approach, the ability of particles to spontaneously attach to the gas bubble in paraffin oil was determined using the variables of equilibrium thermodynamics, based on the experimentally obtained surface energy of particles. In the second approach, the set of experiments that aimed to visualise the presence of particles at the fluid-fluid interface were carried out.

The following, alternative methods for the particles wettability and attachment at the interface were investigated:

(i) Surface energy of catalyst particles

The total surface energy is a sum of dispersive and polar components. The dispersive component of surface free energy of catalyst particles ($Al_2O_3$, $SiO_2$ and $ZrO_2$) was measured experimentally using inverse gas chromatography. The tendency of the particles to attach to bubble suspended in non-polar paraffin oil was subsequently determined based on the gain of the minimum energy in three phase system (thermodynamical approach).

(ii) Particles at fluid/liquid interface

Set of experiments aimed at imagining/visualisation of the catalyst particles at the interface were carried out. The particles attachment to air bubble suspended in water and in oil was investigated. Subsequently the particles adsorption at the water-oil interface was investigated by formation of the droplet of water in paraffin oil and by formation of the droplet of paraffin oil in water. Finally, the ability of particles to stabilise the oil-water emulsion by adsorption at the interface was investigated.

# Chapter 4

# 4 Surface energy of catalyst particles

## 4.1 Surface energy of catalyst particles

Three phase contact angles do not fully describe the interactions between paraffin oil – catalyst particles – gas bubble (Chapter 3, see Appendix). The complete spreading of oil over silica, zirconia and alumina particles (contact angle close to 0) makes differentiation between particles very difficult, and indicate that none are lyophobic therefore none of these particles tend to remain at the gas-liquid interface. Contact angle measured at room temperature however can be misleading when elevated temperature is considered, e.g. in the reaction conditions, since it is known that the surface tension/energy is a function of temperature. The wettability of particles is also affected. Knowledge of the particles surface energy allows calculations of the strength of the interactions between liquid and solid, which ultimately enables establishing the particle position with respect to the gas-liquid interface even at elevated temperature.

The strength of interaction between solid and liquid is directly related to the surface energy of the solid and the surface tension of the liquid, commonly expressed as work of adhesion (Israelachvili 2011):

$$W_{adh} = \gamma_l + \gamma_s - \gamma_{sl} \tag{4.1}$$

This means that the higher the energy of adhesion the stronger the bonding between the liquid and the solid surface, e.g. excellent spreading of liquid on the solid surface. Similarly, the work of cohesion represents the strength of bonding of similar material, and for liquid:

$$W_{coh} = 2\gamma_l \tag{4.2}$$

In the case of partial wetting, where the three phase contact angle is formed, the work of adhesion can be estimated from Young and Dupree equation (Berg 1993):

$$W_{adh} = \gamma_l \left(1 + \cos\theta\right) \tag{4.3}$$

In general, the high energy solids are well wetted by liquids and the lower the surface tension of the liquid the better wetting. On the other hand, the lower the surface energy of solid, the weaker bonding ability and larger contact angles are formed. For example non-polar PTFE tape (surface energy approx. 18 mJ/m$^2$ (Cosgrove 2005)) forms large contact angle with water (150°) and relatively high with low surface tension non-polar liquids (e.g. with n-octane 40°). When the liquid surface tension is significantly lower than the solid surface energy (such as MgO 1,200 mJ/m$^2$ and decane 24 mN/m) liquid completely wets solid surface (Cosgrove 2005).

The relative significance of the relation between surface energy of a solid and the surface tension with a liquid on the wettability is shown in Figure 4.1. Presented differences in wettability result from the balance between the force of adhesion (solid-liquid) and cohesion (liquid-liquid). Larger or comparable adhesive to cohesive forces (Figure 4.1a) cause complete spreading of liquid over the solid surface whereas adhesion forces significantly lower than cohesion results in non-wetting (Figure 4.1c) (Cosgrove 2005).

a) $\gamma_{solid} >> \gamma_{liquid}$ 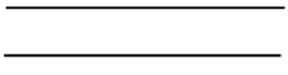 $W_{adh} \geq W_{coh}$

b) $\gamma_{solid} \approx \gamma_{liquid}$  $2W_{adh} = W_{coh}$

c) $\gamma_{solid} << \gamma_{liquid}$ 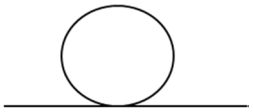 $W_{adh} = 0$

Figure 4.1 The effect of magnitude of surface energy/tension of solid and liquid on the wettability

Wettability, determined by the magnitude of the solid surface energy and liquid tension has a direct impact on the ability of solid particles to stick to the bubble (in liquid). The particle to bubble attachment involves three interfaces solid-gas, solid-liquid and liquid-gas. The change in Gibbs energy of the initially suspended particle in liquid that is attached to the gas bubble and remains there is given by (Norde 2003):

$$\Delta G = \gamma_s - \left(\gamma_{sl} + \gamma_l\right) \tag{4.4}$$

The attachment is favourable/spontaneous for the negative changes of Gibbs energy ($\Delta G<0$); the larger negative value, the stronger attachment occurs (per unit interfacial area). Such reduction of the three phase system energy is driven by the reduction of the solid surface free energy, where the solid contacting gas is replaced with liquid that strongly interacts with solid surface. Equation (4.4) combined with the Young-Dupree equation yields:

$$\Delta G = \gamma_l \left(\cos\theta - 1\right) \tag{4.5}$$

It is therefore clear that energetically favourable particle to bubble attachment occurs when the contact angle is larger than 0 ($\theta > 0°$) and $\theta>20°$ is considered as criteria for efficient attachment (Norde 2003). Therefore the knowledge of the surface energy of particles and the interfacial energy enables prediction of the three phase contact angle and the particles position in respect to the gas-liquid interface.

The interactions between liquid molecules and solid surfaces have the following molecular sources (Grajek *et al.* 2010; Israelachvili 2011):

- non-polar forces where the molecules are attracted by the dispersive (London) forces. Typical groups are hydrocarbons -$C_mH_{2m+1}$ and silicones, where the electrons are not preferentially localized, therefore there is lack of molecule permanent polarization.
- polar forces where polarity is caused by the presence of electronegative atoms and uneven sharing/distribution of the electrons within a bond, hence formation of the partial charge pole. This type of interactions includes the hydrogen bonding, acceptor-donor (Lewis acid-base), π-bonds and any other electrostatic forces; the example of such groups that are responsible for the polar nature of interactions are: -OH, -$NH_2$, -COOH, -$OSO_3H$, -$NH_3^+$, -$COO^-$.

The sum of these fundamental polar and non-polar forces gives the total magnitude of solid-liquid interactions (Fowkes 1987). The dispersive forces are involved whenever two different surfaces (e.g. solid-liquid) are in contact whereas the polar forces are only present when both, contacting liquid and solid, contain the polar components. If one of the materials (solid or liquid) is non-polar, the interactions are only due to the dispersive forces. For instance, the hydrophilic nature of a metal oxide surface is dictated by the presence of polar groups (usually -OH) which are able to form hydrogen bonds with water and once those are not present or accessible for water, the surface reveals hydrophobic nature (Peršin *et al.* 2004).

The forces that are involved in the solid – liquid (both polar) interactions yield the dispersive and polar components of the interfacial energy (Fowkes 1962; Fowkes 1964):

$$\gamma_{sl} = \gamma_l + \gamma_s - 2\left(\gamma_s^{\,d} \cdot \gamma_l^{\,d}\right)^{1/2} - 2\left(\gamma_s^{\,sp} \cdot \gamma_l^{\,sp}\right)^{1/2} \qquad (4.6)$$

and for the non-polar liquid, the solid-liquid interfacial energy depends on the surface tension/energy and dispersive components only (Fowkes 1962):

$$\gamma_{sl} = \gamma_l + \gamma_s - 2\left(\gamma_s^{\,d} \cdot \gamma_l^{\,d}\right)^{1/2} \tag{4.7}$$

Interactions between catalyst supports and paraffin oil are only due to dispersive forces (always present) as the paraffin oil is a non polar liquid. Therefore knowledge of the dispersive component of the particle surface energy enables calculation of the strength of the adhesion between paraffin oil and particles from equations (4.1) and (4.7). Subsequently the contact angle can be calculated from equation (4.3) which in turn allows prediction if the particles to bubble attachment in paraffin oil would be favourable in the reaction temperature (e.g. Fischer Tropsch synthesis ~210°C) based on Gibbs energy of the three phase system determined from equation (4.5).

### 4.1.1 Determination of the solid surface energy

The surface energy of solids is usually unknown and the values cannot be tabularised like surface tensions of liquids because it strongly dependents on the solid surface treatments or the way particles are produced and for the same material can be very different. Amongst the indirect methods for the surface energy measurements of flat solid, the contact angle measurements with selected liquids are the most common. As it was shown in Chapter 3, the measurements of the porous particles contact angle are difficult and for the porous particles, the inverse gas chromatography recently been used for the characterisation of thermodynamical properties of particles (Das *et al.* 2010; Ho *et al.* 2010; Shi *et al.* 2011).

### 4.1.2 Surface energy form the contact angle measurements

This approach can be only used when the liquid does not wet the solid entirely, and the contact angle is formed, i.e. for solids with relatively low surface energies (Schultz *et al.* 1977). Basically, two components of surface energy of solid can be measured separately, the dispersive part and the polar part, depending on the nature of selected liquids (polar, non-polar).

Measurements of contact angles with non-polar liquids of different surface tensions lead to the calculation of the dispersive component of solid surface energy commonly known as Zisman's critical surface tension (Shafrin *et al*. 1967). Zisman's approach is particularly useful for the polymers surface energy calculations since their dispersive part is often equal the total surface energy (no polar groups on the surface). Based on the contact angle measurements with non polar liquids of different surface tensions, the experimental values are plotted against surface tensions of liquids as a straight line. This line is extrapolated to a zero contact angles ($\cos\theta=1$) and such obtained from the cross-section value of surface energy is assumed to be equal to dispersive component of surface energy (Żenkiewicz 2007).

Measured contact angles with polar and non-polar liquids of known surface tensions are used to calculate both, dispersive and polar components of solid surface energy (Fowkes *et al.* 1978; Van Oss *et al.* 1988). Young equation together with Dupree and the Owens-Wendt-Rabel-Kaeble approximation can be rearrange to (Peršin *et al.* 2004):

$$\gamma_l\left(1+\cos\theta\right)=2\left(\gamma_s{}^{d}\cdot\gamma_l{}^{d}\right)^{1/2}+2\left(\gamma_s{}^{sp}\cdot\gamma_l{}^{sp}\right)^{1/2} \tag{4.8}$$

So, from measured contact angles with non-polar liquids, where only dispersive forces affect the interactions, the dispersive component of solid surface energy can be obtained:

$$\gamma_s = \gamma_s^{\,d} = 1/4 \cdot \gamma_l \left(1+\cos\theta\right)^2 \tag{4.9}$$

Subsequently, (for the non-polar solid) the contact angles with polar liquids give the polar (polar) component of solid surface free energy:

$$\gamma_s^{\,sp} = \left(1/2 \cdot \gamma_l \left(1+\cos\theta\right) - \left(\gamma_s^{\,d} \cdot \gamma_l^{\,d}\right)^{1/2}\right)^2 / \gamma_l^{\,sp} \tag{4.10}$$

The sum of the respective, polar and non-polar component gives the total value of surface free energy.

It has to be stressed, that surface free energy of solids obtained from the contact angle measurements gives the values of energy in the presence of vapour and strongly depends on vapour composition and pressure. The difference between absolute surface free energy of solid and the measured in presence of vapour is called surface pressure ($\gamma sv = \gamma s - \pi sl$) (van Oss *et al.* 1998) and this reduction is caused by the adsorption of the liquid molecules from the solid-vapour interface. It is important to notice that the high energy solid surfaces are easily contaminated in the air environment, reducing the surface energy drastically, e.g. in case of mica from thousands of mJ/m2 measured in ultrahigh vacuum to about 500 mJ/m2 in air.

### 4.1.3 Inverse gas chromatography (IGC)

This method is virtually the opposite of the traditional gas chromatography, since here the known liquid probes are injected into a column filled with investigate solid particles. The strength of adsorbate (liquid) – adsorbent (solid) interactions reveals as a retention time of liquid vapour in the column. Using IGC, physical properties, such as adsorption isotherms, heats of adsorption, solubility coefficients, free energy of adsorption, surface free energy,

polar and dispersive components can be determined (Diaz *et al.* 2004). IGC is commonly used to assess thermodynamical properties in pharmaceutical industry (Grimsey *et al.* 2002), coatings (Hegedus *et al.* 1993) and also of composite particles (York *et al.* 1998).

In this method, the chromatographic column is packed with investigated solid. The liquid vapour (probe) is than passed through the column, carried by the inert gas. In order to avoid the adsorbate - adsorbate interactions, the liquid probes are injected in infinite dilution, in which case the Henry's law holds (Mukhopadhyay *et al.* 1995). The interactions between adsorbate (probes) and adsorbent (solids) are characterized by the net retention volume. The retention time ($t_r$) of the liquid probes, i.e. the time that the probe vapour passes through the packed column, is converted into retention volume (Xie *et al.* 2000):

$$V_N = jF\left(t_r - t_0\right)CT \tag{4.11}$$

where the James-Martin factor (j) for the correction of gas compressibility under pressure difference between column inlet ($P_{in}$) and column outlet ($P_{out}$):

$$j = \frac{2}{3}\frac{\left[\frac{P_{in}}{P_{out}}\right]^2 - 1}{\left[\frac{P_{in}}{P_{out}}\right]^3 - 1} \tag{4.12}$$

$$C = 1 - \frac{P_{H_2O}}{P_{out}} \tag{4.13}$$

$$T = \frac{T_{col}}{T_{meter}} \tag{4.14}$$

The retention volume is related to the thermodynamic functions by the adsorption energy (free energy of transfer of molecules from gas to solid phase) (Liu *et al.* 1998; Grajek *et al.* 2010):

$$\Delta G_{ads} = -RT \ln\left(\frac{PV_N}{\pi_0 S_{BET}}\right) \tag{4.15}$$

For a given system the P, $\pi_0$ and $S_{BET}$ are constant, hence the adsorption energy takes the form of:

$$\Delta G_{ads} = -RT \ln V_N + const \tag{4.16}$$

As previously discussed the adsorption of probe molecules results from dispersive and polar types of interactions and it is related to the work of adhesion by:

$$\Delta G_{ads} = -N_A a_p W_{adh} \tag{4.17}$$

where $a_p$ is a molecular area of adsorbed molecule:

$$a_p = 1.09 \cdot 10^{14}\left(\frac{M}{\rho N_A}\right)^{2/3} \tag{4.18}$$

The connection between the adsorption energy and the work of adhesion allows the surface energy of solid particles calculation. For the non-polar liquids (probes) the dispersive component of surface energy can be obtained. Similarly, the adsorption of probe liquids which contain polar groups (polar) can give the magnitude of such polar surface energy of solids.

The dispersive surface energy of solid can be calculated using two approaches:

- Schultz approach (Newell *et al.* 2001)

$$RT \ln V_N = 2N_A\left(y_s^d\right)^{1/2} a\left(\gamma_l^d\right)^{1/2} + const \tag{4.19}$$

- Dorris and Gray (Grajek *et al.* 2010)

$$\frac{-\Delta G_{ads(CH_2)}}{N_A a_{CH_2}} = 2\left(\gamma_{CH_2}\gamma_s^d\right)^{1/2} \tag{4.20}$$

where the free energy of adsorption of single chain of hydrocarbons (methylene group) is experimentally determined from the retention volumes of two consecutive n-alkanes:

$$\Delta G_{ads(CH_2)} = RT \ln \frac{V_{N+1}}{V_N} \tag{4.21}$$

The polar interactions can be subsequently determined once the energy of adsorption of non-polar probe is calculated:

$$I^{sp} = W_{adh}^{sp} = -\frac{\Delta\left(\Delta G_{ads}\right)}{N_A a} \tag{4.22}$$

The total surface energy is the sum of dispersive and polar surface components and are different for different polar probes, strictly dependent on the functional groups of liquid. $I^{sp}$ are the polar component of surface free energy of solid when interact with given (polar) liquid probe (Xie *et al.* 2000).

## 4.2 Materials and methods

Gas chromatograph (GC) Perkin-Elmer 8500 (Figure 4.2a) equipped with the flame ionization detector and copper columns, that can handle both high temperature and pressure (length of 30cm and inner diameter 2mm, Figure 4.2b) was used. The vacuum pump was used to fill these columns with powders and subsequently the columns were sealed with silanized wool at the both ends. It was impossible to fill the column with $TiO_2$ because of its very small size. Each column was left for 24h at 100°C n the GC equipment with inert gas passing through in

order to remove impurities and vapour (at least partially). The temperature of the injection port was set at 230°C to ensure evaporation of injected liquids (above the boiling point of all liquids). Gas flow rates were measured using bubble flowmeter. The injections were repeated 3 times for each liquid and the average time was used in calculations. The time of passing non-adsorbing probe (dead time) was measured using methane. Table 4.1 summarizes conditions used in experiments. The properties of alkanes and acid and base tested liquid probes are summarized in Table 4.2.

Table 4.1 The conditions (T, P) and appropriate flow rates used in experiments

| | | $Al_2O_3$ | $SiO_2$ | $ZrO_2$ |
|---|---|---|---|---|
| Mass, g | | 0.4593 | 0.3691 | 0.5926 |
| P, bar | | 5.11 | 3.44 | 1.72 |
| Flow rates at column temperature, ml/min | 100°C | 10 | 4 | 33 |
| | 140°C | 8.82 | 3.66 | 29.9 |
| | 180°C | 7.69 | 3.22 | 25 |
| | 210°C | 7.14 | 3 | 18.7 |

Table 4.2 Properties of liquid probes used in experiments (Rodriguez *et al.* 1997; Liu *et al.* 1998)

| Liquid probes | $a_p$ Å | $\gamma_l^d$ mN/m | Acid number kcal/mol | Donor number kcal/mol |
|---|---|---|---|---|
| n-hexane | 51.1 | 18.4 | - | - |
| n-heptane | 57 | 20.3 | - | - |
| n-octane | 63 | 21.3 | - | - |
| n-nonane | 69 | 22.7 | - | - |
| Dichloromethane (acid) | 31.5 | 27.6 | 20.4 | 0 |
| Tetrahydrofuran (base) | 45 | 22.5 | 8.0 | 20.1 |

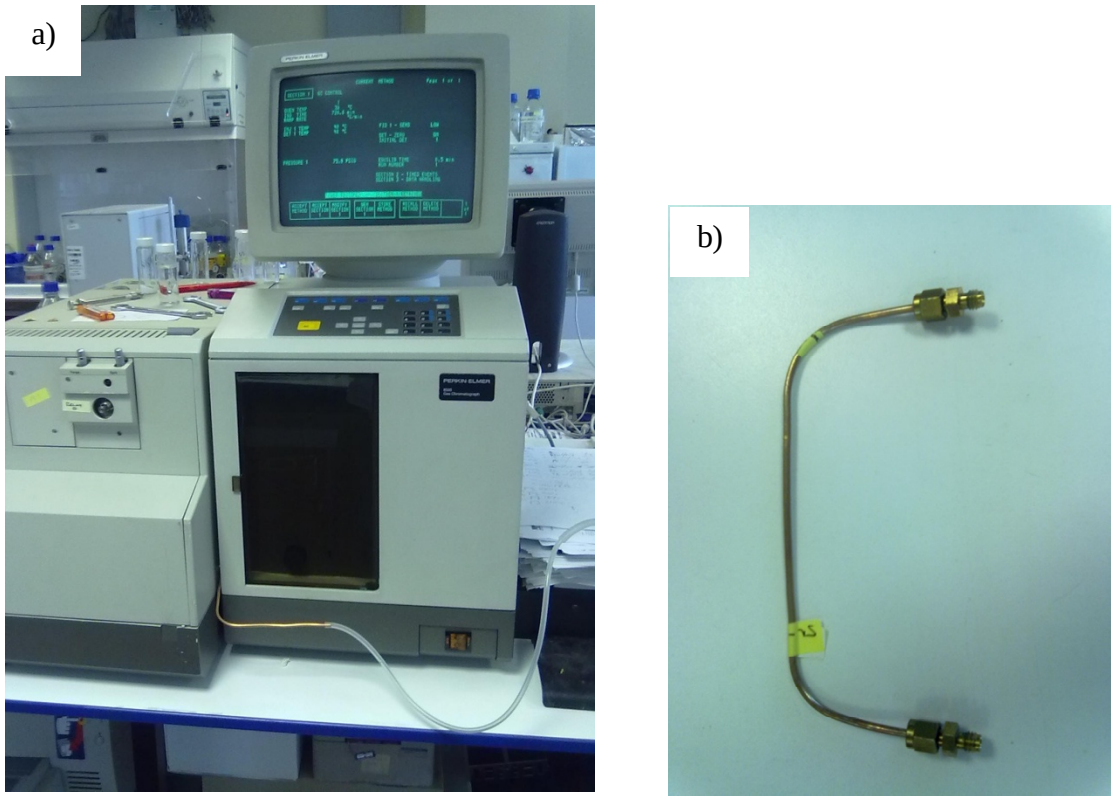


Figure 4.2 Gas chromatograph (a) and column (b) used for the surface energy of catalyst supports measurements

## 4.3 Results and discussion

### 4.3.1 Surface energy from the contact angle measurements

Adhesive glass method (Chapter 3) was used for the measurements of contact angles. Particles were sprinkle over the adhesive tape and the contact angle between the particles and the range of hydrocarbons ($C_6H_{14}$-$C_{16}H_{34}$) were measured. All these liquids spread immediately (< 1s) on the surfaces made of $Al_2O_3$, $SiO_2$, $TiO_2$ and $ZrO_2$ particles therefore the contact angle could not be determined. Therefore the calculation of the dispersive component of particles surface energy from the contact angles formed with non-polar liquids (equation (4.9)) was not possible.

Complete spreading of hydrocarbons ($C_6$-$C_{16}$) indicates that the surface energies of all particles are higher than the surface tension of these liquids (see Figure 4.1). The surface tension of $C_6H_{14}$-$C_{16}H_{34}$ is between 18.5 and 27.5mN/m (Sigma-Aldrich), and hence it can be concluded that measurements of contact angles indicate that the dispersive components of surface energy of all investigated particles are above 27.5mN/m, i.e. higher that the surface tension of $C_{16}H_{34}$.

### 4.3.2 Inverse gas chromatography

#### 4.3.2.1 Dispersive component of surface energy

The accuracy and reproducibility of the measurements using inverse gas chromatography was determined by comparison of the retention time of the same liquid probe injected 3 times into the same column filled with particles. In such a way, the time required for the liquid probe to pass through and leave the column was compared based on triple injection. On the other hand, the effect of column packing on the calculated surface energy of particles was tested by comparing the data from three identically prepared columns, i.e. each was filled with alumina.

The average retention times of the alkane probes passing through the column filled with particles are summarised in Table 4.3. As expected, the larger molecular weight, the longer the time the probe stays in the column. The reproducibility of measurements was very good confirming that the adsorption was reversible.

Table 4.3 Average retention times (tr) with standard deviations of 3 injections of liquid probes

| | | Alumina | | Silica | | Zirconia | |
|---|---|---|---|---|---|---|---|
| Temp. | Probes | $t_r$, min | σ, min | $t_r$, min | σ, min | $t_r$, min | σ, min |
| 100°C | n-hexane | 4.1 | 0.13 | 4.9 | 0.07 | 1.3 | 0.01 |
| | n-heptane | 8.9 | 0.23 | 8.3 | 0.14 | 3.6 | 0.21 |
| | n-octane | 20.4 | 0.12 | 15.4 | 0.21 | 11.6 | 0.08 |
| | n-nonane | 45.5 | 1.35 | 29.4 | 0.23 | 30.2 | 0.95 |
| 140°C | n-hexane | 1.9 | 0.1 | 2.4 | 0.20 | 0.8 | 0.06 |
| | n-heptane | 3.2 | 0.1 | 3.5 | 0.05 | 2.0 | 0.10 |
| | n-octane | 5.8 | 0.14 | 5.3 | 0.08 | 4.9 | 0.28 |
| | n-nonane | 11.1 | 0.51 | 8.5 | 0.01 | 13.1 | 0.86 |
| 180°C | n-hexane | 1.1 | 0.06 | 1.8 | 0.39 | 0.3 | 0.04 |
| | n-heptane | 1.4 | 0.08 | 2.1 | 0.08 | 0.5 | 0.03 |
| | n-octane | 2.3 | 0.05 | 2.9 | 0.22 | 1.0 | 0.04 |
| | n-nonane | 3.9 | 0.1 | 3.7 | 0.19 | 1.9 | 0.05 |
| 210°C | n-hexane | 0.8 | 0.06 | 1.3 | 0.17 | 0.2 | 0.02 |
| | n-heptane | 1.0 | 0.01 | 1.6 | 0.06 | 0.3 | 0.03 |
| | n-octane | 1.4 | 0.03 | 2.0 | 0.08 | 0.5 | 0.03 |
| | n-nonane | 2.0 | 0.01 | 2.5 | 0.22 | 0.8 | 0.02 |

High reproducibility and accuracy was also confirmed by the dispersive component of surface energy of alumina particles obtained from the calculations from three identical columns. The dispersive components of surface free energies were calculated based on the Schultz approach (equation (4.19)) and are shown in Table 4.4, where also standard deviations are given.

Table 4.4 Average values of dispersive component of $Al_2O_3$ surface free energy and standard deviations from 3 different columns

| Temperature °C | $\gamma_s^{disp}$ mJ/m$^2$ | σ |
|---|---|---|
| 100 | 41.38 | 3.46 |
| 140 | 31.33 | 2.92 |
| 180 | 26.87 | 2.03 |
| 210 | 23.18 | 0.79 |

Clearly, the reproducibility is very good. Though differences in column packing are inevitable and in chromatography it is accepted that availability of the high energetic centres on the particles surface might be different, the above results suggest very similar distributions of these centres.

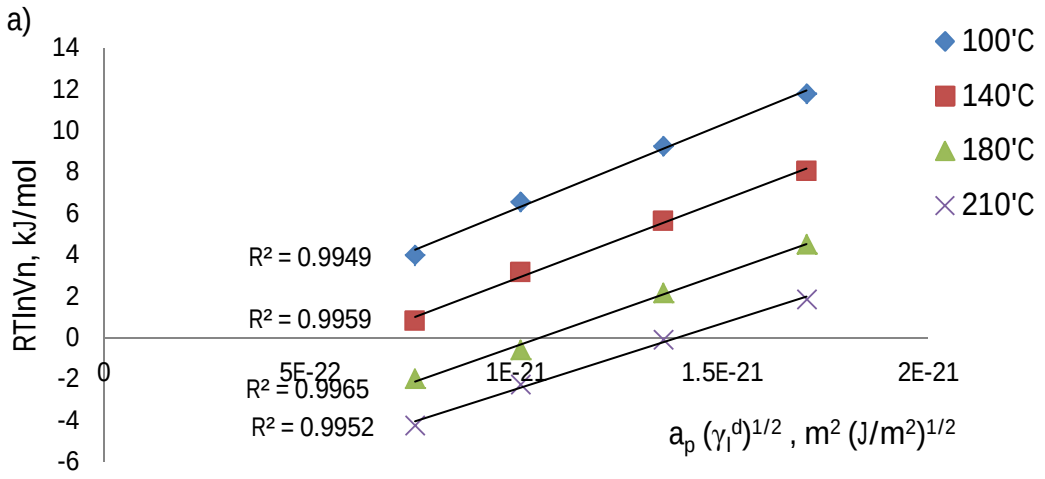

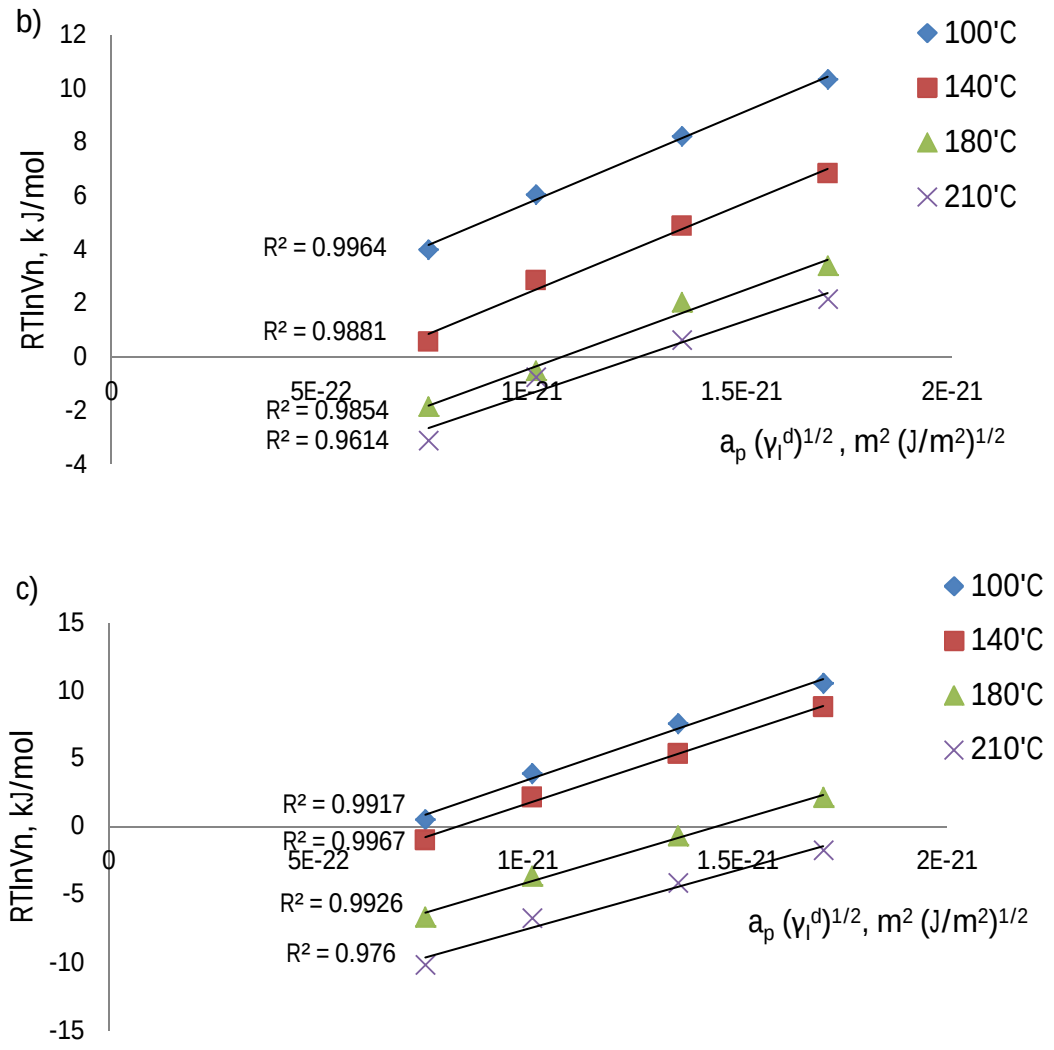


Figure 4.3 The adsorption free energies of the alkanes on the a) $Al_2O_3$, b) $SiO_2$ and c) $ZrO_2$ in a function of temperature

The linear regression show clear proportionality between the adsorption energy, $\Delta G_{ads}$ (equation (4.16)), and the molecular weight of alkane (Figure 4.3). Additionally, the regression coefficients were larger than 0.99 for lower temperatures for all particles, suggesting good correlation between molecule size and adsorption. Regression coefficients were lower than 0.99 for the highest temperatures ($SiO_2$ and $ZrO_2$) what most probably can be attributed to the entropic contribution related to the modification of the surface caused by high temperature (Diaz *et al.* 2004). The free energy of adsorption of the consecutive alkanes

increased with the increasing molecule size , i.e. for larger number of alkyl groups (-$CH_3$) the dispersive forces between particles and non-polar liquids increases. The adsorption energies decrease at higher temperatures which is in good agreement with the van't Hoff equation (Xie *et al.* 2000) according to which there is linear adsorption and retention due to the thermodynamical equilibrium of adsorbent and adsorbant.

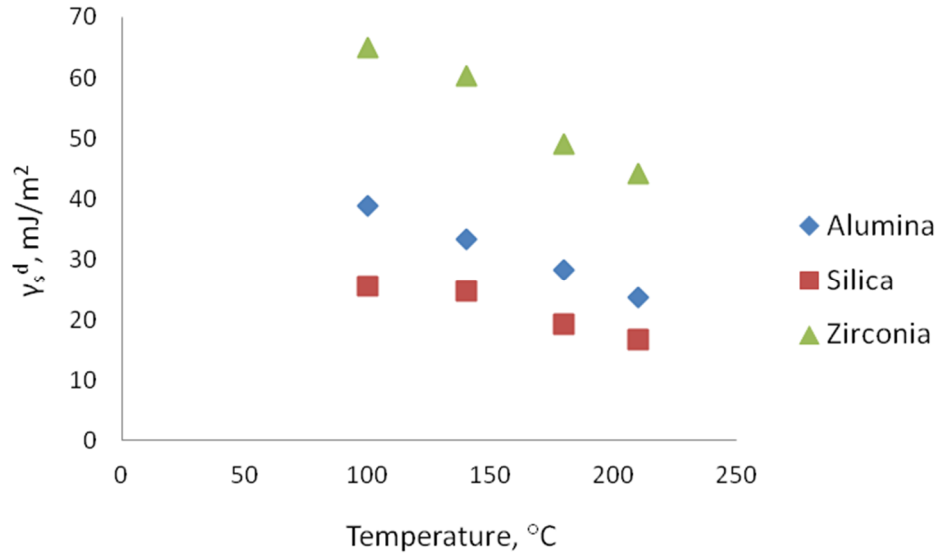


Figure 4.4 Dispersive component of surface energy of catalyst supports as a function of temperature

The dispersive components of surface free energy for $Al_2O_3$, $SiO_2$ and $ZrO_2$ in function of temperature, calculated from equation (4.19), are shown in Figure 4.4 and in Table 4.4. Diaz *et al.* (2004) found surface free energy of γ-$Al_2O_3$ using inverse gas chromatography to be 59.3 mJ/m$^2$ at 200°C whereas this studies gives 25.3 mJ/m$^2$ for alumina at this temperature (Table 4.4). Similarly, literature values for the dispersive parts of surface free energies of crystalline silica and fused silica are 31.78 mJ/m$^2$ and 37.81 mJ/m$^2$ at 140°C respectively and in this study it was found equal to 24.8 mJ/m$^2$ (Yang *et al.* 2007). Though values are rather similar for silica particles, the disagreement between the surface energy of

different batches of similar particles is expected to be different. Obviously, one could not expected the same values of dispersive part of surface free energy of particles used in this project and the literature data since the surface treatment or the catalyst production method significantly affect surface properties therefore surface energy.

Common tendency for all investigated particles is the decrease of dispersive component of surface energy with temperature. Such behaviour was expected since the excess of surface energy at the liquid surface (surface tension) also decreases with temperature. Similar tendency, where the surface free energy of particles decreases with temperature was reported for the $Pd/Al_2O_3$ (Diaz *et al.* 2004), Pd/SDB catalysts (Xie *et al.* 2000) and the activated carbons (Diaz *et al.* 2005).

Knowledge of the dispersive component of the particles surface energy allows estimation of the strength of particle to bubble attachment when they are dispersed in paraffin oil (non-polar liquid). Appropriate equations showed in Introduction allowed the calculations of the dispersive components of surface free energy ($\gamma_s^d$), Gibbs free energy of particle attachment to bubble in vara oil ($\Delta G$), work of adhesion ($W_{adh}$) and finally the contact angles between particle and paraffin oil. All these values were determined for $Al_2O_3$, $SiO_2$ and $ZrO_2$ particles at room temperature and also at temperatures of the Fischer Tropsch process and are summarised in Table 4.5.

Table 4.5 Dispersive component of surface free energy, Gibbs energy of particle to bubble attachment and cosine of contact angle of particles in function of temperature

| | | Alumina | Silica | Zirconia |
|---|---|---|---|---|
| 25°C | $\gamma_s^d$, mJ/m$^2$ | 49 | 33 | 81 |
| | $\Delta G$, mJ/m$^2$ | 16 | 2 | 38 |
| | $W_{adh}$, mJ/m$^2$ | 78 | 64 | 100 |
| | cosθ, - | 1.5* | 1.1* | 2.2* |
| | θ, ° | | | |
| 170°C | $\gamma_s^d$, mJ/m$^2$ | 29 | 21 | 52 |
| | $\Delta G$, mJ/m$^2$ | 7 | -2 | 24 |
| | $W_{adh}$, mJ/m$^2$ | 51 | 43 | 68 |
| | cosθ, - | 1.3* | 0.9 | 2.1* |
| | θ, ° | | 23 | |
| 210°C | $\gamma_s^d$, mJ/m$^2$ | 24 | 17 | 44 |
| | $\Delta G$, mJ/m$^2$ | 4 | -3 | 20 |
| | $W_{adh}$, mJ/m$^2$ | 43 | 36 | 59 |
| | cosθ, - | 1.2* | 0.8 | 2.0* |
| | θ, ° | | 33 | |

* calculated with no physical meaning

At ambient temperature, the dispersive component of surface energy of $Al_2O_3$, $SiO_2$ and $ZrO_2$ particles is higher than the surface tension of paraffin oil (31.15mN/m). Since the surface tension of paraffin oil is relatively low, as compared to the calculated dispersive components of surface energies of particles, it can be concluded that the oil will spread over the particles according to the rule that low surface tension liquid spreads over higher surface energy solid. Similar results, i.e. complete spreading at room temperature was also observed when the measurements of contact angle between the paraffin oil and the particles were carried out (Chapter 3) and zero contact angle was obtained for alumina, silica and zirconia. The non-zero contact angle obtained for the titania particles allows calculation of the dispersive component of the surface energy from equation (4.9). The measured contact angle between titania particles and paraffin oil was 20° using adhesive glass slide technique (Chapter 3) therefore the dispersive component of titania surface energy at room temperature

equals to 29.3mJ/m$^2$. Calculated cos$\theta$ are larger than 1 what indicates complete spreading of paraffin oil on for alumina, silica and zirconia particles (Table 4.5). The consequence of high surface energy (dispersive part) is that in the three phase system (air/paraffin oil/particles) at ambient conditions the particles will tend to remain in the bulk of paraffin oil since the complete spreading is expected. Indeed, calculated Gibbs energy upon the particles attachment ($\Delta G$) is positive for alumina, silica and zirconia particles (Table 4.5), indicating that the particles tend to stay in the bulk of the oil rather than at the oil/gas interface. The contact angle between titania particles and paraffin oil (measured in Chapter 3) enables calculation of Gibbs energy when the particles are attached to bubbles from equation (4.5) giving negative value (-1.9mJ/m$^2$) and the attachment of titania particles to the air bubble in paraffin oil appears to be favourable at room temperature.

Interestingly, the results obtained at temperatures of FTS process show that the dispersive part of surface energy of silica particles are lower than the surface tension of paraffin oil ($\gamma_{oil,\ 170°C}$ = 22.21 mN/m and $\gamma_{oil,\ 210°C}$ = 19.81 mN/m). Subsequently calculated contact angle suggest that paraffin oil does not completely spread on the silica particle at high temperature. Calculated contact angles between silica and paraffin oil are 23° and 33° at 170°C and 210°C respectively. Also, Gibbs energy of the particles attached to bubble is negative, meaning that this position is thermodynamically favourable and that the particles will spontaneously attach to the air-paraffin oil interface. Alumina and zirconia contact angles remain zero, therefore complete spreading is expected at 170-210°C. It is worth to notice that the work of adhesion, i.e. the strength of particle and paraffin oil interaction, decrease with temperature for $Al_2O_3$ and $ZrO_3$, therefore the particles are weaker bounded to oil. Nevertheless, the Gibbs energy (positive) indicates that the particles attachment to the air-paraffin oil interface is not favourable.

#### 4.3.2.2 Polar interactions

The presence of steam in the gas phase, in a contrast to air only, significantly changes the properties of the gas-liquid interface, hence the interaction of particles with this interface. The particles interact with paraffin oil through dispersive forces only but might interact with steam through polar forces and if these are significantly higher than the dispersive, the interaction with polar medium becomes consequently stronger. The presence of hydrophilic groups on the particles surface would reveal the affinity of particle to steam. Detection of particles surface parts that reveal hydrophilic character would prove that the particles are able to interact not only with paraffin oil (as shown previously) but also with water, i.e. the amphiphilic character of surface indicates the ability of particles to remain at the interface made of polar and non-polar medium. Presence of polar groups (able to polarise) on the particle surface indicate the ability to interact with dipoles (negative or positive) such as water molecules (Israelachvili 2011). Commonly, the polar group reveals acidic or basic character, i.e. the group accepts or gives the electron respectively.

The presence of polar groups on the particle surface was measured in the columns filled with particles by passing through the strongly polar (completely acidic or basic character) liquid probe. The interactions of these polar liquids with particles leads to long retention time which indicates the presence of polar forces acting across the particle-probe interfaces, which contributes to the surface energy of particles according to the equation (4.6).

Two liquids were chosen as probes, both reveal non-polar and polar character at the same time. The exact contribution of polar parts into the surface tensions are listed in Table 4.2; the dichloromethane (DCM) is the equivalent of acidic polar solvent and tetrahydrofuran (THF) is basic polar solvent (Liu *et al.* 1998). As long as the particles reveal polar nature of

forces, these solvent probes are able to interact with particles through dispersive and polar forces, hence the interfacial energy (solid-liquid) contains the dispersive and polar parts.

The retention times of polar liquid probes in the chromatography columns filled with alumina, silica and zirconia particles are listed in Table 4.6

Table 4.6 Average retention times (tr) of polar liquid probes in columns filled with particles

| Temp. | Probes | $Al_2O_3$ $t_r$, min | $SiO_2$ $t_r$, min | $ZrO_3$ $t_r$, min |
|---|---|---|---|---|
| 100°C | DCM | 9.4 | 3.7 | 0.3 |
| | THF | 59.2 | 235.3 | 58.5 |
| 140°C | DCM | 1.6 | 2.1 | 0.2 |
| | THF | 49.3 | 43.1 | 37.2 |
| 180°C | DCM | 1.1 | 1.5 | 0.2 |
| | THF | 34.1 | 11.6 | 1.2 |
| 210°C | DCM | 1.0 | 1.4 | 0.1 |
| | THF | 21.1 | 5.6 | 0.1 |

The retention times of THF are significantly larger than DCM regardless of the type of particles. The longer passing of basic probe (THF) results from the fact that its molecule is larger than DCM, i.e. similarly to longer retention time of high molecular alkanes. More significant reason however for such long retention time is that the particles surface contains acidic centres which in turn strongly interact with the basic molecule (THF) significantly extending the time it spends in the column.

The adsorption energies of acid (DCM) and basic (THF) liquid probes are shown on Figure 4.5. On the same figure, the adsorption of alkanes is also given as a reference. The polar probes (DCM and THF) adsorption energy is larger than the hypothetical alkane, i.e. the corresponding alkane with the same molecule size. Polar probe interacts with particles

through dispersive and polar forces and the magnitude of acting dispersive forces is comparable to those of alkanes, hence the reference liquid. The excess of energy of adsorption, i.e. the difference between the reference line and actual $\Delta G_{ads}$ of polar probe give a magnitude of the polar forces across the particles surface (Diaz *et al.* 2004). These forces are responsible for the polar component of surface energy of particles and the adsorption energies of acidic and basic solvent allows estimation of the degree of polar surface energy of particles (Fowkes *et al.* 1978; Fowkes 1987). The polar components of surface free energies were calculated based on equation (4.22) and are listed in Table 4.7 in a function of temperature.

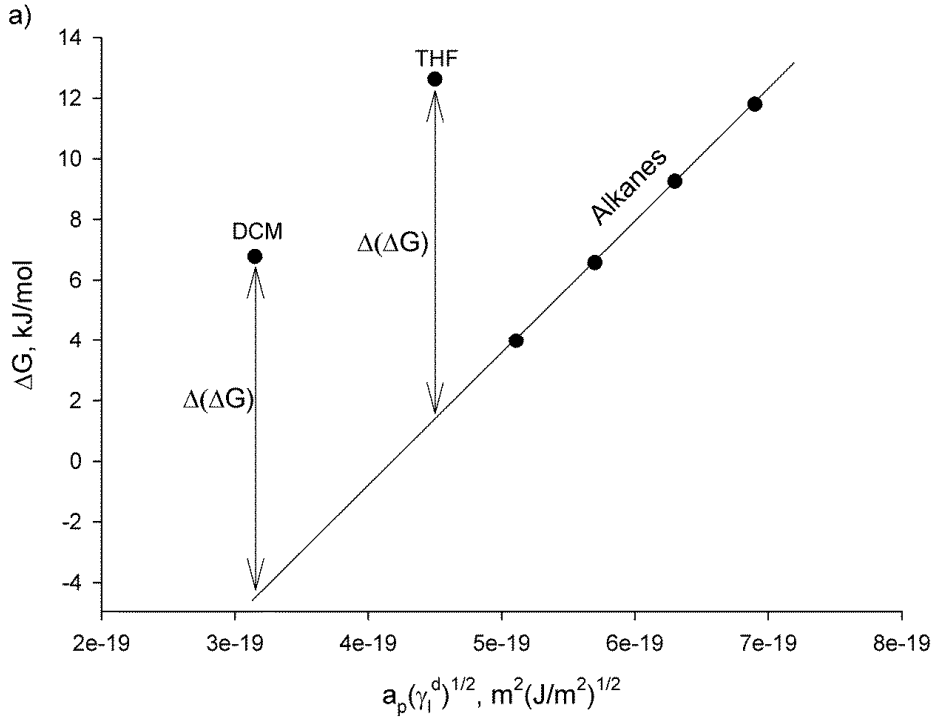

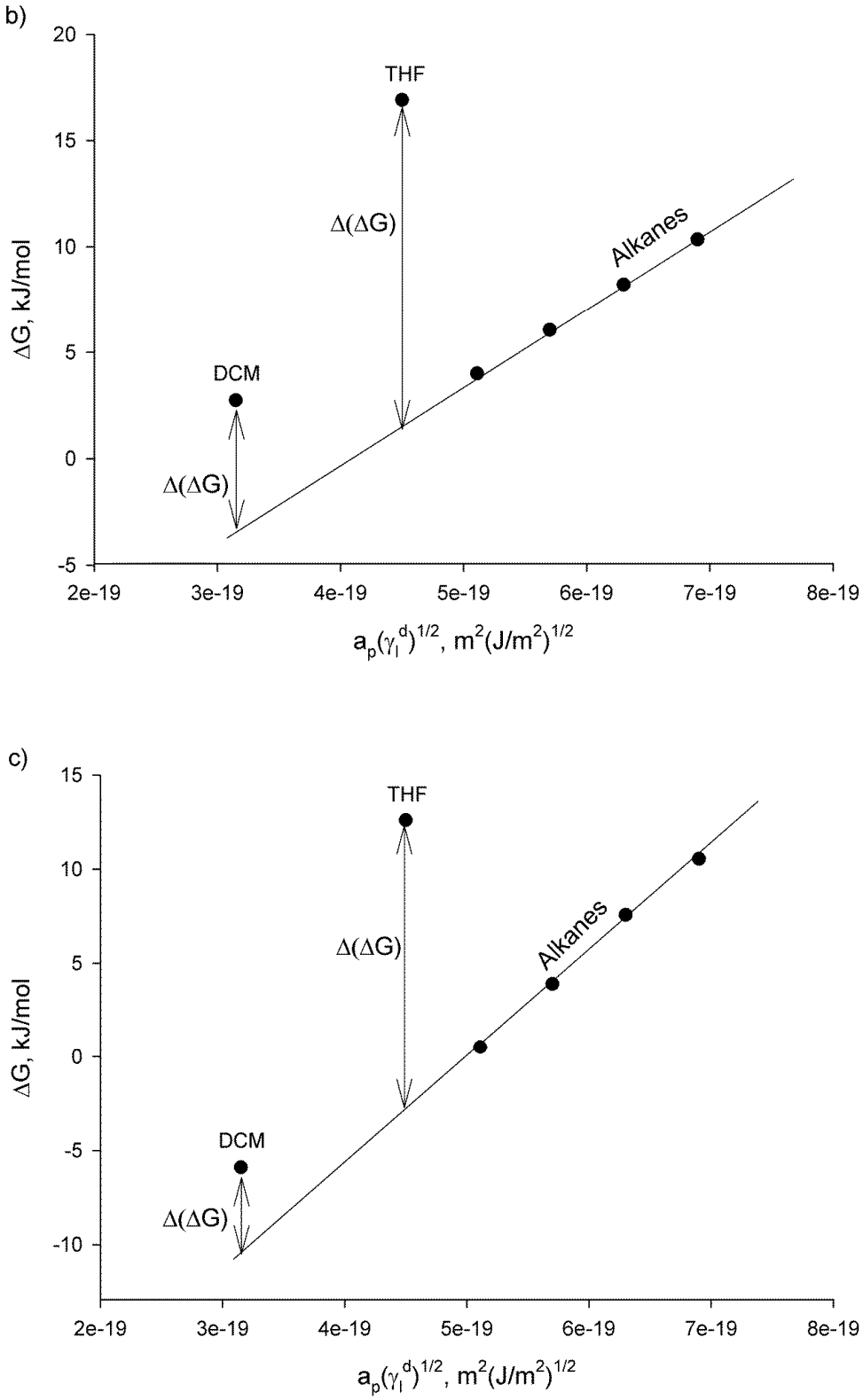


Figure 4.5 Adsorption energies of acidic dichloromethane (DCM) and basic tetrahydrofuran (THF) with a) $Al_2O_3$ b) $SiO_2$ and c) $ZrO_2$ at 100°C particles

Table 4.7 Polar component of surface energy of particles (Isp) as a function of temperature

| Temp. | Solvent | $I^{sp}$, $mJ/m^2$ | | |
|---|---|---|---|---|
| | | $Al_2O_3$ | $SiO_2$ | $ZrO_2$ |
| 100° | DCM | 59.9 | 30.2 | 24.3 |
| | THF | 41.7 | 55.7 | 57.1 |
| 140° | DCM | 36.7 | 30.4 | 13.8 |
| | THF | 55.4 | 52.7 | 61.9 |
| 180° | DCM | 40.1 | 21.8 | 33.0 |
| | THF | 65.6 | 46.7 | 35.9 |
| 210° | DCM | 46.0 | 31.6 | - |
| | THF | 68.2 | 40.1 | - |

Polar components of surface energy (Table 4.7) of particles are relatively high when compared with the dispersive component of surface free energy (Table 4.5). This provides evidence that the particles reveal polar character, i.e. interactions with polar liquids occur due to the dispersive as well as polar forces. Interestingly, the surface appears to have acidic as well as basic character which might enable interactions with water dipoles as acceptor or donor of electron, therefore a variety of forms of interactions with a polar liquid. It can therefore be concluded that all the particles reveal significant contribution of polar forces to the total free energy of solids when interacting with polar solvents.

Values obtained on the polar component of the surface energy are considered as the magnitude of polar interactions between measured liquids and particles. Different polar liquids interacting with particles will convey different values of energy ($I^{sp}$), according to the magnitude of polarity (Swaminathan *et al.* 2006). Though the polar component of particles surface energy differs depending on the liquid in contact and cannot be determined representatively (like dispersive component of surface energy) the ability of particles to interact with polar liquid was nevertheless showed.

## 4.4 Conclusions

A method that employs unconventional technique for the prediction of the particle attachment to gas bubble was presented. One of the advantages of this method is the possibility of prediction of particles attachment in oil at elevated temperatures, i.e. at reaction conditions. For each of the particles it was determined whether the process of particles attachment to air bubbles in paraffin oil is energetically favourable, based on the Gibbs energy of the system. This approach is novel as compared to traditional three phase system description, where the concept of the contact angle is normally used. For investigated system however, the contact angle did not show any differences in particles wettability by paraffin oil (Nowak *et al.* 2013). Inverse gas chromatography appears to be a very attractive tool for the assessment of wettability of solid particles at high temperatures. This technique allows calculation of the contact angle formed between particle and non-polar liquids at high temperatures, which is virtually impossible using the traditional techniques for measurements of particles contact angle.

The strength of interaction between particles and non-polar liquid can be precisely described when the dispersive component of particles surface energy is known. Though such properties are usually unknown and are rather difficult to measure for particulate solids, the inverse gas chromatography proved to be a very useful tool to determine them. Measured energies of adsorption of a set of non-polar liquids enabled calculation of dispersive component of surface energy of particles. Subsequently, the wettability of particles by paraffin oil was assessed not only at room temperature but also at the temperatures that reaction takes place.

It was found that zirconia has the largest dispersive component of surface energy and hence is the best wetted by paraffin oil, i.e. high surface energy solid reveals high reactivity,

therefore very good wettability. Alumina particles showed very good wettability by paraffin oil and complete spreading is expected. The excellent wettability of alumina and zirconia particles was found to be independent of temperature, i.e. at room and at reaction temperatures (170 to 200°C), the complete spreading of paraffin oil is expected. Silica particles however, with the lowest dispersive component of the surface energy, were found to be wetted at room temperature, but at reaction temperatures the wettability is reduced at high temperature and therefore the spreading of oil are not complete. Complete spreading of paraffin oil at room temperature over alumina, silica and zirconia particles was also found when the contact angle between paraffin oil and particles was measured using the adhesive slide method. It was shown that spontaneous attachment to the bubble might only occur for silica particles at reaction temperatures. In those temperatures, the alumina and zirconia attachment was found not to be thermodynamically favourable.

To conclude, silica particles are the least interactive with paraffin oil therefore appear to be prone to remain at the air-oil interface in stagnant conditions rather than in the bulk of liquid. Zirconia particles with the largest dispersive component of surface free energy are the least probable to find at the air-oil interface.

# Chapter 5

# 5 Particles at fluid/liquid interface

## 5.1 Adsorption of the particles at the fluid-liquid interface

Catalyst particles adsorption at the fluid-liquid interface was investigated qualitatively, and the following experiments that aimed to visualise the presence and position of the particles at the interface were carried out:

- Particles to bubble attachment

Catalyst particle to bubble attachment was investigated using bubble pick up method and particles sedimentation method. The model of particle to bubble adhesion based on the forces acting on the particle adhering to gas-liquid interface was employed. Prior to the measurements, both methods (bubble pick up and particles sedimentation) and the model were verified by analysing the interaction between of non-porous glass beads of different sizes and hydrophobicity, and gas bubble suspended in water. Subsequently, the attachment of $Al_2O_3$, $SiO_2$, $ZrO_2$ particles to the air bubbles suspended in water and in paraffin oil was investigated.

- Particles to droplet attachment

The behaviour of the particles at the interface might drastically change when steam is present in the gas phase, therefore the attachment of the catalyst particles to water/paraffin oil interface was investigated. Using the particles sedimentation method, the attachment of $Al_2O_3$, $SiO_2$, and $ZrO_2$ particles to the droplet of paraffin oil suspended in water was investigated. Bubble pick up method was used to examine the particles attachment to the droplet of water suspended in paraffin oil.

- Water/oil emulsions

The adsorption of the particles to the water-paraffin oil interface was investigated. $Al_2O_3$, $SiO_2$, $TiO_2$ and $ZrO_2$ were mixed with equal amounts of water and oil and the particles ability to stabilise such emulsion was tested. Continuous phase of the emulsion stabilised with particles indicate the preferential wettability, i.e. droplets of water in oil indicate preferential particles wetting by oil and formation of oil droplets in water implies that the water wets particles better.

### 5.1.1 Particle to bubble attachment

Particle attachment to bubble is governed by hydrodynamic, capillary and intraparticle forces (Preuss *et al.* 1999). In dynamic conditions, e.g. in flotation column, the attachment of particles to bubble is considered as a multistep process (Nguyen *et al.* 1997; Ralston *et al.* 1999; Albijanic *et al.* 2010). The first step is collision between bubble and particle and its frequency depend on the concentration of dispersed phase (bubbles and particles) and hydrodynamic conditions. After collision, the drainage of thin liquid film surrounding the gas bubble occurs within a time called induction time and subsequently the rupture of liquid film and formation of three phase contact line occurs. In the moment of film rupture the particles slightly protruding into the bubble gas before the equilibrium position is reached, the degree of protruding can increase, i.e. spreading of the three phase contact line occurs. Depending on the strength of attachment and hydrodynamics, the particle can stay on the interface or it can detach.

The thin liquid film drainage/rupture and the three phase contact line formation are mainly determined by the surface forces, especially the hydrophobic attraction between particle and bubble that decides whether the liquid film thins and ruptures (Fielden *et al.*

1996). The capillary forces, hence the wettability of solid particles, dominate the strength of particle to bubble adhesion. There is insufficient knowledge/understanding of the energy dissipation during collision, the bubble deformation, particle-liquid-bubble interfacial forces, when the particle slides on the bubble surface and finally, the development of the dynamic three phase contact line and drainage of thin liquid film (Ralston *et al.* 1999). It therefore appears that the particle to bubble attachment/detachment is a rather complex process.

The origins of the surface forces are the well known long and short range electrostatic and Van de Waals forces as well as hydrophobic ones (Israelachvili 2011) and it was suggested that the hydrophobic attraction is probably the major attracting force between bubble and particle (Butt 1994; Fielden *et al.* 1996; Jiang *et al.* 2010). Also, the same particles with different charge of surface adhere to the bubble differently. It was also shown that the flotation was more efficient for the particles having opposite charge to the bubble and that flotation was not efficient when the charge was the same (Jiang *et al.* 2010). Clearly, the electrostatic attraction strongly enhances the particle solid bubble attachment.

The complexity of the particle to bubble attachment in dynamic conditions with all previously described steps and processes causes the accurate mathematical description impossible (Ralston *et al.* 1999). However, numerous studies on the interactions/attachment between particle and bubble were carried out in stagnant conditions (Wimmers *et al.* 1988; Vinke *et al.* 1991; Omota *et al.* 2006; Omota *et al.* 2006). Depending on the relative strength between the cohesive (particle-particle) and adhesive (particle-bubble) forces the particles can adhere to the gas bubble or not (Omota *et al.* 2006).

### 5.1.2 Force balance of particle attached to the bubble

The particle to bubble attachment is dominated by the capillary force arising from the hydrophobicity of particle. Acting on the adhered particle gravitational force is balanced by the buoyancy force. The forces acting on the single particle attached to bubble (Figure 5.1) in stagnant liquid are as follows (van der Zon *et al.* 2002; Omota *et al.* 2006):

- gravitational force: $F_g = mg = \frac{4}{3}\pi R_p^3 \rho_p g$
- Laplace pressure: $F_p = 2\frac{\gamma_{lv}}{R_b}\pi R_p^2 sin^2\varphi$
- buoyancy force: $F_b = \frac{\pi R_p^3}{3}(1 + cos\varphi)^2(2 - \cos\varphi)\rho_l g$
- capillary force: $F_c = 2\pi R_p \gamma_{lv}\, sin\varphi \sin(\theta - \varphi)$

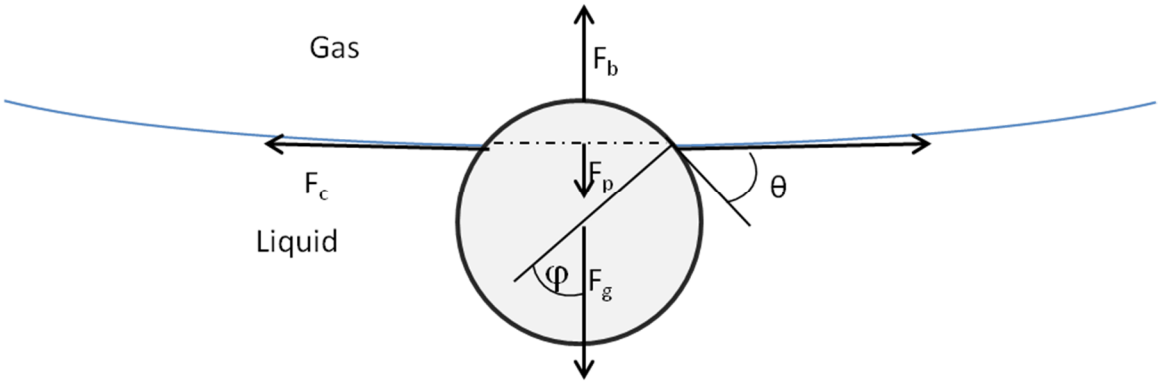


Figure 5.1 Forces acting on the spherical particle attached to the gas bubble

The net adhesion force $F_a$, (not shown in Figure 5.1) determines whether or not particle will remain attached to the surface:

$$F_a = F_c + F_b - F_g - F_p \tag{5.1}$$

and varies with the penetration angle, φ. For the given solid ($R_p$, $\rho_p$), liquid ($\rho_l$, $\gamma_{lv}$) and gas bubble ($R_b$) the three phase contact angle, θ, penetration angle, φ, determines the strength of the adhesion force. The dependency of adhesion force on these angles is shown in Figure 5.2 ($R_p$=50μm, $R_b$=5mm, $\rho_p$=1400kg/m$^3$, $\rho_l$=999kg/m$^3$, $\gamma_{lv}$=72 μN/m).

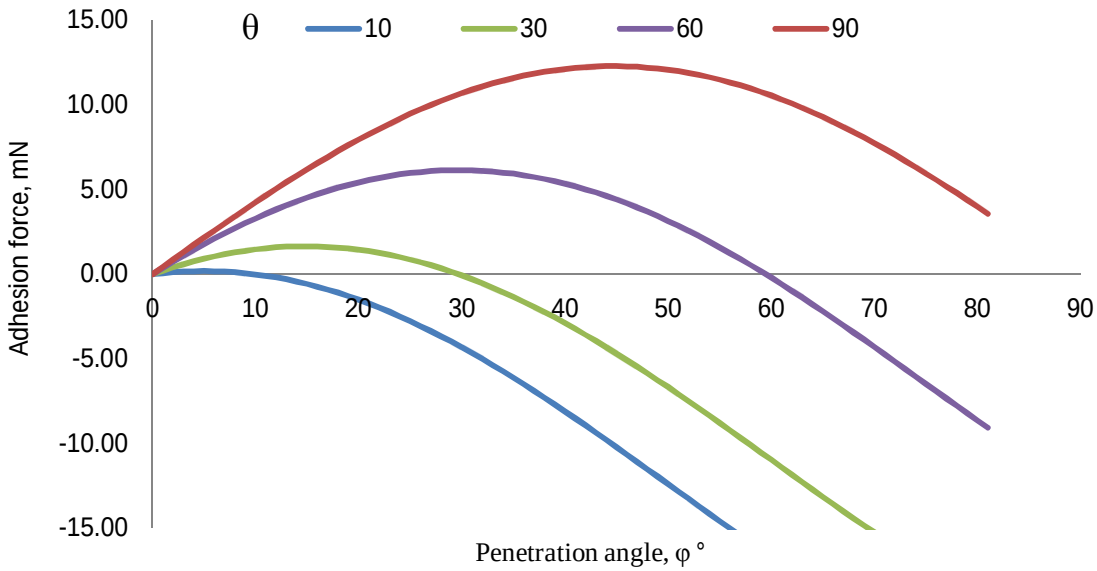


Figure 5.2 The adhesion force as a function of contact (legend) and penetration angle

Table 5.1 The magnitude of forces involved in particle to bubble attachment as a function of penetration and contact angle predicted by model, $F_g$=7.19μN. ($R_p$=50μm, $R_b$=5mm, $\rho_p$=1400kg/m3, $\rho_l$=999kg/m3, $\gamma_{lv}$=72 μN/m)

| φ, ° | Fb, μN | Fp, μN | Fc, μN θ=10° | Fc, μN θ=30° | Fc, μN θ=60° | Fc, μN θ=90° |
|---|---|---|---|---|---|---|
| 1 | 5.13 | 0.1 | 62 | 191 | 338 | 394 |
| 5 | 5.13 | 1.7 | 172 | 832 | 1613 | 1962 |
| 10 | 5.13 | 6.8 | 0 | 1341 | 3005 | 3864 |
| 15 | 5.12 | 15.1 | -509 | 1513 | 4134 | 5648 |
| 20 | 5.12 | 26.4 | -1341 | 1341 | 4966 | 7261 |
| 25 | 5.10 | 40.3 | -2471 | 832 | 5475 | 8653 |
| 30 | 5.06 | 56.5 | -3863 | 0 | 5647 | 9782 |

For $F_a < 0$ the particle will detached from the bubble, otherwise, it will remain attached. Clearly, larger contact angles create the larger (and positive) adhesion force.

Maximum adhesion force is obtained based on the equation (5.1) with the assumption that for small particles the capillary force exceeds all other forces (Table 4.1), the adhesion force can be approximated by (Omota *et al.* 2006):

$$F_{a,\max} = 2\pi R_p \gamma_l \sin^2 \frac{\theta}{2} \tag{5.2}$$

Therefore, it can be concluded that in stagnant conditions and sufficiently small particles, the strength of adhesion of particle to bubble depends on the three phase contact angle.

Force balance for the attachment of single particle can be extended to the case of a layer of particles adhering to the bubble. In such case when the layer of particles is formed on the bubble surface, the coverage angle, $\alpha$, is defined in Figure 5.3.

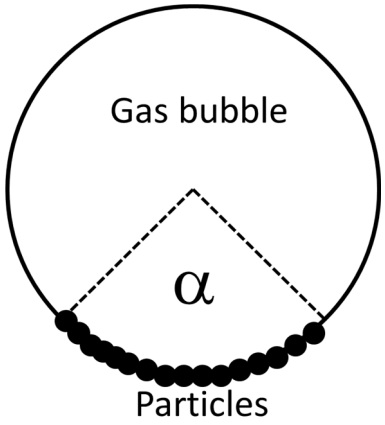


Figure 5.3 Coverage angle of particles attached to the bubble

The maximum adhesion force can be related to the coverage angle and parameters mentioned above, and based on the force balance (Schulze 1977; Wimmers *et al.* 1988; Vinke *et al.* 1991) it can be calculated from:

$$F_{a,\max} = \frac{3\varepsilon_s \left(F_g - F_b\right)\left(R_p - R_b\right)}{2R_p}\left(\alpha - \sin\alpha\cos\alpha\right) \tag{5.3}$$

Above equations enable determination of the effective contact angle of particle attached to the bubbles (Omota *et al.* 2006):

$$\sin^2\frac{\theta_e}{2}=\frac{\varepsilon_s\left(\rho_s-\rho_l\right)gR_p\left(R_p+R_b\right)}{\gamma_l}\left(\alpha-\sin\alpha\cos\alpha\right) \tag{5.4}$$

This simplistic model of particle to bubble attachment was first validated using different size (small and large) non-porous, spherical, glass beads of significantly different hydrophobicity. Accordingly, the glass beads to bubble attachment in water was expected to be stronger for more hydrophobic particles in accordance to equation (5.4), i.e. bubble coverage by highly hydrophobic glass beads ($\theta$>90°) is larger than by hydrophilic ones ($\theta$<90°).

### 5.1.3 Particle adsorption at the paraffin oil-water interface

Investigation of the water – oil interface with the presence of the particles (catalyst) is highly relevant to this project, since the both fluids are present in the Fischer Tropsch synthesis. Though the water is present most probably as a vapour, nevertheless the behaviour of the particles at the liquid water-oil interface can be transferred onto the steam-oil system. It was not possible to investigate particle attachment to a steam bubble suspended in paraffin oil. Therefore particles attachment to two liquids imitating the properties of such interface were analysed instead; particle attachment to a water droplet suspended in paraffin oil and to oil droplet suspended in water was investigated.

The particles behaviour at the water-oil interface not only carries information on the preferential wettability by these liquids but also on the strength of particles adsorption at the interface (Israelachvili 2011). For instance, the particles suspended in the mixture of

immiscible liquids might result in the ejection of particle from one liquid to the other when particles are well wetted by only one of the liquids (Figure 5.4). Such behaviour indicates preferential wettability, i.e. particle is very well wetted by the liquid into which was ejected.

On the other hand, the particle can remain at the interface, in which configuration the system gains the minimum energy (Figure 5.4). The adsorption of particles at the interface is determined by the wettability of particles by both liquids, nevertheless high energy is required to remove particle adsorbed at the interface since is proportional to the particle size (Binks 2002):

$$E = \pi R_p^2 \gamma_{ow} \left(1 \pm \cos\theta_{ow}\right)^2 \tag{5.5}$$

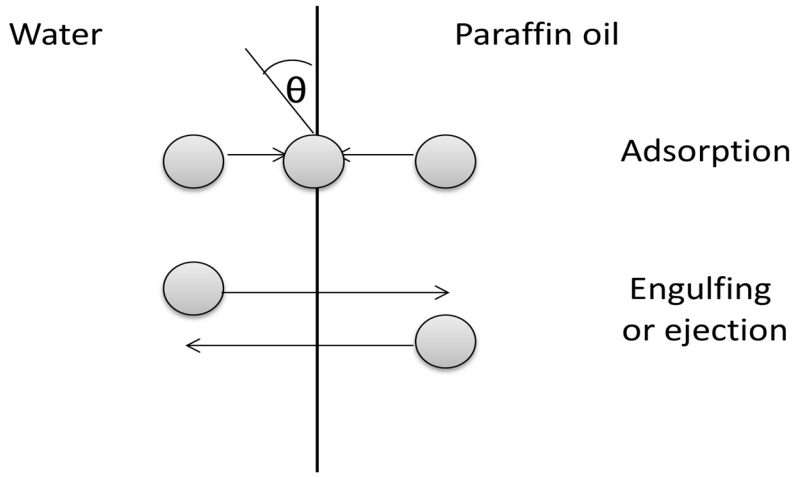


Figure 5.4 Particles adsorption at the interface or transfer from one to the other liquid

This phenomenon is commonly utilized in the emulsion stabilisation. The particles which tend to adsorb at the water/oil interface are usually referred as amphiphilic e.g. they reveal both, hydrophobic and hydrophilic parts at the same time (Binks 2002; Binks *et al.* 2005). Metal oxides usually contain hydrophilic groups at the interface (-OH) therefore are able to form hydrogen bonds with water. The particles in the bulk of liquid do not reveal dipole characteristics, since the centres are saturated by the same interactions with

surrounding liquid. At the interface however, the particle becomes a dipole, i.e. interacts through polar forces with polar liquid from the one side (e.g. water) and through dispersive (non-polar) forces with non-polar liquid from the other side (e.g. oil). The example of energetic heterogeneity of amorphous silica is shown in Figure 5.5. Such heterogeneity of polar and non-polar groups on the metal oxide surface subsequently triggers particles behaviour similar to surfactant, i.e. the particle reveals hydrophilic and hydrophobic parts, dispersed over the particles surface.

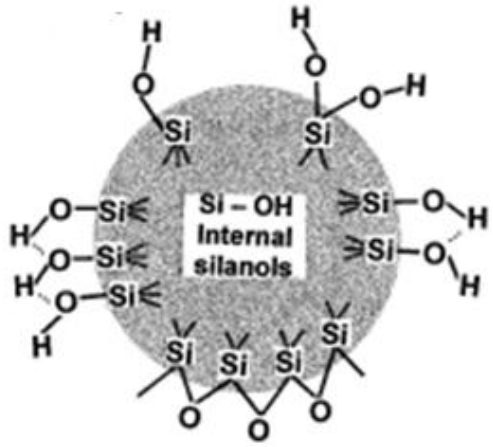


Figure 5.5 Surface chemistry of amorphous silica (Zhuravlev 2000)

The surface energy measurements using inverse gas chromatography revealed that the particles are able to interact with liquids through dispersive (with hydrocarbons) and polar (with acid-base) forces (see Chapter 1). Therefore the set of experiments were performed where the ability of particles to remain at the water-oil interface (adsorption) was tested in stagnant conditions.

The ability of particles to remain at the paraffin oil-water interface was also investigated employing the principles governing the emulsion stabilisation. Frequently,

emulsion of oil droplets in water (or water in oil) is stabilised using emulsifiers. Such emulsifier creates the steric (non-ionic surfactants) hindrance to droplet-droplet coalescence (or flocculation, aggregation) which might be additionally strengthened by the electrostatic repulsion (ionic surfactants) (McClements 2004).

Amongst the several types of the emulsifiers, the most commonly used are surfactants, biopolymers and particles. The adsorption of particles at the water-oil interface is driven by the relative wettability but also the particles size (10nm-5μm), which exceed significantly the size of commonly used surfactants (0.4-1nm) (Tcholakova *et al.* 2008). Such relatively large particle size results in very high desorption energy (equation (5.5)) leading to stable position of particles at the interface caused by very low desorption.

Particles can stabilise droplets of oil in water or droplets of water in oil, in similar way as surfactant, and magnitude of hydrophilic to hydrophobic part decides on the type of dispersion. More hydrophilic particles have ability to stabilise the oil droplets dispersed in water (Figure 5.6a) whereas more hydrophobic particles stabilise water droplets in oil (Figure 5.6b) (Ashby *et al.* 2000). Such ability of formation of different type of dispersed systems can be exploited to characterise the particles wetting properties.

Attempting stabilisation of water-oil emulsion with catalyst supports enables observation of their behaviour at the interface. On the one hand, the particles adsorption and possibly the strength of adsorption at the interface (polar/non-polar liquid) can be determined by simply observation whether mixed dispersion of oil-water is stable. On the other hand, the type of stabilised droplets, water or oil, indicates preferential wettability towards the continuous liquid with which $\Theta < 90^{o}$ (see Figure 5.6a). Nevertheless, too hydrophilic or too hydrophobic particles will tend to remain within the bulk of water and oil respectively.

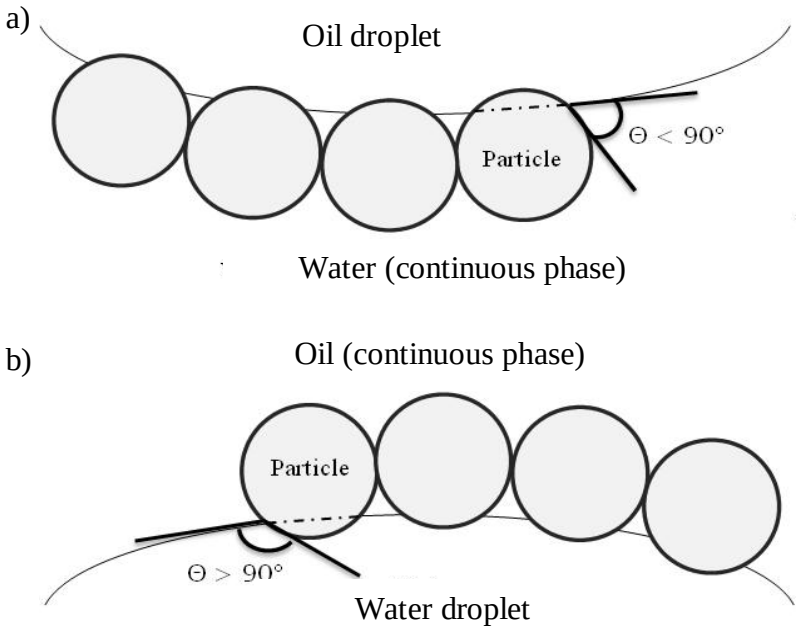


Figure 5.6 The effect of particles partial wettability on the type of dispersed droplets

Therefore the experiments that aim to stabilise the water-oil emulsion with particles allow qualitative evaluation of the particles adsorption at the interface and the wettability. Such knowledge, combined with results of previous experiments (Chapters 2-4) should fully characterize the particles wettability (if preferential) and ability for adsorption at the interface.

## 5.2 Materials and methods

## 5.3 Particles to bubble attachment

Initially, the particle to bubble attachment was measured in stagnant conditions with the method called bubble pick up (Wimmers *et al.* 1988; Vinke *et al.* 1991). Particles were suspended in water (or in oil) in a glass, rectangular container and were left to sediment for 1h (24h for oil). The air bubble was formed at the tip of the syringe needle (1.81 mm diameter)

(Figure 5.7). The container with the particles suspended in the liquid was placed on the adjustable height stand enabling vertical movement of the container towards the stationary gas bubble. Using the stand the container with the particles was moved towards the gas bubble which was completely immersed in the particle bed and subsequently the bubble was withdrawn from the particle bed by lowering the stand.

The particle to bubble attachment was also investigated using particles sedimentation. In this case the bubble was stationary whereas the particles were mobile and were allowed to attach to the bubble whilst sedimenting (falling). This approach enables mimicking the conditions found in slurry reactors, where wet particles interact with gas bubbles. The wet particles were introduced to the container with a stationary air bubble using a syringe filled with particle-liquid suspension (Figure 5.7). This method was also tested for dry particles, i.e. the particles were sprinkled onto a liquid with stationary bubble and were freely sinking. When parafin oil was used, the sedimentation of particles was too long comparing to diminishing air bubble (few hours), hence only the bubble pick up method was employed. It was not possible to investigate titania particles attachment to bubble in water since it created stable suspension over the time and did not sediment. Table 5.2 summarizes all the experiments performed for particle to bubble attachment using both methods.

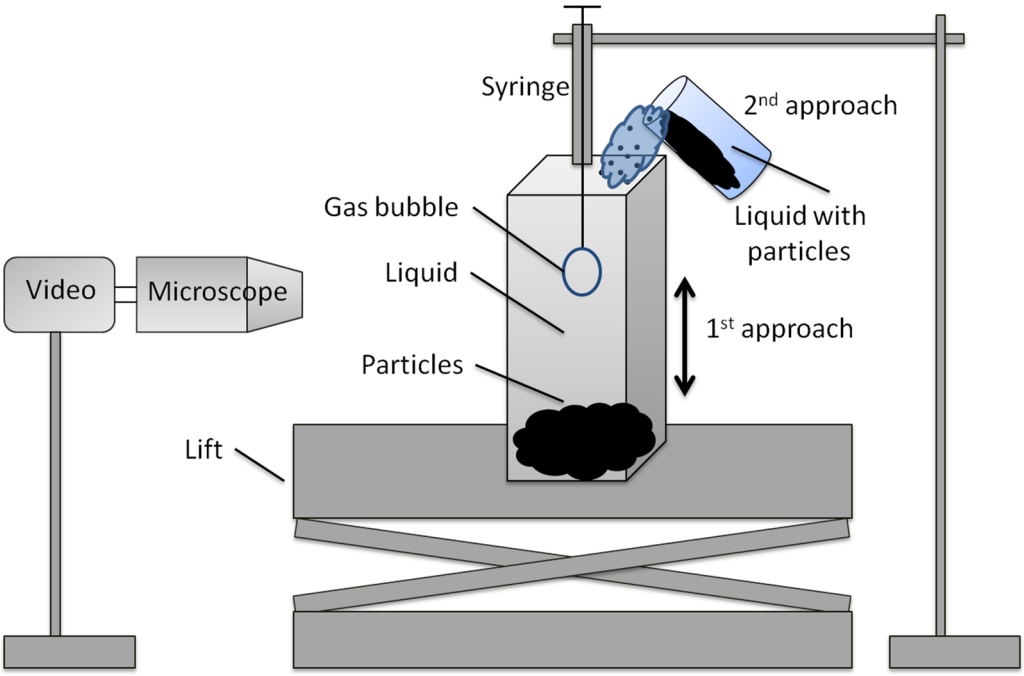


Figure 5.7 Two different methods used to measure particle to bubble attachment

Table 5.2 Summary of carried out experiments - particle to bubble attachment

| | Powders | | Method used with given liquid | |
|---|---|---|---|---|
| | | $d_{32}$, μm | Bubble pick up | Particles sedimentation |
| Porous | $Al_2O_3$ | 16 | water, paraffin oil | water |
| | $SiO_2$ | 13 | water, paraffin oil | water |
| | $ZrO_2$ | 26 | water, paraffin oil | water |
| Non-porous | Small beads | 30 | water | water |
| | Large beaads | 55 | water | water |
| | Small beads treated | 30 | water | water |
| | Large beads treated | 55 | water | water |

Strongly hydrophobic glass beads were prepared in order to ensure the maximum attachment. Glass beads were treated with chlorotrimethylsilane (CTMS, Sigma Aldrich). Following the procedure of silanizing of glassware (Seed 2001) the beads were kept in the concentrated CTMS solution and heated. After the solution evaporated, beads were left in the oven at 100$^{o}$C for 14 hours and subsequently cooled for 12 hours at room temperature. Such prepared hydrophobic particles contact angle was equal to 90° (see Chapter 3 and Appendix).

### 5.3.1 Particles adsorption at interface

Particles to droplet attachment

For the particles adsorption at the interface of the droplet formed in the liquid a similar method was used as in the particle to bubble attachment. The droplet of one liquid was formed at the tip of the needle which was immersed in second liquid. Though the particle sedimentation method was shown to be more efficient (section above) than the bubble pick up, both were used. It was possible to sediment particles over the paraffin oil droplet formed in water since the particles were able to freely sink. With a water droplet in paraffin oil however, the particles sedimentation did not occur, therefore the 'droplet' pick up method was used. Both methods are described above and the principle is shown in Figure 5.7. Using this method, $Al_2O_3$, $SiO_2$ and $ZrO_2$ particles adsorption at the liquid-liquid (polar-non polar) interface was investigated. The $TiO_2$ particles formed the homogenous suspension in water and were not used.

Emulsion

Emulsions were prepared from the equal volume of water and paraffin oil, i.e. 5ml of each, was mixed together in a low shear mixer (shaker). Before the liquids were mixed, the particles (1ml) were added to one of the liquid so that with given particles two similar emulsions were prepared. In one emulsion the particles were initially added to water and then mixed with paraffin oil and in the second emulsion, the particles were initially added to paraffin oil and then mixed with water. The emulsions were prepared with all catalyst supports ($Al_2O_3$, $SiO_2$, $TiO_2$ and $ZrO_2$).

## 5.4 Results and discussion

### 5.4.1 Particles to bubble attachment

#### 5.4.1.1 Glass beads attachment to the bubble in water

Two methods, bubble pick up and particles sedimentation, showed different coverage of bubble by glass beads. Using the bubble pick up method, it was impossible to immerse bubble in the bed made of treated (hydrophobized) glass beads (Figure 5.8a). Strongly hydrophobic particles tend to attract each other and aggregate in water (Hu *et al.* 2003), especially when they are left in contact for prolonged period of time. The complete coverage of bubble by beads was however possible with the untreated glass beads (Figure 5.8b). Limitations of the bubble pick up method when used with hydrophobized beads were overcome by the particles sedimentation method.

The conditions met during the particles sedimentation method, where the beads freely flow over the stationary bubble mimic the dynamic behaviour found during flotation or in slurry bubble columns. Collision of beads with bubble, induction and attachment time in particle sedimentation method is much shorter than in bubble pick up approach. The latter allows for prolonged bead contact with the bubble. Previously discussed steps involved in the particle to bubble attachment process are better met using the particle sedimentation method. In the bubble pick up method, the induction and attachment time depends on the experimental conditions since the adjustable stand is operated manually, the contact of bubble with the bead bed strongly depends on the operator and it can take up to a few seconds. Therefore induction time in both approaches is very different and also might involve additional forces (e.g. bubble is pushed into the bed) affecting the experiments.

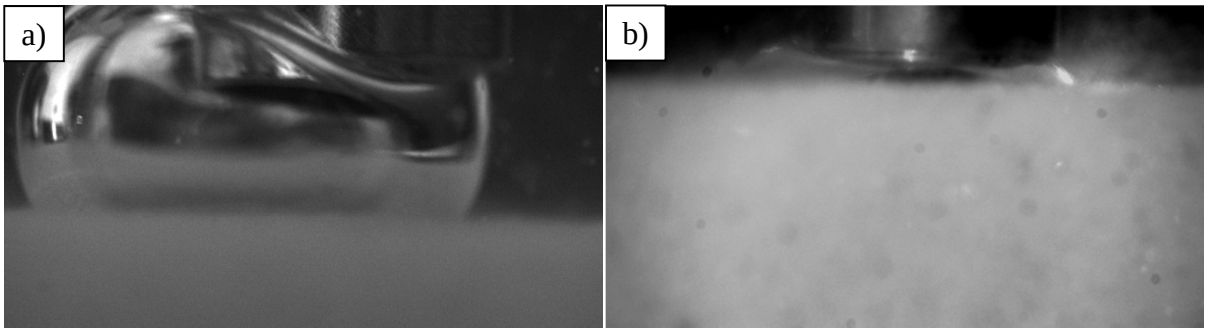


Figure 5.8 Immersion of bubble in the particles bed using bubble pick up approach in particle to bubble attachment: a) silica particles and b) glass beads

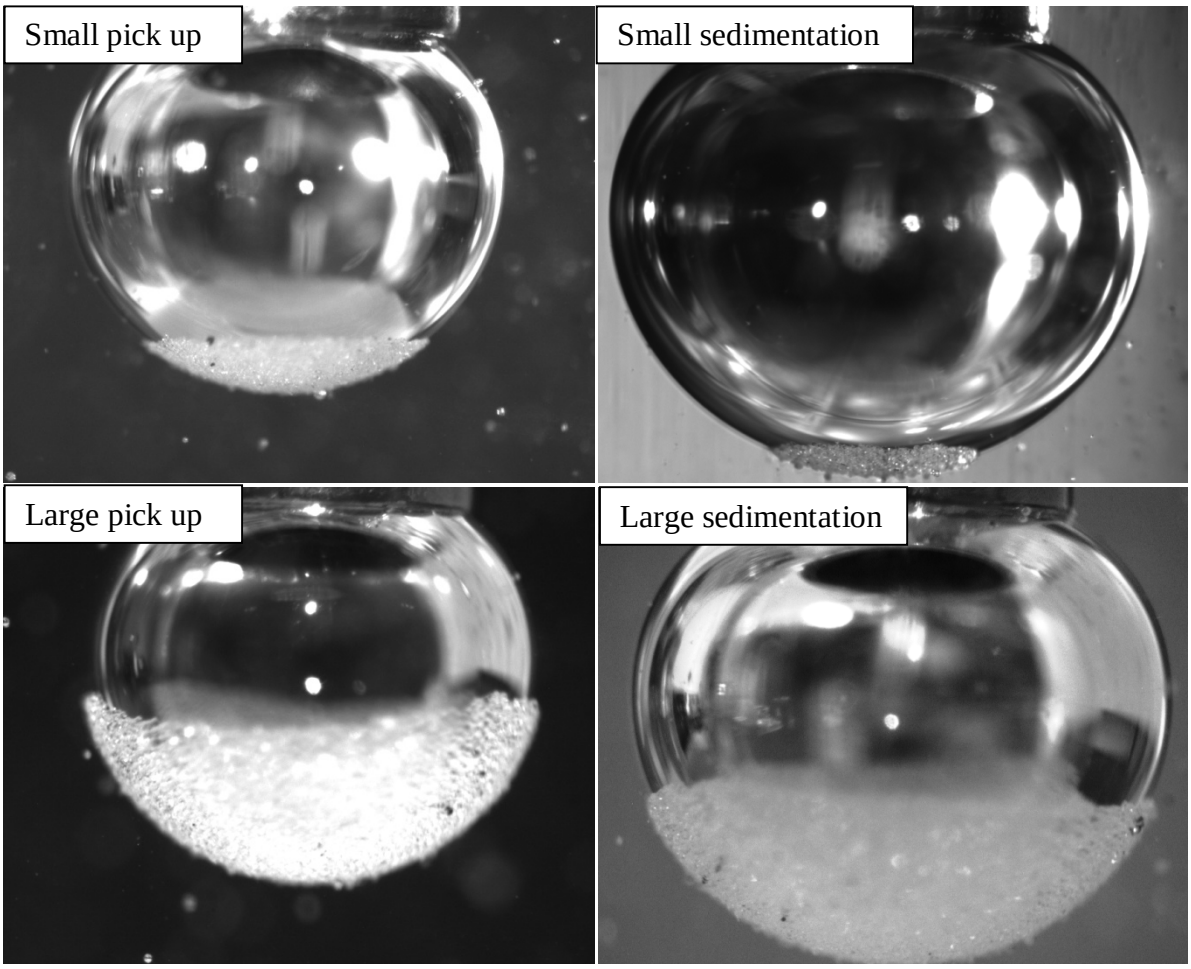


Figure 5.9 Untreated glass beads attachment to the air bubbles in water (size of the images: 3.25 x 2.65mm)

The attachment of the small glass beads (Figure 5.9) shows that the bubble pick up gives larger coverage of the bubble than the particle sedimentation method. Comparable coverage with the large glass beads was observed for both methods. One of the reasons for the

lower coverage by small beads is the size of an air bubble produced at the tip of the needle. The bubble size affects the bubble shape; large number of glass beads attached to the large bubble can cause its elongation. There has to be noted that in the case of a layer of particles attached to the bubble, there occurs tangential force (detachment force) as a result of action of the surrounding particle within the layer. It is directed from the centre of particle at the closest neighbourhood (below and above) within the layer to the centre of the middle particle. At the most upper layer of particles tangential force is minimum and reaches maximum at the lowest (bottom) layer. For the vertically elongated bubble the tangential force acting on the adhering particles increases which causes the lower coverage. Similar tendency of lower coverage for larger bubble was also found for the mesoporous silica particles using bubble pick up method (Omota *et al.* 2006).

The other factor affecting the difference in coverage using both methods is the contact time between particle and bubble. The time where the liquid film is thinning and ruptures and the three phase contact line is formed is much longer in the bubble pick up experiments than in particles sedimentation. Also, when the bubble is pushed towards the particle bed, an additional force acts and affects the thinning and rupture of liquid film. For this reason the liquid film is more effectively removed enabling faster three phase contact formation in bubble pick method.

In particles sedimentation method, the freely moving particles trajectory around the bubble are different for different sized bubbles. It was observed that the attachment of sedimenting particle to the bubble starts at the bottom of the bubble and the next layers of particles build upon the previous (Figure 5.10). Therefore, though the capillary pressure from the smaller bubble repels the particle more effectively than the pressure from the large bubble,

the sliding particle on either side of the bubble might attach easier and build the layers with small diameter of bubble (smaller curvature).

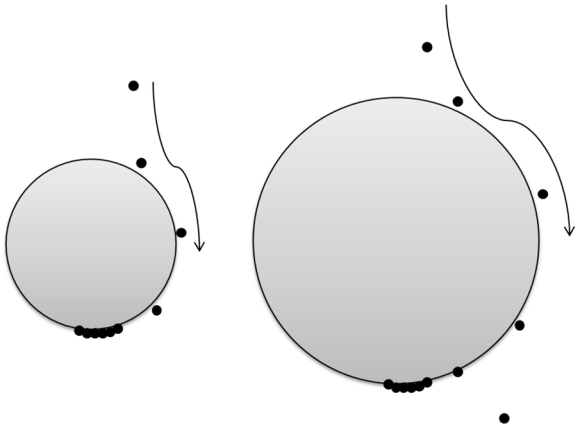

Figure 5.10 Trajectory of sedimenting particles around small and large bubble

The limitation of the bubble pick up method is evident when the hydrophobized glass beads are tested. Comparison of both methods applied to hydrophobic (treated) glass beads clearly indicate that with the bubble pick up method it is not possible to obtain complete coverage, even for the highly hydrophobic glass beads (Figure 5.11). With the particles sedimentation method however, bubbles were almost fully covered with the hydrophobic particles. Dissimilarity of the results obtained using both methods was observed for small (30μm) and large (55μm) treated glass beads. It was previously said that the capillary force is a dominant force responsible for the attachment and determines the adhesion strength. The capillary force is proportional to the particle perimeter, hence increases with the particle size (until gravitational force becomes dominant).

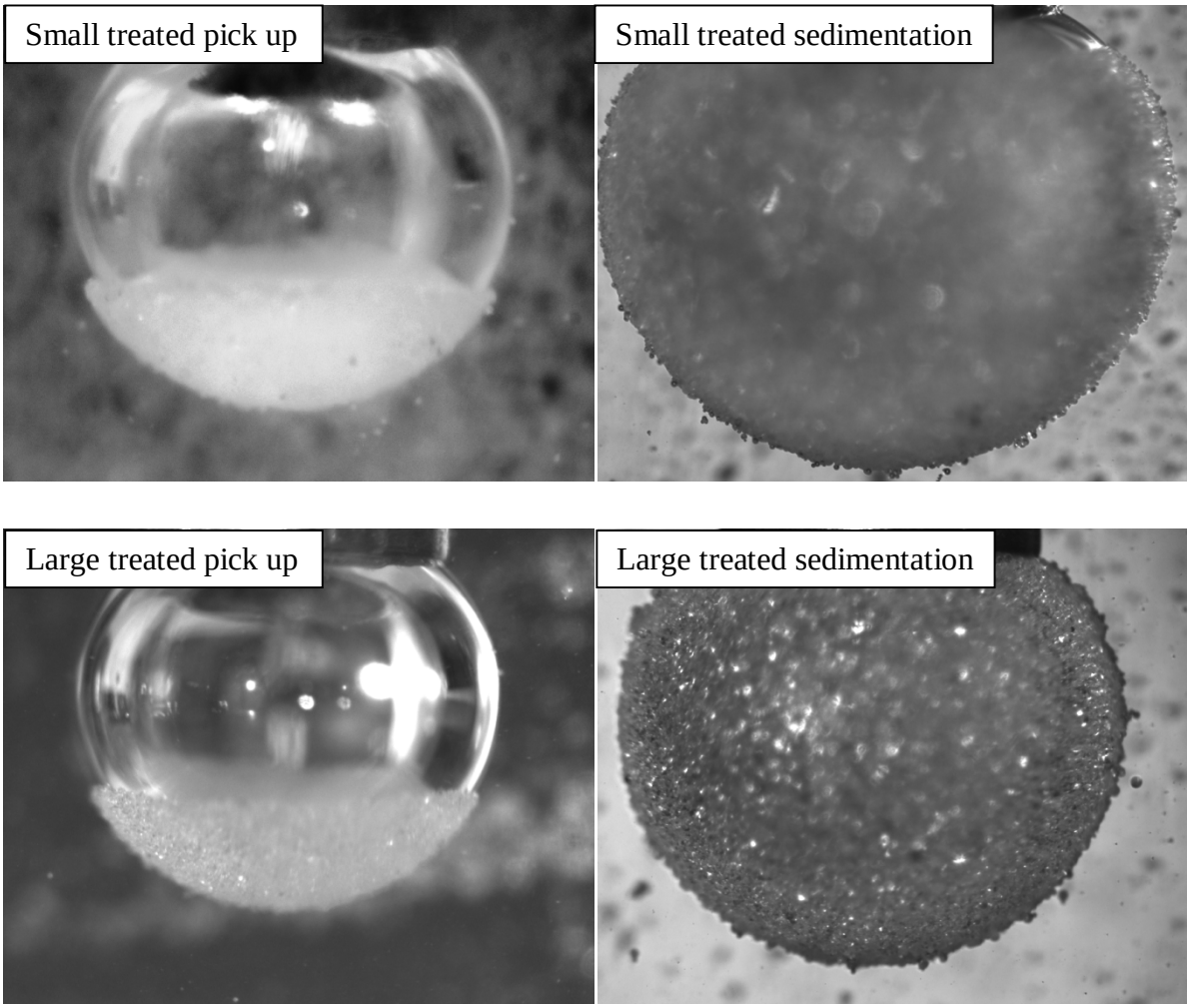

Figure 5.11 Hydrophobic glass beads attached to the air bubbles in water (3.25 x 2.65mm)

The effective contact angles as well as the strength of adhesion were calculated from the equations (5.4) and (5.3) respectively. Table 5.3 summarizes the coverage angles, adhesion forces and the effective contact angles of different size, untreated and treated glass beads.

Table 5.3 The effective contact angles of glass beads calculated from the adhesion model add names of angles to the table

| Glass | Method | $R_b$, mm | Coverage angle $\alpha$, ° | $F_{adh}$, $10^{-9}$ N | Effective contact angle $\theta_e$, ° |
|---|---|---|---|---|---|
| Small | Pick up | 1.18 | 44 | 1.49 | 1.20 |
| Small | Sedimentation | 1.46 | 28 | 0.51 | 0.70 |
| Large | Pick up | 1.20 | 87 | 28.2 | 3.87 |
| Large | Sedimentation | 1.46 | 73 | 23.3 | 3.51 |
| Small treated | Pick up | 1.19 | 65* | 4.21 | 2.02 |
| Small treated | Sedimentation | 1.55 | 131 | 20.2 | 4.42 |
| Large treated | Pick up | 1.16 | 69* | 16.2 | 2.93 |
| Large treated | Sedimentation | 1.36 | 140 | 64.1 | 5.83 |

*inaccurate numbers caused by technique limitations with hydrophobic particles

Clearly, bubble coverage ($\alpha$) is larger for larger glass beads regardless of the method used (pick up or particles sedimentation) and whether the particles were hydrophobized or not. As the model shows (equation (5.1)), the gravitational and buoyancy forces are related to the particle size $R_p^3$, the capillary pressure depends on the $R_p^2$ and the capillary force depends on the $R_p$. It is therefore obvious that for micron sized particles, the $R^2$ and $R^3$ drastically decrease, e.g. $R_p=50\cdot10^{-6}$, $R_p^2=2.5\cdot10^{-9}$ and $R_p^3=1.25\cdot10^{-13}$ therefore for the range of particle sizes used in this study, the capillary force is dominant. This force results from the combined effect of contact angle and particle size. The capillary forces for the small particle with large contact angle and the large particle with small contact angle are of the same magnitude.

The bubble pick up method with untreated small and large glass beads gives slightly higher (by ~0.5°) effective contact angles than the particles sedimentation method (Table 5.3).

This could be attributed to the enhanced liquid film thinning when the air bubble is pushed into the particle bed. In this case the time of particle-bubble contact (~5 seconds) exceeds the time of particle freely moving around the bubble. Furthermore, the additional force, caused by the bubble being pushed into the particles, is unavoidable in bubble pick up experiment and this might also introduce an error.

The bubble pick up method was unsuccessful for the hydrophobic particles. The problem of gas bubble immersion into the strongly hydrophobic particle bed, forming strong aggregates, resulted in limited bubble accessibility (similar to Figure 5.8a). Because the upper surface of bubble remained uncovered by particles during the bubble in particles bed immersion, the coverage angles, therefore the effective contact angles are significantly lower than measured by the particles sedimentation method.

The effective contact angles of small particles are systematically lower than contact angles of large particles. The effect of particle size is less pronounced for the hydrophobic beads where both methods gave very similar coverage angles. The difference between effective contact angles of untreated particles and treated is significantly lower (~50%) than the untreated glass beads (300-500%). The differences caused by particle size diminish when the effective contact angle increases. Obviously, larger contact angle causes larger ‘attaching’ capillary force and according to the model, the adhesion dependency from the capillarity becomes more dominant than from the particle size. Adhesion of untreated as well as hydrophobized glass beads strongly depends on the capillary force which is predicted by the model, hence it is expected that large particle having the same contact angle as small ones will reveal higher adhesion.

#### 5.4.1.2 Particles to bubble attachment in water

Catalyst supports showed similar problems of bubble pick up method as the treated glass beads, because the particles formed firm solid bed and the complete immersion of bubble into it was impossible (Figure 5.12a). Therefore only the particle sedimentation method was used for the effective contact measurement. It was observed, that there was no difference in the coverage angle between dry and wet particles. Dry particles that were sprinkled on the liquid surface had the pores fill with water and by the time (<1min) they approached stationary bubble, they were already saturated.

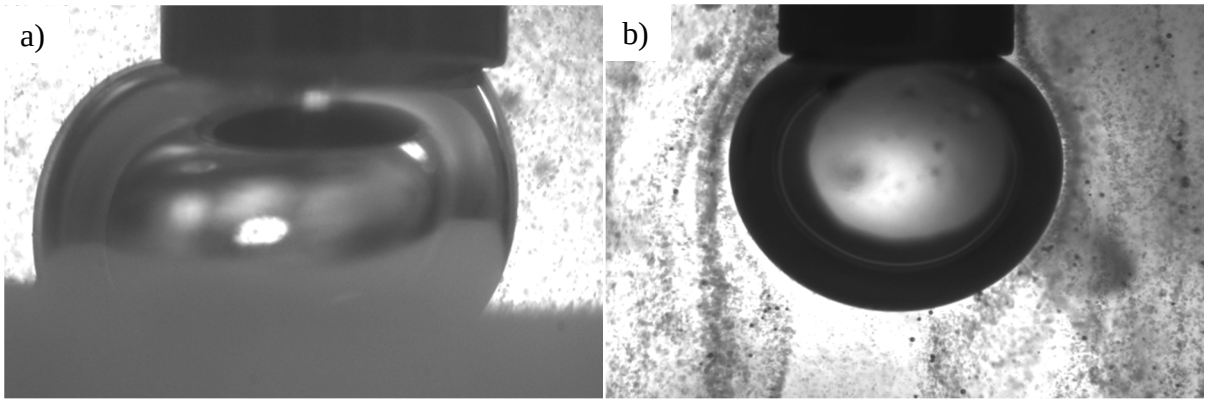


Figure 5.12 Silica to air bubble attachment using a) bubble pick up and b) particles sedimentation methods (1.81 mm needle diameter)

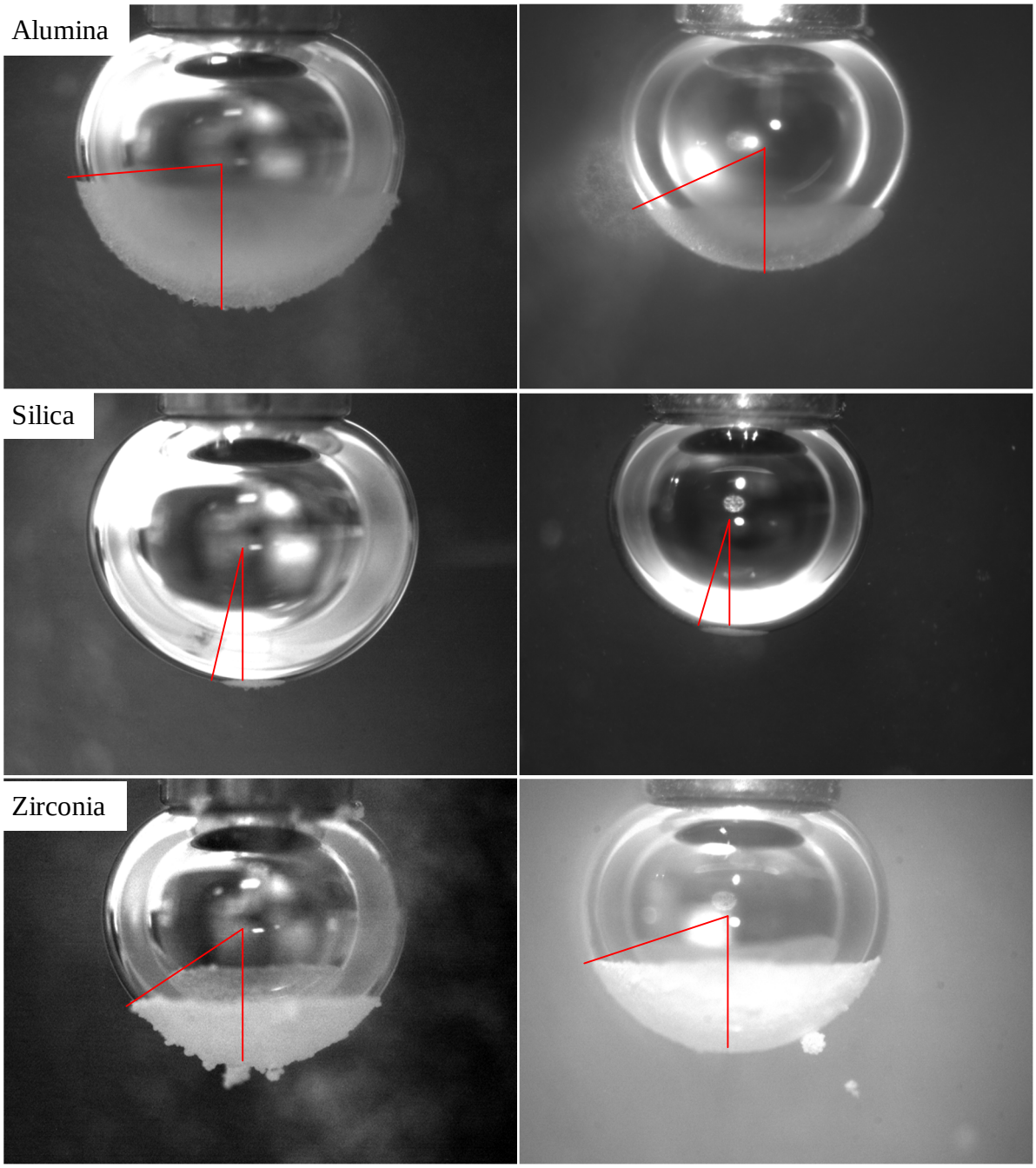


Figure 5.13 Particles attached to the bubble in water using the particles sedimentation (left column) and bubble pick up (right column) method (4.8 x 3.6mm)

Typical images of the particles attached to an air bubble in water using bubble pick up and particles sedimentation method are shown in Figure 5.13. Clearly, different particles reveal very different strength of adhesion to the bubble. The size of alumina (16μm) and silica (13μm) particles is rather comparable and since they form very different coverage, it can be

concluded that hydrophobicity, i.e. contact angle, is the crucial parameter that determines particle to bubble attachment. It appears, that alumina and zirconia particles (Figure 5.13a), c)) are the most hydrophobic whereas the silica particles (Figure 5.13b) are the most hydrophilic. The zirconia aggregates (Figure 5.13c) indicates the attraction to the particles due to a high cohesion forces as compared to alumina and silica.

Measured coverage angles of different particles on the bubble surface as well as 'dry' contact angles between particles and water, measured with the adhesive glass slide method (Nowak *et al.* 2013) are listed in Table 5.4. Based on 'dry' contact angles, the Gibbs free energy upon particle attachment to bubble in water ($\Delta G$) was also calculated and is summarised in Table 5.4

Table 5.4 'Dry' contact angles (Nowak *et al.* 2013), Gibbs energy upon particle to bubble attachment, coverage angle, adhesion force and effective contact angle of particles attached to the bubble

| Catalyst support | $R_p$, μm | $R_b$, mm | 'Dry' contact angle θ, ° | ΔG, $mJ/m^2$ | Coverage angle α, ° | $F_{adh}$, $10^{-9}$ N | Effective contact angle $\theta_e$, ° |
|---|---|---|---|---|---|---|---|
| $Al_2O_3$ | 16 | 1.35<br>1.55 | 91 | -73 | 83<br>81 | 4.45<br>4.77 | 2.84<br>2.94 |
| $SiO_2$ | 13 | 1.40<br>1.49 | 75 | -53 | 14<br>12 | 0.003<br>0.002 | 0.07<br>0.06 |
| $ZrO_2$ | 26 | 1.37<br>1.63 | 49 | -25 | 55<br>37 | 55.0<br>22.0 | 7.86<br>4.96 |

The effective contact angles do not follow the coverage angles which was the case with non-porous glass beads. The lowest coverage angle of silica particles results in the lowest effective contact angle. However, effective contact angles with zirconia and alumina

particles do not follow the coverage angles. The weight and size of the zirconia particles is almost twice that of alumina particles (Table 5.2). According to the force model and to the previously shown calculations (Table 5.3), the adhesion force depends on the size of particle, the larger the particles, the larger the adhesion. Though the hydrophobicity of zirconia is significantly lower than alumina particles, the attachment of heavy zirconia particles requires higher force of adhesion, therefore larger effective contact angles were obtained. Therefore it can be concluded that though the 'dry' contact angle indicates the degree of particles hydrophobicity, the size/weight of particles is also responsible for the particle to bubble attachment. In flotation it was shown (Hewitt *et al.* 1995)that the particles between 35-50 μm were collected more efficiently than the smaller particles (Hewitt *et al.* 1995). On the other hand, the size of bubble affects coverage (Table 5.4). The difference in coverage is most pronounced for the zirconia particles, where the bubble size differs significantly. The capillary pressure is higher for the smaller bubbles resulting in lower adhesion. Omota *et al.* (2006) also showed in experiments that the larger the bubble, the less particles were collected.

The adsorption/attachment of particles to the gas bubble depends on the electrostatic interaction between particle surface and the bubble surface. Whilst oppositely charged particle and bubble surface will attract each other, the electrostatic adsorption barrier will be formed for the similar charge (Tcholakova *et al.* 2008). The surface of air bubble in pure water is charged negatively and has no charge when the water pH is lowered down to 1.5-2.5 (Jiang *et al.* 2010). The zirconia and alumina particles in pure water (pH ~7) have a positive charge and their isoelectric point, (pH of aqueous solution in which particles surface have no charge) are 7.4 and 8.5 respectively (Tang *et al.* 2002). Therefore the attractive electrostatic forces enhance alumina and zirconia particle to bubble attachment. On the other hand, silica particles have negative charge in water, their isoelectric point is 2 (Tang *et al.* 2002) thus the particles

are repelled by the negatively charged air-water interface. The exact magnitude of such electrostatic adsorption barrier is difficult to calculate, not only is system polar but also even the easiest model requires numerical solution (Deriâgin 1989; Tcholakova *et al.* 2008).

During flotation the attraction between oppositely charged particle and bubble was sufficient for the adhesion through the liquid film, i.e. the particle remained 'attached' though the liquid film that was not ruptured and the three phase contact line was not formed (Ralston *et al.* 1999). Accordingly, alumina and zirconia particles can form three phase contact line whilst attached to the bubble which is governed by high contact angle but also can 'stick' to the bubble through the liquid film because of the electrostatic attraction of negatively charged surfaces. However, silica particle attachment is expected to be entirely due to the three phase contact angle formation since the negatively charged surfaces would repulse each other through the liquid film. Therefore the electrostatic adsorption barrier between silica and bubble surface is a contributing factor for the low coverage angles as opposed to alumina and zirconia particles. Indeed, silica contact angle measured with adhesive glass slide method Table 5.4 was larger than the zirconia particles, 75° and 49° respectively, therefore more hydrophobic silica is expected to give larger coverage angles than zirconia. However, the coverage angles with silica are significantly lower than with zirconia particles. The electrostatic adsorption barrier gives satisfactorily explanation of such reversed situation. The attraction is between particle and bubble (if oppositely charged) is stronger for larger particles (Tcholakova *et al.* 2008). Though high contact angle between water and silica particles should result in stronger particle to bubble adhesion and hence in large coverage angle, the repulsion between negative particles and negative bubble surface inhibits the attachment of freely falling silica particles (see Figure 5.12b). Therefore the hydrodynamic forces causing the collision of particle with bubble (which pushes particle to bubble) appears to be insufficient to

exceed such force of electrostatic repulsion and further drain the liquid film between silica particle and bubble. 'Dry' contact angles between silica and zirconia particles and water using glass slide method were lower than alumina particles (Table 5.4). Also, alumina particles have largest coverage angles. The combined effect of largest hydrophobicity and electrostatic attraction between positive alumina particles and negative bubble surface explains the largest coverage angles with these particles.

#### 5.4.1.3 Attachment of particles to bubble suspended in oil

Investigation of the particle to bubble attachment in paraffin oil was more difficult than with water due to the high viscosity of oil (~100 times water). Shear produced during relative motion of bubble and oil (velocity of 0.1 cm/s) caused the sweeping of attached particles (Figure 5.14). Nevertheless, particles attachment to the bubble was observed in a stationary system. The alumina, silica and zirconia particles attachment to air bubble in paraffin oil are shown in Figure 5.15a. The particle to bubble attachment was also investigated in decane (Figure 5.15b) because it has physicochemical properties similar to paraffin oil at 210°C (see Chapter 2, Experimental and methodology). This means that the conditions were similar to Fischer Tropsch synthesis (~210°C) that was used in measurements of the bubble size in paraffin oil at elevated temperature (Chapter 2). Additionally, the bubble pick up method could be used more efficiently, i.e. decane has much lower viscosity (0.84cP, 20°C) than paraffin oil which means, that the shear produced by the bubble movement is significantly reduced and the particles sweeping did not occur.

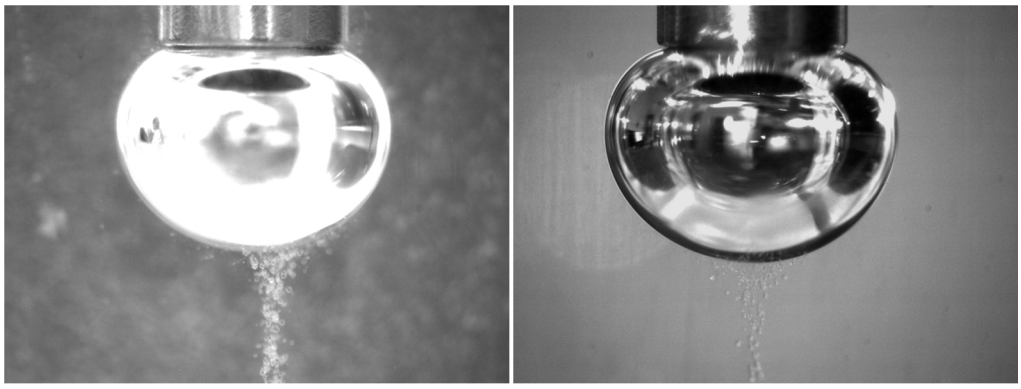

Figure 5.14 Sweeping of the particles off the bubble in oil using bubble pick up method (1.81 mm needle diameter)

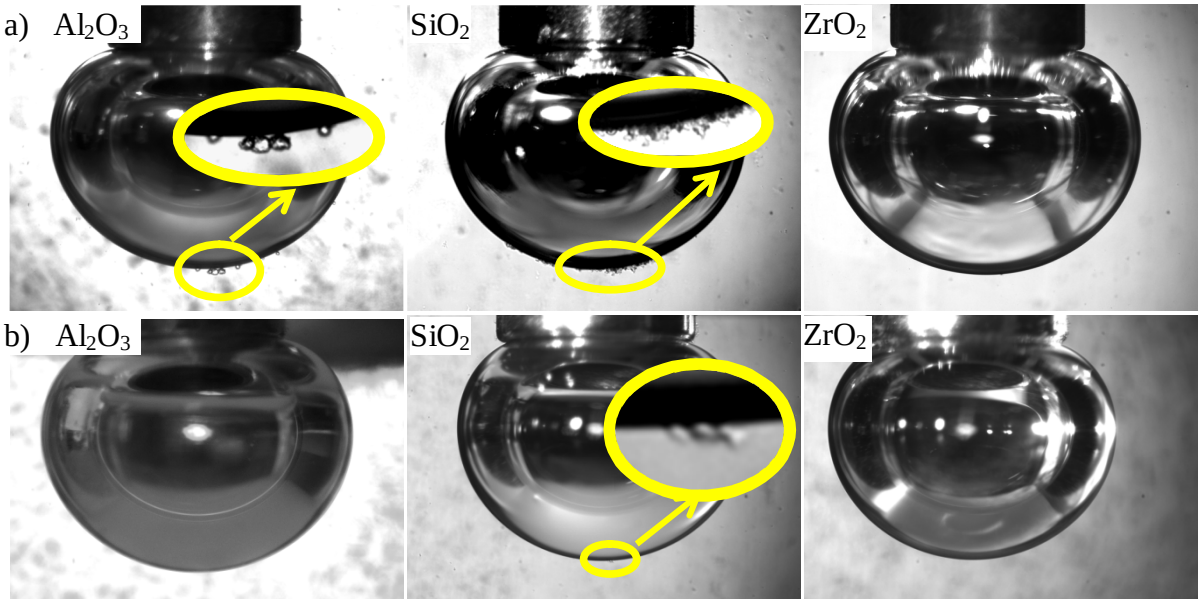


Figure 5.15 Particles to bubble attachment in a) paraffin oil and in b) decane (3.6x2.8 mm)

Figure 5.15a) shows that particles attach to the bubble attachment in paraffin oil. The highest coverage was observed with the silica particles but also alumina particles were attached to the air bubble in paraffin oil but no attachment of zirconia particles was observed. It appears that zirconia is the least lyophobic and the most favourable position that the particles take in the air-paraffin oil dispersion is the bulk of oil. The zirconia particles have the largest dispersive component of surface energy, therefore the interactions between these particles and paraffin oil are the strongest (as compared to alumina and silica). Also, the zero

contact angle between paraffin oil and zirconia particles confirm lyophilic character of particles (Nowak *et al.* 2013). High dispersive component of surface energy indicates the complete spreading of non-polar liquid, therefore the zirconia particles preferential position in respect to the air-oil interface is the oil bulk.

Presence of alumina and silica particles at the air-paraffin oil interface indicates a certain degree of lyophobicity. The lyophobicity is more pronounced for silica particles; it forms larger coverage angles than alumina (Table 5.5). Attached alumina particles (Figure 5.15a) have visibly larger size than the silica particles. The microscopic images of particles pre-suspended in paraffin oil (for approximately 3h) clearly show the alumina aggregates whereas silica particles is uniformly dispersed (Figure 5.16a). In decane, silica particles were the only particles that were attached to the air bubble (Figure 5.15b). Silica particles in decane formed lower coverage angles than in paraffin oil because of lower decane surface tension (25% lower) and hence lower capillary force that is a dominant force in the particle to bubble attachment. The effective contact angles that calculated from the coverage angles of alumina and silica particles are also low (Table 5.5). Measurements of contact angles showed that complete spreading of paraffin oil on the alumina and silica particles occurred, hence that the particles are lyophilic (Nowak *et al.* 2013). Particle to bubble attachment experiments however show that they tend to remain at the interface oil/ air interface.

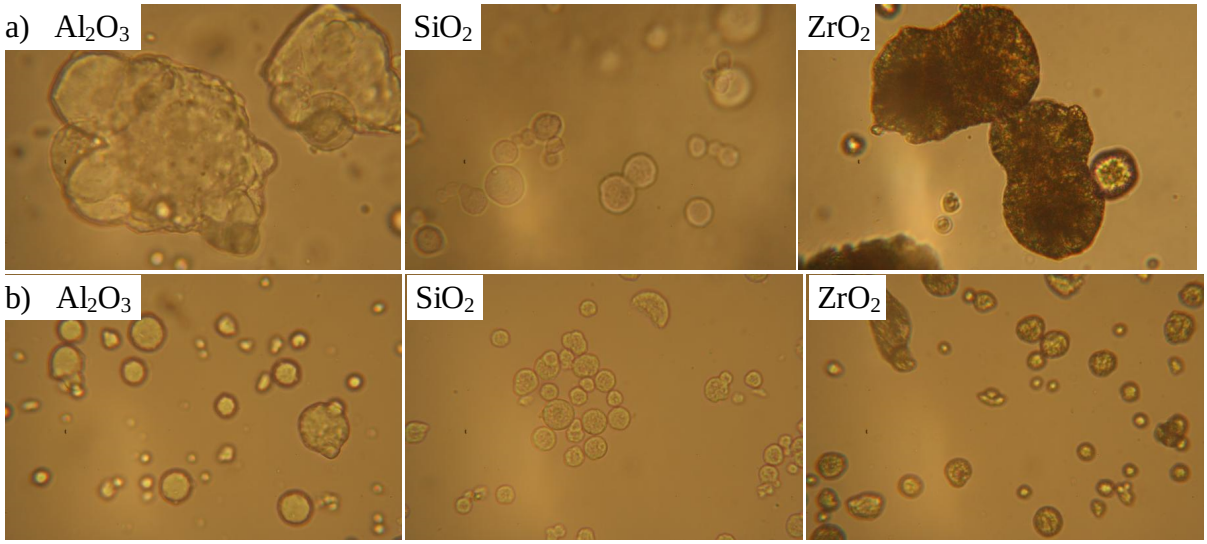


Figure 5.16 Alumina and silica suspended in a) oil and in b) water (210x140 μm)

Table 5.5 The coverage angle, adhesion force and effective contact angle that particles form at the bubble in paraffin oil

| Catalyst support | $R_p$, μm | $R_b$, mm | Coverage angle α, ° | $F_{adh}$, $10^{11}$ N | Effective contact angle $\theta_e$, ° |
|---|---|---|---|---|---|
| $Al_2O_3$ | 16 | 1.42 | 6 | 0.4 | 0.13 |
| $SiO_2$ | 13 | 1.41 | 36 | 14.6 | 0.87 |
| $ZrO_2$ | 26 | 1.46 | 0 | - | - |

### 5.4.2 Particles adsorption at interface

#### 5.4.2.1 Particles to droplet attachment

The investigation of the particles adsorption at the paraffin oil/water interface in stagnant conditions was carried out by initially dispersing the particles either in water or in paraffin oil. Subsequently, images of the particles attachment to formed droplet of water (or oil) were recorded. Figure 5.17 shows the particles adsorption (attachment at the droplet of paraffin oil formed in water. When the droplet of oil was formed in water, the particles was dispersed above such droplet and the images show the particles sedimentation method.

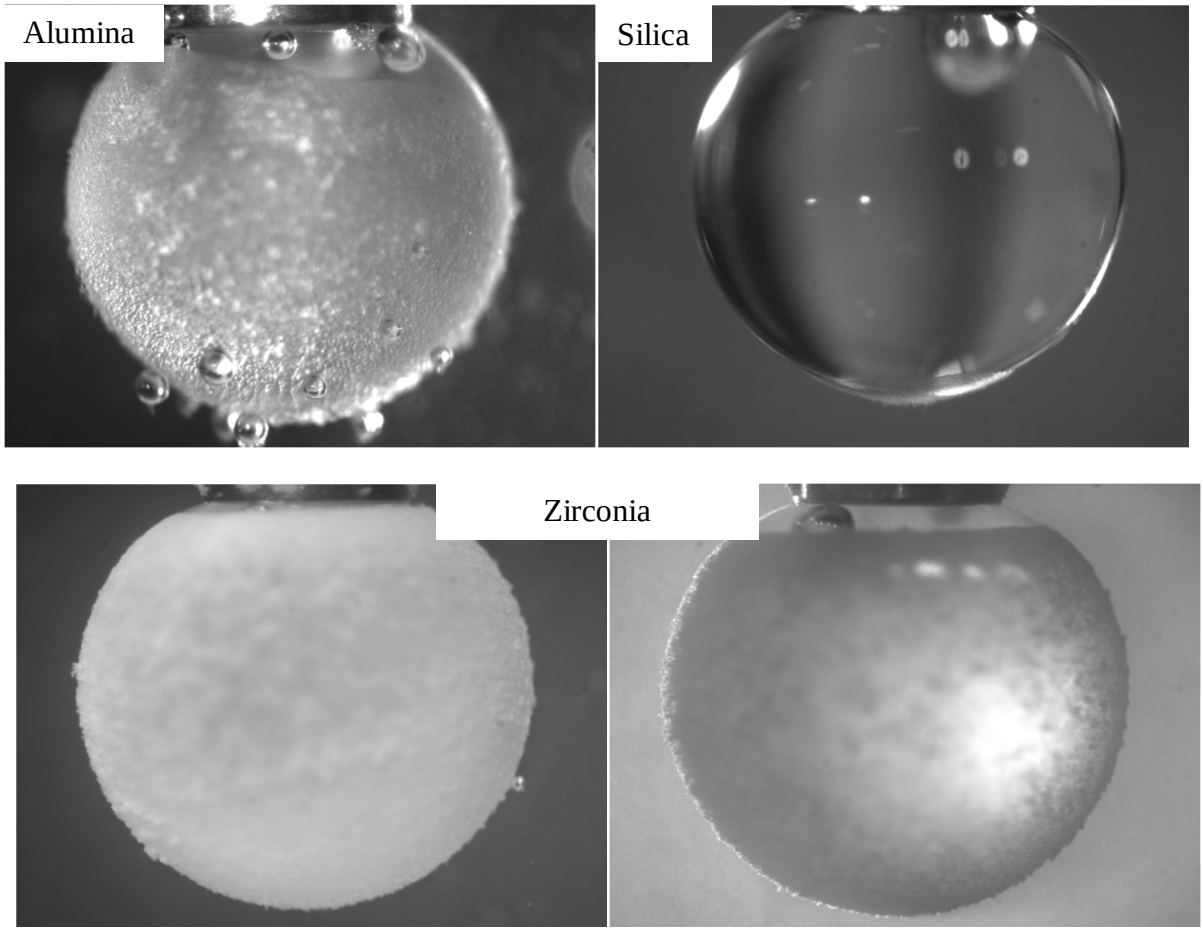


Figure 5.17 Particles to oil droplet attachment in water (1.81mm needle diameter)

Alumina and zirconia particles adsorbed almost on the entire interface whereas silica attachment was scarce. Clearly, the silica particles are strongly hydrophilic and only small attachment at the droplet bottom was observed (coverage angle ~5°). However, such low coverage of paraffin oil droplet with silica particles indicates presence of small fraction of hydrophobic/lyophilic parts on the particles surface. There is clear tendency of alumina and zirconia particles to remain adsorbed at the water/oil interface. These results suggest that alumina and zirconia reveal amphiphilic character, i.e. they can interact with paraffin oil through the dispersive forces but also can interact with water through the polar forces, so the polar groups are present at the surface.

It should be noted that the $OH^-$ ions (dissociation of water) that are adsorbed at the oil-water interface cause the electrostatic, negative charge at the interface (Danov *et al.* 2006). Particle suspended in water are charged because the high dielectric constant of water (~80) facilitate the ions dissociation in the bulk of water and on particle surface (Hsu 2004). So as previously discussed, the alumina and zirconia particles reveal positive electrostatic charge whereas silica is negative. Therefore the low adsorption of silica particles is also (apart from hydrophilicity) caused by the presence of electrostatic repulsion. The positive charge on alumina and zirconia particles dispersed in distilled water produce the large coverage of oil droplet in water.

In the second version of this experiment, the particles were initially suspended in the paraffin oil. Subsequently, the water droplet was formed in the oil and the bubble pick up method was used to attempted attachment of particles attachment to the water/oil interface. The images of particles attached to droplets are shown in Figure 5.18 and Figure 5.19. Alumina and zirconia particles can be seen at the paraffin oil-water interface whereas silica particles were transferred from the bulk of paraffin oil to the bulk of water and no presence at

the interface was detected adsorption was observed. Transfer of silica particles from one liquid to another happened within the fraction of a seconds. Once the silica entered the water droplet, the random movement of particles inside the droplet was observed.

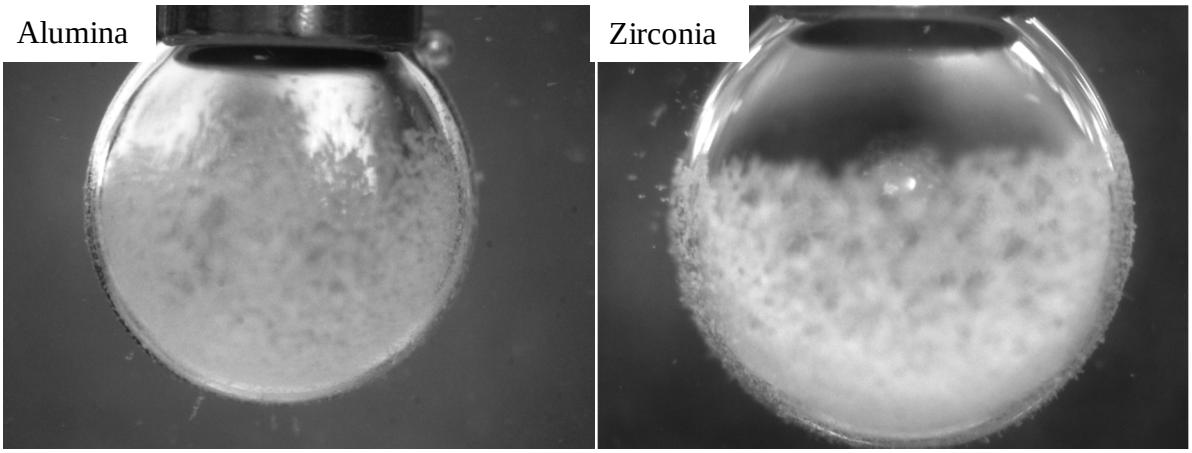


Figure 5.18 Alumina and zirconia attachment to the water droplet in vara oil (1.81 mm needle diameter)

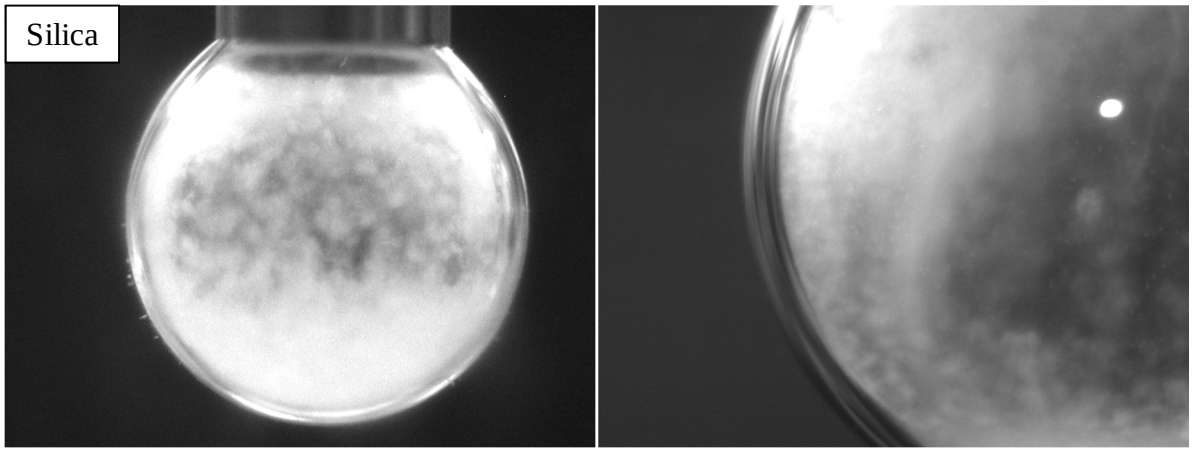


Figure 5.19 Silica particles to water in oil droplet attachment (1.81 mm needle diameter)

The behaviour of silica particles that were initially suspended in paraffin oil is very interesting because the transfer of particles from oil to water phase occurred. Not only proves high hydrophilicity (or lyophobicity) of silica particles but also indicates the amphiphilic

character of alumina and zirconia particles, i.e. the ability to adsorb at the paraffin oil/water interface.

Silica particles are preferentially wetted by water therefore they are transferred from bulk of paraffin oil to water. The work of such particles transfer (egulfing in Figure 5.4) from one liquid to another exceeds the energy of adsorption/desorption at the interface, therefore the energy of desorption is unimportant Clearly, silica particle interfacial energy with water is much lower than with paraffin oil, which cause engulfing of the particles by water ($\Delta W_{tot}<0$). It is essential that the total work is negative which for the transfer of silica particles (3) from oil (1) to water (2) equals:

$$\Delta W_{tot}^{1\to 2} = 4\pi r^2 \cdot (\gamma_{23} - \gamma_{13}) \tag{5.6}$$

When the engulfing occurs, the above equation implies that interfacial energy of particle silica/water is lower than the interfacial energy of silica/paraffin oil ($\gamma_{23}<\gamma_{13}$). This implies that silica is better wetted by the water than by oil. Of course, the adsorption/desorption processes have to be taken into account once the particle is transferred from one liquid to the other through the interface. The final, necessary condition of such particles transfer accounts also the repulsion from one liquid and attraction from another one, so $\Delta\vec{W}$ and $\Delta\overleftarrow{W}$ must have opposite sign, so the necessary condition is that $\gamma_{23} + \gamma_{13} > \gamma_{12}$. The experiments imply that the sum of silica-water and interfacial oil-silica interfacial energies is larger than the water-oil interfacial energy.

It was interesting to notice the presence of long range attraction between droplets of water and alumina or zirconia particles suspended in paraffin. The example is shown in Figure 5.20, where the aggregate of alumina particles is first attracted to the paraffin oil/water

interface, remained there 1-2s and was subsequently repelled. The repulsion of the (adsorbed) small aggregate from the surface was faster than the attraction, and the aggregate behaved as injected back to the bulk of paraffin oil. Apparently, at the interface charge reorientation takes place once the particles/aggregate is attracted to the water/oil surface covered with same particles. Such behaviour was observed many times with alumina and zirconia particles/aggregates (images not shown). Strong interaction between droplet of water/oil and particle suspended in oil were previously also observed (Danov *et al.* 2006; Danov *et al.* 2006; Tcholakova *et al.* 2008). Though the dielectric constant of oils (~2) is normally too low for ion dissociation (from the polar groups on the particle surface) the most probable reason for such particles attraction from the bulk of oil to the droplet of water is the presence of electric charge at the oil-particle interface (Hsu 2004; Danov *et al.* 2006).

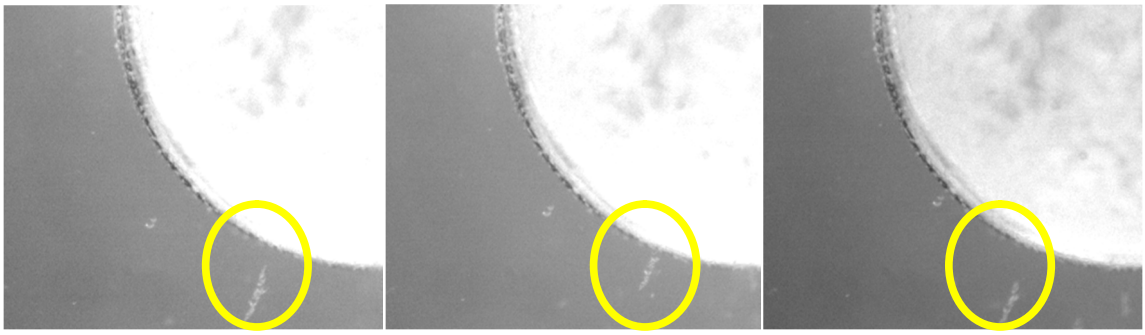

Figure 5.20 Consecutive pictures (2 seconds interval) of attraction/repulsion alumina particles to/from the water/oil interface

The particles layer covering the droplet differs significantly depending on the liquid in which the particles were initially suspended. Clearly, the coverage is much denser with the alumina or zirconia particles that were initially suspended in water (Figure 5.17) than those initially suspended in oil (Figure 5.18). The particles adsorbed at the oil/water interface undergo very long-range (a few particle diameter) repulsive forces and such phenomena was observed only for the particles initially suspended in oil phase. This repulsion is much stronger than that between charged particles in water (Aveyard *et al.* 2002; Danov *et al.*

2006). Particles that are adsorbed at the water/oil (i.e. interface between polar and non-polar liquid) acquire asymmetric charge distribution on their surface, resembling their behaviour dipoles (Figure 5.21) (Aveyard *et al.* 2002). It is caused by dissociation of the polar groups from the part of particles surface immersed in the water. Adsorbed particles at the water/oil interface repel each other because of the electrostatic (negative) charge and such particles form hexagonal arrays at the interface spaced by several diameters (Danov *et al.* 2006).

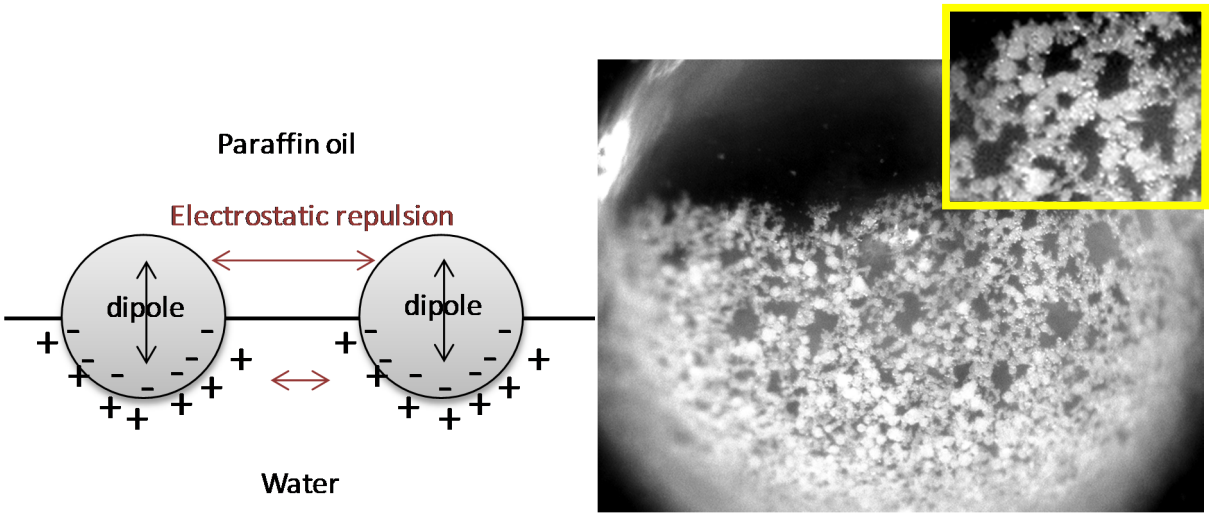


Figure 5.21 Repulsion between zirconia particles adsorbed at the polar (water) and non-polar (paraffin oil) interface

#### 5.4.2.2 Water-oil emulsions

Alumina, titania and zirconia produced stable emulsions (more than few weeks) whereas silica particles did not stopped the water and oil phases separation (Figure 5.22). Lack of emulsion stabilisation proves that the silica particles are highly hydrophilic and lyophobic towards paraffin oil. Also, titania particles show abilities to adsorb at the water/oil interface and stabilise the emulsion. The size of produced oil droplets indicates also the strength of the adsorption, the smaller the droplets the less stable droplets and higher tendency for coalescence/flocculation. The alumina particles produced smaller droplets to titania and

considerably smaller than zirconia. It is worth to notice that the particles initially suspended in water formed more uniform sizes of droplets and particles initially suspended in oil non-uniform sized droplets of oil.

The liquids that formed continuous and dispersed phase in emulsions were detected using water insoluble and oil insoluble pigments. Droplets (dispersed phase) were made of oil. Oil in water emulsion indicates that the particles reveal hydrophilic character, i.e. the continuous phase wets better the particles and the larger particle volume is immersed in water according to the Bancroft rule (Ashby *et al.* 2000). Oil droplets in water indicate that the particles have water contact angle $\Theta < 90^{o}$ according to Figure 5.6a. Clearly, the particles reveal preferential wettability by water, i.e. oil droplets were produced, larger part of alumina, titania and zirconia particles adsorbed at the interface were immersed in water (Tambe *et al.* 1994).

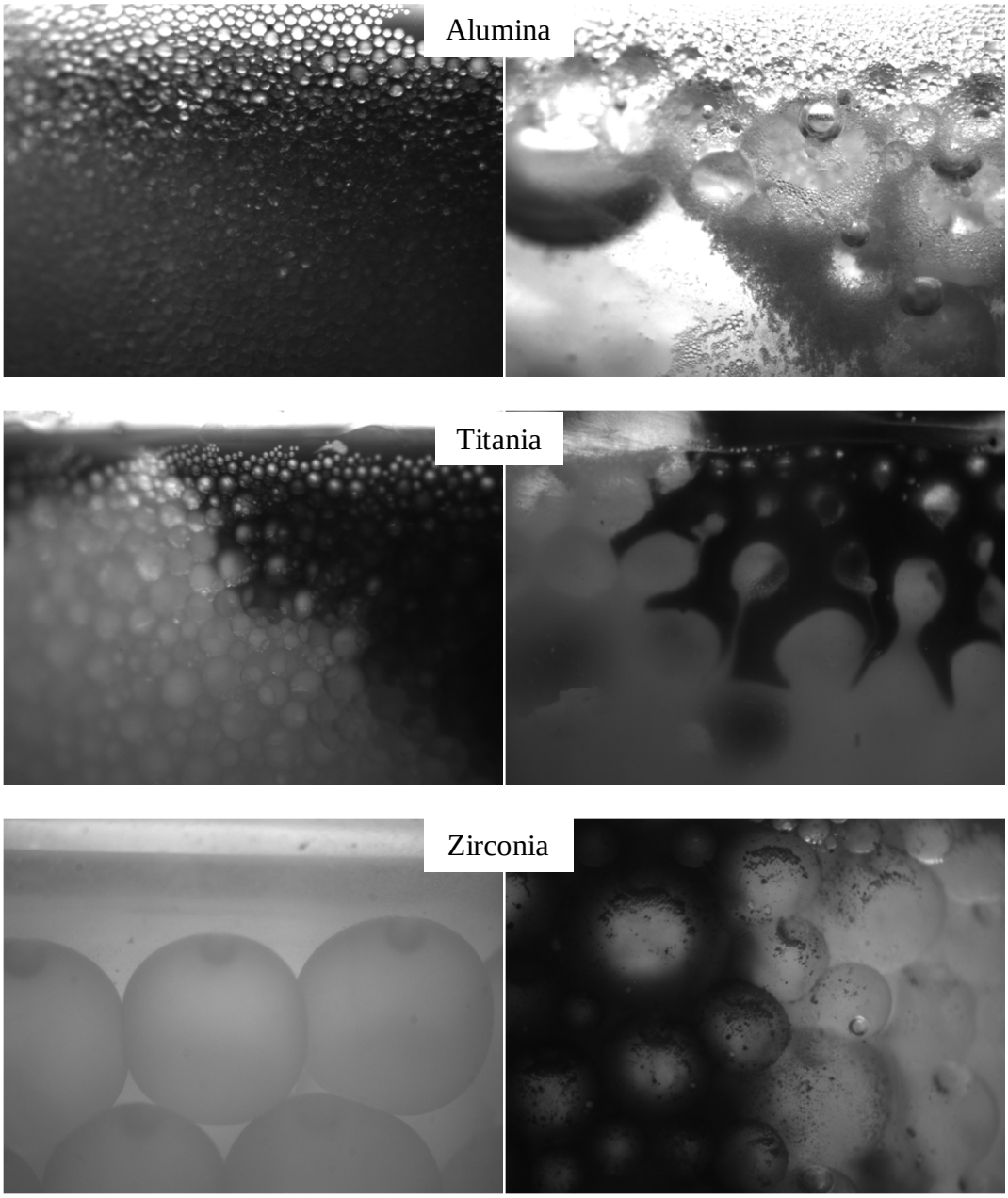


Figure 5.22 Left columns show the mixtures where the particles were initially suspended in water and right column shows the mixtures where the particles were initially suspended in oil (5.0x3.75mm)

## 5.5 Summary and conclusions

Fundamental study that employs single bubble/droplet immersed in liquid as well as practical application, i.e. emulsion stabilisation, clearly showed particles adsorption at the interface. Different behaviour of particles was observed, specifically, there was a clear difference between silica particles and alumina/zirconia at all investigated interfaces. Though the experiments with titania particles were difficult due to opaque suspension they form in water, they stabilised emulsion what proves high adsorption at the water-paraffin oil interface.

Silica particles show the largest degree of lyophobicity in comparison with alumina, titania and zirconia. The ability of silica particles to remain at the air/oil interface indicates that the particles might affect the bubbles coalescence rate. Therefore additional set of experiments was performed in which the effect of particles on the air bubbles coalescence was investigated. The air bubbles, formed at the tip of a needle, were immersed in the oil or oil/particles suspension. The air bubbles were brought in the close proximity and when coalescence did not occur spontaneously, the volume of bubble above was increased until detachment of bubble from the needle occurred.

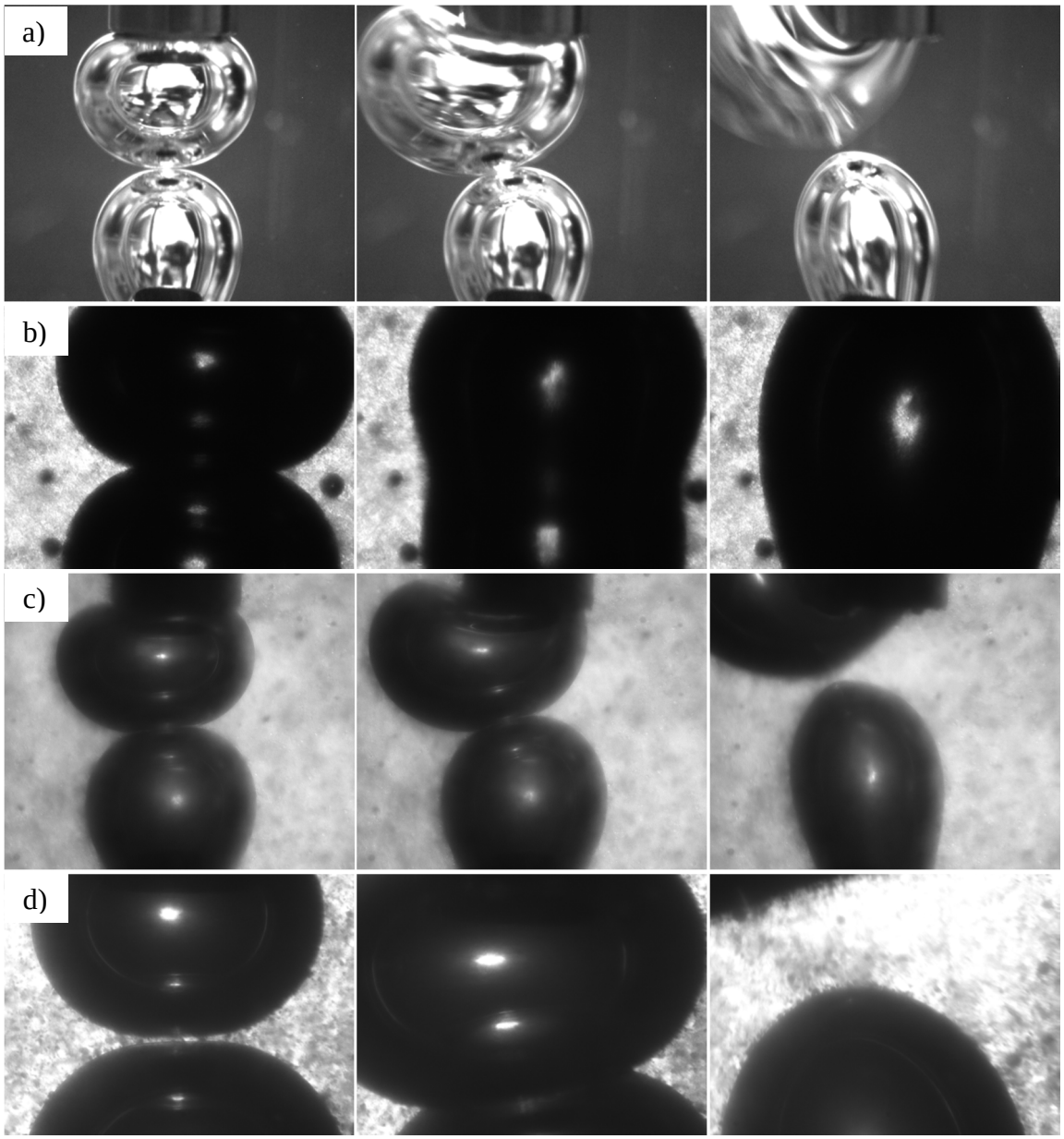


Figure 5.23 Investigation of air bubbles coalescence in a) paraffin oil, b) paraffin oil/silica, c) paraffin oil/alumina, d) paraffin oil/zirconia. Time span for non-coalescing bubbles 0:1:2s, for coalescing bubbles 0:0.06:0.12s (needle diameter 1.81 mm)

Images (Figure 5.23) indicate that the air bubbles in pure paraffin oil did not coalesce and that the presence of alumina (Figure 5.23c) and zirconia (Figure 5.23d) particles did not affect bubbles in paraffin oil, but silica particles enhanced the coalescence (Figure 5.23b). Apparently, silica particles enhances coalescence rate due to the bridging effect, where the particles are pushed towards the gas phase (or try to escape from the oil phase) which lead to

more efficient liquid film drainage. Similar tendency of bubbles covered with highly hydrophobic particles was observed in water (Ata 2009). It must be noted that the “stagnant” conditions can be very different than the conditions present in the stirred tank reactor in turbulent flow. The significant error is expected linked to the difference in contact time between bubbles which is significantly lower and hence less efficient liquid film thinning/drainage. It can be concluded that bubbles coalescence experiments prove that the particles are able to enhance bubble coalescence. The essential step in the bubbles coalescence is the thin liquid film drainage between bubbles and clearly, the presence of particles in such a film increases the rate of its thinning and disruption. Particle in the gas-liquid interface can bridge approaching gas bubbles in liquid, where the three phase contact line is created.

Silica particles proved to be hydrophilic, i.e. very small fraction of particles attached to the bubble in water and the largest amount attached to bubble in paraffin oil. High lyophobicity was clearly seen when the particles transfer from oil to water phase occurred and insignificant attachment to droplet of oil was observed. Finally, the particles did not stabilise emulsion, hence silica particles were not present at the interface.

Alumina and zirconia particles are amphiphilic and experiments confirm high adsorption abilities at the water/paraffin oil interface. Larger number of alumina particles adsorbed at the air bubble/water interface proves particles hydrophobicity which is somewhat greater for alumina. Some degree of alumina lyophobicity was observed since small amount of the particles were attached to the bubble in paraffin oil whereas no attachment with zirconia particles was observed. High adsorption at the paraffin oil/water interface was found with alumina and zirconia particles initially suspended in water. Alumina and zirconia

particles initially suspended in paraffin oil attached to the water droplet and the strong electrostatic repulsion between adsorbed particles occurred. Finally, the ability to stabilise emulsion by producing droplets of oil in water show that the alumina and zirconia particles, though amphiphilic, are better wetted by water.

Particles attachment to the interface made of polar and non-polar media can be extrapolated to the particles effect on the bubble size. For instance, lack of silica particles at the water/oil interface might indicate that the particles are prone to cause bridging effect with the bubbles made of steam since is the hydrophilic and would tend to go ‘inside’ the bubble. Alumina and zirconia however can in principle stabilise steam bubbles via Pickering stabilisation since are prone to remain at the water/oil interface. In air/oil arrangement, only small amount of the silica particles and even less of alumina were found in stagnant conditions whereas no zirconia attachment was observed. This might indicate that when mixing is applied, the particles attachment does not occur. Therefore the coalescence inhibition might occur only when the bubbles were made of steam and the results on the bubble size showed that the reduction of bubbles occurred only for the polar gas/non-polar liquid.

# Chapter 6

# 6 Conclusions and Recommendations

## 6.1 Summary and conclusions

The gas-liquid interfacial area in the multiphase system strongly depends on the gas composition. The bubble size in high molecular paraffin oil increase significantly when the steam is present in the gas phase due to larger restoring forces, i.e. steam-oil interfacial tension is larger than $N_2$-oil. Reduction of mass transfer rates might occur when steam is present in the system caused by decrease of interfacial area due to larger bubbles.

Different catalyst supports have different effect on the bubble size because of different surface properties, however quantification is difficult. The contact angle measurements showed that only $TiO_2$ particles reveal slightly lyophobic character whereas complete spreading on $Al_2O_3$, $SiO_2$ and $ZrO_2$ suggest that particles are lyophilic. Subsequently, water contact angles showed that to different degree all particles reveal hydrophobic character. Therefore such quantified hydro/lyophobicity of particles (contact angles) shows preferential wetting by paraffin oil and non-wetting by water, hence indicates low particles adsorption at the paraffin oil-water or gas-oil interface (remain in bulk) and strong attachment to bubbles in water. However, experiments that aimed to visualise the particles presence at the interface clearly show that particles have high ability to remain adsorbed at the interface. Experiments with the droplets formed in other liquid clearly show that $Al_2O_3$ and $ZrO_2$ strongly adsorb at the paraffin oil-water interface and also these and $TiO_2$ particles stabilise the emulsions. Presence of the polar and non-polar groups at the surface (amphiphilic character) causes the ability of the particle to remain at the liquids interface. Though particle to bubble attachment in water confirmed that $Al_2O_3$ is more hydrophobic than $SiO_2$ and $ZrO_2$, the $ZrO_2$ attachment was stronger than the $SiO_2$ particles in contrary to water contact angles. Contact angle does not fully describe particles/gas/oil interactions. Measured contact angles between oil and particles and between water and particles is insufficient for the prediction of the behaviour of

the particles at the water-oil interface. Particles/gas/oil interaction is more accurately described by interfacial energies, since the favourableness of the particle attachment to bubble followed the trend of the energy of the three phase system upon particle attachment.

Simulation of FT synthesis with dry gas might lead to incorrect conclusions, i.e. alumina increases nitrogen bubbles but reduces bubbles containing steam but zirconia particles do not affect nitrogen bubbles but reduces steam ones. Also, silica particles do not affect nitrogen bubbles but increases steam bubbles. Presence of different particles affects the bubble coalescence rate. The degree of particles lyophobicity and size are the major parameters responsible for the bubbles ($N_2$) size which are either increased (with $Al_2O_3$ and $TiO_2$) or unchanged (with $SiO_2$ and $ZrO_2$). The size of steam bubbles in paraffin oil however is a combined result of particles size, wettability by water and paraffin oil but also the adsorption at interface abilities. Results show that steam bubbles are reduced with presence of alumina and zirconia particles whereas increased with silica particles. Apparently, alumina and zirconia particles have an ability to stabilise and hinder bubble coalescence when steam (polar medium) is present in the gas phase but silica particles enhance such bubble coalescence rate due to the bridge formation between the colliding bubbles. Particles that are able to remain at the water/oil interface characterise with lyophilic and hydrophilic parts on the surface and are sufficiently small, i.e. 20μm particles. Catalysts, characterized by the large amount of lyophilic/hydrophobic centres on the surface, appear to stabilise the steam bubbles against coalescence. Since the contact angle fails to predict particles attachment to the fluid/liquid interface, analysis of particles should be performed using inverse gas chromatography for the magnitude of dispersive component determination and calculation of the three phase system energy followed by the set of experiments that are able to visualise particles at the interface.

## 6.2 Future recommendations

The key recommendations for future work arising from this study are detailed below:

- Bubble size measurements were carried out in stirred tank reactor in a batch mode therefore the future work should include the experiments carried out in continues mode. Thus obtained absolute values as well as observed trends should be compared with the batch mode, where the equilibrium bubble size was measured. Such comparison would be very informative, i.e. the effect of particles on the transient and equilibrium bubble size should follow the same trend.
- As the gas volume dispersed in oil increases when the mixing intensity increases the *Po* number should be measured for the more accurate energy dissipation rate calculations which might lead to more accurate correlations.
- The higher the energy dissipation rate the larger the input of bubble coalescence since there is larger amount of gas dispersed in the liquid therefore the larger the collision probability. In order to exclude the increasing significance of the coalescence at the highest energy dissipation rates it is advisable to study the bubble sizes in non-coalescing system with large gas volume fraction.
- For the largest steam-oil interfacial areas, it is recommended to manufacture catalyst particles with varying size, shape and centres on the surface, i.e. hydrophilic, which are able to form hydrogen bonds with the water molecule but also substantial hydrophobic centres that are able to interact with non-polar oil via dispersive forces. Catalyst surface properties should be subsequently tested for the degree of such centres via inverse gas chromatography (Chapter 4) and attachment at the interface (Chapter 5).

# REFERENCES


Akita, K. and F. Yoshida (1974). "Bubble Size, Interfacial Area, and Liquid-Phase Mass Transfer Coefficient in Bubble Columns." Industrial & Engineering Chemistry Process Design and Development **13**(1): 84-91.

Albal, R. S., Y. T. Shah, N. L. Carr and A. T. Bell (1984). "Mass transfer coefficients and solubilities for hydrogen and carbon monoxide under Fischer-Tropsch conditions." Chemical Engineering Science **39**(5): 905-907.

Albal, R. S., Y. T. Shah, A. Schumpe and N. L. Carr (1983). "Mass transfer in multiphase agitated contactors." The Chemical Engineering Journal **27**(2): 61-80.

Albijanic, B., O. Ozdemir, A. V. Nguyen and D. Bradshaw (2010). "A review of induction and attachment times of wetting thin films between air bubbles and particles and its relevance in the separation of particles by flotation." Advances in Colloid and Interface Science **159**(1): 1-21.

Alper, E. and S. Ozturk (1986). "Effect of fine solid particles on gas-liquid mass transfer in a slurry reactor." Chemical Engineering Communications **46**(1-3): 147-158.

Alper, E., B. Wichtendahl and W. D. Deckwer (1980). "Gas absorption mechanism in catalytic slurry reactors." Chemical Engineering Science **35**(1-2): 217-222.

Alves, S. S., C. I. Maia, J. M. T. Vasconcelos and A. J. Serralheiro (2002). "Bubble size in aerated stirred tanks." Chemical Engineering Journal **89**(1–3): 109-117.

Ashby, N. P. and B. P. Binks (2000). "Pickering emulsions stabilised by Laponite clay particles." Physical Chemistry Chemical Physics **2**(24): 5640-5646.

Ata, S. (2009). "The detachment of particles from coalescing bubble pairs." Journal of Colloid and Interface Science **338**(2): 558-565.

Aveyard, R., B. P. Binks, J. H. Clint, P. D. I. Fletcher, T. S. Horozov, B. Neumann, V. N. Paunov, J. Annesley, S. W. Botchway, D. Nees, A. W. Parker, A. D. Ward and A. N. Burgess (2002). "Measurement of Long-Range Repulsive Forces between Charged Particles at an Oil-Water Interface." Physical Review Letters **88**(24): 246102.

Balasubrahmanyam, S. N. (2008). "Einstein, `parachor' and molecular volume: Some history and a suggestion." CURRENT SCIENCE -BANGALORE- **VOL 94**(NUMB 12,): 1650-1658

Behkish, A., R. Lemoine, L. Sehabiague, R. Oukaci and B. I. Morsi (2007). "Gas holdup and bubble size behavior in a large-scale slurry bubble column reactor operating with an organic liquid under elevated pressures and temperatures." Chemical Engineering Journal **128**(2-3): 69-84.

Behkish, A., Z. Men, J. R. Inga and B. I. Morsi (2002). "Mass transfer characteristics in a large-scale slurry bubble column reactor with organic liquid mixtures." Chemical Engineering Science **57**(16): 3307-3324.

Berg , J. C., Ed. (1993). Wettability. Surfactant Science Series. New York, CRC Press.

Binks, B. P. (2002). "Particles as surfactants—similarities and differences." Current Opinion in Colloid & Interface Science **7**(1–2): 21-41.

Binks, B. P. and C. P. Whitby (2005). "Nanoparticle silica-stabilised oil-in-water emulsions: improving emulsion stability." Colloids and Surfaces a-Physicochemical and Engineering Aspects **253**(1-3): 105-115.

Boode, K. and P. Walstra (1993). "Partial coalescence in oil-in-water emulsions 1. Nature of the aggregation." Colloids and Surfaces A: Physicochemical and Engineering Aspects **81**(0): 121-137.

Boon, M., T. A. Meeder, J. J. Heijnen and K. Luyben (1992). "Influence of oxygen adsorpion of the dynamic kla measurement in 3-phase slurry reactors." Biotechnology and Bioengineering **40**(9): 1097-1106.

Bouaifi, M., G. Hebrard, D. Bastoul and M. Roustan (2001). "A comparative study of gas hold-up, bubble size, interfacial area and mass transfer coefficients in stirred gas-liquid reactors and bubble columns." Chemical Engineering and Processing **40**(2): 97-111.

Bujalski, W., A. W. Nienow, S. Chatwin and M. Cooke (1987). "The dependency on scale of power numbers of Rushton disc turbines." Chemical Engineering Science **42**(2): 317-326.

Butt, H.-J. (1994). "A Technique for Measuring the Force between a Colloidal Particle in Water and a Bubble." Journal of Colloid and Interface Science **166**(1): 109-117.

Calabrese, R. V., M. K. Francis, V. P. Mishra and S. Phongikaroon (2000). Measurement and Analysis of Drop Size in a Batch Rotor-Stator Mixer. 10th European Conference on Mixing. H. E. A. v. d. Akker and J. J. Derksen. Amsterdam, Elsevier Science**:** 149-156.

Calderbank, P. H. (1958). "Physical rate processes in industrial fermentation. Part I: The interfacial area in gas-liquid contacting with mechanical agitation." Trans. Instn Chem. Engrs **36**: 443–463.

Cao, D. B., Y. W. Li, J. G. Wang and H. J. Jiao (2011). "Chain growth mechanism of Fischer-Tropsch synthesis on Fe5C2(001)." Journal of Molecular Catalysis a-Chemical **346**(1-2): 55-69.

Chan, D. Y. C., E. Klaseboer and R. Manica (2011). "Film drainage and coalescence between deformable drops and bubbles." Soft Matter **7**(6): 2235-2264.

Chang, M.-Y. and B. I. Morsi (1992). "Mass transfer in a three-phase reactor operating at elevated pressures and temperatures." Chemical Engineering Science **47**(7): 1779-1790.

Chau, T. T. (2009). "A review of techniques for measurement of contact angles and their applicability on mineral surfaces." Minerals Engineering **22**(3): 213-219.

Chaudhari, R. V. and H. Hofmann (1994). Coalescence of gas bubbles in liquids. Reviews in Chemical Engineering. **10:** 131.

Cheng, J., P. Hu, P. Ellis, S. French, G. Kelly and C. M. Lok (2008). "A DFT study of the chain growth probability in Fischer–Tropsch synthesis." Journal of Catalysis **257**(1): 221-228.

Chesters, A. K. (1991). "The Modeling of Coalescence Processes in Fluid Liquid Dispersions - a Review of Current Understanding." Chemical Engineering Research & Design **69**(4): 259-270.

Chilekar, V. P., J. van der Schaaf, B. F. M. Kuster, J. T. Tinge and J. C. Schouten (2010). "Influence of Elevated Pressure and Particle Lyophobicity on Hydrodynamics and Gas-Liquid Mass Transfer in Slurry Bubble Columns." Aiche Journal **56**(3): 584-596.

Chun, B.-S. and G. T. Wilkinson (1995). "Interfacial tension in high-pressure carbon dioxide mixtures." Industrial & Engineering Chemistry Research **34**(12): 4371-4377.

Clark, K. N. (1990). "The effect of high pressure and temperature on phase distributions in a bubble column." Chemical Engineering Science **45**(8): 2301-2307.

Cosgrove, T. (2005). Colloid Science - Principles, Methods and Applications, Blackwell Publishing.

Dai, Z. F., D. Fornasiero and J. Ralston (1999). "Particle-bubble attachment in mineral flotation." Journal of Colloid and Interface Science **217**(1): 70-76.

Danov, K. D., P. A. Kralchevsky, K. P. Ananthapadmanabhan and A. Lips (2006). "Particle-interface interaction across a nonpolar medium in relation to the production of particle-stabilized emulsions." Langmuir **22**(1): 106-115.

Danov, K. D., P. A. Kralchevsky and M. P. Boneva (2006). "Shape of the capillary meniscus around an electrically charged particle at a fluid interface: Comparison of theory and experiment." Langmuir **22**(6): 2653-2667.

Das, S. C., I. Larson, D. A. V. Morton and P. J. Stewart (2010). "Determination of the Polar and Total Surface Energy Distributions of Particulates by Inverse Gas Chromatography." Langmuir **27**(2): 521-523.

Das, T. K., X. Zhan, J. Li, G. Jacobs, M. E. Dry and B. H. Davis (2007). Fischer-Tropsch synthesis: Kinetics and effect of water for a Co/Al2O3 catalyst. Studies in Surface Science and Catalysis. B. H. Davis and M. L. Occelli, Elsevier. **Volume 163:** 289-314.

Davis, B. H. (2002). "Overview of reactors for liquid phase Fischer–Tropsch synthesis." Catalysis Today **71**(3-4): 249-300.

Deckwer, W.-D., Y. Louisi, A. Zaidi and M. Ralek (1980). "Hydrodynamic Properties of the Fischer-Tropsch Slurry Process." Industrial & Engineering Chemistry Process Design and Development **19**(4): 699-708.

Deimling, A., B. M. Karandikar, Y. T. Shah and N. L. Carr (1984). "Solubility and mass transfer of CO and H2 in Fischer--Tropsch liquids and slurries." The Chemical Engineering Journal **29**(3): 127-140.

Deriâgin, B. V. (1989). Theory of stability of colloids and thin films, Consultants Bureau.

Desnoyer, C., O. Masbernat and C. Gourdon (2003). "Experimental study of drop size distributions at high phase ratio in liquid-liquid dispersions." Chemical Engineering Science **58**(7): 1353-1363.

Diaz, E., S. Ordonez, A. Vega and J. Coca (2004). "Adsorption characterisation of different volatile organic compounds over alumina, zeolites and activated carbon using inverse gas chromatography." Journal of Chromatography A **1049**(1-2): 139-146.

Diaz, E., S. Ordonez, A. Vega and J. Coca (2004). "Adsorption properties of a Pd/gamma-Al2O3 catalyst using inverse gas chromatography." Microporous and Mesoporous Materials **70**(1-3): 109-118.

Diaz, E., S. Ordonez, A. Vega and J. Coca (2005). "Comparison of adsorption properties of a chemically activated and a steam-activated carbon, using inverse gas chromatography." Microporous and Mesoporous Materials **82**(1-2): 173-181.

Dietrich, E., C. Mathieu, H. Delmas and J. Jenck (1992). "Raney-Nickel Catalyzed Hydrogenations - Gas-Liquid Mass-Transfer in Gas-Induced Stirred Slurry Reactors." Chemical Engineering Science **47**(13-14): 3597-3604.

Dry, M. E. (1990). "The fischer-tropsch process - commercial aspects." Catalysis Today **6**(3): 183-206.

Dry, M. E. (1996). "Practical and theoretical aspects of the catalytic Fischer-Tropsch process." Applied Catalysis A: General **138**(2): 319-344.

Dry, M. E. (2002). "The Fischer–Tropsch process: 1950–2000." Catalysis Today **71**(3–4): 227-241.

Dumont, E. and H. Delmas (2003). "Mass transfer enhancement of gas absorption in oil-in-water systems: a review." Chemical Engineering and Processing: Process Intensification **42**(6): 419-438.

Fielden, M. L., R. A. Hayes and J. Ralston (1996). "Surface and Capillary Forces Affecting Air Bubble−Particle Interactions in Aqueous Electrolyte." Langmuir **12**(15): 3721-3727.

Fillion, B. and B. I. Morsi (2000). "Gas−Liquid Mass-Transfer and Hydrodynamic Parameters in a Soybean Oil Hydrogenation Process under Industrial Conditions." Industrial & Engineering Chemistry Research **39**(7): 2157-2168.

Fillion, B., B. I. Morsi, K. R. Heier and R. M. Machado (2002). "Kinetics, Gas−Liquid Mass Transfer, and Modeling of the Soybean Oil Hydrogenation Process." Industrial & Engineering Chemistry Research **41**(4): 697-709.

Fowkes, F. M. (1962). "Determination of interfacial tensions, contact angles, and disperion forces in surfaces by assuming additivity of intermolecular interactions in surfaces." The Journal of Physical Chemistry **66**(2): 382-382.

Fowkes, F. M. (1964). "Attractive forces at interfaces." Industrial & Engineering Chemistry **56**(12): 40-52.

Fowkes, F. M. (1987). "Role of acid-base interfacial bonding in adhesion." Journal of Adhesion Science and Technology **1**(1): 7-27.

Fowkes, F. M. and M. A. Mostafa (1978). "Acid-Base Interactions in Polymer Adsorption." Industrial & Engineering Chemistry Product Research and Development **17**(1): 3-7.

Frye, G. C. and J. C. Berg (1989). "Antifoam action by solid particles." Journal of Colloid and Interface Science **127**(1): 222-238.

Garrett, P. R. (1993). "Recent Developments in the Understanding of Foam Generation and Stability." Chemical Engineering Science **48**(2): 367-392.

Geerlings, J. J. C., J. H. Wilson, G. J. Kramer, H. P. C. E. Kuipers, A. Hoek and H. M. Huisman (1999). "Fischer–Tropsch technology — from active site to commercial process." Applied Catalysis A: General **186**(1–2): 27-40.

Grajek, H., J. Paciura-Zadrozna and Z. Witkiewicz (2010). "Chromatographic characterisation of ordered mesoporous silicas Part I. Surface free energy of adsorption." Journal of Chromatography A **1217**(18): 3105-3115.

Grimsey, I. M., J. C. Feeley and P. York (2002). "Analysis of the surface energy of pharmaceutical powders by inverse gas chromatography." Journal of Pharmaceutical Sciences **91**(2): 571-583.

Guettel, R., U. Kunz and T. Turek (2008). "Reactors for Fischer-Tropsch Synthesis." Chemical Engineering & Technology **31**(5): 746-754.

Harnby, N. and H. Norman (1997). Mixing in the Process Industries: Second Edition, Butterworth-Heinemann.

Hegedus, C. R. and I. L. Kamel (1993). A review of inverse gas chromatography theory used in the thermodynamic analysis of pigment and polymer surfaces. Blue Bell, PA, ETATS-UNIS, Federation of Societies for Coatings Technology.

Hewitt, D., D. Fornasiero and J. Ralston (1995). "Bubble-particle attachment." Journal of the Chemical Society, Faraday Transactions **91**(13): 1997-2001.

Hichri, H., A. Accary, J. P. Puaux and J. Andrieu (1992). "Gas-Liquid Mass-Transfer Coefficients in a Slurry Batch Reactor Equipped with a Self-Gas-Inducing Agitator." Industrial & Engineering Chemistry Research **31**(8): 1864-1867.

Hinze, J. O. (1955). "Fundamentals of the hydrodynamic mechanism of splitting in dispersion processes." Aiche Journal **1**(3): 289-295.

Ho, R., A. S. Muresan, G. A. Hebbink and J. Y. Y. Heng (2010). "Influence of fines on the surface energy heterogeneity of lactose for pulmonary drug delivery." International Journal of Pharmaceutics **388**(1-2): 88-94.

Hobler, T. (1979). Heat transfer and heat exchangers, Wydawnictwa Naukowo-Techniczne.
Hsu, M. F. (2004). Charged Colloidal Particles in Nonpolar Solvents and Self-assembled Colloidal Model Systems, Harvard University.
Hu, B., A. W. Nienow, E. Hugh Stitt and A. W. Pacek (2006). "Bubble sizes in agitated solvent/reactant mixtures used in heterogeneous catalytic hydrogenation of 2-butyne-1,4-diol." Chemical Engineering Science **61**(20): 6765-6774.
Hu, B., A. W. Nienow and A. W. Pacek (2003). "The effect of sodium caseinate concentration and processing conditions on bubble sizes and their break-up and coalescence in turbulent, batch air/aqueous dispersions at atmospheric and elevated pressures." Colloids and Surfaces B: Biointerfaces **31**(1-4): 3-11.
Hu, B., A. W. Nienow, E. H. Stitt and A. W. Pacek (2007). "Bubble Sizes in Agitated Water−Hydrophilic Organic Solvents for Heterogeneous Catalytic Reactions." Industrial & Engineering Chemistry Research **46**(13): 4451-4458.
Hu, B., A. W. Pacek, E. H. Stitt and A. W. Nienow (2005). "Bubble sizes in agitated air–alcohol systems with and without particles: Turbulent and transitional flow." Chemical Engineering Science **60**(22): 6371-6377.
Hu, Y. and J. Dai (2003). "Hydrophobic aggregation of alumina in surfactant solution." Minerals Engineering **16**(11): 1167-1172.
Inga, J. R. and B. I. Morsi (1996). "A Novel Approach for the Assessment of the Rate-Limiting Step in Fischer−Tropsch Slurry Process." Energy & Fuels **10**(3): 566-572.
Inga, J. R. and B. I. Morsi (1997). "Effect of catalyst loading on gasliquid mass transfer in a slurry reactor: A statistical experimental approach." The Canadian Journal of Chemical Engineering **75**(5): 872-881.
Israelachvili, J. N. (2011). Intermolecular and Surface Forces, Third Edition, Academic Press.
Jiang, #160, P., Lin, T.-J., Luo, X., Fan and L.-S. (1995). Flow visualization of high pressure (21 MPa) bubble column: bubble characteristics. Amsterdam, PAYS-BAS, Elsevier.
Jiang, L., M. Krasowska, D. Fornasiero, P. Koh and J. Ralston (2010). "Electrostatic attraction between a hydrophilic solid and a bubble." Physical Chemistry Chemical Physics **12**(43): 14527-14533.
Jin, Y. and F. Wei, Eds. (2006). Multi-phase chemical reaction engineering and technology (Part II), Tsinghua University Press.
Johansson, G. and R. J. Pugh (1992). "The influence of particle size and hydrophobicity on the stability of mineralized froths." International Journal of Mineral Processing **34**(1–2): 1-21.
Joly-Vuillemin, C., C. de Bellefon and H. Delmas (1996). "Solid effects on gas-liquid mass transfer in three-phase slurry catalytic hydrogenation of adiponitrile over raney nickel." Chemical Engineering Science **51**(10): 2149-2158.
Joosten, G. E. H., J. G. M. Schilder and J. J. Janssen (1977). "Influence of Suspended Solid Material on Gas-Liquid Mass-Transfer in Stirred Gas-Liquid Contactors." Chemical Engineering Science **32**(5): 563-566.
Junmei, Z., X. Chunjian and Z. Ming (2006). "The mechanism model of gas-liquid mass transfer enhancement by fine catalyst particles." Chemical Engineering Journal **120**(3): 149-156.
Junmei, Z., D. Zhenya, X. Chunjian and Z. Ming (2008). "Solid effects on gas-liquid mass transfer in catalytic slurry system of isobutene hydration over fine ion exchange resin particles." Chemical Engineering Journal **136**(2-3): 276-281.
Karakashev, S. I. and M. V. Grozdanova (2012). "Foams and antifoams." Advances in Colloid and Interface Science **176–177**(0): 1-17.

Karakashev, S. I., O. Ozdemir, M. A. Hampton and A. V. Nguyen (2011). "Formation and stability of foams stabilized by fine particles with similar size, contact angle and different shapes." Colloids and Surfaces A: Physicochemical and Engineering Aspects **382**(1-3): 132-138.

Karandikar, B. M., B. I. Morsi, Y. T. Shah and N. L. Carr (1986). "Effect of water on the solubility and mass transfer coefficients of CO and H2 in a Fischer-Tropsch liquid." The Chemical Engineering Journal **33**(3): 157-168.

Karandikar, B. M., B. I. Morsi, Y. T. Shah and N. L. Carr (1987). "Effect of water on the solubilities and mass transfer coefficients of gases in a heavy fraction of fischer-tropsch products." The Canadian Journal of Chemical Engineering **65**(6): 973-981.

Klerk, A. d. (2007). "Environmentally friendly refining: Fischer-Tropsch versus crude oil." Green Chemistry **9**(6): 560-565.

Kluytmans, J. H. J., B. G. M. van Wachem, B. F. M. Kuster and J. C. Schouten (2003). "Mass transfer in sparged and stirred reactors: influence of carbon particles and electrolyte." Chemical Engineering Science **58**(20): 4719-4728.

Kollar, M., A. De Stefanis, H. E. Solt, M. R. Mihalyi, J. Valyon and A. A. G. Tomlinson (2010). "The mechanism of the Fischer-Tropsch reaction over supported cobalt catalysts." Journal of Molecular Catalysis a-Chemical **333**(1-2): 37-45.

Kolmogoroff, A. N. (1941). "Dissipation of energy in the locally isotropic turbulence." Comptes Rendus De L Academie Des Sciences De L Urss **32**: 16-18.

Kolmogorov, A. N. (1949). "Disintegration of drops in turbulent flows." Dokl Akad Nauk SSSR **66**: 4.

Kresta, S. M. and M. K. Suzanne (2004). Handbook of Industrial Mixing.

Krishna, R., J. W. A. De Swart, J. Ellenberger, G. B. Martina and C. Maretto (1997). "Gas holdup in slurry bubble columns: Effect of column diameter and slurry concentrations." Aiche Journal **43**(2): 311-316.

Laari, #160, Arto, Turunen and Ilkka (2003). Experimental determination of bubble coalescence and break-up rates in a bubble column reactor. Hoboken, NJ, ETATS-UNIS, Wiley.

Laari, A. and I. Turunen (2005). "Prediction of Coalescence Properties of Gas Bubbles in a Gas–Liquid Reactor Using Persistence Time Measurements." Chemical Engineering Research and Design **83**(7): 881-886.

Lazghab, M., K. Saleh, I. Pezron, P. Guigon and L. Komunjer (2005). "Wettability assessment of finely divided solids." Powder Technology **157**(1-3): 79-91.

Levenspiel, O. (1999). Chemical Reaction Engineering (3rd Edition), John Wiley & Sons.

Lin, T. J., K. Tsuchiya and L. S. Fan (1998). "Bubble flow characteristics in bubble columns at elevated pressure and temperature." Aiche Journal **44**(3): 545-560.

Lindner, D., M. Werner and A. Schumpe (1988). "Hydrogen transfer in slurries of carbon supported catalyst (HPO process)." Aiche Journal **34**(10): 1691-1697.

Liu, F. P., T. G. Rials and J. Simonsen (1998). "Relationship of Wood Surface Energy to Surface Composition." Langmuir **14**(2): 536-541.

Machon, V., A. W. Pacek and A. W. Nienow (1997). "Bubble Sizes in Electrolyte and Alcohol Solutions in a Turbulent Stirred Vessel." Chemical Engineering Research and Design **75**(3): 339-348.

Maretto, C. and R. Krishna (1999). "Modelling of a bubble column slurry reactor for Fischer-Tropsch synthesis." Catalysis Today **52**(2): 279-289.

Massoudi, R. and A. D. King (1974). "Effect of Pressure on Interfacial-Tension of Aqueous-Solutions in Equilibrium with Compressed Gases." Abstracts of Papers of the American Chemical Society: 179-179.

Massoudi, R. and A. D. King (1974). "Effect of Pressure on Surface-Tension of Water - Adsorption of Low-Molecular Weight Gases on Water at 25 Degrees." Journal of Physical Chemistry **78**(22): 2262-2266.

McClements, D. J. (2004). Food Emulsions. Food Emulsions, CRC Press.

Miettinen, T., J. Ralston and D. Fornasiero (2010). "The limits of fine particle flotation." Minerals Engineering **23**(5): 420-437.

Miller, N., Ed. (1985). Surfactant science series. Interfacial phenomena. New York and Basel, Marcel Dekker, INC.

Muganda, S., M. Zanin and S. R. Grano (2011). "Influence of particle size and contact angle on the flotation of chalcopyrite in a laboratory batch flotation cell." International Journal of Mineral Processing **98**(3-4): 150-162.

Mukhopadhyay, P. and H. P. Schreiber (1995). "Aspects of acid-base interactions and use of inverse gas chromatography." Colloids and Surfaces A: Physicochemical and Engineering Aspects **100**: 47-71.

Murray, B. S. and R. Ettelaie (2004). "Foam stability: proteins and nanoparticles." Current Opinion in Colloid & Interface Science **9**(5): 314-320.

Nagaraj, N. and D. J. Gray (1987). "Interfacial area and coalescence frequency in gas-slurry stirred reactors." Aiche Journal **33**(9): 1563-1566.

Newell, H. E., G. Buckton, D. A. Butler, F. Thielmann and D. R. Williams (2001). "The use of inverse phase gas chromatography to measure the surface energy of crystalline, amorphous, and recently milled lactose." Pharm Res **18**(5): 662-666.

Nguyen, A. V., H. J. Schulze and J. Ralston (1997). "Elementary steps in particle—bubble attachment." International Journal of Mineral Processing **51**(1–4): 183-195.

Nienow, A. W. (1968). "Suspension of solid particles in turbine agitated baffled vessels." Chemical Engineering Science **23**(12): 1453-1459.

Nienow, A. W. (1997). The suspension of solid particles. Mixing in the Process Industries. N. Harnby, M. F. Edwards and A. W. Nienow. Oxford, Butterworth-Heinemann**:** 364-393.

Norde, W. (2003). Wetting of Solid Surfaces. Colloids and Interfaces in Life Sciences, CRC Press.

Nowak, E., G. Combes, E. H. Stitt and A. W. Pacek (2013). "A comparison of contact angle measurement techniques applied to highly porous catalyst supports." Powder Technology **233**(0): 52-64.

Omota, F., A. C. Dimian and A. Bliek (2006). "Adhesion of solid particles to gas bubbles. Part 1: Modelling." Chemical Engineering Science **61**(2): 823-834.

Omota, F., A. C. Dimian and A. Bliek (2006). "Adhesion of solid particles to gas bubbles. Part 2: Experimental." Chemical Engineering Science **61**(2): 835-844.

Ozkan, O., A. Calimli, R. Berber and H. Oguz (2000). "Effect of inert solid particles at low concentrations on gas-liquid mass transfer in mechanically agitated reactors." Chemical Engineering Science **55**(14): 2737-2740.

Pacek, A. W., S. Chamsart, A. W. Nienow and A. Bakker (1999). "The influence of impeller type on mean drop size and drop size distribution in an agitated vessel." Chemical Engineering Science **54**(19): 4211-4222.

Pacek, A. W., C. C. Man and A. W. Nienow (1998). "On the Sauter mean diameter and size distributions in turbulent liquid/liquid dispersions in a stirred vessel." Chemical Engineering Science **53**(11): 2005-2011.

Pacek, A. W., I. P. T. Moore, A. W. Nienow and R. V. Calabrese (1994). "Video technique for measuring dynamics of liquid-liquid dispersion during phase inversion." Aiche Journal **40**(12): 1940-1949.

Parthasarathy, R. and N. Ahmed (1994). "Bubble Size Distribution in a Gas Sparged Vessel Agitated by a Rushton Turbine." Industrial & Engineering Chemistry Research **33**(3): 703-711.

Parthasarathy, R., G. J. Jameson and N. Ahmed (1991). Bubble breakup in stirred vessels : predicting the Sauter mean diameter. Amsterdam, PAYS-BAS, Elsevier.

Paul, E. L., V. A. Atiemo-Obeng and S. M. Kresta (2004). Handbook of Industrial Mixing : Science and Practice. Hoboken, NJ, USA, Wiley.

Peršin, Z., K. Stana-Kleinschek, M. Sfiligoj-Smole, T. Kre and V. Ribitsch (2004). "Determining the Surface Free Energy of Cellulose Materials with the Powder Contact Angle Method." Textile Research Journal **74**(1): 55-62.

Pickering, S. U. (1907). "Emulsions." Journal of the Chemical Society, Transactions **91**: 2001-2021.

Pohorecki, R., W. Moniuk, A. Zdrójkowski and P. Bielski (2001). "Hydrodynamics of a pilot plant bubble column under elevated temperature and pressure." Chemical Engineering Science **56**(3): 1167-1174.

Poling, B. E., J. M. Prausnitz and J. P. O'Connell (2001). Properties of Gases and Liquids (5th Edition), McGraw-Hill.

Preuss, M. and H.-J. Butt (1999). "Direct measurement of forces between particles and bubbles." International Journal of Mineral Processing **56**(1–4): 99-115.

Prince, M. J. and H. W. Blanch (1990). "Bubble coalescence and break-up in air-sparged bubble columns." Aiche Journal **36**(10): 1485-1499.

Ralston, J., D. Fornasiero and R. Hayes (1999). "Bubble–particle attachment and detachment in flotation." International Journal of Mineral Processing **56**(1–4): 133-164.

Razzaghi, K. and F. Shahraki (2010). "On the effect of phase fraction on drop size distribution of liquid–liquid dispersions in agitated vessels." Chemical Engineering Research and Design **88**(7): 803-808.

Rodriguez, M. A., J. F. Rubio, M. J. Liso and J. L. Oteo (1997). Application of inverse gas chromatography to the study of the surface properties of slates. Chantilly, Clay Minerals Society.

Ruthiya, K. C. (2005). Mass transfer and hydrodynamic in catalytic slurry reactors. Eindhoven, Technische Universitet Eindhoven**:** 229.

Ruthiya, K. C., B. F. M. Kuster and J. C. Schouten (2003). "Gas-liquid mass transfer enhancement in a surface aeration stirred slurry reactors." Canadian Journal of Chemical Engineering **81**(3-4): 632-639.

Ruthiya, K. C., J. van der Schaaf, B. F. M. Kuster and J. C. Schouten (2003). "Mechanisms of physical and reaction enhancement of mass transfer in a gas inducing stiffed slurry reactor." Chemical Engineering Journal **96**(1-3): 55-69.

Ruthiya, K. C., J. van der Schaaf, B. F. M. Kuster and J. C. Schouten (2005). "Similar effect of carbon and silica catalyst support on the hydrogenation reaction rate in organic slurry reactors." Chemical Engineering Science **60**(22): 6492-6503.

Sagert, N. H. and M. J. Quinn (1977). "Influence of high-pressure gases on the stability of thin aqueous films." Journal of Colloid and Interface Science **61**(2): 279-286.

Samiran, B. (2007). "Design - Development of Fischer - Tropsch Synthesis Reactor & Catalysts and their Interrelationship." Bulletin of the Catalysis Society of India **6**: 1-21.

Saukowski, D. M. and H. W. Yarranton (2005). "Oilfield solids and water-in-oil emulsion stability." Journal of Colloid and Interface Science **285**(2): 821-833.

Schäfer, R., C. Merten and G. Eigenberger (2002). "Bubble size distributions in a bubble column reactor under industrial conditions." Experimental Thermal and Fluid Science **26**(6-7): 595-604.

Schlesinger, M. D., J. H. Crowell, M. Leva and H. H. Storch (1951). "Fischer-Tropsch Synthesis in Slurry Phase." Industrial and Engineering Chemistry **43**(6): 1474-1479.

Schultz, J., K. Tsutsumi and J.-B. Donnet (1977). "Surface properties of high-energy solids: I. Determination of the dispersive component of the surface free energy of mica and its energy of adhesion to water and n-alkanes." Journal of Colloid and Interface Science **59**(2): 272-276.

Schulze, H. J. (1977). "New theoretical and experimental investigations on stability of bubble/particle aggregates in flotation: A theory on the upper particle size of floatability." International Journal of Mineral Processing **4**(3): 241-259.

Seed, B. (2001). Silanizing Glassware. Current Protocols in Immunology, John Wiley & Sons, Inc.

Shafrin, E. G. and W. A. Zisman (1967). "Critical surface tension for spreading on a liquid substrate." The Journal of Physical Chemistry **71**(5): 1309-1316.

Shi, B. L., Y. E. Wang and L. N. Jia (2011). "Comparison of Dorris-Gray and Schultz methods for the calculation of surface dispersive free energy by inverse gas chromatography." Journal of Chromatography A **1218**(6): 860-862.

Shinnar, R. (1961). "On the Behaviour of Liquid Dispersions in Mixing Vessels." Journal of Fluid Mechanics **10**(2): 259-&.

Sridhar, T. and O. E. Potter (1980). "Interfacial-Areas in Gas-Liquid Stirred Vessels." Chemical Engineering Science **35**(3): 683-685.

Stiller, S., H. Gers-Barlag, M. Lergenmueller, F. Pflucker, J. Schulz, K. P. Wittern and R. Daniels (2004). "Investigation of the stability in emulsions stabilized with different surface modified titanium dioxides." Colloids and Surfaces a-Physicochemical and Engineering Aspects **232**(2-3): 261-267.

Storsæter, S., Ø. Borg, E. A. Blekkan, B. Tøtdal and A. Holmen (2005). "Fischer–Tropsch synthesis over Re-promoted Co supported on Al2O3, SiO2 and TiO2: Effect of water." Catalysis Today **100**(3–4): 343-347.

Swaminathan, V., J. Cobb and I. Saracovan (2006). "Measurement of the surface energy of lubricated pharmaceutical powders by inverse gas chromatography." International Journal of Pharmaceutics **312**(1–2): 158-165.

Takahashi, K., W. J. McManamey and A. W. Nienow (1992). "Bubble size distributions in impeller region in a gas-sparged vessel agitated by a rushton turbine " Journal of Chemical Engineering of Japan **25**(4): 427-432.

Tambe, D. E. and M. M. Sharma (1994). "The effect of colloidal particles on fluid-fluid interfacial properties and emulsion stability." Advances in Colloid and Interface Science **52**(0): 1-63.

Tang, Y.-F., A.-D. Li, H.-Q. Ling, Y.-J. Wang, Q.-Y. Shao, Y.-N. Lu and Z.-D. Ling (2002). "Fabrication of composite particles with core-shell structures by a novel processing." Journal of Materials Science **37**(16): 3377-3379.

Tavlarides, L. L. and M. Stamatoudis (1981). The Analysis of Interphase Reactions and Mass Transfer in Liquid-Liquid Dispersions. Advances in Chemical Engineering. G. R. C. J. W. H. Thomas B. Drew and V. Theodore, Academic Press. **Volume 11:** 199-273.

Tcholakova, S., N. D. Denkov and A. Lips (2008). "Comparison of solid particles, globular proteins and surfactants as emulsifiers." Physical Chemistry Chemical Physics **10**(12): 1608-1627.

Tinge, J. T. and A. A. H. Drinkenburg (1995). "The enhancement of the physical absorption of gases in aqueous activated carbon slurries." Chemical Engineering Science **50**(6): 937-942.

van der Zon, A., P. J. Hamersma, E. K. Poels and A. Bliek (2002). "Coalescence of freely moving bubbles in water by the action of suspended hydrophobic particles." Chemical Engineering Science **57**(22-23): 4845-4853.

van der Zon, M., P. J. Hamersma, E. K. Poels and A. Bliek (1999). "Gas-solid adhesion and solid-solid agglomeration of carbon supported catalysts in three phase slurry reactors." Catalysis Today **48**(1-4): 131-138.

van Oss, C. J., R. F. Giese and W. Wu (1998). "On the degree to which the contact angle is affected by the adsorption onto a solid surface of vapor molecules originating from the liquid drop." Journal of Dispersion Science and Technology **19**(6-7): 1221-1236.

Van Oss, C. J., R. J. Good and M. K. Chaudhury (1988). "Additive and nonadditive surface tension components and the interpretation of contact angles." Langmuir **4**(4): 884-891.

Vinke, H., G. Bierman, P. J. Hamersma and J. M. H. Fortuin (1991). "Adhesion of small catalyst particles to gas bubbles: determination of small effective solid—liquid—gas contact angles." Chemical Engineering Science **46**(10): 2497-2506.

Vinke, H., P. J. Hamersma and J. M. H. Fortuin (1991). "Particle-to-bubble adhesion in gas/liquid/solid slurries." Aiche Journal **37**(12): 1801-1809.

Vinke, H., P. J. Hamersma and J. M. H. Fortuin (1993). "Enhancement of the gas-absorption rate in agitated slurry reactors by gas-adsorbing particles adhering to gas bubbles." Chemical Engineering Science **48**(12): 2197-2210.

Voillequin, B. and F. Luck (2011). "Fischer-Tropsch synthesis: a reaction with two limit mechanisms." Actualite Chimique(350): 16-25.

Wilhelm, D. J., D. R. Simbeck, A. D. Karp and R. L. Dickenson (2001). "Syngas production for gas-to-liquids applications: technologies, issues and outlook." Fuel Processing Technology **71**(1-3): 139-148.

Wilkinson, P. M., H. Haringa and L. L. Van Dierendonck (1994). "Mass transfer and bubble size in a bubble column under pressure." Chemical Engineering Science **49**(9): 1417-1427.

Wilkinson, P. M. and L. L. v. Dierendonck (1990). "Pressure and gas density effects on bubble break-up and gas hold-up in bubble columns." Chemical Engineering Science **45**(8): 2309-2315.

Wimmers, O. J. and J. M. H. Fortuin (1988). "The use of adhesion of catalyst particles to gas bubbles to achieve enhancement of gas absorption in slurry reactors--I. Investigation of particle-to-bubble adhesion using the bubble pick-up method." Chemical Engineering Science **43**(2): 303-312.

Xie, J., Q. Zhang and K. T. Chuang (2000). "An IGC Study of Pd/SDB Catalysts for Partial Oxidation of Propylene to Acrylic Acid." Journal of Catalysis **191**(1): 86-92.

Yang, Y.-C. and P.-R. Yoon (2007). "Determination of Dispersive Properties of Silicas by Inverse Gas Chromatography: Variation with Surface Treatment." MATERIALS TRANSACTIONS **48**(6): 1548-1553.

York, P., M. D. Ticehurst, J. C. Osborn, R. J. Roberts and R. C. Rowe (1998). "Characterisation of the surface energetics of milled dl-propranolol hydrochloride using inverse gas chromatography and molecular modelling." International Journal of Pharmaceutics **174**(1–2): 179-186.

Yotsumoto, H. (2006). Flotation. Powder Technology, CRC Press. **null**.

Żenkiewicz, M. (2007). "Methods for the calculation of surface free energy of solids." Journal of Achievements in Materials and Manufacturing Engineering **24**(1): 137-145.

Zhang, L.-j., T. Li, W.-y. Ying and D.-y. Fang (2008). "Rising and descending bubble size distributions in gas–liquid and gas–liquid–solid slurry bubble column reactor." Chemical Engineering Research and Design **86**(10): 1143-1154.

Zhou, G. and S. M. Kresta (1998). "Correlation of mean drop size and minimum drop size with the turbulence energy dissipation and the flow in an agitated tank - relative influence of viscosity and interfacial tension." Chemical Engineering Science **53**(11): 2063-2079.

Zhou, G. and S. M. Kresta (1998). "Evolution of drop size distribution in liquid–liquid dispersions for various impellers." Chemical Engineering Science **53**(11): 2099-2113.

Zhuravlev, L. T. (2000). "The surface chemistry of amorphous silica. Zhuravlev model." Colloids and Surfaces A: Physicochemical and Engineering Aspects **173**(1–3): 1-38.

# APPENDIXES

Appendix contains 2 peer review papers:

1. E. Nowak, G.B. Combes, E.H. Stitt, A.W. Pacek, *A comparison of contact angle measurement techniques applied to highly porous catalyst supports,* Powder Technology 233 (2013) 52–64

2. E. Nowak, P. Robbins, G.B. Combes, E.H. Stitt, A.W. Pacek, *Measurements of contact angle between fine, non-porous particles with varying hydrophobicity and water and non-polar liquids of different viscosities,* Powder Technology 250 (2013) 21–32